THOR INGE FOSSEN

NONLINEAR MODELLING AND CONTROL OF UNDERWATER VEHICLES

DOKTORINGENIØRAVHANDLING 1991:1
INSTITUTT FOR TEKNISK KYBERNETIKK
TRONDHEIM

Nonlinear Modelling and Control of Underwater Vehicles

by

Thor Inge Fossen
M.Sc., Division of Marine Systems Design
Department of Marine Technology
Norwegian Institute of Technology
(October 1987)

Submitted to the Division of Engineering Cybernetics, Department of Electrical Engineering, Norwegian Institute of Technology in partial fulfillment of the requirements for the Dr.ing degree in Engineering Cybernetics

at the

Norwegian Institute of Technology
(June 1991)

To my parents and Heidi

Summary

This thesis is a comprehensive study of nonlinear modelling and control of small underwater vehicles. Most of the findings have been published by the author through recent international conferences and journals.

The 6 degree of freedom (DOF) underwater vehicle equations of motion are written in a compact form inspired by the representation used in robot manipulator control. The model is based on an extensive study of the existing hydrodynamical literature. Particular attention is paid to the modelling of the thruster dynamics. It is shown how a precise model of the highly nonlinear thruster forces can be exploited in the nonlinear control system design. These new results are verified by open water experiments.

It is shown how deterministic and random disturbance models can be augmented to the the vehicle's equations of motion. Statistical descriptions of waves and root-mean-square analyses are discussed in depth.

Some new contributions to stick-fixed and stick-free stability analyses of underwater vehicles in 6 DOF are discussed. These stability criteria are based on well known techniques like the Routh's stability criterion, Lyapunov's linearization method, Lyapunov's direct method for autonomous systems and advanced Lyapunov theory like Barbălat's Lyapunov-like lemma for non-autonomous systems.

Underwater vehicles performing coupled manoeuvres at some speed are known to be highly nonlinear in their dynamics. The obvious way to compensated for these nonlinearities is by applying nonlinear control system techniques. In nonlinear control design emphasis is placed on design simplicity. It is shown how well known properties of the nonlinear equations of motion can be exploited to yield a relatively simple control design. The following three nonlinear design techniques are studied in detail:

- **Feedback linearization techniques.**
- **Sliding control.**
- **Passivity based control.**

These are used to illustrate how adaptive autopilots for velocity, orientation and position control can be designed. It is also shown how environmental disturbances can be relatively easily compensated for when designing the nonlinear autopilot. This study is mainly based on simulation results.

Finally, optimal state estimation is discussed. It is shown how Kalman filtering techniques can be used in state estimation, wild-point detection and filtering. Since the vehicle's hydrodynamic parameters only are partly known for most underwater vehicles, it is desirable to have a navigation system which is independent of the vehicle we are using. Hence, the state estimators are only based on the kinematic equations of motion which implies that we can design two independent state estimators, each designed for:

- **Estimation of linear velocities and position.**
- **Estimation of angular velocities and Euler angles.**

State-of-the-art sensor units are used to illustrate the different concepts. This investigation is partly based on computer simulations and experimental results.

Contents

Nomenclature

Vectors and Matrices

Bold types are used exclusively to denote vectors and matrices.

Symbols

Symbol	Definition
$\boldsymbol{a}$	Commanded acceleration
A	Area, projected area
$\boldsymbol{A}$	System matrix
B	Buoyancy force
$\boldsymbol{B}$	Input matrix, thruster configuration matrix
$\overline{BG}$	Distance between CG and CB
$\overline{BM}$	Distance between the vehicle's metacentre and CB
$\boldsymbol{B}^{\dagger}$	Generalized inverse of $\boldsymbol{B}$
$\boldsymbol{C}$	Matrix of Coriolis and centrifugal terms
$\boldsymbol{C}_A$	Matrix of Coriolis and centrifugal terms due to hydrodynamic added mass
CB	Centre of buoyancy
C_D	Drag coefficient
CG	Centre of gravity
$\boldsymbol{C}_{i,j}$	Rotation matrix describing a rotation j about the i-axis
C_M	Inertia coefficient
CP	Centre of pressure
$\boldsymbol{C}_{RB}$	Matrix of Coriolis and centrifugal terms due to rigid body forces
$\boldsymbol{C}^*$	Matrix of Coriolis and centrifugal terms referred to the earth-fixed coordinate system
$\boldsymbol{d}_Q$	Vector of quadratic damping terms due to skin friction and drag
D	Diameter
$\boldsymbol{D}$	Matrix of dissipative (damping) terms

$\boldsymbol{D_B}$	Matrix of linear damping terms due to potential damping
$\boldsymbol{D_L}$	Matrix of linear damping terms due to skin friction and drag
$\boldsymbol{D_Q}$	Matrix of quadratic damping terms due to skin friction and drag
$\boldsymbol{D_U}$	Damping matrix due to umbilical
$\boldsymbol{D_V}$	Damping matrix due to viscous effects
$\boldsymbol{D^*}$	Damping matrix referred to the earth-fixed coordinate system
$\boldsymbol{e}$	Euler parameter vector, prediction error vector
e_i	Euler parameter i (i=1..4)
E_k	Kinetic energy
$\boldsymbol{f}$	Force vector
$\boldsymbol{f}_o$	Force vector referred to the vehicle-fixed coordinate system
g	Acceleration of gravity
$\boldsymbol{g}$	Vector of gravitational and buoyancy forces
$\boldsymbol{g^*}$	Vector of gravitational and buoyant forces referred to the earth-fixed coordinate sy
$\overline{GM}$	Distance between the vehicle's metacentre and CG
h	Transfer function, water depth
H	Transfer function matrix, wave height
$H_{\frac{1}{3}}$	Significant wave height
k	Wave number
$\overline{KG}$	Distance between the vehicle's CG and keel line
$\boldsymbol{I}$	Identity matrix
$\boldsymbol{I}_o$	Inertia tensor referred to the vehicle-fixed coordinate system
I_x	Moment of inertia about x-axis
I_y	Moment of inertia about y-axis
I_z	Moment of inertia about z-axis
I_{xy}	Product of inertia about x- and y-axes
I_{xz}	Product of inertia about x- and z-axes
I_{yz}	Product of inertia about y- and z-axes
J	Cost function
J_o	Open water advance coefficient
$\boldsymbol{J}$	Linear and Angular velocity transformation matrix
$\boldsymbol{J}_1$	Linear velocity transformation matrix
$\boldsymbol{J}_2$	Angular velocity transformation matrix
K	Hydrodynamic moment component about x-axis (rolling moment)
KC	Keulegan-Carpenter's number
$\boldsymbol{K}_D$	Regulator gain matrix
K_T	Non-dimensional thrust coefficient
K_Q	Non-dimensional torque coefficient
L	Length of vehicle, loop transfer function matrix

l	Loop transfer function
m	Mass of the vehicle
$\boldsymbol{m}$	Moment vector
$\boldsymbol{m}_o$	Moment vector referred to the vehicle-fixed coordinate system
$\overline{m}$	Mass of the displaced fluid
M	Hydrodynamic moment component about y-axis (pitching moment)
$\boldsymbol{M}$	Inertia matrix
$\boldsymbol{M}_A$	Added mass matrix
$\boldsymbol{M}_{FK}$	Froude-Kriloff inertia matrix
$\boldsymbol{M}_{RB}$	Rigid body inertia matrix
$\boldsymbol{M}^*$	Inertia matrix referred to the earth-fixed coordinate system
n	Propeller revolution
N	Hydrodynamic moment component about z-axis (yawing moment)
p	Angular velocity component of $\dot{\boldsymbol{q}}$ about x-axis (roll), pressure
p_D	Dynamic pressure
p_o	Atmospheric pressure on the water surface
$\boldsymbol{P}$	Adaption gain matrix
q	Angular velocity component of $\dot{\boldsymbol{q}}$ about y-axis (pitch)
$\dot{\boldsymbol{q}}$	Vehicle-fixed vector of linear and angular velocities components
$\dot{\boldsymbol{q}}_d$	Desired velocity vector
$\dot{\boldsymbol{q}}_f$	Fluid velocity vector referred to the vehicle-fixed coordinate system
$\dot{\boldsymbol{q}}_r$	Relative fluid velocity vector referred to the vehicle-fixed coordinate system
$\dot{\boldsymbol{q}}_1$	Vehicle-fixed vector of linear velocity components
$\dot{\boldsymbol{q}}_2$	Vehicle-fixed vector of angular velocity components
$\tilde{\dot{\boldsymbol{q}}}$	Velocity tracking error vector
Q	Propeller torque
r	Angular velocity component of $\dot{\boldsymbol{q}}$ about z-axis (yaw)
$\boldsymbol{r}$	Position vector in the earth-fixed coordinate system XYZ
$\boldsymbol{r}_o$	Position vector referring the local coordinate system $X_oY_oZ_o$ to the earth-fixed coordinate system XYZ
$\boldsymbol{r}_G$	Position vector in the local coordinate system $X_oY_oZ_o$
Re	Reynold's number
$\boldsymbol{s}$	Measure of tracking
S	Wave spectrum
t	Time
T	Time constant, wave period, propeller thrust
u	Linear velocity component of $\dot{\boldsymbol{q}}$ in x-direction (surge)
$\boldsymbol{u}$	Control input vector

u_o	Service speed
u_f	Fluid motion velocity component in the x-direction
u_f	Relative fluid motion velocity component in the x-direction
v	Linear velocity component of $\dot{\boldsymbol{q}}$ in y-direction (sway)
$\boldsymbol{v}$	Disturbance vector
$\boldsymbol{v}_e$	Earth-fixed vector of linear velocity components
v_f	Fluid motion velocity component in the y-direction
v_r	Relative fluid motion velocity component in the y-direction
$\boldsymbol{v}_o$	Vehicle-fixed vector of linear velocity components
V	Volume, vehicle speed, noise covariance matrix, Lyapunov function
∇	Volume of displaced fluid
V_A	Advance velocity at the propeller
w	Linear velocity component of $\dot{\boldsymbol{q}}$ in z-direction (heave), wake fraction number
$\boldsymbol{w}$	Measurement noise vector
w_f	Fluid motion velocity component in the z-direction
w_r	Relative fluid motion velocity component in the z-direction
W	Weight of the vehicle
$\boldsymbol{W}$	Measurement noise covariance matrix, positive definite weighting matrix
x	Surge position referred to the earth-fixed reference frame
x_B	The x-coordinate of CB
x_G	The x-coordinate of CG
x_P	The x-coordinate of CP
$\boldsymbol{x}$	Earth-fixed vector of position and Euler angle components
$\boldsymbol{x}_d$	Desired state vector
$\boldsymbol{x}_1$	Earth-fixed vector of linear velocity components
$\boldsymbol{x}_2$	Earth-fixed vector of angular velocity components
$\tilde{\boldsymbol{x}}$	Earth-fixed tracking error vector
X	Hydrodynamic force component along x-axis
$\boldsymbol{X}$	State error covariance matrix
XYZ	Earth-fixed coordinate system
$X_oY_oZ_o$	Vehicle-fixed coordinate system
y	Sway position referred to the earth-fixed reference frame
$\boldsymbol{y}$	Measurement vector
y_B	The y-coordinate of CB
y_G	The y-coordinate of CG
x_P	The y-coordinate of CP
Y	Hydrodynamic force component along y-axis
$\boldsymbol{Y}$	Output covariance matrix
z	Heave position (depth) referred to the earth-fixed reference frame

z_B	The z-coordinate of CB
z_G	The z-coordinate of CG
z_P	The z-coordinate of CP
Z	Hydrodynamic force component along z-axis

Greek Symbols

$\boldsymbol{\Gamma}$	Positive definite weighting matrix
δ	Rudder angle
ζ	Wave elevation
ζ_A	Wave amplitude
ζ_θ	Damping ration in pitch
ζ_ϕ	Damping ratio in roll
η	White noise
$\boldsymbol{\eta}$	Vector of linear and angular velocity components
$\boldsymbol{\eta}_f$	Vector of linear and angular fluid velocity components
η_M	Mechanical efficiency
η_o	Thruster open water efficiency in undisturbed water
$\boldsymbol{\eta}_r$	vector of relative linear and angular velocity components
η_R	Relative rotative efficiency
η_{1-3}	Linear displacements
η_{4-6}	Angular displacements
θ	Angle of pitch, Euler angle
$\boldsymbol{\theta}$	Parameter vector
λ	Wave length, closed loop bandwidth, eigenvalue, forgetting factor
$\boldsymbol{\lambda}$	Vector of Lagrange multiplicators
ρ	Water density
ρ_A	Mass density of vehicle
σ	Standard deviation
$\boldsymbol{\tau}$	Force and moment vector
$\boldsymbol{\tau}_A$	Force and moment vector due to hydrodynamic added mass
$\boldsymbol{\tau}_B$	Force and moment vector due to hydrodynamic potential damping
$\boldsymbol{\tau}_C$	Force and moment vector due to restoring forces
$\boldsymbol{\tau}_D$	Diffraction force and moment vector
$\boldsymbol{\tau}_E$	Force and moment vector due to ϕ_W and ϕ_D
$\boldsymbol{\tau}_{FK}$	Froude-Kriloff force and moment vector
$\boldsymbol{\tau}_H$	Hydrodynamic force and moment vector due to ϕ_R, ϕ_W and ϕ_D
$\boldsymbol{\tau}_o$	Force and moment vector referred to the vehicle-fixed coordinate system

List of Tables

List of Figures

Preface

I am grateful to my supervisor Professor Jens G. Balchen at the Division of Engineering Cybernetics (NTH) whose enthusiasm, creativity and overall knowledge in the general field of control engineering has been of invaluable help in the preparation of this thesis. Professor Jens G. Balchen has also been my main motivation for a doctoral study in engineering cybernetics.

I am particular grateful to my college and friend Svein I. Sagatun at the Division of Engineering Cybernetics (NTH) for his enthusiasm, encouragement and moral support. His help has been invaluable since we started to work together in 1987. Since then, we have designed and built the NEROV underwater vehicle and published several papers together in international journals. Svein I. Sagatun's eagerness and optimism has been extremely appreciated, particularly on days when the realization of the NEROV vehicle, and this thesis, seemed quite unrealistic.

I would like to thank Knut Streitlien at the Department of Ocean Engineering (MIT) for his suggestions concerning Chapter 2 addressing the nonlinear modelling of underwater vehicles. Besides this, Professor Odd M. Faltinsen, Professor Harald Aa. Walderhaug, Associate Professor Bjørn Sortland at the Department of Marine Technology (NTH) have provided many useful suggestions and discussions. Asgeir Sørensen at the Division of Engineering Cybernetics (NTH) should be thanked for his stimulating discussions in marine hydrodynamics.

I am also grateful to Professor Olav Egeland at the Division of Engineering Cybernetics (NTH) for his good support, stimulating discussions and judicious suggestions.

I would like to thank the excellent staff at the mechanical workshop at the Division of Engineering Cybernetics (NTH) for building the NEROV vehicle. Stefano Bertelli's expertise and energy was invaluable in the experimental set-ups and hardware design. I am grateful to Erik Lehn, Senior Research Engineer at MARINTEK who helped us to design the NEROV thruster. His sincere help in the preparation of the NEROV thruster open water test was highly appreciated. I would like to thank Mathias Håndlykken, Senior Research Engineer at SEATEX A/S and Jacob Li Simonsen, Senior Research Engineer at Robertson Tritech A/S for their stimulating discussions and suggestions in the design of the NEROV sensor system.

Øystein Baltzersen, Research Scientist at the Continental Shelf and Petroleum Technology Research Institute (IKU) is also to be thanked for his kind help with the UPOS underwater positioning system.

I am grateful to my colleagues Jan O. Hallset, Geir Mathisen and Ørnulf J. Rødseth at the SINTEF Autonomous System Group for their suggestions and stimulating discussions during the design process of the NEROV vehicle. Jens G. Balchen, Olav Egeland, Ola-Erik Fjellstad, Svein I. Sagatun and Asgeir Sørensen should also be thanked for helping me reducing the number of typographical errors to an acceptable level.

The thesis also benefits from all the useful comments and enthusiasm of many of the students who took my course in Control and Guidance in the spring term 1991 at NTH. I appreciate the assistance from Stewart Clark at NTH, who has helped me improve the English in this thesis. Finally, I am most grateful for the financial support from the Royal Norwegian Council for Scientific and Industrial Research through the Center for Robotic Research (NTH) and the Fulbright Foundation which helped to make this work possible.

Thor I. Fossen

Chapter 1

Introduction

Norway has long recognized the importance of the ocean to its economy, security and environment. Hence, Norway's economic interests are highly tied to areas such as oil and gas exploration, merchant shipping and the fisheries. We believe that the development of a new generation of unmanned underwater vehicles as well as underwater vehicle-manipulator systems will be crucial for future oil and gas exploration. The need will be particular acute as the costs of inspection, maintenance and repair (IMR) of subsea production facilities, pipelines and platform structures will drastically rise with increasing water depths. The use of divers in deep water is hazardous and limited due to obvious physiological limitations. Hence, it is desirable to replace them by underwater robotic vehicles. As major developers of off-shore technology, Norwegian industry and research institutes have recognized the need for more advanced underwater vehicle systems. A result of this is the increased activity in underwater robotics at the Norwegian Institute of Technology.

This thesis considers the nonlinear modelling and control of underwater vehicles. It has been written such that readers that are unfamiliar with hydrodynamics and advanced control theory should be able to understand the mathematical and physical formulations. Both the derivation of the nonlinear mathematical model and control theory are general enough to be applied to a large class of marine vehicles like submarines, submersibles, oil platforms and ships. Nevertheless, the intention with the thesis is to derive and discuss high performance, robust and computionally effective controllers for small unmanned underwater vehicles. These are conveniently classified as remotely operated vehicles (ROVs) and autonomous underwater vehicles (AUVs). The term ROV is used for small untethered and tethered remotely operated underwater vehicles while the term AUV will be used for small untethered underwater vehicles which are autonomous with respect to information and energy. Further it is convenient to distinguish between complete autonomity and semi-autonomity. Complete autonomity implies that the vehicle must be autonomous with respect to both energy and information. Hence, semi-autonomous vehicles could be understood as vehicles which have some communication with a human operator. Though, the sophistication of AUVs has

broken new ground, adequate high energy sources for propulsion as well as good signal transmission in water are the basic limitations of today AUV systems. For instance, a propulsion system based on battery energy greatly limits the vehicle's endurance time. Another problem limiting the commercial use of AUV systems is the insufficiency of underwater navigation systems. Most ROV underwater navigation systems are based on
hydroacoustic transducers and receivers e.g. long base-line systems (LBS), which highly limit the vehicle's operating area.

The control system techniques discussed can be applied to autopilot design, dynamic positioning (DP) and the tracking of general time-varying reference trajectories in 6 degrees of freedom (DOF). Lower DOF controllers where the influence of e.g. the rolling and pitching motion are neglected are easily obtained by a reduction of the general control law. It is shown that for more advanced manoeuvres, nonlinear control design techniques are superior to conventional linear control design techniques when applied to ROVs. Existing ROV systems are usually designed for a simple crab-wise motion with one monovariable controller e.g. using the proportional, integral and derivative (PID) type for each DOF. Nonlinear multivariable controllers allow the ROV to perform more coupled manoeuvres. Improved performance can be further obtained by applying the results from adaptive and robust control theory.

The experiments and simulation studies in this thesis are exclusively based on the use of the Norwegian Experimental Remotely Operated vehicle (NEROV), which was designed by my college Svein I. Sagatun and the author during the academic year 1990-1991, Fossen and Balchen (1991) and Sagatun and Fossen (1991c). The NEROV vehicle is an AUV which is build at the Division of Engineering Cybernetics at the Norwegian Institute of Technology (NTH) in Trondheim. The vehicle is energy-autonomous, but it has an optional communication cable for remote control. Hence, if desirable complete autonomity can be achieved as a routine matter. A general description on the research programme on AUVs in Norway are described in Rødseth (1990) while a description of the Norwegian research programmes in the general field of advanced robotic systems is found in Egeland (1991).

Recently, the control of the combined motion of underwater vehicle-manipulators has been discussed in the technical literature. Coordination of the motion between the underwater vehicle and the manipulator arm is often referred to as macro-micro control. Macro-micro control of underwater vehicle-manipulator systems is not discussed in this thesis. However, some recently results can be found in Fossen (1991) and Mahesh *et al.* (1991).

1.1 Underwater Vehicle Applications

Small underwater vehicles can be used in a large number of applications, such as:

- **Non-destructive testing of underwater structures:** Offshore IMR of underwater structures like oil-platforms, bottom templates etc. are well known ROV applications. The ROV tether is not practical when inspecting complex underwater structures. In such cases the ROV operator has to manoeuvre the vehicle within an underwater structure where a large number of wires and legs are present. AUVs would be easier to operate in such hostile environments.
- **Hydrographic Survey:** Low cost unmanned ROV and AUV systems are expected to replace manned survey launches in hydrographic surveys of offshore waters.
- **Deep seabed mining:** Commercial exploitation of deep seabed minerals like cobol and sulphides has been studied excessively during the last decade. The first full-scale mining test is expected to be performed already in 1994 by a Japanese research team. ROVs and AUVs are expected to play an increasingly role in deep sea surveying and the transport of underwater minerals.
- **Aquaculture:** ROVs and AUVs can be used as instrument platforms for in situ observations and survey of fish without affecting their behaviour. Underwater vehicle systems are expected to be useful tools for fisheries research and sea farming.
- **Military applications:** Military applications for AUVs are numerous, especially in underwater search and intelligence gathering operations. The use of an AUV as a mobile sensor platform will reduce both the costs and risks of such operations. A typical application is detecting of mines by a sonar.

1.2 Why Nonlinear Modelling and Control ?

- **A large number of operating conditions:** Small underwater vehicles are assumed to be able to operate over numerous operating points with no specific speed dominating. Aircraft and submarines are usually linearized about different constant forward speeds. Linear control theory and gain scheduling techniques can then be applied to each of the vehicle's operating points. When designing controllers for small underwater vehicles with dominating speeds in both the longitudinal and lateral directions, nonlinearities caused by e.g. hydrodynamic forces like quadratic lift and drag forces, can be significant. Therefore, in order to obtain high performance for such systems, nonlinear modelling and control techniques should be considered.
- **Design simplicity:** Nonlinear control design of underwater vehicle systems can be simpler and more intuitive than their linear counterparts. Exploring the physics and

a priori information of the underwater vehicle dynamics and kinematics often yields a relative simple control design. A typical example is nonlinear feedback linearization techniques which can be applied for a large number of mechanical systems like robot manipulators, aircraft and underwater vehicles. Successful implementations of robot manipulators are well documented in the technical literature.

- **Improved Robustness and Performance:** Linear control theory is based on the assumption that the physical system is linearizable. However, in mechanical systems there are many hard nonlinearities like Columb friction, hysteresis, actuator dead-zones and saturation. Besides this, nonlinearities are imposed by dynamics and kinematics of the underwater vehicle. Understanding and modelling these effects are crucial to the robustness and performance of the ROV. Nonlinear control design techniques allow the designer to directly compensate for the nonlinear dynamics in the model.

- **Reduced Model Imperfectness:** A linear approximation of a nonlinearity will have both parametric and structural uncertainty. If the structure of the nonlinearity is known, which is often the case for mechanical systems, the nonlinearity can be included directly in the model. Then, only parametric uncertainty has to be considered. Parametric uncertainties can be compensated for by applying adaptive or robust control design techniques.

1.3 The Contribution of the Thesis

1.3.1 Experimental Contribution

The experimental contribution of this thesis is primarily based on the design and building of the the NEROV vehicle. During the design process a large number of laboratory and full-scale experiments have been performed. Some of these results are found in:

(i) *Section 2.8. Open water test of ducted thruster.*
The results from the open water thruster experiments are published in Fossen and Sagatun(1991a, 1991b).

(ii) *Section 2.8. Performance of the inner loop thruster servo.*

(iii) *Chapter 6.3. Experimental verification of the NEROV vehicle's sensor system.* The results are published in Fossen and Balchen (1991).

(iv) *Appendix A. Determination of the hydrodynamical coefficients of the NEROV vehicle.*

The design and testing of the NEROV vehicle is described more closely in the following five internal reports:

- Design Study of the NEROV Vehicle (Sagatun and Fossen (1990b)).
- The NEROV Propulsion System (Sagatun and Fossen (1991a)).
- The NEROV Computer System (Sagatun and Fossen (1991b)).
- The NEROV Equations of Motion (Fossen and Sagatun (1991c)).
- The NEROV Sensor System (Fossen and Sagatun (1991d)).

1.3.2 Theoretical Contribution

The theoretical contribution of the thesis can be briefly summarized as:

(i) Chapter 2. Formalization and derivation of the nonlinear underwater vehicle equations of motion in 6 DOF. Nonlinear modelling of thruster forces, Section 2.8, is considered in detail. The results are published in Fossen (1990), Fossen and Sagatun(1991a, 1991b).

(ii) Sections 4.1.3 - 4.1.4. Derivation of longitudinal and lateral stick-fixed stability criteria for underwater vehicles in 6 DOF.

(iii) Section 4.2.1. Application of Lyapunov stability theory in stick-fixed stability analyses. It is shown how Lyapunov's Direct Method can be used to prove the well known stability criterion of Abkowitz (1964) for straight line stability of marine vehicles.

(iv) Sections 5.2.2-5.2.5. Formalization of 6 DOF nonlinear controllers for underwater vehicles based on feedback linearization techniques. Both vehicle-fixed velocity schemes (q-frame formulation) and earth-fixed position and orientation schemes (x-frame formulation) are considered.

(v) Section 5.3.2. Formalization and derivation of a MIMO sliding controller for nonlinear *minimum phase* systems with arbitrary relative degree. The results are published in Fossen and Foss (1991).

(vi) Section 5.3.4. A first attempt at applying a nonlinear recursive prediction error method to sliding control of underwater vehicles. The results are published in Fossen and Balchen (1988).

(vii) Section 5.4.1. The representation of the adaptive controller of of Slotine and Benedetto (1990) is simplified. The symbolic representation of the new regressor matrix is advantageous when considering systems with a large number of unknown parameters e.g. underwater vehicles in 6 DOF, Fossen and Sagatun(1991a, 1991b).

(viii) Section 5.4.1. A new variable structure passivity based adaptive controller (VS-PBAC) is derived. The control scheme is published in Fossen and Balchen (1991).

(ix) Section 5.4.2. It is shown how slowly-varying environmental disturbances can be compensated for by adding an adaptive feedforward term to the adaptive controller. Global stability is proven for the new scheme, Fossen and Balchen (1991).

(x) Section 5.4.3. Derivation of a new hybrid controller combining adaptive and sliding mode control. The parameter update law estimates unknown parameters in the dynamic equation while a discontinuous (switching) term is added to the control law to compensate for uncertainties in the input matrix. Hence, uncertainties in the thruster characteristics can be compensated for. The results are published in Fossen and Sagatun(1991a, 1991b).

1.4 Outline of the Thesis

The remaining chapters and appendices consider the following:

Chapter 2 is a detailed description of nonlinear modelling of underwater vehicles in 6 DOF. The nonlinear equations of motion are written in a compact form intended for nonlinear control system design and simulation. Kinematics, Newton's laws of angular and linear momentum and general hydrodynamics are discussed in detail.

Chapter 3 describes how deterministic and random disturbances can be incorporated in the vehicle equations of motion. Statistical descriptions of waves and root-mean-square (RMS) analyses are used to illustrate the ideas.

Chapter4 discusses linear and nonlinear stability criteria for underwater vehicles. This includes the definitions of straight line, directional, position motion and metacentric stability. Lyapunov stability theory for autonomous and non-autonomous systems is used to illustrate the concepts of nonlinear stick-fixed and stick-free stability, respectively.

Chapter 5 describes how nonlinear control design techniques can be applied to underwater vehicle autopilot design. Feedback linearization techniques, sliding control and passivity-based adaptive control are discussed in detail. The control of linear and angular velocities of the vehicle as well as the vehicle position and orientation are discussed. Computer simulations are used to illustrate the different control design techniques.

Chapter 6 shows how optimal state estimation (Kalman filtering) can be applied to underwater navigation systems. The sensor systems discussed are based on standard off-the-shelfes sensors for the measuring of position, velocity and acceleration.

Chapter 7 contains the conclusions and recommendations for future work.

Appendix A describes the NEROV nonlinear equations of motion. The weight, balance data and numerical values for hydrodynamic added mass and damping are also enclosed.

Appendix B is a mathematical proof of Eq. 5.21.

Chapter 2

Mathematical Modelling

2.1 Coordinate Systems

In control and guidance applications, the most used kinematic representations are Euler angles and quaternions. Both representations will now be described in more detail.

2.1.1 Euler Angles

It is desirable to describe the orientation of marine and flight vehicles relative to the earth. If we denote the local body-fixed coordinate system $X_oY_oZ_o$ and the earth-fixed coordinate system XYZ, Fig. 2.2 , a vehicle's flight path relative to the earth-fixed coordinate system is given by a linear velocity transformation

$$\boldsymbol{v}_e = \boldsymbol{J}_1(\phi, \theta, \psi)\, \boldsymbol{v}_o$$

where $\boldsymbol{v}_e = (\dot{x}, \dot{y}, \dot{z})^T$ is the linear velocity vector in the earth-fixed coordinate system and $\boldsymbol{v}_o = (u, v, w)^T$ is the linear velocity vector in the local coordinate system. The notation is according to the SNAME (1950) notation. The coordinate transformation matrix $\boldsymbol{J}_1$ is related through the functions of the Euler angles: roll(ϕ), pitch(θ) and yaw(ψ) , Abkowitz (1969) and Roskam (1982). The coordinate transformation matrix $\boldsymbol{J}_1$ is orthogonal i.e. $\boldsymbol{J}_1^T\boldsymbol{J}_1 = \boldsymbol{I}$. The inverse linear velocity transformation can be written as:

$$\boldsymbol{v}_o = \boldsymbol{J}_1^{-1}(\phi, \theta, \psi)\, \boldsymbol{v}_e = \boldsymbol{J}_1^T(\phi, \theta, \psi)\, \boldsymbol{v}_e$$

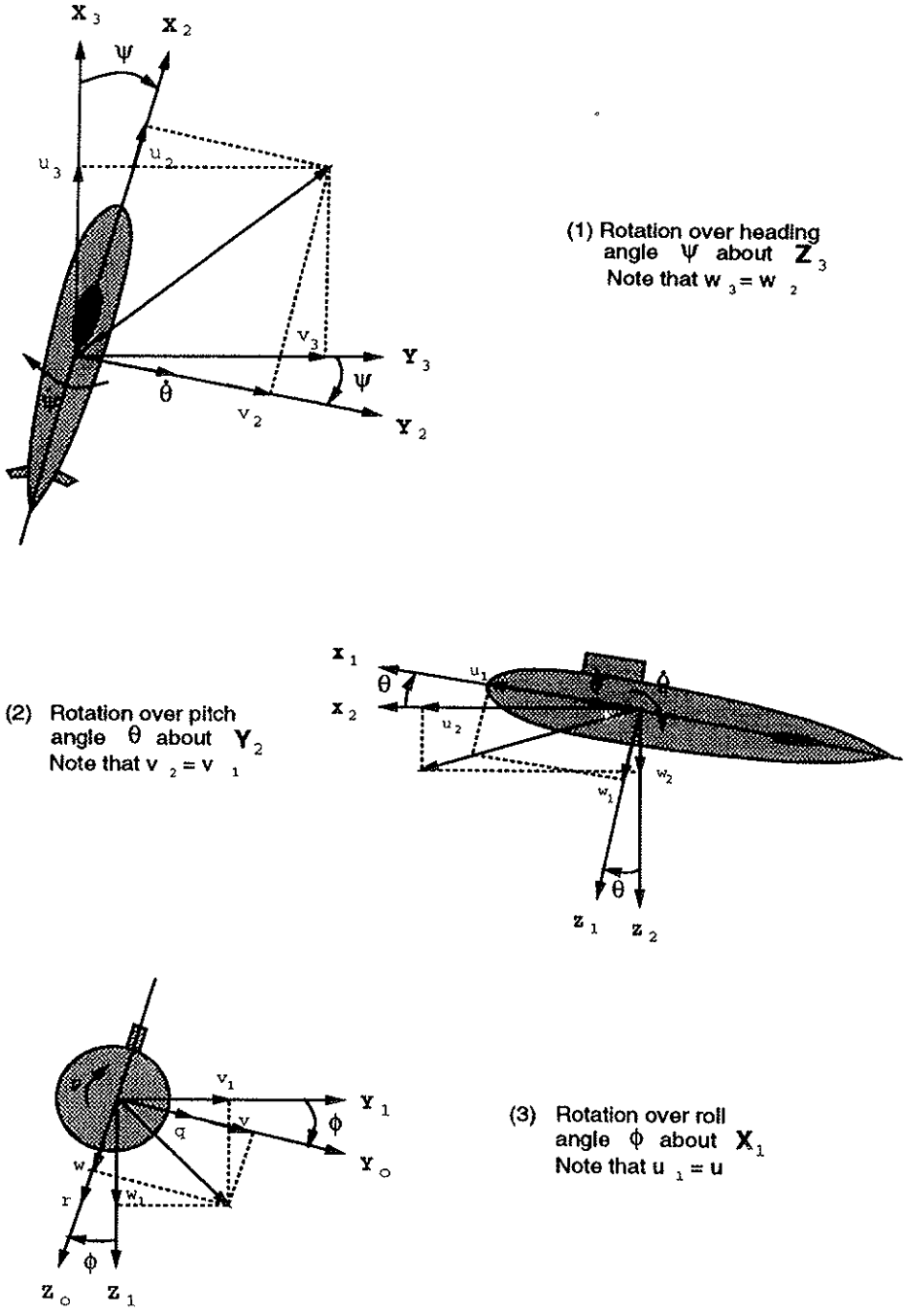

Figure 2.1: The rotation sequence according to the xyz-convention showing both the linear (u, v, w) and angular (p, q, r) velocities.

It is conventional to describe $\boldsymbol{J}_1$ by three rotations. Note, that the order in which these rotations are carried out is not arbitrary. In control and guidance applications it is common to use the xyz-convention specified in terms of Euler angles for the rotations. Let $X_3Y_3Z_3$ be the coordinate system obtained by translating the earth-fixed coordinate system XYZ parallel to itself until its origin coincides with the origin of the body-fixed coordinate system. Then, the coordinate system $X_3Y_3Z_3$ is rotated a *yaw* angle ψ about the Z_3 axis. This yields the coordinate system $X_2Y_2Z_2$. The coordinate system $X_2Y_2Z_2$ is rotated a *pitch* angle θ about the Y_2 axis. This yields the coordinate system $X_1Y_1Z_1$. Finally, the coordinate system $X_1Y_1Z_1$ is rotated a *bank* or *roll* angle ϕ about the X_1 axis. This yields the body-fixed coordinate system $X_oY_oZ_o$, see Fig. 2.1. The rotation sequence is written as:

$$\boldsymbol{J}_1^{-1}(\phi,\theta,\psi) = \boldsymbol{C}_{x,\phi}\boldsymbol{C}_{y,\theta}\boldsymbol{C}_{z,\psi}$$

Here $\boldsymbol{C}_{i,j}$ is a rotation matrix describing a rotation angle j about the i-axis. The basic rotation matrices are defined as:

$$\boldsymbol{C}_{x,\phi} = \begin{bmatrix} 1 & 0 & 0 \\ 0 & c\phi & s\phi \\ 0 & -s\phi & c\phi \end{bmatrix} \quad \boldsymbol{C}_{y,\theta} = \begin{bmatrix} c\theta & 0 & -s\theta \\ 0 & 1 & 0 \\ s\theta & 0 & c\theta \end{bmatrix} \quad \boldsymbol{C}_{z,\psi} = \begin{bmatrix} c\psi & s\psi & 0 \\ -s\psi & c\psi & 0 \\ 0 & 0 & 1 \end{bmatrix}$$

where $s\cdot = \sin(\cdot), c\cdot = \cos(\cdot)$ and $t\cdot = \tan(\cdot)$. Since the coordinate transformation matrices $\boldsymbol{C}_{i,j}$ are orthogonal matrices, $\boldsymbol{J}_1$ is simply found as:

$$\boldsymbol{J}_1(\phi,\theta,\psi) = (\boldsymbol{C}_{x,\phi}\boldsymbol{C}_{y,\theta}\boldsymbol{C}_{z,\psi})^T = \boldsymbol{C}_{z,\psi}^T\boldsymbol{C}_{y,\theta}^T\boldsymbol{C}_{x,\phi}^T$$

which yields

$$\boldsymbol{J}_1(\phi,\theta,\psi) = \begin{bmatrix} c\psi c\theta & -s\psi c\phi + c\psi s\theta s\phi & s\psi s\phi + c\psi c\phi s\theta \\ s\psi c\theta & c\psi c\phi + s\phi s\theta s\psi & -c\psi s\phi + s\theta s\psi c\phi \\ -s\theta & c\theta s\phi & c\theta c\phi \end{bmatrix}$$

The body-fixed angular velocity vector $\boldsymbol{\omega}_o = (p,q,r)^T$ and the Euler rate vector $\boldsymbol{\omega}_e = (\dot{\psi},\dot{\theta},\dot{\phi})^T$ are related through a transformation matrix $\boldsymbol{J}_2$ as:

$$\boldsymbol{\omega}_e = \boldsymbol{J}_2(\phi,\theta,\psi)\,\boldsymbol{\omega}_o$$

This relationship should not be interpreted as a coordinate transformation because the Euler angles can not be treated as coordinates. They simply express how the body-fixed coordinate system is orientated with respect to the inertial reference frame. Hence, the transformation matrix $\boldsymbol{J}_2$ does not satisfy the orthogonal coordinate transformation property i.e. $\boldsymbol{J}_2^{-1} \neq \boldsymbol{J}_2^T$. The transformation can be expressed as:

$$\boldsymbol{\omega}_o = \begin{bmatrix} \dot{\phi} \\ 0 \\ 0 \end{bmatrix} + \boldsymbol{C}_{x,\phi}\begin{bmatrix} 0 \\ \dot{\theta} \\ 0 \end{bmatrix} + \boldsymbol{C}_{x,\phi}\boldsymbol{C}_{y,\theta}\begin{bmatrix} 0 \\ 0 \\ \dot{\psi} \end{bmatrix} = \boldsymbol{J}_2^{-1}(\phi,\theta,\psi)\,\boldsymbol{\omega}_e \tag{2.1}$$

This relationship is verified by inspection of Fig. 2.1. Equating Eq. 2.1 yields

$$\boldsymbol{J}_2^{-1}(\phi,\theta,\psi) = \begin{bmatrix} 1 & 0 & -s\theta \\ 0 & c\phi & c\theta s\phi \\ 0 & -s\phi & c\theta c\phi \end{bmatrix}$$

$\boldsymbol{J}_2$ is then

$$\boldsymbol{J}_2(\phi,\theta,\psi) = \begin{bmatrix} 1 & s\phi t\theta & c\phi t\theta \\ 0 & c\phi & -s\phi \\ 0 & s\phi/c\theta & c\phi/c\theta \end{bmatrix}$$

Notice that $\boldsymbol{J}_2$ is singular for a pitch angle of $\theta = \pm\, 90°$. For ships this is not a problem while both underwater vehicles and aircraft may operate close to this singularity. In such cases, the kinematic equations can be described by two Euler angle representations with different singularities. Another possibility is to use a quaternion representation. This is the topic of the next section.

Summarizing the results from this section implies that the kinematic equations can be expressed in a compact form as:

$$\begin{bmatrix} \boldsymbol{v}_e \\ \boldsymbol{\omega}_e \end{bmatrix} = \boldsymbol{J}(\phi,\theta,\psi) \begin{bmatrix} \boldsymbol{v}_o \\ \boldsymbol{\omega}_o \end{bmatrix} \quad \text{where} \quad \boldsymbol{J} = \begin{bmatrix} \boldsymbol{J}_1(\phi,\theta,\psi) & 0 \\ 0 & \boldsymbol{J}_2(\phi,\theta,\psi) \end{bmatrix} \tag{2.2}$$

or according to the SNAME (1950) notation:

$$\begin{bmatrix} \dot{\boldsymbol{x}}_1 \\ \dot{\boldsymbol{x}}_2 \end{bmatrix} = \begin{bmatrix} \boldsymbol{J}_1(\boldsymbol{x}_2) & 0 \\ 0 & \boldsymbol{J}_2(\boldsymbol{x}_2) \end{bmatrix} \begin{bmatrix} \dot{\boldsymbol{q}}_1 \\ \dot{\boldsymbol{q}}_2 \end{bmatrix} \quad \Longleftrightarrow \quad \dot{\boldsymbol{x}} = \boldsymbol{J}(\boldsymbol{x})\dot{\boldsymbol{q}}$$

Here $\boldsymbol{x}_1 = (x,y,z)^T$ is the position vector and $\boldsymbol{x}_2 = (\phi,\theta,\psi)^T$ is a vector of Euler angles, both referred to the inertial reference frame. The vehicle-fixed linear and angular velocity vectors are denoted as $\dot{\boldsymbol{q}}_1 = (u,v,w)^T$ and $\dot{\boldsymbol{q}}_2 = (p,q,r)^T$, respectively.

2.1.2 Quaternions

An alternative to the Euler angle representation is a four-parameter method based on quaternions or Cayley-Klein parameters, Kane *et al.* (1983). The singularity of the matrix $\boldsymbol{J}_2(\boldsymbol{x}_2)$ for $\boldsymbol{\theta} = \pm\, 90°$ can be avoided by using four parameters to describe the three basic rotations. Euler's theorem of rotation states that:

> *Every change in the relative orientation of two rigid bodies or reference frames $\boldsymbol{R}_A$ and $\boldsymbol{R}_B$ can be produced by means of a simple rotation of $\boldsymbol{R}_B$ in $\boldsymbol{R}_A$.*

Let $\boldsymbol{\lambda} = (\lambda_1, \lambda_2, \lambda_3)^T$ be the unit vector which $\boldsymbol{R_B}$ is rotated about and θ the angle frame $\boldsymbol{R_B}$ is rotated. The Euler parameter vector $\boldsymbol{e}$ is defined as:

$$\boldsymbol{e} = \begin{bmatrix} e_1 \\ e_2 \\ e_3 \\ e_4 \end{bmatrix} = \begin{bmatrix} \boldsymbol{\lambda} \sin\frac{\theta}{2} \\ \cos\frac{\theta}{2} \end{bmatrix}$$

Hence, the transformation between the inertial reference frame and the vehicle-fixed reference frame can be expressed as:

$$\begin{bmatrix} \dot{\boldsymbol{x}}_1 \\ \dot{\boldsymbol{e}} \end{bmatrix} = \begin{bmatrix} \boldsymbol{J}_1(\boldsymbol{e}) & 0 \\ 0 & \boldsymbol{J}_2(\boldsymbol{e}) \end{bmatrix} \begin{bmatrix} \dot{\boldsymbol{q}}_1 \\ \dot{\boldsymbol{q}}_2 \end{bmatrix}$$

where the Euler parameter vector must be integrated subject to the constraint $e_1^2 + e_2^2 + e_3^2 + e_4^2 = 1$. The transformation matrices are, Sagatun (1991),

$$\boldsymbol{J}_1(\boldsymbol{e}) = \begin{bmatrix} e_1^2 - e_2^2 - e_3^2 + e_4^2 & 2(e_1e_2 - e_3e_4) & 2(e_1e_3 + e_2e_4) \\ 2(e_1e_2 + e_3e_4) & -e_1^2 + e_2^2 - e_3^2 + e_4^2 & 2(e_2e_3 - e_1e_4) \\ 2(e_1e_3 - e_2e_4) & 2(e_2e_3 + e_1e_4) & -e_1^2 - e_2^2 + e_3^2 + e_4^2 \end{bmatrix} \quad , \quad \boldsymbol{J}_1^{-1}(\boldsymbol{e}) = \boldsymbol{J}_1^T(\boldsymbol{e})$$

and

$$\boldsymbol{J}_2(\boldsymbol{e}) = \frac{1}{2}\begin{bmatrix} e_4 & -e_3 & e_2 \\ e_3 & e_4 & -e_1 \\ -e_2 & e_1 & e_4 \\ -e_1 & -e_2 & -e_3 \end{bmatrix} \quad , \quad \boldsymbol{J}_2(\boldsymbol{e})^T\boldsymbol{J}_2(\boldsymbol{e}) = \frac{1}{4}\boldsymbol{I}_{3\times 3}$$

The relationship between the Euler angles $\boldsymbol{x}_2 = (\phi, \theta, \psi)^T$ (xyz-convention) and the Euler parameters is simply, Egeland (1985),

$$\begin{aligned} \psi &= atan\left(\frac{J_1(\boldsymbol{e})_{21}}{J_1(\boldsymbol{e})_{11}}\right) \\ \theta &= atan2\left(\frac{-J_1(\boldsymbol{e})_{31}}{\cos\psi\, J_1(\boldsymbol{e})_{11} + \sin\psi\, J_1(\boldsymbol{e})_{21}}\right) \\ \phi &= atan2\left(\frac{\sin\psi\, J_1(\boldsymbol{e})_{13} - \cos\psi\, J_1(\boldsymbol{e})_{23}}{\sin\psi\, J_1(\boldsymbol{e})_{12} + \cos\psi\, J_1(\boldsymbol{e})_{22}}\right) \end{aligned}$$

When transforming the gravitational forces to the vehicle-fixed reference frame, the gravitational components may be expressed as functions of the Euler angles or the Euler parameters. This will be discussed more detailed in Section 2.4.3.

2.2 Newton's Second Law

For underwater vehicles it is desirable to derive the equations of motion for an arbitrary origin in a local body-fixed coordinate system to take advantages of the vehicle's geometrical properties. The dynamic behaviour of an underwater vehicle is described through Newton's laws of linear and angular momentum. By formulating Newton's laws in a body-fixed coordinate system, hydrodynamic and kinematics forces and moments remain constant due to changes of the vehicle's orientation relative to the global earth-fixed reference frame. When deriving the equations of motion it will be assumed: (1) the vehicle is rigid and (2) the earth is fixed in space. The first assumption eliminates the consideration of forces acting between individual elements of mass while the second eliminates forces due to the earth's motion relative a star-fixed reference system. In space based control and guidance applications it is usual to use a star-fixed reference frame while marine vehicles like ships and underwater vehicles, usually are related to an earth-fixed reference frame.

Consider Newton's 2nd laws in terms of conservation of both linear and angular momentum:

$$\int_V \frac{d}{dt}(\frac{d\boldsymbol{r}}{dt})\rho_A dV = \int_V \rho_A \boldsymbol{g} dV + \int_S \boldsymbol{f} dS \tag{2.3}$$

$$\int_V \frac{d}{dt}(\boldsymbol{r} \times \frac{d\boldsymbol{r}}{dt})\rho_A dV = \int_V \boldsymbol{r} \times \rho_A \boldsymbol{g} dV + \int_S \boldsymbol{r} \times \boldsymbol{f} dS \tag{2.4}$$

where $\boldsymbol{r} = \boldsymbol{r}_o + \boldsymbol{r}_G$ is defined in Fig. 2.2 and ρ_A is the mass density of the vehicle. The applied forces are divided into surface forces and volume forces denoted with the volume integration $\int_V dV$ and the surface integration $\int_S dS$, respectively. Time derivatives measured in XYZ and $X_oY_oZ_o$ are related through:

$$\dot{\mathbf{c}} = \acute{\mathbf{c}} + \boldsymbol{\omega}_o \times \mathbf{c} \tag{2.5}$$

Here $\dot{\mathbf{c}} = \frac{d\mathbf{c}}{dt}$ is the time derivative in XYZ, $\acute{\mathbf{c}}$ is the time derivative in $X_oY_oZ_o$ and $\boldsymbol{\omega}_o$ is the angular velocity vector. Notice that

$$\dot{\boldsymbol{\omega}}_o = \acute{\boldsymbol{\omega}}_o + \boldsymbol{\omega}_o \times \boldsymbol{\omega}_o = \acute{\boldsymbol{\omega}}_o$$

which states that the angular acceleration vector $\dot{\boldsymbol{\omega}}_o$ is independent of the reference system. Evaluating the left-hand-side of Eq. 2.3 yields:

$$\int_V \frac{d}{dt}(\frac{d\boldsymbol{r}}{dt})\rho_A dV = \int_V \frac{d}{dt}(\frac{d\boldsymbol{r}_o}{dt} + \frac{d\boldsymbol{r}_G}{dt})\rho_A dV = \int_V (\dot{\boldsymbol{v}}_o + \ddot{\boldsymbol{r}}_G)\rho_A dV \tag{2.6}$$

Here we have used the fact that: $\boldsymbol{v}_o = \frac{d\boldsymbol{r}_o}{dt}$ and $\ddot{\boldsymbol{r}}_G = \frac{d^2\boldsymbol{r}_G}{dt^2}$. The assumption of a rigid vehicle and that the origin in $X_oY_oZ_o$ is fixed implies that: $\acute{\boldsymbol{r}}_G = 0$. Applying Eq. 2.5, yields the following useful relations:

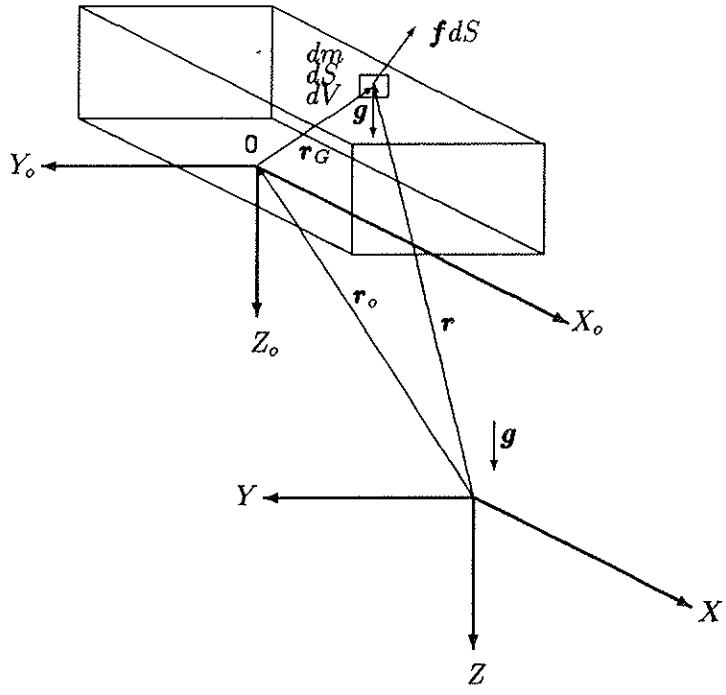

Figure 2.2: The inertial, earth-fixed non-rotating coordinate system XYZ and the body-fixed rotating coordinate system $X_oY_oZ_o$.

$$\begin{aligned}
\dot{\boldsymbol{r}}_G &= \dot{\boldsymbol{r}}_G + \boldsymbol{\omega}_o \times \boldsymbol{r}_G = \boldsymbol{\omega}_o \times \boldsymbol{r}_G \\
\ddot{\boldsymbol{r}}_G &= \dot{\boldsymbol{\omega}}_o \times \boldsymbol{r}_G + \boldsymbol{\omega}_o \times \dot{\boldsymbol{r}}_G = \dot{\boldsymbol{\omega}}_o \times \boldsymbol{r}_G + \boldsymbol{\omega}_o \times (\boldsymbol{\omega}_o \times \boldsymbol{r}_G) \\
\ddot{\boldsymbol{r}}_o &= \dot{\boldsymbol{v}}_o = \dot{\boldsymbol{v}}_o + \boldsymbol{\omega}_o \times \boldsymbol{v}_o
\end{aligned} \tag{2.7}$$

Substituting Eq. 2.7 into Eq. 2.6 yields:

$$\int_V (\dot{\boldsymbol{v}}_o + \boldsymbol{\omega}_o \times \boldsymbol{v}_o + \dot{\boldsymbol{\omega}}_o \times \boldsymbol{r}_G + \boldsymbol{\omega}_o \times (\boldsymbol{\omega}_o \times \boldsymbol{r}_G))\, \rho_A dV = \int_V \rho_A \boldsymbol{g} dV + \int_S \boldsymbol{f} dS \tag{2.8}$$

If we assume that the vehicle has constant mass i.e. $m = \int_V \rho_A dV$, Eq. 2.8 simplifies to:

$$\boxed{m\,(\dot{\boldsymbol{v}}_o + \boldsymbol{\omega}_o \times \boldsymbol{v}_o + \dot{\boldsymbol{\omega}}_o \times \boldsymbol{r}_G + \boldsymbol{\omega}_o \times (\boldsymbol{\omega}_o \times \boldsymbol{r}_G)) = \mathrm{f}_o} \tag{2.9}$$

Here we have collected all the external forces in the term $\boldsymbol{f}_o$. The equation for the angular momentum can be rewritten in a similar manner. Consider Eq. 2.4,

$$\int_V \left(\frac{d\boldsymbol{r}}{dt} \times \frac{d\boldsymbol{r}}{dt}\right) \rho_A dV + \int_V \boldsymbol{r} \times \frac{d}{dt}\left(\frac{d\boldsymbol{r}}{dt}\right) \rho_A dV = \int_V \boldsymbol{r} \times \rho_A \boldsymbol{g} dV + \int_S \boldsymbol{r} \times \boldsymbol{f} dS$$

Since $\frac{d\boldsymbol{r}}{dt} \times \frac{d\boldsymbol{r}}{dt} = 0$ and $\boldsymbol{r} = \boldsymbol{r}_o + \boldsymbol{r}_G$, we obtain:

$$\int_V (\boldsymbol{r}_o + \boldsymbol{r}_G) \times \ddot{\boldsymbol{r}} \rho_A dV = \int_V (\boldsymbol{r}_o + \boldsymbol{r}_G) \times \rho_A \boldsymbol{g} dV + \int_S (\boldsymbol{r}_o + \boldsymbol{r}_G) \times \boldsymbol{f} dS$$

From this expression we can eliminate the terms recognized as the linear momentum, Eq. 2.3, i.e.

$$\boldsymbol{r}_o \times \underbrace{\left(\int_V \ddot{\boldsymbol{r}}\, \rho_A dV - \int_V \rho_A \boldsymbol{g} dV - \int_S \boldsymbol{f} dS\right)}_{0} = 0$$

which yields:

$$\int_V \boldsymbol{r}_G \times (\ddot{\boldsymbol{r}}_o + \ddot{\boldsymbol{r}}_G) \rho_A dV = \int_V \boldsymbol{r}_G \times \rho_A \boldsymbol{g} dV + \int_S \boldsymbol{r}_G \times \boldsymbol{f} dS \tag{2.10}$$

Substituting the result of Eq. 2.7 into Eq. 2.10 we finally obtain:

$$\int_V \boldsymbol{r}_G \times (\dot{\boldsymbol{v}}_o + \boldsymbol{\omega}_o \times \boldsymbol{v}_o + \dot{\boldsymbol{\omega}}_o \times \boldsymbol{r}_G + \boldsymbol{\omega}_o \times (\boldsymbol{\omega}_o \times \boldsymbol{r}_G)) \rho_A dV = \int_V \boldsymbol{r}_G \times \rho_A \boldsymbol{g} dV + \int_S \boldsymbol{r}_G \times \boldsymbol{f} dS \tag{2.11}$$

Observe that it is possible to rewrite the last term on the left-hand-side of Eq. 2.11 by using the vector triple product expansion $a \times (b \times c) = b\,(a \cdot c) - c\,(a \cdot b)$ with $a = b = \boldsymbol{\omega}_o$ and $c = \boldsymbol{r}_G$, which yields:

$$\begin{aligned}\int_V \boldsymbol{r}_G \times (\boldsymbol{\omega}_o \times (\boldsymbol{\omega}_o \times \boldsymbol{r}_G))\, \rho_A dV &= \int_V \boldsymbol{r}_G \times (\boldsymbol{\omega}_o\, (\boldsymbol{\omega}_o \cdot \boldsymbol{r}_G) - \boldsymbol{r}_G\, (\boldsymbol{\omega}_o \cdot \boldsymbol{\omega}_o))\ \rho_A dV \\ &= \int_V \boldsymbol{r}_G \times \boldsymbol{\omega}_o\, (\boldsymbol{\omega}_o \cdot \boldsymbol{r}_G)\, \rho_A dV - \int_V \underbrace{\boldsymbol{r}_G \times \boldsymbol{r}_G}_{0} (\boldsymbol{\omega}_o \cdot \boldsymbol{\omega}_o)\, \rho_A dV\end{aligned}$$

By using the definition of the inertia tensor $\boldsymbol{I}_o$ (calculated with respect to the local origin), it is possible to rewrite:

$$\begin{aligned}\int_V \boldsymbol{r}_G \times (\dot{\boldsymbol{\omega}}_o \times \boldsymbol{r}_G)\, \rho_A dV &= \boldsymbol{I}_o \dot{\boldsymbol{\omega}}_o \\ \int_V \boldsymbol{r}_G \times \boldsymbol{\omega}_o\, (\boldsymbol{\omega}_o \cdot \boldsymbol{r}_G)\, \rho_A dV &= \boldsymbol{\omega}_o \times (\boldsymbol{I}_o \boldsymbol{\omega}_o)\end{aligned}$$

where

$$\boldsymbol{I}_o = \begin{bmatrix} I_x & -I_{xy} & -I_{xz} \\ -I_{xy} & I_y & -I_{yz} \\ -I_{xz} & -I_{yz} & I_z \end{bmatrix}$$

Here I_x, I_y and $I_z$are the moments of inertia about the x,y and z-axes and I_{xy}, I_{xz} and I_{yz} are the products of inertia defined as:

$$\begin{aligned} I_x &= \int_V (y^2 + z^2)\, \rho_A dV \quad , \quad I_{xy} = \int_V xy\, \rho_A dV \\ I_y &= \int_V (x^2 + z^2)\, \rho_A dV \quad , \quad I_{xz} = \int_V xz\, \rho_A dV \\ I_z &= \int_V (x^2 + y^2)\, \rho_A dV \quad , \quad I_{yz} = \int_V yz\, \rho_A dV \end{aligned}$$

Applying these definitions implies that Eq. 2.11 finally can be written as:

$$\boxed{m\boldsymbol{r}_G \times \dot{\boldsymbol{v}}_o + m\boldsymbol{r}_G \times (\boldsymbol{\omega}_o \times \boldsymbol{v}_o) + \boldsymbol{I}_o\dot{\boldsymbol{\omega}}_o + \boldsymbol{\omega}_o \times (\boldsymbol{I}_o\boldsymbol{\omega}_o) = \mathbf{m}_o} \tag{2.12}$$

Here we have collected the external moments on the right-hand-side of Eq. 2.11 into the vector term $\boldsymbol{m}_o$ and assumed the mass and inertia tensor to be constant. Eqs. 2.9 and 2.12 are usually written in the notation of SNAME (1950) i.e.,

$$\begin{aligned} \mathbf{f_o} &= (X_o, Y_o, Z_o)^T && \text{, the external forces} \\ \mathbf{m_o} &= (K_o, M_o, N_o)^T && \text{, the moment of external forces} \\ \boldsymbol{v}_o &= (u, v, w)^T && \text{, the velocity of the origin} \\ \boldsymbol{\omega}_o &= (p, q, r)^T && \text{, the angular velocity about the origin} \\ \boldsymbol{r}_G &= (x_G, y_G, z_G)^T && \text{, the body-fixed centre of gravity (CG)} \end{aligned}$$

Applying this notation to Eqs. 2.9 and 2.12 yields:

$$\begin{aligned} m\left[\dot{u} - vr + wq - x_G(q^2 + r^2) + y_G(pq - \dot{r}) + z_G(pr + \dot{q})\right] &= X_o \\ m\left[\dot{v} - wp + ur - y_G(r^2 + p^2) + z_G(qr - \dot{p}) + x_G(qp + \dot{r})\right] &= Y_o \\ m\left[\dot{w} - uq + vp - z_G(p^2 + q^2) + x_G(rp - \dot{q}) + y_G(rq + \dot{p})\right] &= Z_o \\ I_x\dot{p} + (I_z - I_y)qr - (\dot{r} + pq)I_{xz} + (r^2 - q^2)I_{yz} + (pr - \dot{q})I_{xy} & \\ \quad + m\left[y_G(\dot{w} - uq + vp) - z_G(\dot{v} - wp + ur)\right] &= K_o \\ I_y\dot{q} + (I_x - I_z)rp - (\dot{p} + qr)I_{xy} + (p^2 - r^2)I_{zx} + (qp - \dot{r})I_{yz} & \\ \quad + m\left[z_G(\dot{u} - vr + wq) - x_G(\dot{w} - uq + vp)\right] &= M_o \\ I_z\dot{r} + (I_y - I_x)pq - (\dot{q} + rp)I_{yz} + (q^2 - p^2)I_{xy} + (rq - \dot{p})I_{zx} & \\ \quad + m\left[x_G(\dot{v} - wp + ur) - y_G(\dot{u} - vr + wq)\right] &= N_o \end{aligned} \tag{2.13}$$

This is probably the most used representation of Newton's laws in control and guidance applications i.e. Newton's laws formulated in a body-fixed coordinate system with an arbitrary origin and constant mass and inertia tensor. The three first equations represent the translational motion while the three last equations represent the rotational motion, totally 6 degrees of freedom (DOF). It is desirable to select the axes of the local coordinate system to

be the principal axes of inertia of the vehicle. This simplifies the equations above, because the terms including the products of inertia become zero. This is automatically satisfied if the xy- , xz- and yz-planes are planes of symmetry. If the local origin is chosen to coincide with the CG i.e. $\boldsymbol{r}_G = (0,0,0)^T$, the complexity of the above equations will be further reduced. Applying these assumptions to Eq. 2.13 yields:

$$\begin{aligned} m(\dot{u} - vr + wq) &= X_o \\ m(\dot{v} - wp + ur) &= Y_o \\ m(\dot{w} - uq + vp) &= Z_o \\ I_x\dot{p} + (I_z - I_y)qr &= K_o \\ I_y\dot{q} + (I_x - I_z)rp &= M_o \\ I_z\dot{r} + (I_y - I_x)pq &= N_o \end{aligned}$$

It is usual to describe ships only in sway and yaw. Assuming the forward speed $u = u_o$ to be constant and that $\boldsymbol{r}_g = (x_G, 0, z_G)^T$, suggests:

$$\begin{aligned} m(\dot{v} + u_o r + x_G\dot{r}) &= Y_o \\ I_z\dot{r} + mx_G(\dot{v} + u_o r) &= N_o \end{aligned}$$

The 6 DOF nonlinear equations, Eq. 2.13, can be written in a more compact form as:

$$\boldsymbol{M}_{RB}\,\ddot{\boldsymbol{q}} + \boldsymbol{C}_{RB}(\dot{\boldsymbol{q}})\dot{\boldsymbol{q}} = \boldsymbol{\tau}_o \tag{2.14}$$

Here $\dot{\boldsymbol{q}} = (u, v, w, p, q, r)^T$ is the body-fixed linear and angular velocity vector and $\boldsymbol{\tau}_o = (X_o, Y_o, Z_o, K_o, M_o, N_o)^T$ is a generalized vector of external forces and moments. The rigid-body inertia matrix $\boldsymbol{M}_{RB}$ is recognized as:

$$\boldsymbol{M}_{RB} = \begin{bmatrix} m & 0 & 0 & 0 & mz_G & -my_G \\ 0 & m & 0 & -mz_G & 0 & mx_G \\ 0 & 0 & m & my_G & -mx_G & 0 \\ 0 & -mz_G & my_G & I_x & -I_{xy} & -I_{xz} \\ mz_G & 0 & -mx_G & -I_{xy} & I_y & -I_{yz} \\ -my_G & mx_G & 0 & -I_{xz} & -I_{yz} & I_z \end{bmatrix}$$

Notice that the rigid-body inertia matrix $\boldsymbol{M}_{RB}$ is symmetrical i.e. $\boldsymbol{M}_{RB} = \boldsymbol{M}_{RB}^T$. The Coriolis terms $\boldsymbol{\omega}_o \times \boldsymbol{v}_o$ and centrifugal terms $\boldsymbol{\omega}_o \times \boldsymbol{\omega}_o$ are collected in the matrix:

$$\boldsymbol{C}_{RB}(\dot{\boldsymbol{q}}) = \begin{bmatrix} 0 & -mr & mq & m(y_Gq + z_Gr) & -mx_Gq & -mx_Gr \\ mr & 0 & -mp & -my_Gp & m(z_Gr + x_Gp) & -my_Gr \\ -mq & mp & 0 & -mz_Gp & -mx_Gq & m(x_Gp + y_Gq) \\ -m(y_Gq + z_Gr) & my_Gp & mz_Gp & 0 & -I_{yz}q - I_{xz}p + I_zr & I_{yz}r + I_{xy}p - I_yq \\ mx_Gq & -m(z_Gr + z_Gp) & mz_Gq & I_{yz}q + I_{xz}p - I_zr & 0 & -I_{xz}r - I_{xy}q + I_xp \\ mx_Gr & my_Gr & -m(x_Gp + y_Gq) & -I_{yz}r - I_{xy}p + I_yq & I_{xz}r + I_{xy}q - I_xp & 0 \end{bmatrix}$$

This particular choice implies that the matrix $\boldsymbol{C}_{RB}$ is skew-symmetrical i.e. $\boldsymbol{C}_{RB} = -\boldsymbol{C}_{RB}^T$. The skew-symmetric property will be exploited in the adaptive control design in Section

5.4.1. The generalized vector τ_o consists of a large number of external forces and moments acting on the vehicle. It is convenient to write τ_o as a sum of vectors components, namely:

$$\tau_o = \tau_H + \tau_V + \tau_U + \tau_P$$

where the subscripts correspond to the following forces:

- Hydrodynamic forces due to radiation and excitation τ_H :
  1. Radiation induced forces due to the forced body oscillations:
     - added mass
     - potential damping
     - restoring forces
  2. Excitation forces due to a restrained body:
     - Froude-Kriloff forces
     - diffraction forces
- Viscous damping τ_V :
  - linear damping
  - quadratic damping
- Umbilical forces τ_U :
- Propulsion forces τ_P :
  - thruster forces
  - thruster momentum drag
  - control surfaces
  - variable ballast-displacement system

The contribution from each of these terms will be discussed more detailed in the next sections. If no excitation forces are present it will be shown that the n DOF equations of motion for an underwater vehicle can be expressed in a compact form as:

$$\boldsymbol{M}\ddot{\boldsymbol{q}} + \boldsymbol{C}(\dot{\boldsymbol{q}})\dot{\boldsymbol{q}} + \boldsymbol{D}(\dot{\boldsymbol{q}})\dot{\boldsymbol{q}} + \boldsymbol{g}(\boldsymbol{x}) = \boldsymbol{B}(\dot{\boldsymbol{q}})\,\boldsymbol{u}$$

$$\dot{\boldsymbol{x}} = \boldsymbol{J}(\boldsymbol{x})\dot{\boldsymbol{q}}$$

where $\boldsymbol{x} \in \Re^n$, $\boldsymbol{q} \in \Re^n$ and $\boldsymbol{u} \in \Re^p$. $\boldsymbol{M}$ is an $n \times n$ inertia matrix including hydrodynamic added mass, $\boldsymbol{C}$ is an $n \times n$ nonlinear matrix including Coriolis, centrifugal and added mass terms, $\boldsymbol{D}$ is an $n \times n$ matrix of dissipative terms, such as potential damping, viscous damping

and skin friction, $\boldsymbol{B}$ is an $n \times p$ input matrix including the thruster characteristics and $\boldsymbol{g}$ is an $n \times 1$ vector of restoring forces and moments. These terms will be interpreted in the next sections. The transformation matrix $\boldsymbol{J}$ has already been described in Section 2.1. For a 6 DOF model the state vectors are defined as: $\boldsymbol{x} = (x, y, z, \phi, \theta, \psi)^T$ and $\dot{\boldsymbol{q}} = (u, v, w, p, q, r)^T$, where $\boldsymbol{q}$ is a virtual vector, c.f. Table 2.1. If excitation forces are considered the nonlinear equations of motion can be written in terms of the relative fluid motion. This will be described more closely at the end of Chapter 2. For readers that are unfamiliar with basic hydrodynamics, the next section addressing regular wave theory is recommended to study.

Table 2.1: Notation used in the 6 DOF underwater vehicle equations of motion.

DOF	body-fixed forces and moments	body-fixed linear and angular velocities	earth-fixed positions and Euler angles
1 surge	X	u	x
2 sway	Y	v	y
3 heave	Z	w	z
4 roll	K	p	ϕ
5 pitch	M	q	θ
6 yaw	N	r	ψ

2.3 Basic Hydrodynamics

The wave induced motions and loads on ships, underwater vehicles and offshore structures can be described by regular waves i.e. incident regular sinusoidal waves of small steepness. Small wave steepness implies that the waves are far from breaking. It is possible to obtain results in irregular sea by linearly superposing the results from regular wave components. This is done by adding a large number of regular waves of different amplitudes, wavelengths and propagation directions.

2.3.1 Regular Wave Theory

Regular wave theory is based on potential theory. The derivation of linear wave theory (Airy theory) for propagating waves is found in many textbooks e.g. Newman (1977) and Faltinsen (1990a). Let ϕ be a velocity potential describing the fluid velocity vector: $\boldsymbol{v}(x, y, z, t) = (u, v, w)^T$ at time t at a point $\boldsymbol{x} = (x, y, z)^T$ in a Cartesian coordinate system which is fixed in space. The relationship between the fluid velocity and the velocity potential is

$$\boldsymbol{v} = \nabla\phi = \left[\frac{\partial\phi}{\partial x}, \frac{\partial\phi}{\partial y}, \frac{\partial\phi}{\partial z}\right]^T \tag{2.15}$$

The derivation of the velocity potential is based on the following assumptions:

(1) The velocity potential should satisfy the Laplace's equation. This is based on the assumption that the water is incompressible i.e. the fluid density $\rho = const$. The continuity equation for an incompressible fluid is:

$$div\ \boldsymbol{v} = \nabla \cdot \boldsymbol{v} = \frac{\partial u}{\partial x} + \frac{\partial v}{\partial y} + \frac{\partial w}{\partial z} = 0 \tag{2.16}$$

Combining Eqs. 2.15 and Eq. 2.16 yields *Laplace's equation:*

$$\nabla^2\phi = \frac{\partial^2\phi}{\partial x^2} + \frac{\partial^2\phi}{\partial y^2} + \frac{\partial^2\phi}{\partial z^2} = 0$$

A potential flow is said to be irrotational if

$$\nabla \times \boldsymbol{v} = \left[\left(\frac{\partial w}{\partial y} - \frac{\partial v}{\partial z}\right), \left(\frac{\partial u}{\partial z} - \frac{\partial w}{\partial x}\right), \left(\frac{\partial v}{\partial x} - \frac{\partial u}{\partial y}\right)\right]^T = 0$$

everywhere in the fluid. The velocity potential of an irrotational, incompressible fluid is then found by solving the *Laplace's equation* with relevant boundary conditions on the fluid.

(2) The sea bottom condition is simply that

$$\left(\frac{\partial\phi}{\partial z}\right)_{z=h} = 0$$

This ensures that the vertical velocity at the seabed $z = h$ (z positive downwards) where h is the mean water depth, should be zero.

(3) The dynamic free-surface condition is simply that the water pressure is equal to the constant atmospheric pressure p_o on the surface. For inviscid fluids the pressure p follows from *Bernoulli's equation:*

$$p - \rho g z + \frac{1}{2}\rho \boldsymbol{v}^T\boldsymbol{v} + \rho\frac{\partial\phi}{\partial t} = C(t)$$

Here $C(t)$ depends on time only. The dynamic pressure p_D is defined as:

$$p_D = -\rho \frac{\partial \phi}{\partial t}$$

Let the free-surface be defined as

$$z = \zeta(x, y, t) \tag{2.17}$$

where ζ is the wave elevation. If we choose C as the constant atmospheric pressure on the surface p_o, then

$$-g\zeta + \frac{\partial \phi}{\partial t} + \frac{1}{2}\left[\left(\frac{\partial \phi}{\partial x}\right)^2 + \left(\frac{\partial \phi}{\partial y}\right)^2 + \left(\frac{\partial \phi}{\partial z}\right)^2\right] = 0 \text{ on } z = \zeta(x, y, t) \tag{2.18}$$

Notice that the free-surface condition, Eq.2.18, is nonlinear. Linear theory is based on a first order Taylor expansion of Eq. 2.18 around the mean free-surface $z = 0$ i.e.

$$\phi(\zeta, t) = \phi(0, t) + \frac{\partial \phi(0, t)}{\partial z}\zeta + O(\zeta^2) \approx \phi(0, t)$$

Indeed, this is a good approximation for small waves. This finally yields:

$$g\zeta = \left(\frac{\partial \phi}{\partial t}\right)_{z=0}$$

This approximation can be improved by introducing higher order terms e.g. a Stoke's expansion, Newman (1977).

(4) The kinematic free-surface condition simply states that a fluid particle is assumed to stay on the free surface. Defining

$$F(x, y, z, t) = z - \zeta(x, y, t)$$

implies that the substantial derivative

$$\frac{DF(x, y, t)}{Dt} = \frac{\partial F}{\partial t} + \boldsymbol{v} \cdot \nabla F = 0$$

or equivalently

$$\frac{\partial \zeta}{\partial t} + \frac{\partial \phi}{\partial x}\frac{\partial \zeta}{\partial x} + \frac{\partial \phi}{\partial y}\frac{\partial \zeta}{\partial y} - \frac{\partial \phi}{\partial z} = 0 \text{ on } z = \zeta(x, y, t)$$

where the expression for v has been used in Eq. 2.15. By a first order Taylor expansion it is possible to transfer the free surface position $\zeta(x, y, t)$ to the mean surface at $z = 0$ which yields the kinematic surface condition:

$$\frac{\partial \zeta}{\partial t} = \left(\frac{\partial \phi}{\partial z}\right)_{z=0}$$

It is straightforward to show, see e.g. Walderhaug (1990), that the wave velocity potential satisfying all these assumptions is

$$\phi_W = \frac{g\zeta_A}{\omega}\frac{\cosh k(h-z)}{\cosh kh}\sin(\omega t - kx)$$

Here ζ_A is the wave amplitude, h is the mean water depth, g is the acceleration of gravity, t is the time variable, x is the direction of wave propagation and z is the vertical coordinate (z is positive downwards). The complete expressions are given in Table 2.2. The wave number k is defined as:

$$k = \frac{2\pi}{\lambda}$$

where λ is the wave length. The connection between the circular frequency ω and the wave period T is

$$\omega = \frac{2\pi}{T}$$

According to potential theory, the total pressure in the fluid is the sum of the dynamic and static pressure i.e.: $p_{TOT} = p_D + \rho g z + p_0$, where p_0 is the constant atmospheric pressure on the surface. Let λ be the wave length and h be the water depth, then it is common to classify the water depth as:

- Infinite water depth: $\frac{h}{\lambda} > \frac{1}{2}$
- Finite water depth: $\frac{1}{20} < \frac{h}{\lambda} < \frac{1}{2}$
- Shallow water: $\frac{h}{\lambda} > \frac{1}{20}$

Table 2.2: Velocity potential, dispersion relation, pressure, velocity and acceleration for regular sinusoidal propagating waves on finite and infinite water depth according to linear (Airy) theory.

	Finite water depth	Infinite water depth
Velocity potential:	$\phi_W = \frac{g\zeta_A}{\omega}\frac{\cosh k(h-z)}{\cosh kh}\sin(\omega t - kx)$	$\phi_W = \frac{g\zeta_A}{\omega}e^{-kz}\sin(\omega t - kx)$
Connection between wave number k and circular frequency ω:	$\omega^2 = kg\tanh kh$	$\omega^2 = kg$
Connection between wavelength λ and wave period T:	$\lambda = \frac{g}{2\pi}T^2\tanh\frac{2\pi}{\lambda}h$	$\lambda = \frac{g}{2\pi}T^2$
Wave profile:	$\zeta = \zeta_A\cos(\omega t - kx)$	$\zeta = \zeta_A\cos(\omega t - kx)$
Dynamic pressure:	$p_D = -\rho g\zeta_A\frac{\cosh k(h-z)}{\cosh kh}\cos(\omega t - kx)$	$p_D = -\rho g\zeta_A e^{-kz}\cos(\omega t - kx)$
x-component of velocity:	$u_f = -\omega\zeta_A\frac{\cosh k(h-z)}{\cosh kh}\cos(\omega t - kx)$	$u_f = -\omega\zeta_A e^{-kz}\cos(\omega t - kx)$
z-component of velocity:	$w_f = -\omega\zeta_A\frac{\sinh k(h-z)}{\cosh kh}\sin(\omega t - kx)$	$w_f = -\omega\zeta_A e^{-kz}\sin(\omega t - kx)$
x-component of acceleration:	$\dot{u}_f = \omega^2\zeta_A\frac{\cosh k(h-z)}{\cosh kh}\sin(\omega t - kx)$	$\dot{u}_f = \omega^2\zeta_A e^{-kz}\sin(\omega t - kx)$
z-component of acceleration:	$\dot{w}_f = -\omega^2\zeta_A\frac{\sinh k(h-z)}{\cosh kh}\cos(\omega t - kx)$	$\dot{w}_f = -\omega^2\zeta_A e^{-kz}\cos(\omega t - kx)$

2.3.2 Wave Induced Forces in Regular Waves

For small motions (assuming no currents) the total velocity potential ϕ_{TOT} is written as a sum of three components, Faltinsen (1990b),

$$\phi_{TOT} = \phi_W + \phi_D + \phi_R$$

where

- ϕ_W is the incident regular wave velocity potential.
- ϕ_D is the diffraction potential caused by reflection when the vehicle is restrained.
- $\phi_R = \sum_{j=1}^{6}\phi_{Rj}$ is the sum of the radiation potentials in 6 DOF caused by forcing the vehicle to oscillate with the wave excitation frequency, when there are no incident waves.

The wave induced force due to the velocity potential ϕ_{TOT} is simply found by integrating the expression for the total pressure over the vehicle's surface S:

$$\boldsymbol{f} = \rho \int\int \frac{\partial \phi_{TOT}}{\partial t} \boldsymbol{n}\, dS$$

where $\boldsymbol{n} = (n_1, n_2, n_3)^T$ is the unit vector normal to the body surface defined to be positive into the fluid. Linear regular wave theory implies that wave induced forces acting on a rigid vehicle can be superpositioned into two sub-problems, Faltinsen (1990a), (1) radiation induced forces and moments and (2) excitation forces and moments.

(1) Radiation induced forces and moments

Radiation induced forces and moments act on the vehicle when the vehicle is forced to oscillate with the wave excitation frequency. There are no incident waves. The hydrodynamic forces are identified as:

- **Added mass** *due to the inertia of the surrounding fluid.*

- **Potential damping** *due to the energy carried away by generated surface waves.*

- **Restoring terms** *due to Archimedes.*

These forces are due to the radiation potential, i.e. the potential ϕ_R created by the forced oscillation of the vehicle when there are no incident waves. It is possible to show that the total forces and moments due to the radiation potential can be written as

$$\boldsymbol{\tau}_R = \rho \int\int \frac{\partial \phi_R}{\partial t} \approx -\boldsymbol{A}(\omega)\ddot{\boldsymbol{\eta}} - \boldsymbol{B}(\omega)\dot{\boldsymbol{\eta}} - \boldsymbol{C}\boldsymbol{\eta} \tag{2.19}$$

where $\boldsymbol{\eta}$ is a 1×6 vector of linear (η_1, η_2, η_3) and angular (η_4, η_5, η_6) displacements. This expression is found from solving a boundary layer problem for the radiation velocity potential, Faltinsen (1990a). Both the added mass matrix $\boldsymbol{A}(\omega)$ and the damping matrix $\boldsymbol{B}(\omega)$ depend on the wave excitation frequency ω, the shape of the body, the distance from the free-surface, the seabed and nearby structures. On the contrary, the $\boldsymbol{C}$ matrix representing the restoring forces and moments, will be independent of the wave excitation frequency. All these terms will be described more closely in the following sections.

(2) Excitation forces and moments

Excitation forces and moments are acting on the vehicle when the vehicle is restrained from oscillating and there are incident regular waves. They are classified as:

- **Froude-Kriloff (FK) forces** *due to* ϕ_W.

- **Diffraction forces** *due to* ϕ_D.

The FK-forces and moments are found by integrating the pressure induced by the undisturbed waves while the diffraction forces and moments are due to the pressure created by the vehicle when the waves are reflected from the vehicle, i.e.

$$\boldsymbol{\tau}_E = \rho \int\int \frac{\partial \phi_W}{\partial t} \boldsymbol{n}\, dS + \rho \int\int \frac{\partial \phi_D}{\partial t} \boldsymbol{n}\, dS \tag{2.20}$$

Here ϕ_W is the wave potential and ϕ_D is the diffraction potential i.e. the velocity potential created from the reflection. The most commonly used wave potential is that of Table 2.2. The diffraction potential can be solved from a boundary value problem similar to that of the radiation problem. If only the wave excitation loads are of interest and not the detailed pressure distribution, the so-called Haskind relation can be applied. Haskind (1954) developed relations, based on Green's identities of potential theory, that allow diffraction forces for the 6 DOF's to be found from the radiation potential for the appropriate DOF. This makes it unnecessary to find ϕ_D. In its original form it is assumed that the structure has zero forward speed and that no currents are present. If the body is totally submerged, has a "small volume" and the whole body surface is wetted, a special solution of Eq. 2.20 exists. By "small volume" we mean that a characteristic cross-sectional dimension of the body is small relative to the wavelength λ. For a vertical cylinder "small volume" means that $\lambda > 5D$, where D is the cylinder diameter. ROVs are usually within this limit. If the subscript f denotes the fluid motion, Eq. 2.20 can then be approximated as:

$$\boldsymbol{\tau}_E \approx \boldsymbol{M}_{FK}\, \ddot{\boldsymbol{\eta}}_f + \boldsymbol{A}(\omega)\ddot{\boldsymbol{\eta}}_f + \boldsymbol{B}(\omega)\dot{\boldsymbol{\eta}}_f \tag{2.21}$$

The first term corresponds to the FK-force while the last terms represent the diffraction forces. The matrix $\boldsymbol{M}_{FK}$ may be interpreted as the FK-inertia matrix i.e. the inertia matrix of the displaced fluid.

Linearizing Newton's laws of linear and angular momentum about zero velocity with only wave induced forces as external forces, yields:

$$\boldsymbol{M}_{RB}\, \ddot{\boldsymbol{\eta}} = \boldsymbol{\tau}_R + \boldsymbol{\tau}_E$$

Note that viscous and control forces are neglected in this expression. Substituting the expressions for $\boldsymbol{\tau}_R$ and $\boldsymbol{\tau}_E$ into the expression for Newton's laws, yields the linear equations of motion:

$$(\boldsymbol{M}_{RB} + \boldsymbol{A}(\omega))\,\ddot{\boldsymbol{\eta}} + \boldsymbol{B}(\omega)\dot{\boldsymbol{\eta}} + \boldsymbol{C}\boldsymbol{\eta} - (\boldsymbol{M}_{FK} + \boldsymbol{A}(\omega))\,\ddot{\boldsymbol{\eta}}_f - \boldsymbol{B}(\omega)\dot{\boldsymbol{\eta}}_f = 0$$

Note that the added mass and damping matrices are functions of the incident wave frequency i.e. $\boldsymbol{A}(\omega)$ and $\boldsymbol{B}(\omega)$. For bodies that are small compared to the wavelength, totally submerged and satisfying $\boldsymbol{M}_{FK} = \boldsymbol{M}_{RB}$ i.e. neutrally buoyant vehicles with homogeneous mass distribution, the linear equations of motion can be combined to give

$$(\boldsymbol{M}_{RB} + \boldsymbol{A}(\omega))\,\ddot{\boldsymbol{\eta}}_r + \boldsymbol{B}(\omega)\dot{\boldsymbol{\eta}}_r + \boldsymbol{C}\boldsymbol{\eta} = 0$$

where $\boldsymbol{\eta}_r = \boldsymbol{\eta} - \boldsymbol{\eta}_f$ is the relative fluid velocity over the submersible. It should be noted that this is based on the assumption that water is an inviscid fluid. This implies that viscous damping terms e.g. skin friction and drag should be added to yield a complete model. This problem will be addressed in Section 2.4.3. Another effect to be considered, is the change in the frequency of encounter. If the vehicle is moving with a velocity U and ω is the incident wave frequency, then the frequency of encounter ω_e can be expressed as:

$$\omega_e = \omega + kU\cos\beta$$

Here β is the heading angle between the vehicle and the wave propagation direction and k is the wavenumber. This simple relationship is based on the Doppler effect. In deep water, the dispersion relation $\omega^2 = kg$ implies that:

$$\omega_e = \omega + \frac{\omega^2 U}{g}\cos\beta$$

2.3.3 Morison's Equation

Since a typical ROV has many cylindrical elements exposed to the surroundings, it is important to estimate the forces on these. According to Morison *et al.* (1950) the horizontal force dF on a strip dz of a vertical cylinder can be written as:

$$dF = \underbrace{\rho\frac{\pi D^2}{4}\,dz\,C_M\,\dot{u}_f}_{\text{Mass force}} + \underbrace{\frac{1}{2}\,\rho\,C_D\,D\,dz\,u_f|u_f|}_{\text{Drag force}}$$

Here D is the cylinder diameter and u_f is the horizontal component of the undisturbed fluid velocity. *Morison's equation* can only be applied for small-volume structures, c.f. Fig. 2.3. Both the drag coefficient C_D and inertia coefficient C_M will be functions of the Reynolds number, the Keulegan-Carpenter number, the relative current number and the roughness ratio Faltinsen (1990a). The Reynolds number and Keulegan-Carpenter number are defined as:

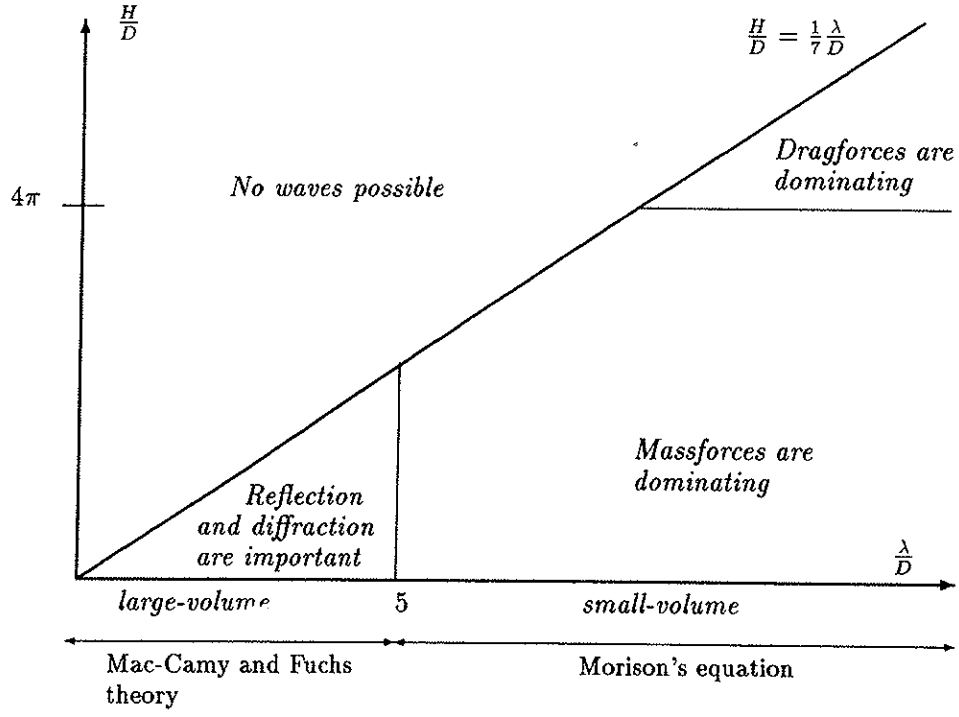

Figure 2.3: Breaking limit: $\frac{H}{D} = \frac{1}{7}\frac{\lambda}{D}$, small-volume and large-volume limit: $\frac{\lambda}{D} = 5$ and dragforce dominated and massforce dominated limit: 4π. H is the wave height, D is the cylinder diameter and λ is the wave length.

$$Re = \frac{UD}{\nu} \qquad KC = \frac{U_M T}{D}$$

where U is the characteristic free-stream velocity, ν is the kinematic viscosity coefficient, U_M is the amplitude of the oscillatory planar flow velocity and T is the wave period. When applying potential theory for a circular cylinder: $C_M = 2$. In this case, half the contribution comes from the FK-force and the other half from the diffraction force. If viscous effects are accounted for, C_M will differ from 2. The last term in *Morison's equation* suggests that the viscous damping force should include a quadratic damping term.

2.4 Radiation Induced Forces

As described in the previous section, the radiation induced forces involves the problem of finding the *added mass, potential damping and restoring* terms. For an underwater vehicle in 6 DOF these terms will generally be nonlinear. The radiation induced forces and moments can be expressed as:

$$\boldsymbol{\tau}_R(\ddot{\boldsymbol{q}}, \dot{\boldsymbol{q}}, \boldsymbol{x}) = \boldsymbol{\tau}_A(\ddot{\boldsymbol{q}}, \dot{\boldsymbol{q}}) + \boldsymbol{\tau}_B(\dot{\boldsymbol{q}}) + \boldsymbol{\tau}_C(\boldsymbol{x})$$

where the subscripts A, B and C denote the nonlinear added mass, damping and restoring terms, respectively.

2.4.1 Added Mass

Like the rigid-body kinematics, it is desirable to separate the added mass terms in terms which belong to an added mass matrix $\boldsymbol{M}_A$ and a matrix of Coriolis and centrifugal terms $\boldsymbol{C}_A(\dot{\boldsymbol{q}})$. For underwater vehicles this implies that the added mass forces and moments can be written as:

$$\boldsymbol{\tau}_A(\ddot{\boldsymbol{q}}, \dot{\boldsymbol{q}}) = -\boldsymbol{M}_A\ddot{\boldsymbol{q}} - \boldsymbol{C}_A(\dot{\boldsymbol{q}})\dot{\boldsymbol{q}}$$

where $\boldsymbol{\tau}_A = (X_A, Y_B, Z_A, K_A, M_A, N_A)^T$ is the total added mass force and moment vector. The added mass terms represent the fluid particles surrounding the submerged body that are accelerated with it. Any motion of the vehicle induces a motion in the otherwise stationary fluid. In order to allow the vehicle to pass through the fluid, the fluid must move aside and then close behind the vehicle. As a consequence, the fluid passage processes kinetic energy that it would lack if the vehicle was not in motion. Lamb (1932) gives the following expression for the fluid kinetic energy E_k expressed as a quadratic form of the body axis velocity vector components:

$$E_k = \frac{1}{2}\dot{\boldsymbol{q}}^T\boldsymbol{M}_A\dot{\boldsymbol{q}} \tag{2.22}$$

Here $\boldsymbol{M}_A$ is a 6×6 added mass matrix. For a rigid body body moving in an ideal fluid the added mass matrix is symmetrical i.e. $\boldsymbol{M}_A = \boldsymbol{M}_A^T$. In a real fluid these 36 elements may all be distinct. Experience has shown that the numerical values of added mass in a real fluid are usually in good agreement with those obtained from ideal theory, Wendel (1956). The added mass matrix is simply written as:

$$\boldsymbol{M}_A = -\begin{bmatrix} X_{\dot{u}} & X_{\dot{v}} & X_{\dot{w}} & X_{\dot{p}} & X_{\dot{q}} & X_{\dot{r}} \\ Y_{\dot{u}} & Y_{\dot{v}} & Y_{\dot{w}} & Y_{\dot{p}} & Y_{\dot{q}} & Y_{\dot{r}} \\ Z_{\dot{u}} & Z_{\dot{v}} & Z_{\dot{w}} & Z_{\dot{p}} & Z_{\dot{q}} & Z_{\dot{r}} \\ K_{\dot{u}} & K_{\dot{v}} & K_{\dot{w}} & K_{\dot{p}} & K_{\dot{q}} & K_{\dot{r}} \\ M_{\dot{u}} & M_{\dot{v}} & M_{\dot{w}} & M_{\dot{p}} & M_{\dot{q}} & M_{\dot{r}} \\ N_{\dot{u}} & N_{\dot{v}} & N_{\dot{w}} & N_{\dot{p}} & N_{\dot{q}} & N_{\dot{r}} \end{bmatrix}, \quad \boldsymbol{M}_A > 0$$

The notation of SNAME (1950) is used in this expression; e.g. the hydrodynamic added mass force Y_A along the Y-axis due to an acceleration $\dot{u}$ in the x-direction is written as:

$$Y_A = Y_{\dot{u}}\dot{u} \quad \text{where} \quad Y_{\dot{u}} = \frac{\partial Y}{\partial \dot{u}}$$

This definition implies that the hydrodynamic derivatives $X_{\dot{u}}, Y_{\dot{v}}, Z_{\dot{w}}, K_{\dot{p}}, M_{\dot{q}}, N_{\dot{r}}$ corresponding to the diagonal of the added mass matrix $\boldsymbol{M}_A$, will all be negative. Equating Eq. 2.22 (assuming $\boldsymbol{M}_A = \boldsymbol{M}_A^T$) yields:

$$\begin{aligned} 2E_k = \; & -X_{\dot{u}}u^2 - Y_{\dot{v}}v^2 - Z_{\dot{w}}w^2 - 2Y_{\dot{w}}vw - 2X_{\dot{w}}wu - 2X_{\dot{v}}uv \\ & -K_{\dot{p}}p^2 - M_{\dot{q}}q^2 - N_{\dot{r}}r^2 - 2M_{\dot{r}}qr - 2K_{\dot{r}}rp - 2K_{\dot{q}}pq \\ & -2p(X_{\dot{p}}u + Y_{\dot{p}}v + Z_{\dot{p}}w) \\ & -2q(X_{\dot{q}}u + Y_{\dot{q}}v + Z_{\dot{q}}w) \\ & -2r(X_{\dot{r}}u + Y_{\dot{r}}v + Z_{\dot{r}}w) \end{aligned} \tag{2.23}$$

The added mass terms are obtained from potential theory. The method is based on assuming inviscid fluid, no circulation and that the body is completed submerged in an unbounded fluid. The last assumption is violated at the seabed, near underwater installations and at the surface. Consider *Kirchhoff's equations* in component form, Milne-Thomson (1968):

$$\begin{aligned} \frac{d}{dt}\frac{\partial E_k}{\partial u} &= r\frac{\partial E_k}{\partial v} - q\frac{\partial E_k}{\partial w} - X_A \\ \frac{d}{dt}\frac{\partial E_k}{\partial v} &= p\frac{\partial E_k}{\partial w} - r\frac{\partial E_k}{\partial u} - Y_A \\ \frac{d}{dt}\frac{\partial E_k}{\partial w} &= q\frac{\partial E_k}{\partial u} - p\frac{\partial E_k}{\partial v} - Z_A \\ \frac{d}{dt}\frac{\partial E_k}{\partial p} &= w\frac{\partial E_k}{\partial v} - v\frac{\partial E_k}{\partial w} + r\frac{\partial E_k}{\partial q} - q\frac{\partial E_k}{\partial r} - K_A \\ \frac{d}{dt}\frac{\partial E_k}{\partial q} &= u\frac{\partial E_k}{\partial w} - w\frac{\partial E_k}{\partial u} + p\frac{\partial E_k}{\partial r} - r\frac{\partial E_k}{\partial p} - M_A \\ \frac{d}{dt}\frac{\partial E_k}{\partial r} &= v\frac{\partial E_k}{\partial u} - u\frac{\partial E_k}{\partial v} + q\frac{\partial E_k}{\partial p} - p\frac{\partial E_k}{\partial q} - N_A \end{aligned} \tag{2.24}$$

Substituting Eq. 2.23 into Eq. 2.24 gives the following expressions for the added mass terms, Imlay (1961):

$$
\begin{aligned}
X_A &= X_{\dot{u}}\dot{u} + X_{\dot{w}}(\dot{w} + uq) + X_{\dot{q}}\dot{q} + Z_{\dot{w}}wq + Z_{\dot{q}}q^2 \\
&\quad + X_{\dot{v}}\dot{v} + X_{\dot{p}}\dot{p} + X_{\dot{r}}\dot{r} - Y_{\dot{v}}vr - Y_{\dot{p}}rp - Y_{\dot{r}}r^2 \\
&\quad - X_{\dot{v}}ur - Y_{\dot{w}}wr \\
&\quad + Y_{\dot{w}}vq + Z_{\dot{p}}pq - (Y_{\dot{q}} - Z_{\dot{r}})qr \\
Y_A &= X_{\dot{v}}\dot{u} + Y_{\dot{w}}\dot{w} + Y_{\dot{q}}\dot{q} \\
&\quad + Y_{\dot{v}}\dot{v} + Y_{\dot{p}}\dot{p} + Y_{\dot{r}}\dot{r} + X_{\dot{v}}vr - Y_{\dot{w}}vp + X_{\dot{r}}r^2 + (X_{\dot{p}} - Z_{\dot{r}})rp - Z_{\dot{p}}p^2 \\
&\quad - X_{\dot{w}}(up - wr) + X_{\dot{u}}ur - Z_{\dot{w}}wp \\
&\quad - Z_{\dot{q}}pq + X_{\dot{q}}qr \\
Z_A &= X_{\dot{w}}(\dot{u} - wq) + Z_{\dot{w}}\dot{w} + Z_{\dot{q}}\dot{q} - X_{\dot{u}}uq - X_{\dot{q}}q^2 \\
&\quad + Y_{\dot{w}}\dot{v} + Z_{\dot{p}}\dot{p} + Z_{\dot{r}}\dot{r} + Y_{\dot{v}}vp + Y_{\dot{r}}rp + Y_{\dot{p}}p^2 \\
&\quad + X_{\dot{v}}up + Y_{\dot{w}}wp \\
&\quad - X_{\dot{v}}vq - (X_{\dot{p}} - Y_{\dot{q}})pq - X_{\dot{r}}qr \\
K_A &= X_{\dot{p}}\dot{u} + Z_{\dot{p}}\dot{w} + K_{\dot{q}}\dot{q} - X_{\dot{v}}wu + X_{\dot{r}}uq - Y_{\dot{w}}w^2 - (Y_{\dot{q}} - Z_{\dot{r}})wq + M_{\dot{r}}q^2 \\
&\quad + Y_{\dot{p}}\dot{v} + K_{\dot{p}}\dot{p} + K_{\dot{r}}\dot{r} + Y_{\dot{w}}v^2 - (Y_{\dot{q}} - Z_{\dot{r}})vr + Z_{\dot{p}}vp - M_{\dot{r}}r^2 - K_{\dot{q}}rp \\
&\quad + X_{\dot{w}}uv - (Y_{\dot{v}} - Z_{\dot{w}})vw - (Y_{\dot{r}} + Z_{\dot{q}})wr - Y_{\dot{p}}wp - X_{\dot{q}}ur \\
&\quad + (Y_{\dot{r}} + Z_{\dot{q}})vq + K_{\dot{r}}pq - (M_{\dot{q}} - N_{\dot{r}})qr \\
M_A &= X_{\dot{q}}(\dot{u} + wq) + Z_{\dot{q}}(\dot{w} - uq) + M_{\dot{q}}\dot{q} - X_{\dot{w}}(u^2 - w^2) - (Z_{\dot{w}} - X_{\dot{u}})wu \\
&\quad + Y_{\dot{q}}\dot{v} + K_{\dot{q}}\dot{p} + M_{\dot{r}}\dot{r} + Y_{\dot{p}}vr - Y_{\dot{r}}vp - K_{\dot{r}}(p^2 - r^2) + (K_{\dot{p}} - N_{\dot{r}})rp \\
&\quad - Y_{\dot{w}}uv + X_{\dot{v}}vw - (X_{\dot{r}} + Z_{\dot{p}})(up - wr) + (X_{\dot{p}} - Z_{\dot{r}})(wp + ur) \\
&\quad - M_{\dot{r}}pq + K_{\dot{q}}qr \\
N_A &= X_{\dot{r}}\dot{u} + Z_{\dot{r}}\dot{w} + M_{\dot{r}}\dot{q} + X_{\dot{v}}u^2 + Y_{\dot{w}}wu - (X_{\dot{p}} - Y_{\dot{q}})uq - Z_{\dot{p}}wq - K_{\dot{q}}q^2 \\
&\quad + Y_{\dot{r}}\dot{v} + K_{\dot{r}}\dot{p} + N_{\dot{r}}\dot{r} - X_{\dot{v}}v^2 - X_{\dot{r}}vr - (X_{\dot{p}} - Y_{\dot{q}})vp + M_{\dot{r}}rp + K_{\dot{q}}p^2 \\
&\quad - (X_{\dot{u}} - Y_{\dot{v}})uv - X_{\dot{w}}vw + (X_{\dot{q}} + Y_{\dot{p}})up + Y_{\dot{r}}ur + Z_{\dot{q}}wp \\
&\quad - (X_{\dot{q}} + Y_{\dot{p}})vq - (K_{\dot{p}} - M_{\dot{q}})pq - K_{\dot{r}}qr
\end{aligned}
\tag{2.25}
$$

Imlay (1961) has arranged the equations in four lines with longitudinal components on the first line and lateral components on the second line. The third line consists of mixed terms involving u or w as one factor. If one or both of these velocities are large enough to be treated as a constant the third line may be treated as an additional term to the lateral equation of motion. The fourth line contains mixed terms that usually can be neglected as second order terms. Many of the added mass derivatives contained in the general expressions for added mass are either zero or mutually related when the body has various symmetries, Imlay (1961). A more detailed discussion of added mass terms is found in Humphreys and

Watkinson (1978). Extracting the added mass derivatives corresponding to the velocity coupling terms yields:

$$\boldsymbol{C}_A(\dot{\boldsymbol{q}}) = \begin{bmatrix} 0 & 0 & 0 & 0 & C_A^{15} & C_A^{16} \\ 0 & 0 & 0 & C_A^{24} & 0 & C_A^{26} \\ 0 & 0 & 0 & C_A^{34} & C_A^{35} & 0 \\ 0 & -C_A^{24} & -C_A^{34} & 0 & C_A^{45} & C_A^{46} \\ -C_A^{15} & 0 & -C_A^{35} & -C_A^{45} & 0 & C_A^{56} \\ -C_A^{16} & -C_A^{26} & 0 & -C_A^{46} & -C_A^{56} & 0 \end{bmatrix}$$

where

$$\begin{aligned} C_A^{15} &= -X_{\dot{w}}u - Y_{\dot{w}}v - Z_{\dot{w}}w - Z_{\dot{p}}p - Z_{\dot{q}}q - Z_{\dot{r}}r \\ C_A^{16} &= X_{\dot{v}}u + Y_{\dot{v}}v + Y_{\dot{w}}w + Y_{\dot{p}}p + Y_{\dot{q}}q + Y_{\dot{r}}r \\ C_A^{24} &= X_{\dot{w}}u + Y_{\dot{w}}v + Z_{\dot{w}}w + Z_{\dot{p}}p + Z_{\dot{q}}q + Z_{\dot{r}}r \\ C_A^{26} &= -X_{\dot{u}}u - X_{\dot{v}}v - X_{\dot{w}}w - X_{\dot{p}}p - X_{\dot{q}}q - X_{\dot{r}}r \\ C_A^{34} &= -X_{\dot{v}}u - Y_{\dot{v}}v - Y_{\dot{w}}w - Y_{\dot{p}}p - Y_{\dot{q}}q - Y_{\dot{r}}r \end{aligned}$$

$$\begin{aligned} C_A^{35} &= X_{\dot{u}}u + X_{\dot{v}}v + X_{\dot{w}}w + X_{\dot{p}}p + X_{\dot{q}}q + X_{\dot{r}}r \\ C_A^{45} &= -X_{\dot{r}}u - Y_{\dot{r}}v - Z_{\dot{r}}w - K_{\dot{r}}p - M_{\dot{r}}q - N_{\dot{r}}r \\ C_A^{46} &= X_{\dot{q}}u + Y_{\dot{q}}v + Z_{\dot{q}}w + K_{\dot{q}}p + M_{\dot{q}}q + M_{\dot{r}}r \\ C_A^{56} &= -X_{\dot{p}}u - Y_{\dot{p}}v - Z_{\dot{p}}w - K_{\dot{p}}p - K_{\dot{q}}q - K_{\dot{r}}r \end{aligned}$$

This particular choice implies that the matrix $\boldsymbol{C}_A$ is skew-symmetrical i.e. $\boldsymbol{C}_A = -\boldsymbol{C}_A^T$. A common assumption is to neglect the contribution from the off-diagonal elements in the added mass matrix $\boldsymbol{M}_A$. This yields the following simple $\boldsymbol{C}_A$ matrix:

$$\boldsymbol{C}_A(\dot{\boldsymbol{q}}) = \begin{bmatrix} 0 & 0 & 0 & 0 & -Z_{\dot{w}}w & Y_{\dot{v}}v \\ 0 & 0 & 0 & Z_{\dot{w}}w & 0 & -X_{\dot{u}}u \\ 0 & 0 & 0 & -Y_{\dot{v}}v & X_{\dot{u}}u & 0 \\ 0 & -Z_{\dot{w}}w & Y_{\dot{v}}v & 0 & -N_{\dot{r}}r & M_{\dot{q}}q \\ Z_{\dot{w}}w & 0 & -X_{\dot{u}}u & N_{\dot{r}}r & 0 & -K_{\dot{p}}p \\ -Y_{\dot{v}}v & X_{\dot{u}}u & 0 & -M_{\dot{q}}q & K_{\dot{p}}p & 0 \end{bmatrix}$$

2.4.2 Potential Damping

The contribution from the potential damping terms compared to other dissipative terms like viscous damping terms are usually neglectable for underwater vehicles operating at great depth. Nevertheless, underwater vehicles operating close to the free surface should consider the potential damping effect. Especially, small underwater vehicles with a non-streamlined body e.g. vehicles build as an open space-frame with buoyant elements and equipment mounted within the frame, should consider the effect from the potential damping terms. The linear potential damping can be modelled as:

$$\boldsymbol{\tau}_B(\dot{\boldsymbol{q}}) = -\boldsymbol{D}_B\dot{\boldsymbol{q}}$$

where $\boldsymbol{D}_B$ is a positive definite matrix ($\boldsymbol{D}_B > 0$), of linear damping coefficients:

$$\boldsymbol{D}_B = -\begin{bmatrix} X_u & X_v & X_w & X_p & X_q & X_r \\ Y_u & Y_v & Y_w & Y_p & Y_q & Y_r \\ Z_u & Z_v & Z_w & Z_p & Z_q & Z_r \\ K_u & K_v & K_w & K_p & K_q & K_r \\ M_u & M_v & M_w & M_p & M_q & M_r \\ N_u & N_v & N_w & N_p & N_q & N_r \end{bmatrix}$$

Often it is convenient to include the linear potential damping terms in the viscous forces rather than separating these effects.

2.4.3 Restoring Forces and Moments

In the hydrodynamic terminology, the gravitational and buoyant forces are called restoring forces. The restoring forces and moments can be written as:

$$\boldsymbol{\tau}_C(\boldsymbol{x}) = -\boldsymbol{g}(\boldsymbol{x})$$

where $\boldsymbol{g}(\boldsymbol{x})$ is a 6×1 nonlinear vector. The gravitational force $\boldsymbol{f}_G$ acting on the underwater vehicle acts through the centre of gravity: $\boldsymbol{r}_G = (x_G, y_G, z_G)^T$ of the vehicle. Similar the buoyant force $\boldsymbol{f}_B$ acts through the centre of buoyancy: $\boldsymbol{r}_B = (x_B, y_B, z_B)^T$. The restoring forces will have components along the respective body axes. Both the gravitational force and the buoyant force will also produce moments about these axes.

Let m be the mass of the vehicle including water in free floating spaces, ∇ the volume of fluid displaced by the vehicle, g the acceleration of gravity and ρ the fluid density. According to the SNAME (1950) notation, the vehicle's weight is defined as: $W = mg$ while the buoyancy force is defined as: $B = \rho g \nabla$. By applying the results from Section 2.1, the weight and buoyancy force can be transformed to the body-fixed coordinate system with:

$$\boldsymbol{f}_G = \boldsymbol{J}_1^{-1}(\phi, \theta, \psi) \begin{bmatrix} 0 \\ 0 \\ W \end{bmatrix} \quad , \quad \boldsymbol{f}_B = \boldsymbol{J}_1^{-1}(\phi, \theta, \psi) \begin{bmatrix} 0 \\ 0 \\ B \end{bmatrix}$$

where $\boldsymbol{J}_1$ is a coordinate transformation matrix defined in Section 2.1. Let $\boldsymbol{\tau}(\boldsymbol{x})$ be a generalized vector in the body-fixed coordinate system consisting of both the gravitational and the buoyant forces and moments, namely:

$$\boldsymbol{\tau}_C(\boldsymbol{x}) = \begin{bmatrix} \boldsymbol{f}_G - \boldsymbol{f}_B \\ \boldsymbol{r}_G \times \boldsymbol{f}_G - \boldsymbol{r}_B \times \boldsymbol{f}_B \end{bmatrix}$$

Notice that the z-axis is positive downwards. Equating this expression yields

$$\boldsymbol{g}(\boldsymbol{x}) = \begin{bmatrix} & (W-B)\, s\theta & & \\ - & (W-B)\, c\theta s\phi & & \\ - & (W-B)\, c\theta c\phi & & \\ - & (y_G W - y_B B)\, c\theta c\phi & + & (z_G W - z_B B)\, c\theta s\phi \\ & (z_G W - z_B B)\, s\theta & + & (x_G W - x_B B)\, c\theta c\phi \\ - & (x_G W - x_B B)\, c\theta s\phi & - & (y_G W - y_B B)\, s\theta \end{bmatrix} \tag{2.26}$$

Eq. 2.26 is the Euler angle representation of the hydrostatic forces and moments. An alternative representation is found by applying the quaternion representation:

$$\boldsymbol{g}(\boldsymbol{e}) = \begin{bmatrix} - & 2(W-B)\,(e_1e_3 - e_2e_4) \\ - & 2(W-B)\,(e_2e_3 + e_1e_4) \\ & (W-B)\,(e_1^2 + e_2^2 - e_3^2 - e_4^2) \\ & (y_G W - y_B B)\,(e_1^2 + e_2^2 - e_3^2 - e_4^2) + 2(z_G W - z_B B)\,(e_2e_3 + e_1e_4) \\ - & 2(z_G W - z_B B)\,(e_1e_3 - e_2e_4) - (x_G W - x_B B)\,(e_1^2 + e_2^2 - e_3^2 - e_4^2) \\ - & 2(x_G W - x_B B)\,(e_2e_3 + e_1e_4) + (y_G W - y_B B)\,(e_1e_3 - e_2e_4) \end{bmatrix} \tag{2.27}$$

where the Euler parameters e_i (i=1..4) are defined in Section 2.1. For neutrally buoyant underwater vehicles with homogeneous mass distribution ($W = B$) the expression for the restoring forces and moments is quite simple. Let the distance between the centre of gravity and the centre of buoyancy be denoted as $\overline{\boldsymbol{BG}}$ where:

$$\overline{\boldsymbol{BG}} = (\overline{BG}_x,\ \overline{BG}_y,\ \overline{BG}_z)^T = (x_G - x_B,\ y_G - y_B,\ z_G - z_B)^T$$

Hence, Eq. 2.26 can be written as:

$$\boldsymbol{g}(\boldsymbol{x}) = \begin{bmatrix} 0 \\ 0 \\ 0 \\ -\overline{BG}_y W\, c\theta c\phi + \overline{BG}_z W\, c\theta s\phi \\ \overline{BG}_z W\, s\theta + \overline{BG}_x W\, c\theta c\phi \\ -\overline{BG}_x W\, c\theta s\phi - \overline{BG}_y W\, s\theta \end{bmatrix}$$

2.5 Excitation Forces

When applying potential theory, the fluid motion was assumed to be irrotational. This implies that we only consider the linear velocity components of the fluid i.e.

$$\dot{\boldsymbol{q}}_f \triangleq (u_f, v_f, w_f, 0, 0, 0)^T$$

Let $u_r \triangleq u - u_f$, $v_r \triangleq v - v_f$ and $w_r \triangleq w - w_f$ be the relative linear fluid velocity components. Hence, $\dot{\boldsymbol{q}}_r = (u_r, v_r, w_r, p, q, r)^T$ can be interpreted as the relative fluid velocity vector.

Linear Theory:

In linear theory the wave induced forces and moments acting on the vehicle can be written as the sum of the radiation induced forces and moments and the excitation forces and moments, c.f. Section 2.3.2:

$$\boldsymbol{\tau}_H = \underbrace{\overbrace{\boldsymbol{M}_{FK}\ddot{\boldsymbol{q}}_f}^{\boldsymbol{\tau}_{FK}} + \overbrace{\boldsymbol{A}\ddot{\boldsymbol{q}}_f + \boldsymbol{B}\dot{\boldsymbol{q}}_f}^{\boldsymbol{\tau}_D}}_{\boldsymbol{\tau}_E} - \underbrace{\boldsymbol{A}\ddot{\boldsymbol{q}} - \boldsymbol{B}\dot{\boldsymbol{q}} - \boldsymbol{C}\boldsymbol{x}}_{\boldsymbol{\tau}_R} \tag{2.28}$$

where

$\boldsymbol{\tau}_{FK}$ is the Froude-Kriloff forces and moments
$\boldsymbol{\tau}_D$ is the diffraction forces and moments
$\boldsymbol{\tau}_E$ is the excitation forces and moments
$\boldsymbol{\tau}_R$ is the radiation induced forces and moments

Nonlinear Theory:

In the nonlinear case, $\boldsymbol{\tau}_H$ cannot be written as a sum of linear elements. The forces and moments due to the radiation and diffraction potential are nonlinear functions of the relative velocity vector $\dot{\boldsymbol{q}}_r$ and relative acceleration vector $\ddot{\boldsymbol{q}}_r$. Let the contribution from the radiation and diffraction induced forces and moments be denoted with the combined vector term $\boldsymbol{\tau}_{R+D}$, then the sum:

$$\boldsymbol{\tau}_H = \boldsymbol{\tau}_{FK} + \boldsymbol{\tau}_{R+D}$$

could be used to describe the nonlinear hydrodynamic forces and moments caused by waves. These new terms are described more closely in the next sections.

2.5.1 Froude-Kriloff Forces

The Froude-Kriloff force and moment vector can be expressed as:

$$\boldsymbol{\tau}_{FK}(\dot{\boldsymbol{q}}_f, \ddot{\boldsymbol{q}}_f) = \boldsymbol{M}_{FK}\ddot{\boldsymbol{q}}_f$$

Here $\boldsymbol{M}_{FK}$ can be interpreted as the FK-inertia matrix. Coriolis and centrifugal terms will not appear in the general expression for the FK forces and moments since we have assumed the rotational fluid motion to be zero i.e. $p_f = q_f = r_f = 0$. Let ∇ be the volume of the displaced fluid and ρ be the fluid density, hence the mass of the displaced fluid must be

$$\overline{m} = \rho\nabla$$

The moments and products of the inertia of the displaced fluid are:

$$\begin{aligned} \overline{I}_x &= \int_\nabla (y^2+z^2)\rho d\nabla \quad , \quad \overline{I}_{xy} = \int_\nabla xy\rho d\nabla \\ \overline{I}_y &= \int_\nabla (x^2+z^2)\rho d\nabla \quad , \quad \overline{I}_{xz} = \int_\nabla xz\rho d\nabla \\ \overline{I}_z &= \int_\nabla (x^2+y^2)\rho d\nabla \quad , \quad \overline{I}_{yz} = \int_\nabla yz\rho d\nabla \end{aligned}$$

Applying the results from Section 2.3.2 the FK-inertia matrix for a small volume completely submerged body, c.f. Eq. 2.14, is:

$$\boldsymbol{M}_{FK} = \begin{bmatrix} \overline{m} & 0 & 0 & 0 & \overline{m}z_B & -\overline{m}y_B \\ 0 & \overline{m} & 0 & -\overline{m}z_B & 0 & \overline{m}x_B \\ 0 & 0 & \overline{m} & \overline{m}y_B & -\overline{m}x_B & 0 \\ 0 & -\overline{m}z_B & \overline{m}y_B & \overline{I}_x & -\overline{I}_{xy} & -\overline{I}_{xz} \\ \overline{m}z_B & 0 & -\overline{m}x_B & -\overline{I}_{xy} & \overline{I}_y & -\overline{I}_{yz} \\ -\overline{m}y_B & \overline{m}x_B & 0 & -\overline{I}_{xz} & -\overline{I}_{yz} & \overline{I}_z \end{bmatrix}$$

Since we have assumed that $\ddot{\boldsymbol{q}}_f \triangleq (\dot{u}_f, \dot{v}_f, \dot{w}_f, 0, 0, 0)^T$, we only have to calculate the first three columns of $\boldsymbol{M}_{FK}$ to obtain the vector $\boldsymbol{M}_{FK}\ddot{\boldsymbol{q}}_f$.

2.5.2 Diffraction Forces

Linear Theory:

We recall that in the linear case, the diffraction forces and moments were linearly superpositioned as:

$$\boldsymbol{\tau}_D(\dot{\boldsymbol{q}}_f, \ddot{\boldsymbol{q}}_f) = -\boldsymbol{A}\ddot{\boldsymbol{q}}_f - \boldsymbol{B}\dot{\boldsymbol{q}}_f$$

Nonlinear Theory:

In the nonlinear case it was suggested writing the diffraction forces and moments directly as functions of the relative fluid motion. Hence, the combined expression for the nonlinear radiation and diffraction induced forces and moments can be expressed as:

$$\boldsymbol{\tau}_{R+D}(\boldsymbol{x}, \dot{\boldsymbol{q}}_r, \ddot{\boldsymbol{q}}_r) = -\boldsymbol{M}_A\ddot{\boldsymbol{q}}_r - \boldsymbol{C}_A(\dot{\boldsymbol{q}}_r)\dot{\boldsymbol{q}}_r - \boldsymbol{D}_B\dot{\boldsymbol{q}}_r - \boldsymbol{g}(\boldsymbol{x})$$

which yields:

$$\boldsymbol{\tau}_H(\boldsymbol{x}, \dot{\boldsymbol{q}}_r, \ddot{\boldsymbol{q}}_r) = \boldsymbol{\tau}_{FK} + \boldsymbol{\tau}_{R+D} = \boldsymbol{M}_{FK}\ddot{\boldsymbol{q}}_f - \boldsymbol{M}_A\ddot{\boldsymbol{q}}_r - \boldsymbol{C}_A(\dot{\boldsymbol{q}}_r)\dot{\boldsymbol{q}}_r - \boldsymbol{D}_B\dot{\boldsymbol{q}}_r - \boldsymbol{g}(\boldsymbol{x})$$

This is simply the nonlinear counterpart to Eq. 2.28. When no excitation forces are present, the general expression for $\boldsymbol{\tau}_H$ simplifies to

$$\boldsymbol{\tau}_H(\boldsymbol{x}, \dot{\boldsymbol{q}}, \ddot{\boldsymbol{q}}) \equiv \boldsymbol{\tau}_R(\boldsymbol{x}, \dot{\boldsymbol{q}}, \ddot{\boldsymbol{q}}) = -\boldsymbol{M}_A\ddot{\boldsymbol{q}} - \boldsymbol{C}_A(\dot{\boldsymbol{q}})\dot{\boldsymbol{q}} - \boldsymbol{D}_B\dot{\boldsymbol{q}} - \boldsymbol{g}(\boldsymbol{x})$$

2.6 Viscous Wave Loads and Damping

The viscous effects for underwater vehicles are mainly caused by

- Linear skin friction due to laminar boundary layers.
- Quadratic skin friction due to turbulent boundary layers.
- Quadratic drag due to vortex shedding (Morison's equation).

The viscous damping forces and moments $\boldsymbol{\tau}_V$ will be functions of the relative fluid motion. In the range of Reynold's numbers in which underwater vehicles typically operate, flow is turbulent. Hence the drag force is approximated by the square law resistance arising from Morison's equation. We recall that the quadratic drag force in the x-direction can be expressed as, c.f. Section 2.3.3:

$$f = -\frac{1}{2}\rho\, C_D\, A\, u_r|u_r|$$

where A is the projected cross-sectional area , C_D is the drag-coefficient based on the representative area and ρ is the fluid density. The drag coefficient C_D depends on both the Reynolds number and the orientation of the vehicle. The skin friction will give a linear and quadratic contribution to the drag force. Experiments verify that the total drag on the vehicle could be fairly described as the sum of a linear and quadratic drag component. This is illustrated in Figure 2.4
A generalization of Morison's equation could be to use a truncated second order Taylor series expansion to describe the viscous damping in 6 DOF. This suggests that the viscous damping could be written as:

$$\boldsymbol{\tau}_V(\dot{\boldsymbol{q}}_r) = -\boldsymbol{D}_L\, \dot{\boldsymbol{q}}_r - \boldsymbol{d}_Q(\dot{\boldsymbol{q}}_r) - \boldsymbol{h.o.t.} \tag{2.29}$$

where $\boldsymbol{D}_L$ is a 6×6 positive definite matrix ($\boldsymbol{D}_L > 0$) of linear damping terms and $\boldsymbol{d}_Q(\dot{\boldsymbol{q}}_r)$ is 6×1 vector of non-negative quadratic damping terms. The linear coefficients can be expressed as:

$$\boldsymbol{D}_L = -\begin{bmatrix} X_u & X_v & X_w & X_p & X_q & X_r \\ Y_u & Y_v & Y_w & Y_p & Y_q & Y_r \\ Z_u & Z_v & Z_w & Z_p & Z_q & Z_r \\ K_u & K_v & K_w & K_p & K_q & K_r \\ M_u & M_v & M_w & M_p & M_q & M_r \\ N_u & N_v & N_w & N_p & N_q & N_r \end{bmatrix}$$

while the quadratic counterpart is written as:

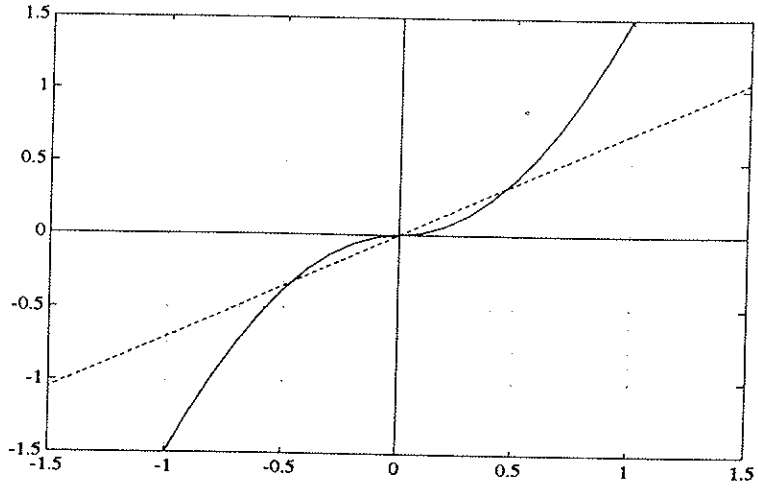

Figure 2.4: Linear (dotted) and quadratic damping (solid) versus relative velocity u_r.

$$\boldsymbol{d}_Q(\dot{\boldsymbol{q}}_r) = - \begin{bmatrix} \dot{\boldsymbol{q}}_r^T \boldsymbol{X}_Q \, |\dot{\boldsymbol{q}}_r| \\ \dot{\boldsymbol{q}}_r^T \boldsymbol{Y}_Q \, |\dot{\boldsymbol{q}}_r| \\ \dot{\boldsymbol{q}}_r^T \boldsymbol{Z}_Q \, |\dot{\boldsymbol{q}}_r| \\ \dot{\boldsymbol{q}}_r^T \boldsymbol{K}_Q \, |\dot{\boldsymbol{q}}_r| \\ \dot{\boldsymbol{q}}_r^T \boldsymbol{M}_Q \, |\dot{\boldsymbol{q}}_r| \\ \dot{\boldsymbol{q}}_r^T \boldsymbol{N}_Q \, |\dot{\boldsymbol{q}}_r| \end{bmatrix}$$

where $|\dot{\boldsymbol{q}}_r| = (\, |u_r|, |v_r|, |w_r|, |p|, |q|, |r| \,)^T$. The matrices $\boldsymbol{X}_Q$, $\boldsymbol{Y}_Q$, $\boldsymbol{Z}_Q$, $\boldsymbol{K}_Q$, $\boldsymbol{M}_Q$ and $\boldsymbol{N}_Q$ are 6×6 negative definite matrices of hydrodynamic coefficients. The first matrix is written as:

$$\boldsymbol{X}_Q = \begin{bmatrix} X_{u|u|} & X_{u|v|} & X_{u|w|} & X_{u|p|} & X_{u|q|} & X_{u|r|} \\ Y_{v|u|} & Y_{v|v|} & Y_{v|w|} & Y_{v|p|} & Y_{v|q|} & Y_{v|r|} \\ Z_{w|u|} & Z_{w|v|} & Z_{w|w|} & Z_{w|p|} & Z_{w|q|} & Z_{w|r|} \\ K_{p|u|} & K_{p|v|} & K_{p|w|} & K_{p|p|} & K_{p|q|} & K_{p|r|} \\ M_{q|u|} & M_{q|v|} & M_{q|w|} & M_{q|p|} & M_{q|q|} & M_{q|r|} \\ N_{r|u|} & N_{r|v|} & N_{r|w|} & N_{r|p|} & N_{r|q|} & N_{r|r|} \end{bmatrix}$$

Similar expression are obtained for the other matrices in $\boldsymbol{d}_Q$. The expression Eq. 2.29 includes both the effects from the skin friction and the vortex shedding. It is quite complicated to determine the hydrodynamic coefficients in this expression, especially the off-diagonal elements. The cross-coupling terms can be neglected in many applications. On the other hand,

the diagonal elements can be obtained from simple experiments. Hence, a frequently used approximation to Eq. 2.29 is

$$\boldsymbol{\tau}_V(\dot{\boldsymbol{q}}_r) = \begin{bmatrix} X_u + X_{u|u|}\,|u_r| & 0 & 0 & 0 & 0 & 0 \\ 0 & Y_u + Y_{v|v|}\,|v_n| & 0 & 0 & 0 & 0 \\ 0 & 0 & Z_w + Z_{w|w|}\,|w_r| & 0 & 0 & 0 \\ 0 & 0 & 0 & K_p + K_{p|p|}\,|p| & 0 & 0 \\ 0 & 0 & 0 & 0 & M_q + M_{q|q|}\,|q| & 0 \\ 0 & 0 & 0 & 0 & 0 & N_r + N_{r|r|}\,|r| \end{bmatrix} \dot{\boldsymbol{q}}_r$$

A more convenient representation of Eq. 2.29 is

$$\boldsymbol{\tau}_V(\dot{\boldsymbol{q}}_r) = -\boldsymbol{D}_V(\dot{\boldsymbol{q}}_r)\,\dot{\boldsymbol{q}}_r$$

where $\boldsymbol{D}_V$ is a positive definite matrix of both linear and quadratic damping terms.

2.7 Umbilical Forces

Umbilical cables are used for both power supply and communication to underwater vehicles. Ship heave may cause large dynamic loads which can lead to vibrations (strumming) of the cable. Hence, hydrodynamic drag may be so dominating that it overcomes the vehicle's propulsion system. The hydrodynamical loads can be split into three components; normal drag force f_n, tangential drag force f_t and lift force f_l, Dand and Every (1983). The steady state normal force, tangential force and lift force per unit length acting on the cable can be described as:

$$f_n = \frac{1}{2}\rho C_{D_n} D v_n^2 \qquad f_t = \frac{1}{2}\rho C_{D_t} D v_t^2 \qquad f_l = \frac{1}{2}\rho C_{D_l} D v_n^2$$

where v_n and v_t are the normal and tangential velocity, respectively while C_{D_n}, C_{D_t} and C_{D_l} are the drag coefficients. It is usual to treat f_n, f_t and f_l independently. The total umbilical forces and moments can be expressed as

$$\boldsymbol{\tau}_U = -\boldsymbol{D}_U(\dot{\boldsymbol{q}}_r)\,\dot{\boldsymbol{q}}_r$$

The umbilical cable configuration can be optimized by numerical simulations. In particular it is desirable to reduce the static and dynamic force at the lower end of the cable such that ROV operations are less affected by strumming effects. This is described in more detail by Lie *et al.* (1989).

2.8 Propulsion and Control Forces

Small underwater vehicles are usually manoeuvred with thrusters and control surfaces. The efficiency of the control surfaces depends on the speed of the vehicle. This is due to the fact that the lift force is proportional to the square of the velocity. However, control surfaces are particularly useful in trim and depth changing manoeuvres. Submersibles can also be designed with variable ballast-buoyancy systems for trim and depth control. Besides this, more modern devices like water jets can be used. In this section it will be shown that the propulsion forces and moments $\boldsymbol{\tau}_P \in \Re^n$ can be described as

$$\boldsymbol{\tau}_P = \boldsymbol{B}(\dot{\boldsymbol{q}})\,\boldsymbol{u} \tag{2.30}$$

where $\boldsymbol{u} \in \Re^p$ is an input vector and $\boldsymbol{B}$ is an $n \times p$ input matrix depending on the vehicle's speed. To obtain a unique expression for $\boldsymbol{B}$ is a non-trivial task due to a large number of complex unmodelled hydrodynamic effects e.g. cavitation or interactive forces and moments due to a number of thrusters mounted within an open ROV frame. The thruster forces are determined by performing an *open water test* where the propeller revolution, thruster force and thruster moment are all measured. Control surfaces can be tested in a similar manner e.g. in a *cavitation tunnel.* Finally, these tests can be used to determine the elements in the $\boldsymbol{B}$ matrix.

2.8.1 Thruster Forces

In this section the thruster forces and moments will be described by Eq. 2.30. The experimental results are based on the thruster shown in Figure 2.5.

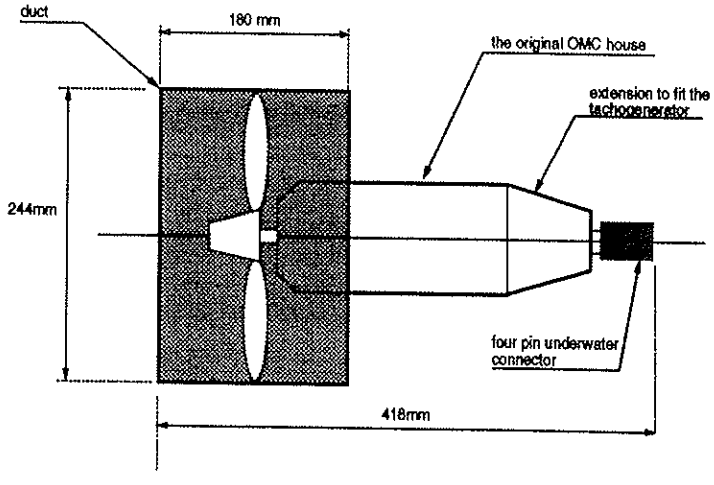

Figure 2.5: The NEROV ducted thruster, Sagatun and Fossen (1991a)

Actuator dynamics:

A thruster can simply be a small DC motor designed for underwater operating conditions. A speed-controlled motor can be described as, see e.g. Balchen (1963),

$$\begin{aligned} L\frac{di}{dt} &= -Ri - K_M\omega + v_S \\ J\frac{d\omega}{dt} &= K_M i - Q \end{aligned} \tag{2.31}$$

where i is the current, v_S is the input voltage, L is the inductance, R is the resistance and J is the moment of inertia. The field current i_f is assumed to be constant and $K_M = k_f i_f$ where k_f is a motor constant. Q is the propeller torque. From Eq. 2.31 it is straightforward to find the motor transfer function

$$h_{motor}(s) = \frac{\omega(s)}{v_s(s)} = \frac{K}{(1+T_1 s)(1+T_2 s)}$$

Here K is a motor constant while T_1 and T_2 are two time constants.

Experimental Results: Inner Loop PID-Controller

The NEROV propulsion system is based on six 24 V 400 W permanent magnet motors which are made by the Outboard Marine Corporation, Sagatun and Fossen (1991a). By extending the motor house we were able to fit a tachogenerator inside the unit, see Fig. 2.5. A frequency response generator was used to obtain the open loop frequency response. The experimental results are shown in Figure 2.7. The tachogenerator was used to design an analog inner loop PID-controller. A block diagram illustrating the inner loop feedback control system is shown in Figure 2.6.

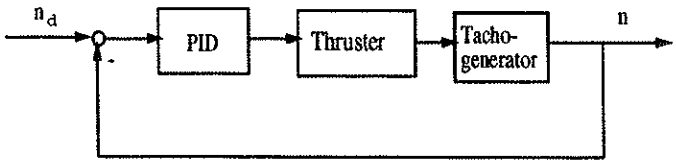

Figure 2.6: Block diagram of the thruster inner loop feedback control system where n is the propeller revolution measurement and n_d is the desired propeller revolution.

Consider the regulator transfer function

$$h_{PID}(s) = \frac{K_P}{T_I s}\frac{(1+T_I s)(1+T_D s)}{1+T_f s}$$

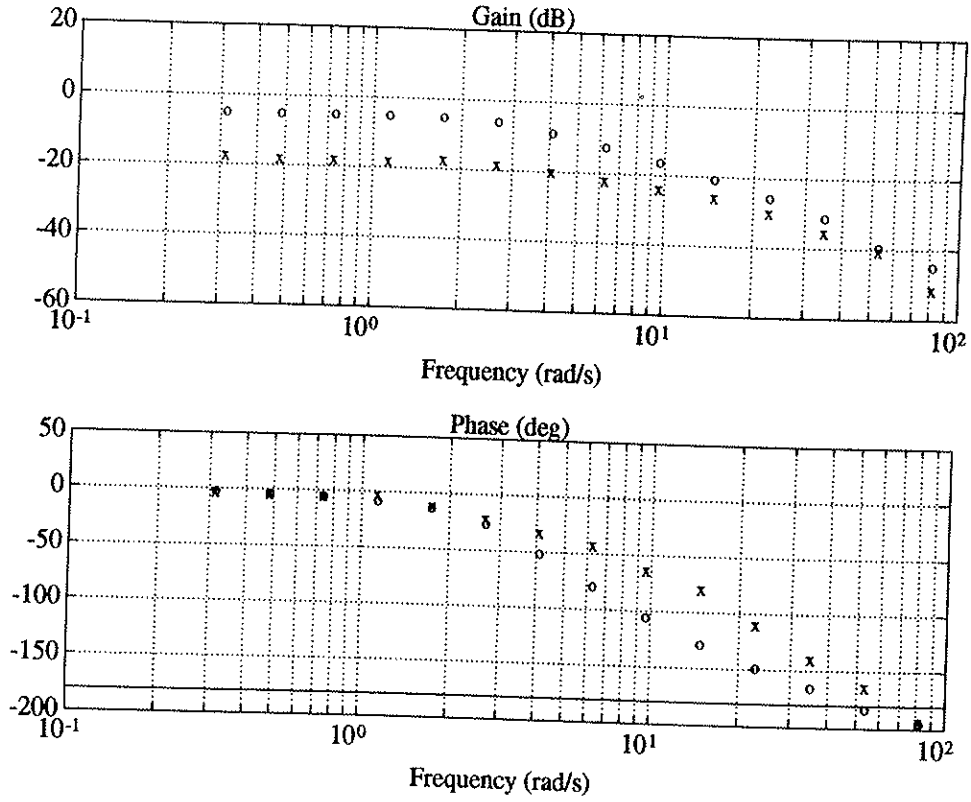

Figure 2.7: Open loop frequency response of the NEROV thruster, Sagatun and Fossen (1991a). The upper plot illustrates the thruster gain in air (marked by o) and water (marked by x) as a function of the logarithmic frequency. The lower plot is the corresponding phase.

This suggests that the regulator time constants should be selected as $T_I \approx T_1 = 0.13\ s$, $T_D \approx T_2 = 0.05\ s$ *and* $T_f \approx 0.1\ T_D = 0.005\ s$ *which yields the loop transfer function*

$$l(s) = h_{PID}(s)\ h_{motor}(s) = \frac{K_P K}{T_I s\ (1 + T_f s)}$$

The thruster bandwidth can be improved by simply increasing the regulator gain K_P. *For the NEROV thruster the closed loop bandwidth was found to be* $\omega_c = 20\, rad/s$. *The performance of the control system for a sampling rate of* $50 Hz$ *is shown in Figure 2.8. If the PID-controller yields poor performance e.g. as a result of significant actuator dynamics and non-linearities like hysteresis, a model-based controller should be considered. Adaptive sliding controllers for systems with significant actuator nonlinear dynamics are described in Yoerger* et al. *(1990) and Fossen (1990).*

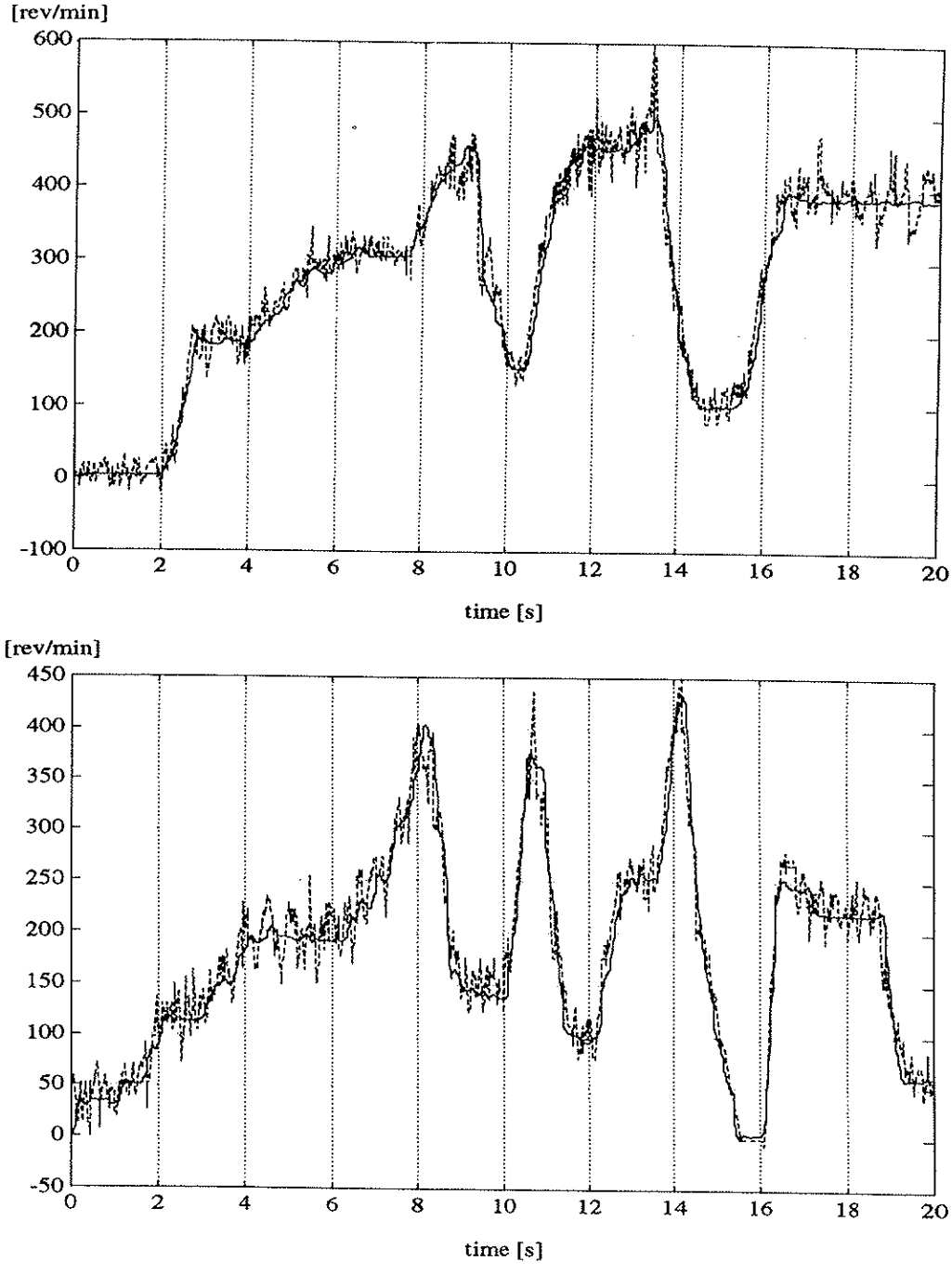

Figure 2.8: Experimental results showing the actual (broken line) and the desired (line) propeller revolution versus time for the NEROV thruster.

Thruster Hydrodynamics

Small underwater vehicles usually operate over a considerable speed range with no specific speed dominating. For such vehicles the performance of the ducted thrusters will be a function of advance velocity V_A at the propeller, propeller revolutions n and propeller diameter D. The non-dimensional open water characteristics are defined in terms of the open water advance coefficient J_o, Dand and Every (1983),

$$J_o = \frac{V_A}{nD}$$

The non-dimensional thrust and torque coefficients K_T and K_Q and thruster open water efficiency η_o i.e. the efficiency in undisturbed water, are defined as

$$K_T = \frac{T}{\rho n|n| D^4} \quad ; \quad K_Q = \frac{Q}{\rho n|n| D^5} \quad ; \quad \eta_o = \frac{J_o}{2\pi} \cdot \frac{K_T}{K_Q} \tag{2.32}$$

where ρ is the water density and T and Q are the propeller thrust and torque, respectively. The total thruster efficiency is defined as

$$\eta_{TOT} = \eta_o \cdot \eta_D \cdot \eta_M$$

where η_M is the mechanical efficiency (typically 0.8-0.9) and η_D is the propulsion efficiency defined as:

$$\eta_D = \eta_H \cdot \eta_o \cdot \eta_R \quad \text{where} \quad \eta_H = \frac{1-t}{1-w}$$

Here the relative rotative efficiency η_R is defined as: $\eta_R = \eta_B/\eta_o$ which simply is the ratio between the propeller efficiency when wakes are present and the open water efficiency. t is the thrust deduction number (typically 0.05-0.2) and w is the wake fraction number (typically 0.05-0.3) relating the advance speed at the propeller V_A with the vehicle speed V as

$$V_A = (1-w)V$$

By carrying out an open water test a unique curve is obtained, see Figure 2.9, where J_o is plotted against K_T and K_Q.

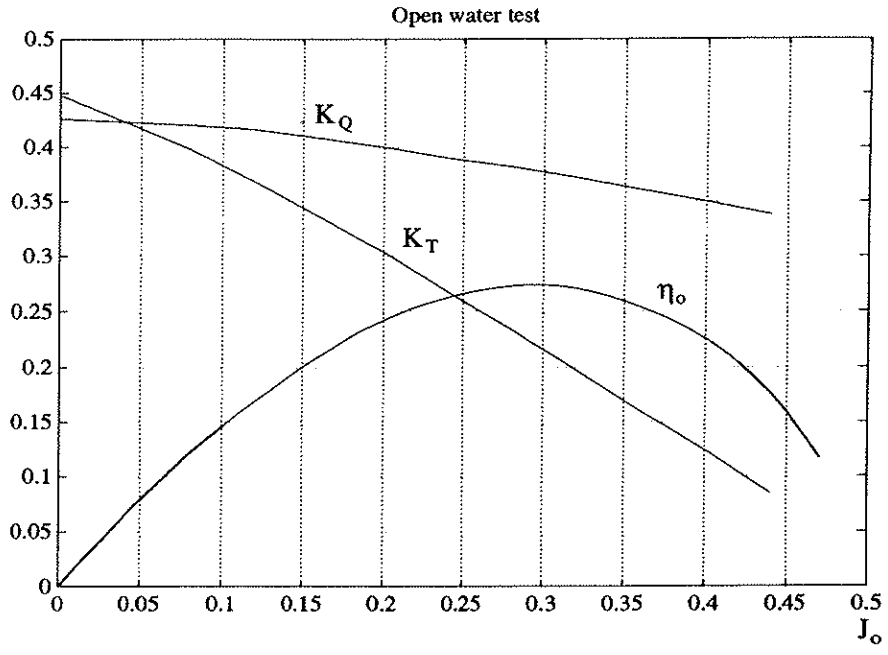

Figure 2.9: Non-dimensional thruster characteristics K_T, K_Q and η_o as a function of positive advance coefficient J_o (ahead direction).

Experimental Results: Open Water Test

For the NEROV thruster an open water test was performed in the towing tank at the Norwegian Marine Technology Research Institute (MARINTEK) in Trondheim. The experimental results from this test are shown in Figures 2.10 and 2.11. It should be noted that the K_T and K_Q curves will depend on the orientation of the thruster relative to the direction of the speed of the vehicle. An experiment showing this effect for the NEROV thruster is shown in Figure 2.11.

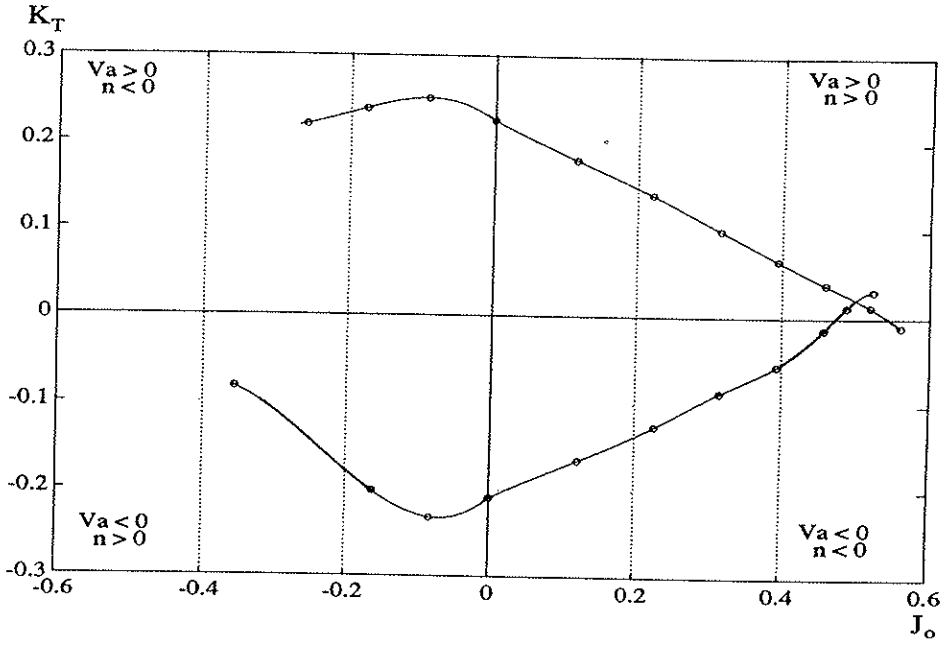

Figure 2.10: Non-dimensional experimental thruster characteristics K_T versus the advance coefficient J_o for the NEROV vehicle, Sagatun and Fossen (1991a).

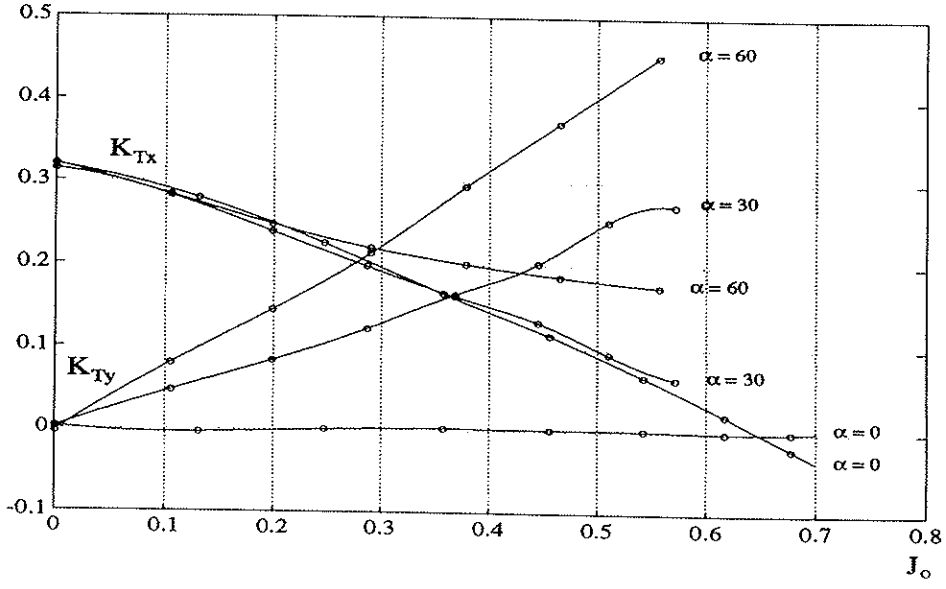

Figure 2.11: Non-dimensional thruster characteristics K_{Tx} and K_{Ty} in the x- and y-directions respectively as functions of J_o and angle α (deg) between the thruster and vehicle speed.

From the K_T curves it is seen that the thruster force T is highly nonlinear. This is best illustrated in Figure 2.12, where

$$T = \rho\, D^4\, K_T\left(J_o(V_A, n, D)\right)\, n\,|n|$$

is plotted versus the speed of advance V_A and propeller revolutions n. When designing the control system the effect of this nonlinearity should be compensated for.

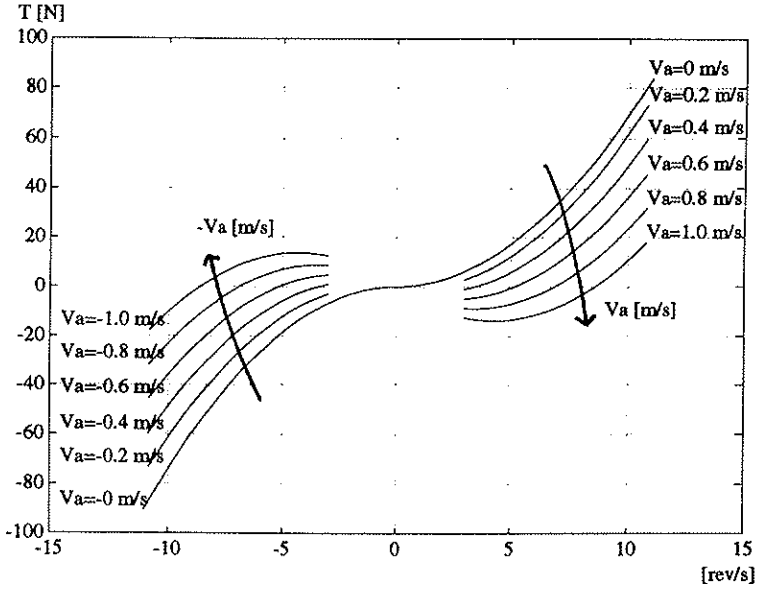

Figure 2.12: Thruster force T as a function of propeller revolutions n for different speeds of advance V_A.

Approximation of Nonlinear Thruster Characteristics

Fossen and Sagatun(1991a, 1991b) suggest that the thruster force can be approximated as

$$T \approx \rho\, D^4\, \hat{K}_T(J_o)\, n\,|n|$$

Here $\hat{K}_T$ is the estimate of the non-dimensional thrust coefficient. For positive J_o, Fig. 2.10 suggests that $\hat{K}_T$ can be linearly interpolated as

$$\hat{K}_T(J_o) \approx \alpha + \beta\, J_o$$

where α and β are two constants. If the vehicle's velocity V_k is measured at time k, the advance coefficient $J_{o,\,k}$ can be approximated as

$$J_{o,\,k} \approx \frac{(1-w)V_k}{n_{k-1}D}$$

Here w is the wake fraction number and n_{k-1} is the measurement of the propeller revolution at time $k-1$. A control input vector $\boldsymbol{u} = (u_1, ..., u_p)^T$ with elements

$$u_j = n_j|n_j| \quad \Longleftrightarrow \quad n_j = sgn(u_j)\sqrt{|u_j|}$$

where n_j is the propeller revolution of thruster j and sgn is signum function

$$sgn(x) = \begin{cases} 1 & \text{if } x > 0 \\ 0 & \text{if } x = 0 \\ -1 & \text{if } x < 0 \end{cases}$$

shows that the elements in the input matrix $\boldsymbol{B}$ can be expressed as

$$B_{ij}(\dot{\boldsymbol{q}}) \approx \rho D^4 \hat{K}_{T_{ij}}(J_o) \;\; , \;\; i = 1..n, \;\; j = 1..p \tag{2.33}$$

Here $\hat{K}_{T_{ij}}$ is the nonlinear approximation corresponding to thruster input $u_j = n_j|n_j|$. Hence, the thruster force and moment vector can be expressed as

$$\boldsymbol{\tau}_P = \boldsymbol{B}(\dot{\boldsymbol{q}})\,\boldsymbol{u} \tag{2.34}$$

where $\boldsymbol{B}$ is an $n \times p$ input matrix. Feedback linearization techniques as well as monovariable control design techniques e.g. of PID-type, require that $\boldsymbol{u}$ can be calculated through an inverse transformation

$$\boldsymbol{u} = \boldsymbol{B}^{\dagger}(\dot{\boldsymbol{q}})\boldsymbol{\tau}_P \tag{2.35}$$

where $\boldsymbol{B}^{\dagger}$ can be interpreted as a generalized inverse of $\boldsymbol{B}$. This raises the question of whether it is possible to select $\boldsymbol{B}^{\dagger}$ in some optimal manner. The answer is yes, if excessive use of control efforts, i.e. means of saving energy are important. Hence, the minimization of an energy cost function should be considered. This matter is discussed in Section 2.8.4.

Experimental Results: Force Controlled Thruster

Although the NEROV thruster is a speed controlled thruster, force control can be obtained by exploiting the results from the open water test i.e. Eqs. 2.33 and 2.34. For simplicity we assumed that the advance speed at the propeller was zero i.e. $V_A = 0\ m/s$. *Hence, the relationship between the desired thruster force* $\tau_d\ (N)$ *and the desired propeller revolution* $n_d\ (rev/s)$ *can be expressed as*

$$\tau_d \approx \rho\, D^4\, \hat{K}_T(0)\, n_d|n_d|$$

For the NEROV vehicle $D = 0.24\ m$, $\rho = 1000\ kg/m^3$ *and* $\hat{K}_T(0) \approx 0.23$ *(Bollard pull). Hence* n_d *can be calculated by applying the inverse transformation*

$$n_d \approx sgn(\tau_d)\sqrt{\frac{|\tau_d|}{\rho\, D^4\, \hat{K}_T(0)}}$$

corresponding to the more general expression Eq. 2.35. The desired thruster force corresponding to the lower plot in Figure 2.8 is shown in Figure 2.13.

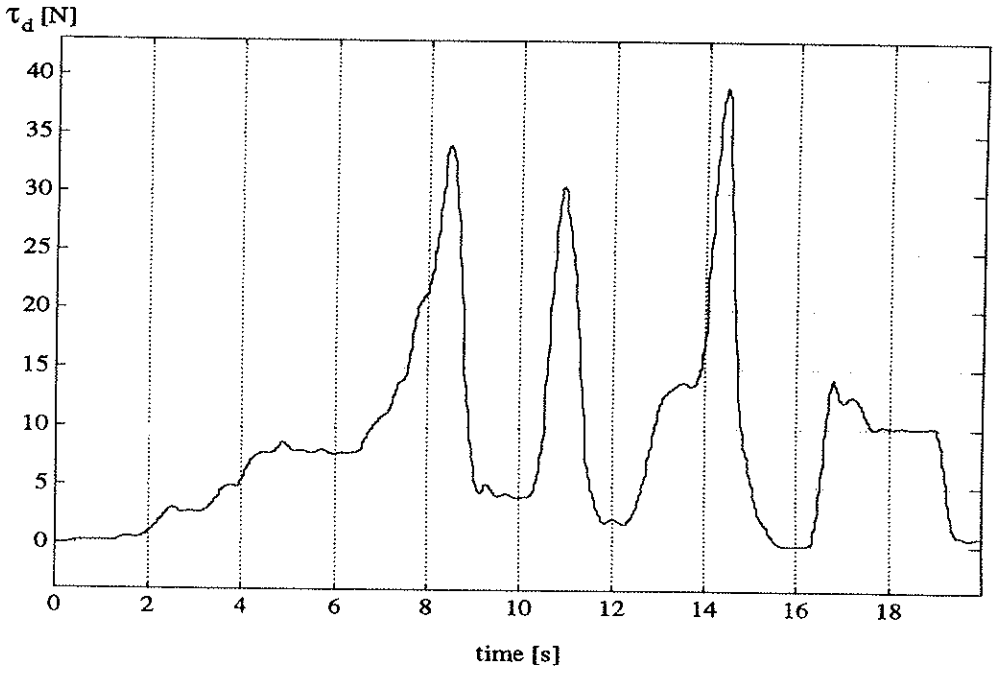

Figure 2.13: Desired thruster force τ_d versus time for $V_A = 0\ m/s$.

Uncertainties in the experimental data, $\hat{K}_T$*, can be compensated for in the outer loop control design. This is described more closely in Section 5.4.3.*

2.8.2 Thruster Momentum Drag

Momentum drag is a hydrodynamic effect that couples the thruster jet velocity with the vehicle's speed. An active thruster that moves at an angle to the main motion of the vehicle will change the momentum in the fluid, Dand and Every (1983). This is because the fluid which passes through the thruster must be accelerated from rest up to the speed of the vehicle. This change in momentum is balanced by an additional drag acting on the vehicle.

For underwater vehicles this effect can be significant because such vehicles often have a large number of thrusters mounted in different directions within a space-frame structure. Hence an underwater vehicle will suffer from momentum drag when performing numerous coupled manoeuvres. The contribution of momentum drag can be found from open water tests. For a thruster which is perpendicular to the vehicle speed vector

$$U = \sqrt{u^2 + v^2 + w^2}$$

momentum drag f_j is shown to satisfy

$$f_j = k\,\rho\,A_D\,v_j U \qquad j = 1..p$$

where k is a coefficient, ρ is the water density, A_D is the duct cross-sectional area, v_j is the thruster jet velocity and u is vehicle speed. Open water tests of the thruster can give satisfactory values for k. Interactions between the thruster and the vehicle can affect k significantly. Hence, best results are obtained by performing the test with the whole vehicle when trying to decide the coefficient k. The drag forces will also cause a moment

$$\boldsymbol{m} = \boldsymbol{r}_P \times \boldsymbol{f}$$

where $\boldsymbol{r}_P = (x_p, y_P, z_P)^T$ is the centre of pressure.

2.8.3 Variable Buoyancy Systems

These systems can be used separately or combined with the existing propulsion and trim system. A variable buoyancy system (VBS) can be used for depth and trim changing operations. In dynamic positioning (DP) applications neutral buoyancy and a constant trim are of particular interest. Variable buoyancy systems are limited in practical applications for underwater vehicles mainly because they are cost excessive, Triantafyllou and Amzallag (1984). A small AUV based on a variable buoyancy system was built and tested in Norway by SIMRAD Subsea A/S and SINTEF Automatic Control in 1985. This vehicle was also equipped with two thrusters, two control surfaces and a built-in television camera, Kleppaker *et al.* (1986). The control surfaces were used to pitch the vehicle while the VBS was used for the depth changing operations.

A gas generation system can be used to vary the buoyancy force f_B. Consider a tank which contains both water and gas. The area of the water surface $A(h)$ will be a function of the water height h. Hence, the buoyancy force is simply

$$f_B = \int_h^H \rho g A(h) dh$$

where ρ is the water density and H is the total height of the tank. The control philosophy for a variable buoyancy system is based on volume control i.e. controlling the volume of the displaced water. A more general discussion on variable ballast-displacement and trim systems is found in Allmendinger (1990).

2.8.4 Optimal Distribution of Propulsion and Control Forces

For underwater vehicles where the input matrix $\boldsymbol{B}$ is an non-square matrix and $p \geq n$, i.e. equal or more control inputs than controllable DOF, it is possible to find an "optimal" distribution of control energy, for each DOF, Fossen and Sagatun (1991b). A comprehensive study of the thruster allocation of dynamic positioned ships is found in Jenssen (1980). Consider the linear quadratic energy cost function

$$\text{Min } J = \frac{1}{2}\boldsymbol{u}^T\boldsymbol{W}\boldsymbol{u} \quad \text{subject to} \quad \boldsymbol{\tau}_P = \boldsymbol{B}\boldsymbol{u}$$

where $\boldsymbol{W}$ is positive definite, usually diagonal energy weighting matrix. For underwater vehicles which have both control surfaces and thrusters, the elements in $\boldsymbol{W}$ should be selected such that using the control surfaces is much more inexpensive than using the thrusters i.e. providing a means of saving battery energy. Defining the Lagrangian

$$L(\boldsymbol{u}, \boldsymbol{\lambda}) = \frac{1}{2}\boldsymbol{u}^T\boldsymbol{W}\boldsymbol{u} + \boldsymbol{\lambda}^T(\boldsymbol{\tau}_P - \boldsymbol{B}\boldsymbol{u})$$

where the parameter vector $\boldsymbol{\lambda}$ is the Lagrange multipliers. Differentiating the Lagrangian L with respect to $\boldsymbol{u}$ yields

$$\nabla_u L = \boldsymbol{W}\boldsymbol{u} - \boldsymbol{B}^T\boldsymbol{\lambda} = 0$$

From this we obtain:

$$\boldsymbol{u} = \boldsymbol{W}^{-1}\boldsymbol{B}^T\boldsymbol{\lambda} \tag{2.36}$$

By using the fact that

$$\boldsymbol{\tau}_P = \boldsymbol{B}\boldsymbol{u} = \boldsymbol{B}\boldsymbol{W}^{-1}\boldsymbol{B}^T\boldsymbol{\lambda}$$

and assuming that $\boldsymbol{B}\boldsymbol{W}^{-1}\boldsymbol{B}^T$ is nonsingular, we find the following optimal solution for the Lagrange multiplicators

$$\boldsymbol{\lambda} = (\boldsymbol{B}\boldsymbol{W}^{-1}\boldsymbol{B}^T)^{-1}\boldsymbol{\tau}$$

Substituting this result into Eq. (2.36) yields the generalized inverse

$$\boldsymbol{B}_W^{\dagger} = \boldsymbol{W}^{-1}\boldsymbol{B}^T(\boldsymbol{B}\boldsymbol{W}^{-1}\boldsymbol{B}^T)^{-1} \tag{2.37}$$

In the case when all inputs are equality weighted, i.e. $\boldsymbol{W} = \boldsymbol{I}$, Eq. (2.37) simplifies to

$$\boldsymbol{B}^{\dagger} = \boldsymbol{B}^T(\boldsymbol{B}\boldsymbol{B}^T)^{-1}$$

Notice that for the square case $\boldsymbol{B}^{\dagger}$ is simply equal to $\boldsymbol{B}^{-1}$.

2.9 Determination of Hydrodynamic Coefficients

A large number of experimental methods can be used to determine forces and moments associated with variations in linear and angular velocity and acceleration. Typical facilities are the rotating arm, the free oscillator, the forced oscillator, the curved-flow tunnel and the curved models in a straight flow facility. Nevertheless, it is difficult to determine all hydrodynamic coefficients for an underwater vehicle in 6 DOF. It is necessary to know these coefficients with reasonable accuracy to obtain a a good model of the vehicle. One promising technique has been developed by a research team at the David Taylor Model Basin in 1957. They applied a device called the Planar Motion Mechanism (PMM) System, Gertler (1959). The PMM system can be used to experimentally determining all of hydrodynamic stability coefficients in 6 DOF. These includes static stability coefficients, rotary stability coefficients and acceleration derivatives.
Besides this some hydrodynamic coefficients can be determined by theoretical and semi-empirical methods. For ships strip theory has been successfully applied, for instance. Another promising approach is system identification (SI) techniques, Tinker (1982). SI techniques are economical in tank time and provide a more direct answer free from the cumulative error of measuring many coefficients individually. The disadvantage is the quite harsh requirement of persistent excitation of the control input sequence. Indeed, this requirement can be hard to satisfy for a general vehicle in 6 DOF.

2.10 Underwater Vehicle Equations of Motion

The linear and nonlinear underwater vehicle equations of motion can be expressed in compact forms by applying the results from the previous sections.

2.10.1 Nonlinear Equations of Motion

The nonlinear underwater vehicle equations of motion will first be derived for an undisturbed underwater vehicle (*no fluid motion*) and secondly for an underwater vehicle exposed to sinusoidal waves (*equations of relative motion*).

No Fluid Motion

In this case the nonlinear underwater vehicle equations of motion can be expressed in a compact form as:

- Vehicle dynamics:

$$\boldsymbol{M}\ddot{\boldsymbol{q}} + \boldsymbol{C}(\dot{\boldsymbol{q}})\dot{\boldsymbol{q}} + \boldsymbol{D}(\dot{\boldsymbol{q}})\dot{\boldsymbol{q}} + \boldsymbol{g}(\boldsymbol{x}) = \boldsymbol{B}(\dot{\boldsymbol{q}})\boldsymbol{u} \tag{2.38}$$

- Kinematics

$$\dot{\boldsymbol{x}} = \boldsymbol{J}(\boldsymbol{x})\dot{\boldsymbol{q}} \tag{2.39}$$

Here $\boldsymbol{x} \in \Re^n$, $\boldsymbol{q} \in \Re^n$ and $\boldsymbol{u} \in \Re^p$. The scalar n corresponds to the number of DOF while p is simply the number of control inputs. The kinematic transformation matrix $\boldsymbol{J}$ is defined in Section 2.1. $\boldsymbol{M}$ is an $n \times n$ inertia matrix including hydrodynamic added mass. The inertia matrix $\boldsymbol{M}$ can be written as:

$$\boldsymbol{M} = \boldsymbol{M}_{RB} + \boldsymbol{M}_A$$

where $\boldsymbol{M}_{RB}$ is defined in Section 2.2 and $\boldsymbol{M}_A$ is defined in Section 2.4. This yields the following inertia matrix (n = 6):

$$\boldsymbol{M} = \begin{bmatrix} m - X_{\dot{u}} & -X_{\dot{v}} & -X_{\dot{w}} & -X_{\dot{p}} & mz_G - X_{\dot{q}} & -my_G - X_{\dot{r}} \\ -X_{\dot{v}} & m - Y_{\dot{v}} & -Y_{\dot{w}} & -mz_G - Y_{\dot{p}} & -Y_{\dot{q}} & mx_G - Y_{\dot{r}} \\ -X_{\dot{w}} & -Y_{\dot{w}} & m - Z_{\dot{w}} & my_G - Z_{\dot{p}} & -mx_G - Z_{\dot{q}} & -Z_{\dot{r}} \\ -X_{\dot{p}} & -mz_G - Y_{\dot{p}} & my_G - Z_{\dot{p}} & Ix - K_{\dot{p}} & -Ixy - K_{\dot{q}} & -Izx - K_{\dot{r}} \\ mz_G - X_{\dot{q}} & -Y_{\dot{q}} & -mx_G - Z_{\dot{q}} & -Ixy - K_{\dot{q}} & Iy - M_{\dot{q}} & -Iyz - M_{\dot{r}} \\ -my_G - X_{\dot{r}} & mx_G - Y_{\dot{r}} & -Z_{\dot{r}} & -Izx - K_{\dot{r}} & -Iyz - M_{\dot{r}} & Iz - N_{\dot{r}} \end{bmatrix}$$

By applying the results from the previous sections, the $\boldsymbol{C}$ and $\boldsymbol{D}$ matrix can be found in a similar manner as:

$$\boldsymbol{C}(\dot{\boldsymbol{q}}) = \boldsymbol{C}_{RB}(\dot{\boldsymbol{q}}) + \boldsymbol{C}_A(\dot{\boldsymbol{q}})$$
$$\boldsymbol{D}(\dot{\boldsymbol{q}}) = \boldsymbol{D}_B + \boldsymbol{D}_U(\dot{\boldsymbol{q}}) + \boldsymbol{D}_V(\dot{\boldsymbol{q}})$$

These expressions will be quite complicated in the general case. It is common to reduce the complexity of the model by neglecting a large number of coupling terms from symmetry considerations. The $n \times p$ input matrix $\boldsymbol{B}$ is defined in Section 2.8 while the $n \times 1$ vector of restoring forces and moments $\boldsymbol{g}$ is defined in Section 2.4.3.

Nonlinear Equations of Relative Motion

A more general representation of the nonlinear equations of motion is found when including the fluid motion due to waves. Recall that the fluid velocity vector was defined as: $\dot{\boldsymbol{q}}_f \triangleq (u_f, v_f, w_f, 0, 0, 0)^T$ while the relative fluid velocity vector is $\dot{\boldsymbol{q}}_r = \dot{\boldsymbol{q}} - \dot{\boldsymbol{q}}_f$. Hence, the combined equations of motion can be written as:

$$M_{RB}\ddot{q} - M_{FK}\ddot{q}_f + M_A\ddot{q}_r + [C_{RB}(\dot{q}_r) + C_A(\dot{q}_r)]\,\dot{q}_r$$

$$+ [D_B + D_U(\dot{q}_r) + D_V(\dot{q}_r)]\,\dot{q}_r + g(x) = B(\dot{q})u$$

For a neutrally buoyant underwater vehicle with homogeneous mass distribution:

$$M_{FK} = M_{RB}$$

Hence, the nonlinear equations of relative motion simplify to:

$$M\ddot{q}_r + C(\dot{q}_r)\dot{q}_r + D(\dot{q}_r)\dot{q}_r + g(x) = B(\dot{q})u \tag{2.40}$$

The kinematic equations will of course be equal to the case with no fluid motion. The equations of relative motion are quite useful for the simulation of underwater vehicles when sealoads are of interest. The fluid motion vector can be found from linear wave theory.

Simplicity Considerations of the Inertia Matrix

The general expression for the inertia matrix M can be considerably simplified by exploiting different body symmetries. It is straightforward to verify the following three cases:

(i) xz-plane of symmetry (port/starboard symmetry).

$$M = \begin{bmatrix} m_{11} & 0 & m_{13} & 0 & m_{15} & 0 \\ 0 & m_{22} & 0 & m_{24} & 0 & m_{26} \\ m_{31} & 0 & m_{33} & 0 & m_{35} & 0 \\ 0 & m_{42} & 0 & m_{44} & 0 & m_{46} \\ m_{51} & 0 & m_{53} & 0 & m_{55} & 0 \\ 0 & m_{62} & 0 & m_{64} & 0 & m_{66} \end{bmatrix}$$

(ii) xz- and yz-planes of symmetry (port/starboard and fore/aft symmetries).

$$M = \begin{bmatrix} m_{11} & 0 & 0 & 0 & m_{15} & 0 \\ 0 & m_{22} & 0 & m_{24} & 0 & 0 \\ 0 & 0 & m_{33} & 0 & 0 & 0 \\ 0 & m_{42} & 0 & m_{44} & 0 & 0 \\ m_{51} & 0 & 0 & 0 & m_{55} & 0 \\ 0 & 0 & 0 & 0 & 0 & m_{66} \end{bmatrix}$$

(iii) xz-, yz- and xy-planes of symmetry (port/starboard, fore/aft and bottom/top symmetries).

$$M = \begin{bmatrix} m_{11} & 0 & 0 & 0 & 0 & 0 \\ 0 & m_{22} & 0 & 0 & 0 & 0 \\ 0 & 0 & m_{33} & 0 & 0 & 0 \\ 0 & 0 & 0 & m_{44} & 0 & 0 \\ 0 & 0 & 0 & 0 & m_{55} & 0 \\ 0 & 0 & 0 & 0 & 0 & m_{66} \end{bmatrix}$$

Useful Properties of the Nonlinear Equations of Motion

The nonlinear representation Eqs. 2.38 and 2.39 have some useful properties which can be exploited in the nonlinear control design. From linear algebra a square matrix $\boldsymbol{A}$ is said to be:

(i) Positive definite: $\boldsymbol{s}^T\boldsymbol{A}\boldsymbol{s} > 0 \ \forall \ \boldsymbol{s}$.

(ii) Symmetric: $\boldsymbol{A} = \boldsymbol{A}^T$.

(iii) Skew-symmetric: $\boldsymbol{A} = -\boldsymbol{A}^T \ \Rightarrow \ \boldsymbol{s}^T\boldsymbol{A}\boldsymbol{s} = 0 \ \forall \ \boldsymbol{s}$.

These properties can be observed for different matrices in the nonlinear equations of motion. The nonlinear control design techniques discussed in the next sections are based on the following properties:

$\boldsymbol{M} = \boldsymbol{M}^T > 0$. The inertia matrix is symmetrical and positive definite. Newman (1977) has shown that for a rigid body moving in an ideal fluid the inertia matrix is symmetrical. In a real fluid these 36 elements may all be distinct. Experience has shown that the numerical values of added mass in a real fluid are usually in good agreement with those obtained from ideal theory, Wendel (1956).

$\boldsymbol{s}^T(\dot{\boldsymbol{M}} - 2\boldsymbol{C})\boldsymbol{s} = 0 \ \ \forall \ \ \boldsymbol{s}$. This requires that the dissipative forces are not included in $\boldsymbol{C}$. In robotics it is usual to calculate $\boldsymbol{C}$ by using the Christoffel symbols, Ortega and Spong (1988). For a marine vehicle, $\boldsymbol{M}$ will depend on the wave frequency and thus the vehicle's speed. This relationship is hardly known. Nevertheless, by assuming that $\dot{\boldsymbol{M}} = 0$ for each sea condition, this implies that only $\boldsymbol{C}$ must be skew-symmetrical. Indeed, this is satisfied.

$\boldsymbol{D} > 0$. The damping matrix will always be dissipative.

Alternative Representation of the Nonlinear Equations of Motion

Differentiating Eq. 2.39 yields

$$\ddot{\boldsymbol{x}} = \boldsymbol{J}\ddot{\boldsymbol{q}} + \dot{\boldsymbol{J}}\dot{\boldsymbol{q}} \quad \Longleftrightarrow \quad \ddot{\boldsymbol{q}} = \boldsymbol{J}^{-1}(\ddot{\boldsymbol{x}} - \dot{\boldsymbol{J}}\boldsymbol{J}^{-1}\dot{\boldsymbol{x}})$$

Applying this result to the nonlinear ROV equations of motion, Eqs. 2.38 and 2.39 yields

$$\boldsymbol{M}^*(\boldsymbol{x})\ddot{\boldsymbol{x}} + \boldsymbol{C}^*(\boldsymbol{x},\dot{\boldsymbol{x}})\dot{\boldsymbol{x}} + \boldsymbol{D}^*(\boldsymbol{x},\dot{\boldsymbol{x}})\dot{\boldsymbol{x}} + \boldsymbol{g}^*(\boldsymbol{x}) = \boldsymbol{B}^*(\boldsymbol{x})\boldsymbol{u} \tag{2.41}$$

where

$$\begin{aligned} \boldsymbol{M}^*(\boldsymbol{x}) &= \boldsymbol{J}^{-T}\boldsymbol{M}\boldsymbol{J}^{-1} \\ \boldsymbol{C}^*(\boldsymbol{x},\dot{\boldsymbol{x}}) &= \boldsymbol{J}^{-T}(\boldsymbol{C}-\boldsymbol{M}\boldsymbol{J}^{-1}\dot{\boldsymbol{J}})\boldsymbol{J}^{-1} \\ \boldsymbol{D}^*(\boldsymbol{x},\dot{\boldsymbol{x}}) &= \boldsymbol{J}^{-T}\boldsymbol{D}\boldsymbol{J}^{-1} \\ \boldsymbol{g}^*(\boldsymbol{x}) &= \boldsymbol{J}^{-T}\boldsymbol{g} \\ \boldsymbol{B}^*(\boldsymbol{x},\dot{\boldsymbol{x}}) &= \boldsymbol{J}^{-T}\boldsymbol{B} \end{aligned} \tag{2.42}$$

It is straightforward to show that $\boldsymbol{M} = \boldsymbol{M}^T > 0$ implies that $\boldsymbol{M}^* = (\boldsymbol{M}^*)^T > 0$. Similar $\boldsymbol{D} > 0$ implies that $\boldsymbol{D}^* > 0$. The skew-symmetric property can be verified by differentiating $\boldsymbol{M}^*$ with respect to time, which yields

$$\dot{\boldsymbol{M}}^* = \boldsymbol{J}^{-T}(\dot{\boldsymbol{M}} - 2\boldsymbol{M}\boldsymbol{J}^{-1}\dot{\boldsymbol{J}})\boldsymbol{J}^{-1}$$

This in turn implies that

$$\dot{\boldsymbol{M}}^* - 2\boldsymbol{C}^* = \boldsymbol{J}^{-T}(\dot{\boldsymbol{M}} - 2\boldsymbol{C})\boldsymbol{J}^{-1}$$

Since $\dot{\boldsymbol{M}} - 2\boldsymbol{C}$ is skew-symmetric, $\dot{\boldsymbol{M}}^* - 2\boldsymbol{C}^*$ must also be skew-symmetrical.

2.10.2 Linear Equations of Motion

The linearized equations of motion are obtained by defining the state vector as $\boldsymbol{x} = (\boldsymbol{x}_1^T, \boldsymbol{x}_2^T)^T$ where $\boldsymbol{x}_1 = (u, v, w, p, q, r)^T$ and $\boldsymbol{x}_2 = (x, y, z, \phi, \theta, \psi)^T$. The control input vector is simply denoted as $\boldsymbol{u}$. Hence, Eqs. 2.38 and 2.39 can be linearized about an equilibrium point $\boldsymbol{x}_o = (\boldsymbol{x}_{1o}^T, \boldsymbol{x}_{2o}^T)^T$ as:

$$\begin{aligned} \boldsymbol{M}\,\Delta\dot{\boldsymbol{x}}_1 &= \overline{\boldsymbol{A}}_{11}\,\Delta\boldsymbol{x}_1 + \overline{\boldsymbol{A}}_{12}\,\Delta\boldsymbol{x}_2 + \overline{\boldsymbol{B}}_1\,\Delta\boldsymbol{u} \\ \Delta\dot{\boldsymbol{x}}_2 &= \overline{\boldsymbol{A}}_{21}\,\Delta\boldsymbol{x}_1 \end{aligned} \tag{2.43}$$

Here $\Delta\boldsymbol{x} = \boldsymbol{x} - \boldsymbol{x}_o$, $\Delta\boldsymbol{u} = \boldsymbol{u} - \boldsymbol{u}_o$ and $\boldsymbol{M}$ is the vehicle's inertia matrix while the matrices $\overline{\boldsymbol{A}}$ and $\overline{\boldsymbol{B}}$ are defined as

$$\overline{\boldsymbol{A}}_{11} = -\left(\frac{\partial(\boldsymbol{C}(\boldsymbol{x}_1)+\boldsymbol{D}(\boldsymbol{x}_1))}{\partial\boldsymbol{x}_1}\right)_{\boldsymbol{x}_1=\boldsymbol{x}_{10}} \qquad \overline{\boldsymbol{A}}_{12} = -\left(\frac{\partial\boldsymbol{g}(\boldsymbol{x}_2)}{\partial\boldsymbol{x}_2}\right)_{\boldsymbol{x}_2=\boldsymbol{x}_{20}}$$

$$\overline{\boldsymbol{A}}_{21} = \left(\frac{\partial\boldsymbol{J}(\boldsymbol{x}_2)}{\partial\boldsymbol{x}_2}\right)_{\boldsymbol{x}_2=\boldsymbol{x}_{2o}} \qquad \overline{\boldsymbol{B}}_1 = \left(\frac{\partial\boldsymbol{B}(\boldsymbol{x}_1)}{\partial\boldsymbol{x}_1}\right)_{\boldsymbol{x}_1=\boldsymbol{x}_{1o}}$$

If we linearize $\boldsymbol{J}(\boldsymbol{x}_2)$ about the zero roll, pitch and yaw angles, then $\overline{\boldsymbol{A}}_{21}$ is simply equal to the identity matrix. Letting

$$\boldsymbol{A} = \begin{bmatrix} \boldsymbol{M}^{-1}\overline{\boldsymbol{A}}_{11} & \boldsymbol{M}^{-1}\overline{\boldsymbol{A}}_{12} \\ \hline \overline{\boldsymbol{A}}_{21} & 0 \end{bmatrix} \qquad \boldsymbol{B} = \begin{bmatrix} \boldsymbol{M}^{-1}\overline{\boldsymbol{B}}_{1} \\ \hline 0 \end{bmatrix}$$

and dropping the delta notation for the perturbed state and control input vector, yields the standard state space representation:

$$\dot{\boldsymbol{x}} = \boldsymbol{A}\boldsymbol{x} + \boldsymbol{B}\boldsymbol{u} \tag{2.44}$$

Linear Decoupled Equations of Motion

In the stability analysis of underwater vehicles it is convenient to decouple the linear motion into (1) the *longitudinal* and (2) the *lateral* motion. This is based on the following assumptions:

- It will be assumed that the deviations from the linear model are so small that higher order terms can be neglected. This assumption may be quite unrealistic if the vehicle is performing coupled manoeuvres at some speed.
- The kinematic transformation matrix will be chosen as the identity matrix i.e. $\boldsymbol{J}(\boldsymbol{x}) = \boldsymbol{I}$. This corresponds to linearizing the kinematic equations about the zero roll, pitch and yaw angles.
- Constant or zero control inputs. This is of particular interest in "stick-fixed" stability analyses of the vehicle.
- The xz-plane is a plane of symmetry (port/starboard symmetry).
- The vehicle is neutrally buoyant i.e. $B = W$ with $B = mg$ and $W = \rho g \nabla$.

(1) Equations of Longitudinal Motion

The longitudinal equations of motion can be used to describe the vehicle's motion in surge, heave and pitch. This includes diving, climbing and forward speed changing manoeuvres. For small underwater vehicles the longitudinal equations of motion are obtained from Eq. 2.43, which yields:

$$\begin{bmatrix} m - X_{\dot{u}} & -X_{\dot{w}} & mz_G - X_{\dot{q}} & 0 \\ -X_{\dot{w}} & m - Z_{\dot{w}} & -mx_G - Z_{\dot{q}} & 0 \\ mz_G - X_{\dot{q}} & -mx_G - Z_{\dot{q}} & I_y - M_{\dot{q}} & 0 \\ 0 & 0 & 0 & 1 \end{bmatrix} \begin{bmatrix} \dot{u} \\ \dot{w} \\ \dot{q} \\ \dot{\theta} \end{bmatrix} + \begin{bmatrix} -X_u & -X_w & -X_q & 0 \\ -Z_u & -Z_w & -Z_q & 0 \\ -M_u & -M_w & -M_q & \overline{BG}_z W \\ 0 & 0 & -1 & 0 \end{bmatrix} \begin{bmatrix} u \\ w \\ q \\ \theta \end{bmatrix} = \begin{bmatrix} X(t) \\ Z(t) \\ M(t) \\ 0 \end{bmatrix}$$

Here $X(t)$, $Z(t)$ and $M(t)$ are externally applied disturbances.

(2) Equations of Lateral Motion

The lateral equations of motion describe the vehicle's motion in sway, roll and yaw. They are written as:

$$\begin{bmatrix} m-Y_{\dot v} & -mz_G-Y_{\dot p} & mx_G-Y_{\dot r} & 0 & 0 \\ -mz_G-Y_{\dot p} & Ix-K_{\dot p} & -Izx-K_{\dot r} & 0 & 0 \\ mx_G-Y_{\dot r} & -Izx-K_{\dot r} & Iz-N_{\dot r} & 0 & 0 \\ 0 & 0 & 0 & 1 & 0 \\ 0 & 0 & 0 & 0 & 1 \end{bmatrix} \begin{bmatrix} \dot v \\ \dot p \\ \dot r \\ \dot\phi \\ \dot\psi \end{bmatrix} + \begin{bmatrix} -Y_v & -Y_p & -Y_r & 0 & 0 \\ -K_v & -K_p & -K_r & \overline{BG}_x W & 0 \\ -N_v & -N_p & -N_r & -\overline{BG}_x W & 0 \\ 0 & -1 & 0 & 0 & 0 \\ 0 & 0 & -1 & 0 & 0 \end{bmatrix} \begin{bmatrix} v \\ p \\ r \\ \phi \\ \psi \end{bmatrix} = \begin{bmatrix} Y(t \\ K(t \\ N(t \\ 0 \\ 0 \end{bmatrix}$$

Here $Y(t)$, $K(t)$ and $N(t)$ are externally applied disturbances.

This representation can also be used to describe the linear motion of ships.

Linear Ship Steering Equations of Motion

The standard linear ship steering equations of motion are usually obtained by neglecting the roll mode from the general linear expression for the lateral motion, Åström and Källström (1976), Källström (1979), Blanke (1981) etc. The 3 DOF equations of motion can be written as:

$$\begin{bmatrix} m-Y_{\dot v} & mx_G-Y_{\dot r} & 0 \\ mx_G-N_{\dot v} & Iz-N_{\dot r} & 0 \\ 0 & 0 & 1 \end{bmatrix} \begin{bmatrix} \dot v \\ \dot r \\ \dot\psi \end{bmatrix} + \begin{bmatrix} -Y_v & mu_o-Y_r & 0 \\ -N_v & mx_G u_o-N_r & 0 \\ 0 & -1 & 0 \end{bmatrix} \begin{bmatrix} v \\ r \\ \psi \end{bmatrix} = \begin{bmatrix} Y_\delta \\ N_\delta \\ 0 \end{bmatrix} \delta$$

which corresponds to the compact form:

$$\boldsymbol{M}\ddot{\boldsymbol{x}} + \boldsymbol{D}\dot{\boldsymbol{x}} = \boldsymbol{B}\,\delta$$

Here $\boldsymbol{x} = (v, r, \psi)^T$ is the state vector, δ is the rudder angle and $u = u_o = constant$ is the ship's service speed. Note that for ships it is common to use a non-symmetric inertia matrix i.e. $Y_{\dot r} \neq N_{\dot v}$. Especial care most be taken since $\boldsymbol{D}$ can be *negative definite* in this representation. This is due to the fact that $\boldsymbol{D}$ consists of both Coriolis terma ($mu_o r$) and damping terms (Y_v, Y_r, N_v, N_r). Indeed, the off-diagonal term $u_o > 0$ can make the matrix negative definite. The corresponding state space representation is

$$\begin{bmatrix} \dot v \\ \dot r \\ \dot\psi \end{bmatrix} = \begin{bmatrix} a_{11} & a_{12} & 0 \\ a_{21} & a_{22} & 0 \\ 0 & 1 & 0 \end{bmatrix} \begin{bmatrix} v \\ r \\ \psi \end{bmatrix} + \begin{bmatrix} b_1 \\ b_2 \\ 0 \end{bmatrix} \delta$$

It follows that the transfer function relating the rudder angle and heading angle can be written as:

$$h(s) = \frac{\psi(s)}{\delta(s)} = \frac{K(1 + T_3 s)}{s(1 + T_1 s)(1 + T_2 s)}$$

For large tankers this expression is usually approximated as:

$$h(s) = \frac{K}{s(1 + Ts)}$$

which is the so-called Nomoto model. Nonlinear versions of the ship steering equations are discussed by Abkowitz (1964), Norrbin (1970), Blanke (1981), Zhou (1987), etc.

Standard Equations of Motion for Underwater Vehicle Simulation

In Kalske (1989) a survey of the motion dynamics of subsea vehicles is given. This report includes a survey of the equations of motion for submarine simulation and remotely operated vehicles. Modelling and simulation of small underwater vehicles are discussed in Lewis *et al.* (1984). A detailed description of the nonlinear and linear motion dynamics of the University of New-Hampshire Experimental Underwater Vehicle (UNH-EAVE) is found in Humphreys and Watkinson (1982). The Norwegian Experimental Remotely Operated Vehicle (NEROV) nonlinear equations of motion, Fossen and Sagatun (1991c), are given in Appendix A. The standard equations of motion for submarine simulation from the David Taylor Model Basin Naval Ship Research and Development Center (DTMSRDC) are described in detail by Gertler and Hagen (1967) and Feldman (1979).

Chapter 3

Disturbance Analysis

This chapter discusses deterministic and random disturbances. Statistical descriptions of waves and root-mean-square (RMS) analyses are discussed in depth. The wave disturbance model used in this chapter is general enough to be applied to most marine vehicles. For simplicity, the linear ship steering equations of motion are used in the numerical example.

3.1 Linear Equations of Motion

Consider the linear state space model of a marine vehicle

$$\begin{aligned} \dot{\boldsymbol{x}} &= \boldsymbol{A}\boldsymbol{x} + \boldsymbol{C}\boldsymbol{v} \\ \boldsymbol{y} &= \boldsymbol{D}\boldsymbol{x} + \boldsymbol{w} \quad \text{with} \quad \boldsymbol{W} = E(\boldsymbol{w}(t)\boldsymbol{w}^T(\tau)) \end{aligned} \tag{3.1}$$

where $\boldsymbol{x}$ is the state vector, $\boldsymbol{v}$ is the disturbance vector and $\boldsymbol{y}$ is the output vector. The more general state space model

$$\begin{aligned} \dot{\boldsymbol{x}} &= \boldsymbol{A}\boldsymbol{x} + \boldsymbol{B}\boldsymbol{u} + \boldsymbol{C}\boldsymbol{v} \\ \boldsymbol{y} &= \boldsymbol{D}\boldsymbol{x} + \boldsymbol{w} \end{aligned}$$

where $\boldsymbol{u}$ is the control input vector e.g. chosen as

$$\boldsymbol{u} = \boldsymbol{G}_1\boldsymbol{x} + \boldsymbol{G}_2\boldsymbol{v}$$

can also be expressed in the form of Eq. 3.1, since

$$\begin{aligned} \dot{\boldsymbol{x}} &= (\boldsymbol{A} + \boldsymbol{B}\boldsymbol{G}_1)\boldsymbol{x} + (\boldsymbol{C} + \boldsymbol{B}\boldsymbol{G}_2)\boldsymbol{v} \\ \boldsymbol{y} &= \boldsymbol{D}\boldsymbol{x} + \boldsymbol{w} \end{aligned} \tag{3.2}$$

Hence, we will exclusively consider systems with no control inputs.

3.2 Disturbance Descriptions

It is convenient to distinguish between deterministic and random disturbances. These two disturbance descriptions are briefly described in this section.

3.2.1 Responses to Deterministic Disturbances

Responses of the system states $\boldsymbol{x}(t)$ and outputs $\boldsymbol{y}(t)$ can be derived for arbitrary disturbances $\boldsymbol{v}(t)$ by using the Duhamel integral or by time convolution. We have

$$\boldsymbol{x}(t) = e^{\boldsymbol{A}t}\boldsymbol{x}(0) + \int_o^t e^{\boldsymbol{A}(t-\tau)}\boldsymbol{C}\ \boldsymbol{v}(\tau)\ d\tau$$

and

$$\boldsymbol{y}(t) = \boldsymbol{D}e^{\boldsymbol{A}t}\boldsymbol{x}(0) + \int_o^t \boldsymbol{D}e^{\boldsymbol{A}(t-\tau)}\boldsymbol{C}\ \boldsymbol{v}(\tau)\ d\tau + \boldsymbol{w}(t)$$

3.2.2 Responses to Random Disturbances

If the disturbances are random variables with statistical mean $E(\boldsymbol{v}(t)) = \overline{\boldsymbol{v}}(t)$ and covariance matrix $E(\boldsymbol{v}(t)\boldsymbol{v}^T(\tau)) = \boldsymbol{V}(t,\tau)$, then the response of the system states and outputs will have to be described in statistical terms. It can be shown that the mean is (assuming $\boldsymbol{x}(0)$ and $\boldsymbol{v}(t)$ to be uncorrelated)

$$\overline{\boldsymbol{x}}(t) = e^{\boldsymbol{A}t}\boldsymbol{x}(0) + \int_o^t e^{\boldsymbol{A}(t-\tau)}\boldsymbol{C}\ \overline{\boldsymbol{v}}(\tau)\ d\tau$$

while the covariance matrix is

$$E(\boldsymbol{x}(t)\boldsymbol{x}^T(\tau)) = e^{\boldsymbol{A}t}E(\boldsymbol{x}(0)\boldsymbol{x}^T(0))e^{\boldsymbol{A}^T\tau} + \int_o^t\int_o^\tau e^{\boldsymbol{A}(t-\tau)}\boldsymbol{C}E(\boldsymbol{v}(\tau)\boldsymbol{v}^T(s))\boldsymbol{C}^T e^{\boldsymbol{A}^T(\tau-s)}\ d\tau ds$$

A special solution is obtained if $\boldsymbol{v}(t)$ is white-noise i.e. $E(\boldsymbol{v}(t)\boldsymbol{v}^T(\tau)) = \boldsymbol{V}_o\boldsymbol{\delta}(t-\tau)$. The steady-state covariance matrix of the system states is defined as

$$\boldsymbol{X} = \lim_{t\to\infty} E(\boldsymbol{x}(t)\boldsymbol{x}^T(\tau))$$

which satisfies the Lyapunov equation

$$\boldsymbol{A}\boldsymbol{X} + \boldsymbol{X}\boldsymbol{A}^T + \boldsymbol{C}\boldsymbol{V}_o\boldsymbol{C}^T = 0$$

provided that $\boldsymbol{A}$ is stable. In a similar manner, the steady-state output covariance matrix is defined as

$$\boldsymbol{Y} = \lim_{t\to\infty} E(\boldsymbol{y}(t)\boldsymbol{y}^T(\tau))$$

which yields (assuming $E(\boldsymbol{w}(t)\boldsymbol{w}^T(\tau)) = \boldsymbol{W}_o$)

$$\boldsymbol{Y} = \boldsymbol{D}\boldsymbol{X}\boldsymbol{D}^T + \boldsymbol{W}_o$$

3.2.3 Power Spectral Density Definitions

The system outputs can be written as

$$\boldsymbol{y}(s) = \boldsymbol{H}(s)\boldsymbol{v}(s) \quad \text{where} \quad \boldsymbol{H}(s) = \boldsymbol{D}(s\boldsymbol{I} - \boldsymbol{A})^{-1}\boldsymbol{C}$$

The power spectral density (PSD) is defined as

$$\boldsymbol{\Phi_{yy}}(\omega) = \boldsymbol{H}(j\omega)\boldsymbol{\Phi_{vv}}(\omega)\boldsymbol{H}^*(j\omega)$$

where $\boldsymbol{H}^*(j\omega) = \boldsymbol{H}^T(-j\omega)$. For monovariable systems the PSD is simply

$$\phi_{yy}(\omega) = |h(j\omega)|^2\, \phi_{vv}(\omega)$$

The PSD describes how the output energy is distributed at different frequencies. If $\boldsymbol{v}$ is white noise, it can be shown that the mean-square response of the output y_i is equal to the area under the corresponding PSD curve i.e.

$$Y_{ii} = \lim_{t\to\infty} E(y_i(t)y_i^T(\tau)) = \sigma_{y_i}^2 = \frac{1}{\pi}\int_o^\infty \Phi_{y_iy_i}(\omega)\, d\omega$$

where σ_{y_i} is the root mean square (RMS) of output y_i. In a similar manner the cross covariance is defined as

$$Y_{ij} = \lim_{t\to\infty} E(y_i(t)y_j^T(\tau)) = \frac{1}{\pi}\int_o^\infty \Phi_{y_iy_j}(\omega)\, d\omega$$

The requirement that $\boldsymbol{v}(t)$ should be white noise can be relaxed by simply generating $\boldsymbol{v}(t)$ as

$$\boldsymbol{v}(s) = \boldsymbol{H}_v(s)\boldsymbol{\eta}(s)$$

with $\boldsymbol{\eta}(s)$ as white noise. Hence, $\boldsymbol{v}(s)$ can be can be used to describe coloured noise by defining an adequate transfer function matrix $\boldsymbol{H}_v(s)$. This is the topic for the next sections.

3.3 Statistical Description of Waves

The wave elevation of a long-crested irregular sea propagating along the positive x-axis can be written as the sum of a large number of wave components i.e.

$$\zeta = \sum_{j=1}^{N} A_j \sin(\omega_j t - k_j x + \epsilon_j) \tag{3.3}$$

where, A_j is the wave amplitude, ω_j is the wave frequency, ϵ_j is a random phase angle and

$$k_j = \frac{2\pi}{\lambda_j}$$

is the wave number, with λ_j as the wave length. The wave amplitude can be expressed as a wave spectrum $S(\omega)$ as

$$A_j^2 = 2S(\omega_j)\Delta\omega$$

where, $\Delta\omega$ is a constant difference between successive frequencies. The instantaneous wave elevation is Gaussian distributed with zero mean and variance σ^2 defined as:

$$\sigma^2 = \int_o^\infty S(\omega)\, d\omega$$

The wave spectrum can be estimated from wave measurements. For fully developed seas it is common to use the so-called Pierson-Moskowitz (PM) spectrum, Myrhaug (1986), which can be expressed as:

$$S(\omega) = \frac{A}{\omega^5}\, e^{-(B/\omega^4)}$$

where A and B can depend on a variety of parameters. The PM-spectrum is shown in Figure 3.1. Some classifications are as follows:

- **The Pierson-Moskowitz (PM) Spectrum.** A frequently used one-parameter description of the (PM) spectrum for fully developed sea (North-Atlantic Ocean) is

  $$A = 0.0081\, g^2 \qquad B = 0.74\, (\frac{g}{U})^4$$

  where U is the velocity of the wind 19.5 m over the water surface.

- **The ITTC (International Towing Tank Conference) Spectrum.** Instead of using the velocity of the wind as a parameter, significant wave height $H_{1/3}$ (mean of the highest one third of the waves) can be used. The ITTC spectrum is defined as:

  $$A = 0.0081\, g^2 \qquad B = 0.0323\, (\frac{g}{H_{1/3}})^2 = \frac{3.11}{H_{1/3}^2}$$

  The relationship between $H_{1/3}$ and U is:

  $$H_{1/3} = 0.21\, \frac{U^2}{g}$$

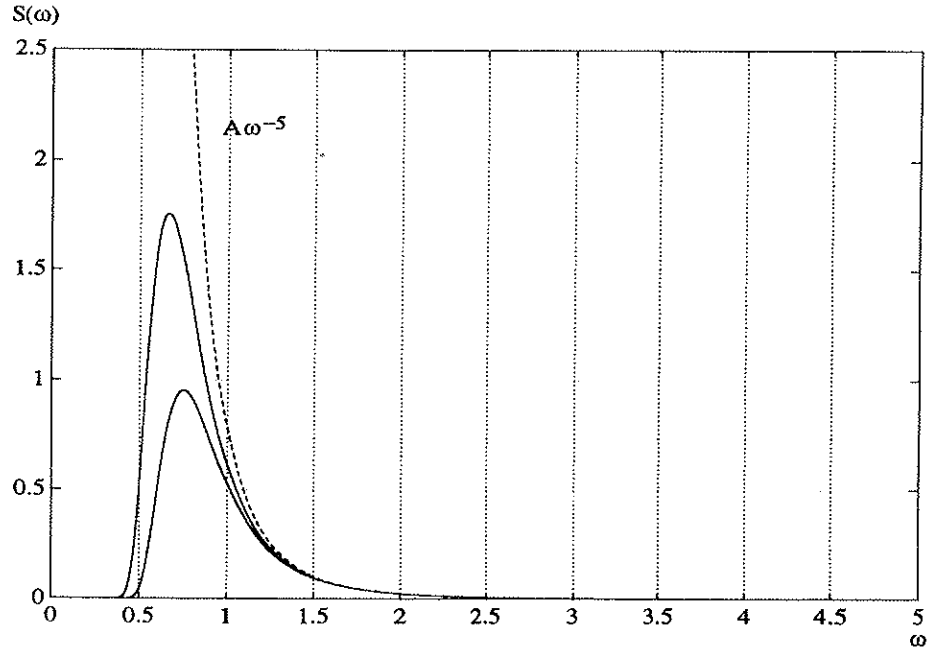

Figure 3.1: PM-spectrum: $S(\omega) = \frac{A}{\omega^5}\, e^{-(B/\omega^4)}$.

- **The ISSC (International Ship and Offshore Structure Congress) Spectrum.** This representation uses the mean frequency $\overline{\omega}$ i.e. the frequency corresponding to the spectrum's centre of area. The parameters are

$$A = 0.11\, H_{1/3}^2\, \overline{\omega}^4 \qquad B = 0.44\, \overline{\omega}^4$$

Hence, the mean wave period is defined as $\overline{T} = \frac{2\pi}{\overline{\omega}}$.

- **JONSWAP (Joint North Sea Wave Project) Spectrum.**

The JONSWAP spectrum can be used to describe a not fully developed sea. Thus, the JONSWAP spectrum is more peaked than the fully developed spectra. The parameters in the JONSWAP spectrum are based on measurements from the North Sea (finite water depth). The parameters are

$$A = \alpha\, g^2 \qquad B = \frac{5}{4}\, \omega_P^4$$

where, $\alpha = 0.0081$ for the PM-spectrum. The peak frequency ω_P is related to the velocity of the wind as:

$$\omega_P = 0.87\,\frac{g}{U}$$

The peak value of the JONSWAP spectrum is increased by multiplying $S(\omega)$ with a factor

$$\gamma^{exp\left[-\frac{1}{2}\left(\frac{\omega-\omega_P}{\sigma\,\omega_P}\right)^2\right]}$$

where

$1 < \gamma < 7$ where $\gamma = \dfrac{S(\omega_P)_{JONSWAP}}{S(\omega_P)_{PM}}$

$\sigma = \begin{cases} \sigma_a & \text{for } \omega \leq \omega_P \\ \sigma_b & \text{for } \omega > \omega_P \end{cases}$

α is a parameter which is used to shape the high frequency part of the spectrum

ω_P is the peak frequency

Hasselmann et al. (1973) suggest the following values for the spectrum's parameters:

$$\gamma = 3.3$$
$$\sigma_a = 0.07 \text{ and } \sigma_b = 0.09$$
$$\alpha = 0.076\left(\frac{g\,x}{U^2}\right)^{-0.22}$$
$$\omega_P = 7.0\,\pi\left(\frac{g}{U}\right)\left(\frac{g\,x}{U^2}\right)^{-0.33}$$

where x is the length of the water surface exposed to wind and U is the velocity of the wind.

We can simulate irregular sea by using the following expression for the horizontal fluid velocity component, Faltinsen (1990a),

$$u_f = \sum_{j=1}^{N} \omega_j A_j e^{k_j z} \sin(\omega_j t - k_j x + \epsilon_j)$$

Here ω_j should be chosen as a random frequency in each frequency interval $(\omega_j - \Delta\omega/2, \omega_j + \Delta\omega/2)$ to avoid the expressions repeating themselves. ϵ_j is a random phase angle. N should be chosen as a large number, typically $N = 1000$. This depends on the selection of the maximum and minimum frequency components. The wave elevation is found from Eq. 3.3.

3.4 Applications to Marine Vehicles

In this section we will show how root-mean-square analyses can be used when designing autopilots.

Linear Approximation of the PM-Spectrum

A linear approximation of the PM spectrum can be obtained by writing

$$y(s) = h(s)\,\eta(s) \quad , \quad \eta(s) \text{ is white noise}$$

$$\phi_{yy}(\omega) = |h(j\omega)|^2\,\phi_{\eta\eta} = |h(j\omega)|^2$$

Here $y(s)$ is the wave amplitude and $\eta(s)$ is a white noise source with power spectrum

$$\phi_{\eta\eta}(\omega) = 1.0$$

Sælid *et al.* (1983) suggest choosing the transfer function $h(s)$ as

$$h(s) = \frac{2\zeta\sigma(\frac{s}{\omega_o})}{1 + 2\zeta(\frac{s}{\omega_o}) + (\frac{s}{\omega_o})^2} \tag{3.4}$$

where σ, ζ and ω_o are the spectrum's parameters. Hence, substituting $s = j\omega$ yields

$$h(j\omega) = \frac{j2\zeta\sigma(\frac{\omega}{\omega_o})}{(1 - (\frac{\omega}{\omega_o})^2) + j2\zeta(\frac{\omega}{\omega_o})}$$

This in turn implies that

$$|h(j\omega)| = \frac{2\zeta\sigma(\frac{\omega}{\omega_o})}{\sqrt{(1 - (\frac{\omega}{\omega_o})^2)^2 + 4\zeta^2(\frac{\omega}{\omega_o})^2}}$$

Hence,

$$\phi_{yy}(\omega) = |h(j\omega)|^2\,\phi_{\eta\eta}(\omega) = \frac{4\zeta^2\sigma^2(\frac{\omega}{\omega_o})^2}{(1 - (\frac{\omega}{\omega_o})^2)^2 + 4\zeta^2(\frac{\omega}{\omega_o})^2}$$

From this it is seen that $\phi_{yy}(0) = 0$ and that the maximum value of $\phi_{yy}(\omega)$ is obtained for $\omega = \omega_o$ i.e.

$$\max_{\omega} \phi_{yy}(\omega) = \phi_{yy}(\omega_o) = \sigma^2$$

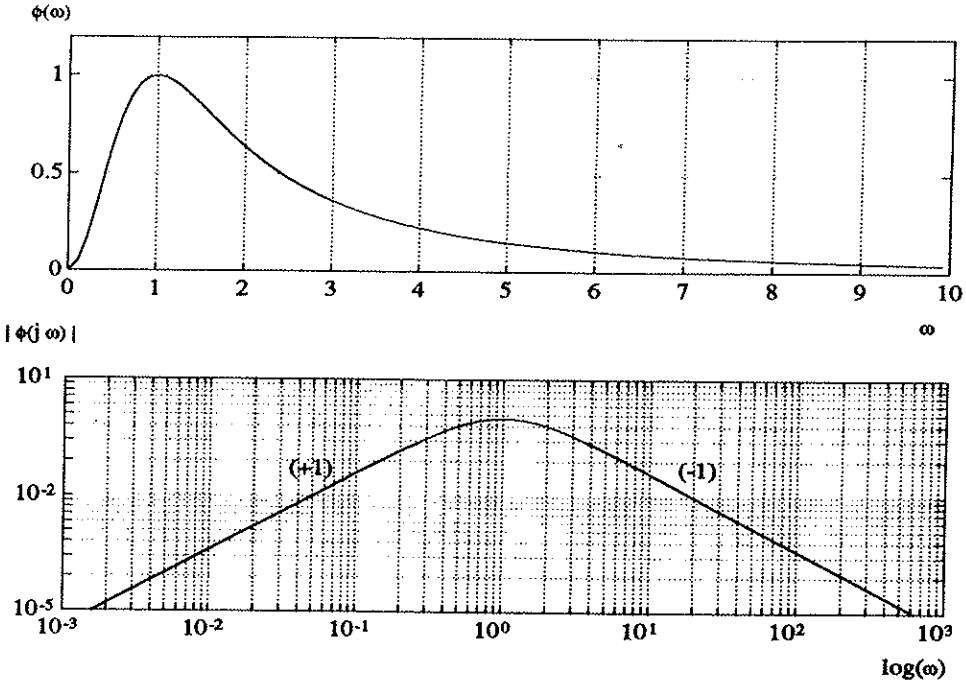

Figure 3.2: Wave spectrum approximation ($\omega_o = 1$, $\zeta = 1$ and $\sigma = 1$).

A linear state space model can be derived from

$$\dot{y} + 2\zeta\omega_o\, y + \omega_o^2 \int_o^t y(\tau)\, d\tau = 2\zeta\sigma\omega_o\, \eta$$

by letting $x_1 = \int_o^t y(\tau)\, d\tau$ and $x_2 = y$. Hence,

$$\begin{bmatrix} \dot{x}_1 \\ \dot{x}_2 \end{bmatrix} = \begin{bmatrix} 0 & 1 \\ -\omega_o^2 & -2\zeta\omega_o \end{bmatrix} \begin{bmatrix} x_1 \\ x_2 \end{bmatrix} + \begin{bmatrix} 0 \\ 2\zeta\sigma\omega_o \end{bmatrix} \eta$$

$$y = \begin{bmatrix} 0 & 1 \end{bmatrix} \begin{bmatrix} x_1 \\ x_2 \end{bmatrix}$$

The transfer function, Eq. 3.4, cannot be used to generate $\dot{y}$. This is easily seen from

$$\lim_{s\to\infty} s\, y(s) = 2\zeta\sigma\omega_o$$

Nevertheless, this problem can be solved by using the strictly proper transfer function:

$$\frac{\dot{y}}{\eta}(s) = \frac{2\zeta\sigma(\frac{s}{\omega_o})\, s}{(1 + 2\zeta(\frac{s}{\omega_o}) + (\frac{s}{\omega_o})^2)^2}$$

Example: Horizontal Motion of a Ship

Consider the linear ship steering equations of motion

$$\begin{bmatrix} \dot{v} \\ \dot{r} \\ \dot{\psi} \end{bmatrix} = \begin{bmatrix} a_{11} & a_{12} & 0 \\ a_{21} & a_{22} & 0 \\ 0 & 1 & 0 \end{bmatrix} \begin{bmatrix} v - v_f \\ r \\ \psi \end{bmatrix} + \begin{bmatrix} b_1 \\ b_2 \\ 0 \end{bmatrix} \delta$$

Let the fluid velocity component v_f in the y-direction be described by

$$\frac{v_f}{\eta}(s) = \frac{k\, s^2}{(a + b\, s + s^2)^2} \quad , \quad \eta(s) \text{ is white noise}$$

This in turn implies that

$$(s^2 + 2\, b\, s + (2a + b^2) + 2ab\, s^{-1} + a^2\, s^{-2})\, v_f(s) = k\, \eta(s)$$

Augmenting the ship steering equations of motion with the wave disturbance model, yields

$$\begin{bmatrix} \dot{v} \\ \dot{r} \\ \dot{\psi} \\ \dot{x}_{1,f} \\ \dot{x}_{2,f} \\ \dot{x}_{3,f} \\ \dot{x}_{4,f} \end{bmatrix} = \begin{bmatrix} a_{11} & a_{12} & 0 & 0 & 0 & -a_{11} & 0 \\ a_{21} & a_{22} & 0 & 0 & 0 & -a_{21} & 0 \\ 0 & 1 & 0 & 0 & 0 & 0 & 0 \\ 0 & 0 & 0 & 0 & 1 & 0 & 0 \\ 0 & 0 & 0 & 0 & 0 & 1 & 0 \\ 0 & 0 & 0 & -a^2 & -2ab & -(2a + b^2) & -2b \end{bmatrix} \begin{bmatrix} v \\ r \\ \psi \\ x_{1,f} \\ x_{2,f} \\ x_{3,f} \\ x_{4,f} \end{bmatrix} + \begin{bmatrix} b_1 \\ b_2 \\ 0 \\ 0 \\ 0 \\ 0 \\ 0 \end{bmatrix} \delta + \begin{bmatrix} 0 \\ 0 \\ 0 \\ 0 \\ 0 \\ 0 \\ k \end{bmatrix} \eta$$

If the heading angle ψ is measured by a flux-gate compass, for instance, the corresponding measurement equation is:

$$\psi = [\, 0\, 0\, 1\, 0\, 0\, 0\, 0\,] \begin{bmatrix} v \\ r \\ \psi \\ x_{1,f} \\ x_{2,f} \\ x_{3,f} \\ x_{4,f} \end{bmatrix} + w$$

Numerical Values:

Consider the following model of a typical cargo vessel, Åström and Wittenmark (1989),

$$\begin{array}{lll} a_{11} = -0.77 & a_{12} = -0.34 & b_1 = 0.17 \\ a_{21} = -3.39 & a_{22} = -1.63 & b_2 = -1.63 \end{array}$$

Let the wave disturbance model be described by: $a = c = k = 1$ and $b = 2$. Hence,

$$\boldsymbol{A} = \begin{bmatrix} -0.77 & -0.34 & 0 & 0 & 0 & 0.77 & 0 \\ -3.99 & -1.63 & 0 & 0 & 0 & 3.99 & 0 \\ 0 & 1 & 0 & 0 & 0 & 0 & 0 \\ 0 & 0 & 0 & 0 & 1 & 0 & 0 \\ 0 & 0 & 0 & 0 & 0 & 1 & 0 \\ 0 & 0 & 0 & 0 & 0 & 0 & 1 \\ 0 & 0 & 0 & -1 & -4 & -6 & -4 \end{bmatrix} \quad \boldsymbol{B} = \begin{bmatrix} 0.17 \\ -1.63 \\ 0 \\ 0 \\ 0 \\ 0 \\ 0 \end{bmatrix}$$

$$\boldsymbol{C} = \begin{bmatrix} 0 & 0 & 0 & 0 & 0 & 0 & 1 \end{bmatrix}^T \qquad \boldsymbol{D} = \begin{bmatrix} 0 & 0 & 1 & 0 & 0 & 0 & 0 \end{bmatrix}$$

The system eigenvalues are

$$\lambda(\boldsymbol{A}) = \begin{Bmatrix} 0 \\ -2.4416 \\ 0.0416 \\ -1 \\ -1 \\ -1 \\ -1 \end{Bmatrix}$$

which implies that the vehicle is open-loop unstable. A simple PD-controller

$$u = \boldsymbol{G}\boldsymbol{x} \quad , \quad \boldsymbol{G} = [\, 0\ 3\ 1\ 0\ 0\ 0\ 0 \,]$$

can be used to stabilize the ship. This yields the following closed-loop eigenvalues

$$\lambda(\boldsymbol{A} + \boldsymbol{B}\boldsymbol{G}) = \begin{Bmatrix} -0.6746 \\ -0.4661 \\ -6.1493 \\ -1 \\ -1 \\ -1 \\ -1 \end{Bmatrix}$$

Solving the Lyapunov equation

$$(\boldsymbol{A}+\boldsymbol{BG})\boldsymbol{X}+\boldsymbol{X}(\boldsymbol{A}+\boldsymbol{BG})^T+\boldsymbol{C}\boldsymbol{V}_o\boldsymbol{C}^T=0$$

with $\boldsymbol{V}_o=\boldsymbol{I}$*, yields the steady-state covariance matrix:*

$$\boldsymbol{X}=\begin{bmatrix} 0.0115 & -0.0009 & 0.0072 & -0.0188 & 0.0127 & 0.0101 & -0.0196 \\ -0.0009 & 0.0079 & 0.0000 & -0.0056 & -0.0073 & 0.0120 & 0.0058 \\ 0.0072 & -0.0000 & 0.0051 & -0.0126 & 0.0056 & 0.0073 & -0.0120 \\ -0.0188 & -0.0056 & -0.0126 & 0.1563 & -0.0000 & -0.0313 & 0.0000 \\ 0.0127 & -0.0073 & 0.0056 & -0.0000 & 0.0313 & -0.0000 & -0.0312 \\ 0.0101 & 0.0120 & 0.0073 & -0.0313 & 0.0000 & 0.0312 & 0.0000 \\ -0.0196 & 0.0058 & -0.0120 & 0.0000 & -0.0313 & -0.0000 & 0.1563 \end{bmatrix}$$

Hence, the expression for the steady-state output covariance matrix:

$$\boldsymbol{Y}=\boldsymbol{D}\boldsymbol{X}\boldsymbol{D}^T$$

yields

$$Y_{\psi\psi}=0.0051$$

This in turn implies that:

$$\sigma_{\psi\psi}=\sqrt{Y_{\psi\psi}}=0.0712$$

If we want to calculate the RMS-value for the lateral acceleration $a_{y_{cg}}$*, c.f. Eq. 2.13, we must consider the expression*

$$a_{y_{cg}}=\dot{v}+u_o r$$

where u_o *is the ship's service speed. By using the fact that* $\dot{v}$ *is*

$$\dot{v}=a_{21}(v-v_f)+a_{22}r+b_2g_2r+b_2g_3\psi$$

we obtain

$$\boldsymbol{D}=[\ a_{21}\ \ (a_{22}+b_2g_2+u_o)\ \ b_2g_3\ \ 0\ \ \ 0\ \ -a_{21}\ \ \ 0\ ]$$

Hence, the RMS-value for the lateral acceleration $a_{y_{cg}}$ *with* $u_o=5m/s$ *is*

$$\sigma_{a_{ycg}a_{ycg}}=0.0492\ g$$

According to Table 3.2 this satisfies the lateral acceleration requirement for "intellectual work". The vertical acceleration criterion can be checked in a similar manner by considering the vehicle's longitudinal equations of motion i.e. the state vector $\boldsymbol{x} = (u, w, q, \phi, \theta)^T$.

Operability Limiting Criteria for Marine Vehicles

Some operability limiting criteria for marine vehicles based on RMS-values are shown in Table 3.1 and 3.2.

Table 3.1: General operability limiting criteria for marine vehicles, Faltinsen (1990a).

	Merchant ships	Naval vessels	Fast small craft
Vertical acceleration at forward perpendicular (RMS-value)	0.275 g (L $\leq$ 100 m) 0.05 g (L $\geq$ 330 m) [1]	0.275 g	0.65 g
Vertical acceleration at bridge (RMS-value)	0.15 g	0.2 g	0.275 g
Lateral acceleration at bridge (RMS-value)	0.12 g	0.1 g	0.1 g
Roll (RMS-value)	6.0 deg	4.0 deg	4.0 deg

Table 3.2: Criteria with regard to accelerations and roll, Faltinsen (1990a).

Root mean square criterion			
Vertical acceleration	Lateral acceleration	Roll	Description
0.20 g	0.10 g	6.0 deg	Light manual work
0.15 g	0.07 g	4.0 deg	Heavy manual work
0.10 g	0.05 g	3.0 deg	Intellectual work
0.05 g	0.04 g	2.5 deg	Transit passengers
0.02 g	0.03 g	2.0 deg	Cruise liner

[1] The limiting criterion for lengths between 100 and 330 m varies almost linearly between the values L = 100m and L = 330 m, where L is the length of the ship.

Chapter 4

Stability Analysis

4.1 Basic Stability Definitions

Stability of an underwater vehicle can be defined as the ability of returning to an equilibrium state of motion after a disturbance without any corrective action, such as use of thruster power or control surfaces. Hence, manoeuvrability can be defined as the capability of the vehicle to carry out specific manoeuvres. Excessive stability implies that the control effort will be excessive while a marginally stable vehicle is easy to control. Thus, a compromise between stability and manoeuvrability must be made. For aircraft as well as underwater vehicles it is common to distinguish between *stick-fixed* and *stick-free* stability. These terms can be understood as:

- **Stick-fixed stability** implies investigating the vehicle's stability when the control surfaces are fixed and when the thrust from all the thrusters is constant.
- **Stick-free stability** refers to the case when both the control surfaces and the thruster power are allowed to vary. This implies that the dynamics of the control system also must be considered in the stability analysis.

These terms will be described more closely in the next sections.

4.1.1 Straight line, Directional and Position Motion Stability

Straight line, directional and position motion stability can be understood by considering a linear second order system in the form:

$$m\ddot{x} + d\dot{x} + kx = f(t)$$

Here m is the mass, $d\dot{x}$ represent the damping force, kx is the restoring force and $f(t)$ is a function of external disturbances and control inputs. From a physical point of view,

mass is known to be positive ($m > 0$) and damping is known to be dissipative ($d > 0$). The eigenvalues $\lambda_{1,2}$, the natural frequency ω and the damping ratio ζ for the second order system are:

$$\lambda_{1,2} = \frac{-d \mp \sqrt{d^2 - 4mk}}{2m}; \qquad \omega = \sqrt{\frac{k}{m}}; \qquad \zeta = \frac{d}{2\sqrt{k\,m}}$$

In control and guidance applications stability can be classified according to how external disturbances affect the vehicle's motion. The following cases are of particular interest, c.f. Figure 4.1:

- **Instability (k < 0):** For the unstable vehicle one of the eigenvalues will have a positive real part. This occurs when $Re\{\lambda_1\} < 0$ and $Re\{\lambda_2\} > 0$.

- **Straight Line Stability (k = 0):**

  Consider an uncontrolled underwater vehicle moving in a straight path. If the new path is straight after a disturbance in yaw the vehicle is said to have straight line stability. The direction of the new path will usually differ from the initial path because no restoring forces are present. This property is observed in surge, sway, heave and yaw for marine vehicles. The eigenvalues are: $\lambda_1 = -\frac{d}{m} < 0$ and $\lambda_2 = 0$.

- **Directional Stability (k > 0):**

  Directional stability is a much stronger requirement than straight line stability. Directional stability requires the final path to be parallel to the initial path. The vehicle is said to be directionally stable if both eigenvalues have negative real parts i.e. $Re\{\lambda_{1,2}\} < 0$. Two types of directional stability are observed:

  1. **Non-oscillatoric ($d^2 - 4mk \geq 0$):**
     This implies that both eigenvalues are negative and real.
  2. **Oscillatoric ($d^2 - 4mk < 0$):**
     This corresponds to two imaginary eigenvalues with negative real parts.

  Directional stability is observed for the uncontrolled vehicle in roll and pitch where metacentric restoring forces are present. For a fully submerged vehicle the condition $k > 0$ simply implies that the centre of gravity must be below the centre of buoyancy. Directional stability in yaw cannot be obtained without corrective action from a control system, for example.

- **Positional Motion Stability**

  Positional motion stability implies that the underwater vehicle should return to its original path after a disturbance. This is generally impossible in surge, sway, heave and yaw for an uncontrolled submersible without using thrust or control surfaces.

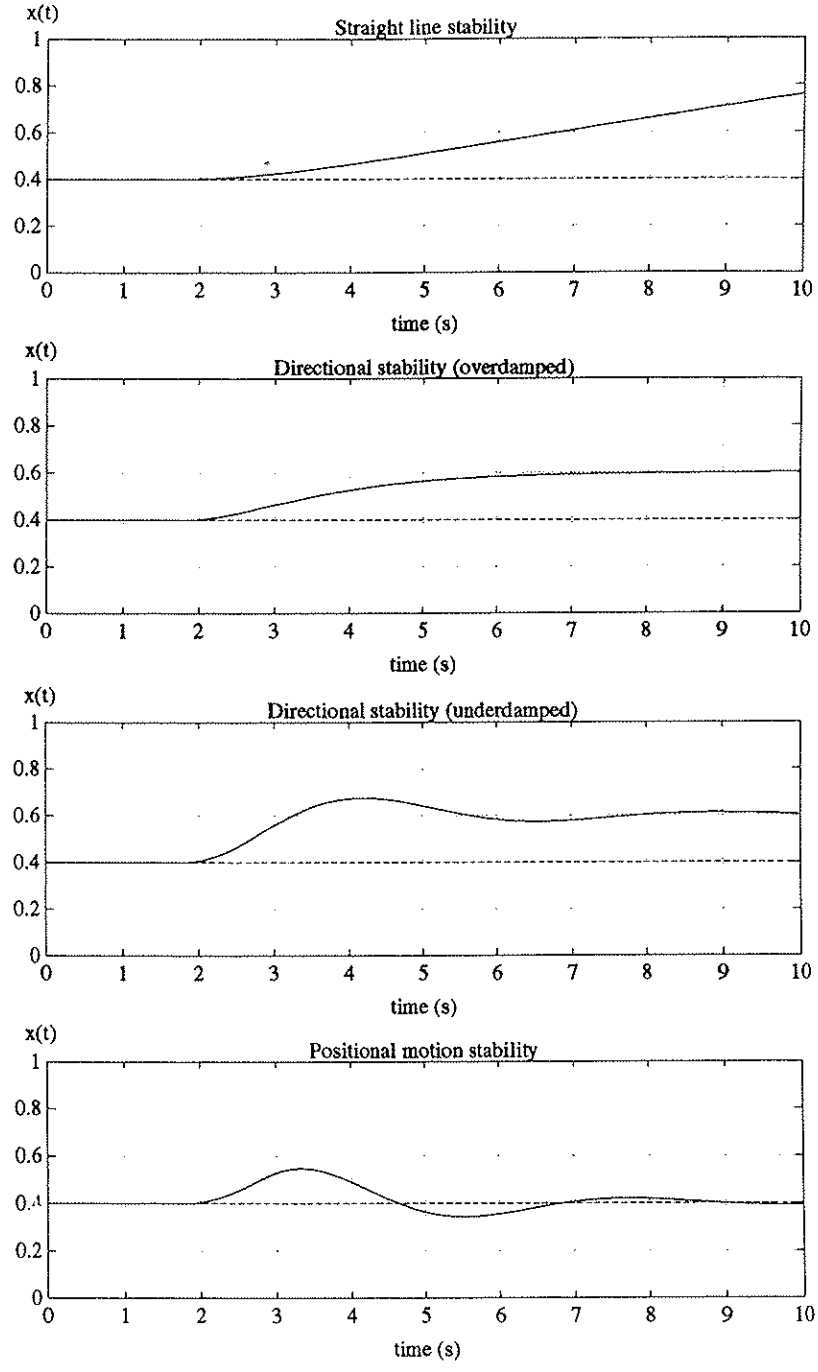

Figure 4.1: Straight line, directional and position motion stability for a typical small underwater vehicle when a constant disturbance $f(t) = v_o$ is injected for $t \geq 2\ s$.

4.1.2 Metacentric Stability

A frequently used term in hydrostatics is metacentric stability. For underwater vehicles the transition period i.e. the period when the vehicle is diving from a surfaced position to the vehicle is completed submerged, is of particular interest. Consider a surfaced vehicle where G denotes the centre of gravity, B denotes the centre of buoyancy, K is the keel line and M is the vehicle's metacentre. Hence, it is straightforward to verify that, c.f. Figure 4.2,

$$\begin{aligned} \overline{GM}_T &= \overline{KB} + \overline{BM}_T - \overline{KG} \\ \overline{GM}_L &= \overline{KB} + \overline{BM}_L - \overline{KG} \end{aligned}$$

where the subscripts T and L denote transverse and lateral quantities, respectively.

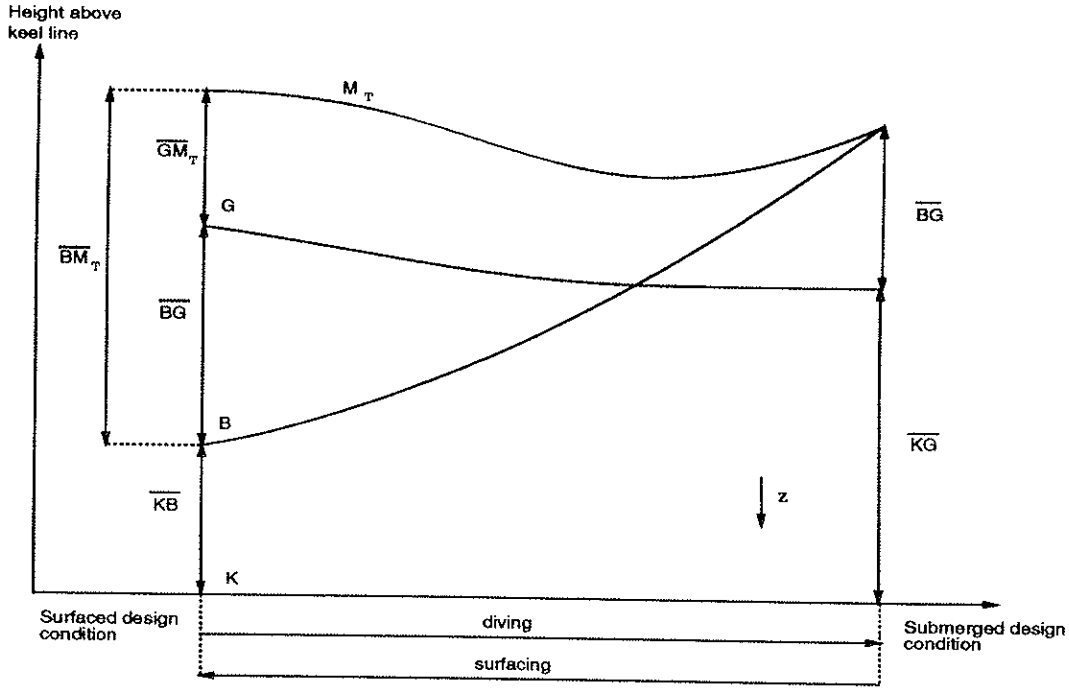

Figure 4.2: Transverse transition stability, Allmendinger (1990).

For small roll and pitch angles $\overline{BM}_T$ and $\overline{BM}_L$ are given by

$$\overline{BM}_T = \frac{I_x}{\nabla} \qquad \overline{BM}_L = \frac{I_y}{\nabla}$$

where I_x and I_y are the moments of area of the waterplane about the x- and y-axes, respectively and ∇ is the volume of the displaced water. For surfaced marine vehicles transverse and longitudinal metacentric stability are obtained by requiring that, Allmendinger (1990):

$$\overline{GM}_T > 0 \qquad \overline{GM}_L > 0$$

Transverse metacentric stability implies that the vehicle will return to its original path after a disturbance in roll while lateral metacentric stability guarantees stability of the pitching motion. For a completely submerged vehicle, the conditions $\overline{GM}_T > 0$ and $\overline{GM}_L > 0$ simply reduce to

$$\overline{BG} > 0$$

which is the well known requirement that the centre of gravity should be below the centre of buoyancy for a metacentric stable underwater vehicle. This is shown in Figure 4.2.

4.1.3 Longitudinal Stability Criterion

In the stability analysis of underwater vehicles it is convenient to use the linearized equations of motion such that the well known stability techniques of Routh and Hurwitz, for example, can be applied. It is also desirable to use a non-dimensional version of the equations of motion based on $U^2 = u^2 + v^2 + w^2$, since the hydrodynamic derivatives depend upon the square of the forward speed. Another parameter used in the scaling procedure is the vehicle's length L. Hence, the non-dimensional time could be defined as $t' = \frac{U}{L}t$. The non-dimensional system will be described as the "prime-system". Consider the non-dimensional longitudinal equations of motion

$$\begin{bmatrix} m' - X'_{\dot{u}} & -X'_{\dot{w}} & m'z'_G - X'_{\dot{q}} & 0 \\ -X'_{\dot{w}} & m' - Z'_{\dot{w}} & -m'x'_G - Z'_{\dot{q}} & 0 \\ m'z'_G - X'_{\dot{q}} & -m'x'_G - Z'_{\dot{q}} & I'_y - M'_{\dot{q}} & 0 \\ 0 & 0 & 0 & 1 \end{bmatrix} \begin{bmatrix} \dot{u}' \\ \dot{w}' \\ \dot{q}' \\ \dot{\theta}' \end{bmatrix} + \begin{bmatrix} -X'_u & -X'_w & -X'_q & 0 \\ -Z'_u & -Z'_w & -Z'_q & 0 \\ -M'_u & -M'_w & -M'_q & m'\gamma_z \\ 0 & 0 & -1 & 0 \end{bmatrix} \begin{bmatrix} u' \\ w' \\ q' \\ \theta' \end{bmatrix} = \begin{bmatrix} X'(t) \\ Z'(t) \\ M'(t) \\ 0 \end{bmatrix}$$

where the prime notation denotes the non-dimensional quantities defined as:

$$\begin{array}{lllll} u' = \frac{u}{U} & w' = \frac{w}{U} & q' = \frac{qL}{U} & \theta' = \theta & m' = \frac{m}{\frac{1}{2}\rho L^3} \\ x'_G = \frac{x_G}{L} & z'_G = \frac{z_G}{L} & \gamma_z = \frac{g\overline{BG}_z}{U^2} & X'_{\dot{u}} = \frac{X_{\dot{u}}}{\frac{1}{2}\rho L^3} & X'_{\dot{w}} = \frac{X_{\dot{w}}}{\frac{1}{2}\rho L^3} \\ X'_{\dot{q}} = \frac{X_{\dot{q}}}{\frac{1}{2}\rho L^5} & I'_y = \frac{I_y}{\frac{1}{2}\rho L^5} & Z'_{\dot{w}} = \frac{Z_{\dot{w}}}{\frac{1}{2}\rho L^3} & Z'_{\dot{q}} = \frac{Z_{\dot{q}}}{\frac{1}{2}\rho L^5} & M'_{\dot{q}} = \frac{M_{\dot{q}}}{\frac{1}{2}\rho L^5} \\ X'_u = \frac{X_u}{\frac{1}{2}\rho UL^2} & X'_w = \frac{X_w}{\frac{1}{2}\rho UL^2} & X'_q = \frac{X_q}{\frac{1}{2}\rho UL^3} & Z'_u = \frac{Z_u}{\frac{1}{2}\rho UL^2} & Z'_w = \frac{Z_w}{\frac{1}{2}\rho UL^2} \\ Z'_q = \frac{Z_q}{\frac{1}{2}\rho UL^4} & M'_u = \frac{M_u}{\frac{1}{2}\rho UL^3} & M'_w = \frac{M_w}{\frac{1}{2}\rho UL^3} & M'_q = \frac{M_q}{\frac{1}{2}\rho UL^4} & \end{array}$$

From the longitudinal equations of motion the pure pitching motion can be expressed as

$$(I_y - M_{\dot{q}})\,\ddot{\theta} - M_q\,\dot{\theta} + \overline{BG}_z W\,\theta = M^*(t)$$

where all interactions and disturbances are collected in the term $M^*(t)$. This equation can be used to describe the oscillatoric behaviour in pitch. Let the characteristic equation of the second-order pitching motion be written as:

$$\lambda^2 + 2\zeta_\theta \, \omega_\theta \, \lambda + \omega_\theta^2 = 0.$$

The roots of the characteristic equation are

$$\lambda_{1,2} = -\zeta_\theta \, \omega_\theta \pm j \, \omega_\theta \sqrt{1 - \zeta_\theta^2}$$

Hence, the natural frequency ω_θ and the damping ratio ζ_θ for the pitching motion are:

$$\omega_\theta = \sqrt{\frac{\overline{BG}_z W}{I_y - M_{\dot{q}}}}; \qquad \zeta_\theta = \frac{-M_q}{2\sqrt{\overline{BG}_z W (I_y - M_{\dot{q}})}}$$

This in turn implies that the natural period in pitch can be expressed as

$$T_\theta = \frac{2\pi}{\omega_\theta} = 2\pi \sqrt{\frac{I_y - M_{\dot{q}}}{\overline{BG}_z W}}$$

This expression is quite useful when designing marine vehicles. It is seen that a reduction in the moment of inertia $(I_y - M_{\dot{q}})$ or an increase of the vertical distance between the centre of gravity and centre of buoyancy $\overline{BG}_z$, and the vehicle's weight W, will reduce the natural pitch period. To derive a stability criterion for the overall longitudinal motion, let us consider the quatric characteristic equation

$$A\lambda^4 + B\lambda^3 + C\lambda^2 + D\lambda + E = 0$$

corresponding to the longitudinal equations of motion. After some laborious calculations, the following expressions were found for the coefficients A, B, C, D and E:

$$\begin{aligned}
A &= m_{11}m_{33}m_{55} - m_{15}^2 m_{33} + 2m_{13}m_{15}m_{35} - m_{11}m_{35}^2 - m_{13}^2 m_{55} \\
B &= -d_{55}m_{13}^2 + d_{35}m_{13}m_{15} + d_{53}m_{13}m_{15} - d_{33}m_{15}^2 + d_{55}m_{11}m_{33} - d_{15}m_{15}m_{33} - d_{51}m_{15}m_{33} \\
&\quad -d_{35}m_{11}m_{35} - d_{53}m_{11}m_{35} + d_{15}m_{13}m_{35} + d_{51}m_{13}m_{35} + d_{13}m_{15}m_{35} + d_{31}m_{15}m_{35} - d_{11}m_{35}^2 \\
&\quad +d_{33}m_{11}m_{55} - d_{13}m_{13}m_{55} - d_{31}m_{13}m_{55} + d_{11}m_{33}m_{55} \\
C &= m\gamma_z(m_{11}m_{33} - m_{13}^2) + -d_{35}d_{53}m_{11} + d_{33}d_{55}m_{11} + d_{35}d_{51}m_{13} + d_{15}d_{53}m_{13} - d_{13}d_{55}m_{13} \\
&\quad -d_{31}d_{55}m_{13} - d_{15}d_{33}m_{15} + d_{13}d_{35}m_{15} - d_{33}d_{51}m_{15} + d_{31}d_{53}m_{15} - d_{15}d_{51}m_{33} + d_{11}d_{55}m_{33} \\
&\quad +d_{15}d_{31}m_{35} - d_{11}d_{35}m_{35} + d_{13}d_{51}m_{35} - d_{11}d_{53}m_{35} - d_{13}d_{31}m_{55} + d_{11}d_{33}m_{55} \\
D &= -d_{15}d_{33}d_{51} + d_{13}d_{35}d_{51} + d_{15}d_{31}d_{53} - d_{11}d_{35}d_{53} - d_{13}d_{31}d_{55} + d_{11}d_{33}d_{55} \\
&\quad +m\gamma_z(d_{33}m_{11} - d_{13}m_{13} - d_{31}m_{13} + d_{11}m_{33}) \\
E &= m\gamma_z(d_{11}d_{33} - d_{13}d_{31})
\end{aligned}$$

Here m_{ij} and d_{ij} are the elements of the non-dimensional inertia matrix $\boldsymbol{M}'$ and damping matrix $\boldsymbol{D}'$, respectively. The longitudinal stability criterion can be derived by requiring that the roots of the characteristic quatric have negative real parts. A simple way to do this is by applying Routh's stability criterion. Forming the so-called Routh array from the characteristic quatric yields:

$$\begin{array}{lll} A & C & E \\ B & D & 0 \\ \frac{BC-AD}{B} & E & 0 \\ \frac{D(BC-AD)-B^2E}{BC-AD} & 0 & \\ E & & \end{array}$$

Hence, sufficient and necessary conditions for the underwater vehicle to be stable are:

$$\begin{array}{ll} \text{(i)} & A, B, C, D, E > 0 \\ \text{(ii)} & BC - AD > 0 \\ \text{(iii)} & D(BC - AD) - B^2E > 0 \end{array}$$

This corresponds to requiring that all coefficients should be positive and that the elements in the first column of the Routh array should be positive. The first condition $A > 0$ is automatically satisfied because A is recognized as the determinant of the inertia matrix which is known to be positive. Since the vehicle is a dissipative system, we have:

$$\begin{vmatrix} d_{11} & d_{13} \\ d_{31} & d_{33} \end{vmatrix} = \begin{vmatrix} -X'_u & -X'_w \\ -Z'_u & -Z'_w \end{vmatrix} = X'_u Z'_w - X'_w Z'_u > 0$$

Hence, the condition $E > 0$ reduces to $m\gamma_z > 0$ which is satisfied if:

$$\overline{BG}_z > 0$$

This expression simply states that the centre of gravity should be vertically below the centre of buoyancy. Indeed, this is the well known condition for *metacentric stability* of a fully submerged vehicle. At high speed $\gamma_z \to 0$ which implies that the stability quatric becomes a cubic polynomial. This can be explained by the vehicle being oscillatoric at low speed (directional stable) while at infinite speed the vehicle only has straight-line stability.

4.1.4 Lateral Stability Criterion

Recall that the lateral equations of motion were written as:

$$\begin{bmatrix} m'-Y'_{\dot{v}} & -m'z'_G-Y'_{\dot{p}} & m'x'_G-Y'_{\dot{r}} & 0 & 0 \\ -m'z'_G-Y'_{\dot{p}} & I'_x-K'_{\dot{p}} & -I'_{xz}-K'_{\dot{r}} & 0 & 0 \\ m'x'_G-Y'_{\dot{r}} & -I'_{xz}-K'_{\dot{r}} & I'_z-N'_{\dot{r}} & 0 & 0 \\ 0 & 0 & 0 & 1 & 0 \\ 0 & 0 & 0 & 0 & 1 \end{bmatrix} \begin{bmatrix} \dot{v}' \\ \dot{p}' \\ \dot{r}' \\ \dot{\phi}' \\ \dot{\psi}' \end{bmatrix} + \begin{bmatrix} -Y'_v & -Y'_p & -Y'_r & 0 & 0 \\ -K'_v & -K'_p & -K'_r & m'\gamma_z & 0 \\ -N'_v & -N'_p & -N'_r & -m'\gamma_x & 0 \\ 0 & -1 & 0 & 0 & 0 \\ 0 & 0 & -1 & 0 & 0 \end{bmatrix} \begin{bmatrix} v' \\ p' \\ r' \\ \phi' \\ \psi' \end{bmatrix} = \begin{bmatrix} Y'(t) \\ K'(t) \\ N'(t) \\ 0 \\ 0 \end{bmatrix}$$

where the prime denotes the non-dimensional quantities defined in a similar manner as in the longitudinal case. It is straightforward to verify that the vehicle's rolling motion can be described by:

$$(I_x - K_{\dot{p}})\,\ddot{\phi} - K_p\,\dot{\phi} + \overline{BG}_z W\,\phi = K^*(t)$$

Here all cross-coupling terms and disturbances are collected in the term $K^*(t)$. Hence, the natural frequency ω_ϕ and the damping ratio ζ_ϕ for the rolling motion are:

$$\omega_\phi = \sqrt{\frac{\overline{BG}_z W}{I_x - K_{\dot{p}}}}; \qquad \zeta_\phi = \frac{-K_p}{2\sqrt{\overline{BG}_z W (I_x - K_{\dot{p}})}}$$

which suggests the following expression for the natural period of the oscillatoric behaviour in roll:

$$T_\phi = \frac{2\pi}{\omega_\phi} = 2\pi \sqrt{\frac{I_x - K_{\dot{p}}}{\overline{BG}_z W}}$$

The characteristic equation corresponding to the lateral equations of motion can be expressed as:

$$(A\lambda^4 + B\lambda^3 + C\lambda^2 + D\lambda + E)\,\lambda = 0$$

where

$$\begin{aligned}
A &= m_{22}m_{44}m_{66} - m_{26}^2 m_{44} + 2m_{24}m_{26}m_{46} - m_{22}m_{46}^2 - m_{24}^2 m_{66} \\
B &= -d_{66}m_{24}^2 + d_{46}m_{24}m_{26} + d_{64}m_{24}m_{26} - d_{44}m_{26}^2 + d_{66}m_{22}m_{44} - d_{26}m_{26}m_{44} - d_{62}m_{26}m_{44} \\
&\quad -d_{46}m_{22}m_{46} - d_{64}m_{22}m_{46} + d_{26}m_{24}m_{46} + d_{62}m_{24}m_{46} + d_{24}m_{26}m_{46} + d_{42}m_{26}m_{46} - d_{22}m_{46}^2 \\
&\quad +d_{44}m_{22}m_{66} - d_{24}m_{24}m_{66} - d_{42}m_{24}m_{66} + d_{22}m_{44}m_{66} \\
C &= -d_{46}d_{64}m_{22} + d_{44}d_{66}m_{22} + d_{46}d_{62}m_{24} + d_{26}d_{64}m_{24} - d_{24}d_{66}m_{24} - d_{42}d_{66}m_{24} + d_{24}d_{46}m_{26} \\
&\quad -d_{44}d_{26}m_{26} - d_{44}d_{62}m_{26} + d_{42}d_{64}m_{26} - d_{26}d_{62}m_{44} + d_{22}d_{66}m_{44} - d_{22}d_{46}m_{46} + d_{42}d_{26}m_{46} \\
&\quad +d_{24}d_{62}m_{46} - d_{22}d_{64}m_{46} - d_{24}d_{42}m_{66} + d_{22}d_{44}m_{66} \\
&\quad +m\gamma_z(m_{22}m_{66} - m_{26}^2) + m\gamma_x(m_{22}m_{46} - m_{24}m_{26}) \\
D &= d_{24}d_{46}d_{62} - d_{44}d_{26}d_{62} - d_{22}d_{46}d_{64} + d_{42}d_{26}d_{64} - d_{24}d_{42}d_{66} + d_{22}d_{44}d_{66} \\
&\quad +m\gamma_x(d_{46}m_{22} - d_{26}m_{24} - d_{42}m_{26} + d_{22}m_{46}) + m\gamma_z(d_{66}m_{22} - d_{26}m_{26} - d_{62}m_{26} + d_{22}m_{66}) \\
E &= m\gamma_x(d_{22}d_{46} - d_{42}d_{26}) + m\gamma_z(d_{22}d_{66} - d_{26}d_{62})
\end{aligned}$$

Here m_{ij} and d_{ij} are the elements of the non-dimensional inertia matrix $\boldsymbol{M}'$ and damping matrix $\boldsymbol{D}'$, respectively. Hence, the lateral stability criterion is derived by forming a Routh array similar to the longitudinal case, which yields:

$$\begin{array}{ll} \text{(i)} & A, B, C, D, E > 0 \\ \text{(ii)} & BC - AD > 0 \\ \text{(iii)} & D(BC - AD) - B^2 E > 0 \end{array}$$

These are the necessary and sufficient conditions for stick-fixed stability. As in the longitudinal case, the condition $A > 0$ is trivial due to the positiveness of the inertia matrix while the condition $E > 0$ simply states that:

$$\frac{\overline{BG}_x}{\overline{BG}_z} > \frac{Y'_v N'_r - Y'_r N'_v}{Y'_r K'_v - Y'_v K'_r}$$

At infinite speed $\gamma_x \to 0$ and $\gamma_z \to 0$. This in turn implies that $E \to 0$. Hence, the metacentric righting moment in the rolling motion is lost. We also note that metacentric stability has no effect on the yawing motion. The longitudinal and lateral stability criteria indicate whether a submarine is stable or not, but they give little or no indication as to the degree of stability.

4.1.5 Stability Requirements Based on Eigenvalues

In stick-fixed stability analyses, the eigenstructure decomposition can be used to determine whether the nonlinear system is local stable. The fundamental way to do this is by applying Lyapunov's linearization method which was published in 1893 by the Russian mathematician Alexandr Mikhailovich Lyapunov. Lyapunov's work (*Problème Gènèrale de la Stabilitè de Mouvement*) includes both Lyapunov's linearization method and Lyapunov's direct method. A translation of this work is found in Lyapunov (1907). Consider the nonlinear system

$$\dot{\boldsymbol{x}} = \boldsymbol{f}(\boldsymbol{x})$$

which can be linearized around the equilibrium point $\boldsymbol{x} = 0$ as:

$$\dot{\boldsymbol{x}} = \boldsymbol{A}\boldsymbol{x} + \boldsymbol{f}_{h.o.t.} \qquad \boldsymbol{A} = \left(\frac{\partial \boldsymbol{f}}{\partial \boldsymbol{x}}\right)_{\boldsymbol{x}=0}$$

Let the eigenvalues be denoted as λ. Then the following theorem can be used to determine if the original nonlinear system is locally stable at the equilibrium point $\boldsymbol{x} = 0$.

Theorem 1 (Lyapunov's Linearization Method)

- *If the linearized system is strictly stable i.e.*

$$Re\{\lambda_i(A)\} < 0 \quad for \quad i = 1..n$$

then the equilibrium point is asymptotically stable for the nonlinear system.

- *If the linearized system is marginally stable i.e.*

$$Re\{\lambda_i(A)\} \leq 0 \quad for \quad i = 1..n$$

then the equilibrium point may be stable, asymptotically stable or unstable for the nonlinear system.

- *If the linearized system is unstable i.e.*

$$Re\{\lambda_i(A)\} > 0 \quad for\ some \quad i$$

then the equilibrium point is unstable for the nonlinear system.

It should be noted that for marine vehicles the A matrix will depend on the vehicle's speed. This suggests that the linear model should be made non-dimensional before an eigenstructure decomposition is performed. A typical plot of the open loop poles (eigenvalues) of a metacentric stable underwater vehicle is shown in Figure 4.3. The two complex conjugate poles represent the rolling and pitching motion, respectively. For a metacentric stable vehicle their real parts will be strictly negative while they are positive for the metacentric unstable vehicle. The 4 negative real poles correspond to stable modes in surge, sway, heave and yaw while the 4 multiple poles in the origin are caused by pure integrations of the linear and angular velocities in surge, sway, heave and yaw.

4.2 Nonlinear Stability Theory

Nonlinear stability analysis of underwater vehicles is non-trivial due to the relatively complex structure of the nonlinear underwater vehicle equations of motion. Nevertheless, advanced Lyapunov theory for autonomous and non-autonomous systems is applicable in both the stick-fixed and stick-free stability analysis.

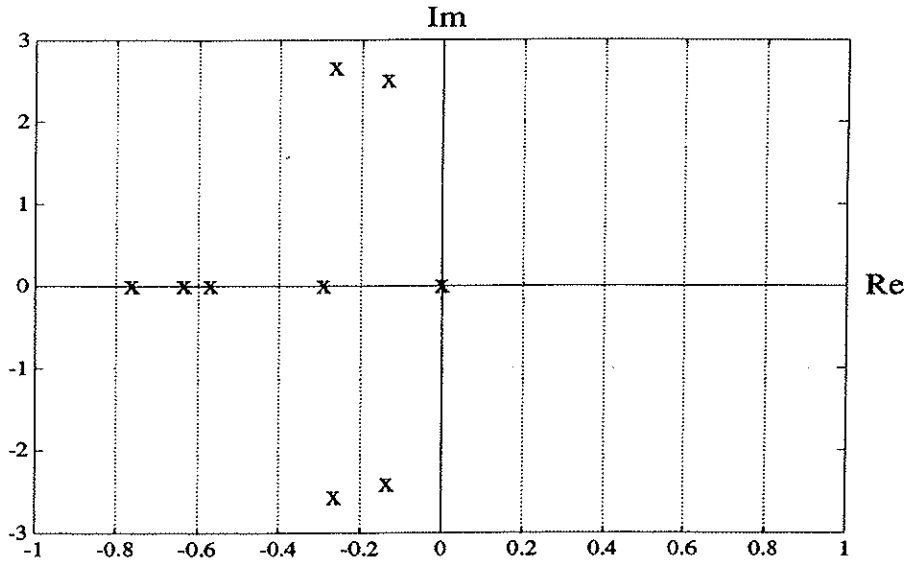

Figure 4.3: A typical plot of the open-loop poles of a metacentric stable underwater vehicle.

4.2.1 Lyapunov's Direct Method Applied to Stick-Fixed Stability Analyses

Stick-fixed stability analyses for marine vehicles concerns the problem of finding stability criteria based on the hydrodynamic derivatives. For a linear model of ships this is quite simple, thanks to the well known techniques of Routh and Hurwitz. This section shows that an alternative approach based on Lyapunov's direct method, Lyapunov (1907), can be applied in the nonlinear case. Indeed, this approach also verifies well known criteria for linear stick-fixed stability. Lyapunov' s direct method only has validation for autonomous systems. A nonlinear system is said to be *autonomous* if the system's state equation can be expressed as

$$\dot{\boldsymbol{x}} = \boldsymbol{f}(\boldsymbol{x})$$

where the nonlinear function $\boldsymbol{f}$ is not allowed to explicitly depend on time. For such systems, a scalar Lyapunov function can be applied to determine whether the system is stable or not. *Lyapunov's direct method* for autonomous systems, see e.g. Balchen (1990) or Slotine and Li (1991), simply states:

Theorem 2 (Lyapunov's Theorem for Global Stability)
Assume that there exists a scalar function $V(\boldsymbol{x})$ with continuous first derivatives satisfying:

- $V(\boldsymbol{x})$ *is positive definite*
- $\dot{V}(\boldsymbol{x})$ *is negative definite*
- $V(\boldsymbol{x}) \rightarrow \infty$ *as* $||\boldsymbol{x}|| \rightarrow \infty$

then the equilibrium point $\boldsymbol{x}^*$ satisfying $\boldsymbol{f}(\boldsymbol{x}^*) = 0$ is globally asymptotic stable.

For marine vehicles the Lyapunov function V can be chosen to represent the system's total mechanical energy. Consider the Lyapunov function candidate

$$V(\boldsymbol{x}, \dot{\boldsymbol{x}}) = \frac{1}{2}\, \dot{\boldsymbol{x}}^T\, \boldsymbol{M}^*(\boldsymbol{x})\, \dot{\boldsymbol{x}} + \int_o^{\boldsymbol{x}} \boldsymbol{g}^*(\boldsymbol{z})\, d\boldsymbol{z}$$

where $\boldsymbol{M}^*$ and $\boldsymbol{g}^*$ are defined in Eq. 2.42. V can be interpreted as the sum of the kinetic and potential energy of the vehicle. Hence, zero energy corresponds to the equilibrium point $\boldsymbol{x} = 0$ and $\dot{\boldsymbol{x}} = 0$. Instability corresponds to a growth in mechanical energy while asymptotic stability implies the convergence of mechanical energy to zero. Differentiating V with respect to time (assuming $\boldsymbol{M}^* = (\boldsymbol{M}^*)^T$) yields:

$$\dot{V} = \dot{\boldsymbol{x}}^T\, (\boldsymbol{M}^*(\boldsymbol{x})\ddot{\boldsymbol{x}} + \boldsymbol{g}^*(\boldsymbol{x})) + \frac{1}{2}\, \dot{\boldsymbol{x}}^T\, \dot{\boldsymbol{M}}^*\, \dot{\boldsymbol{x}}$$

Hence the expression for $\dot{V}$ can be rewritten as:

$$\dot{V} = \dot{\boldsymbol{x}}^T\, (\boldsymbol{M}^*(\boldsymbol{x})\ddot{\boldsymbol{x}} + \boldsymbol{C}^*(\boldsymbol{x}, \dot{\boldsymbol{x}})\dot{\boldsymbol{x}} + \boldsymbol{g}^*(\boldsymbol{x})) + \frac{1}{2}\dot{\boldsymbol{x}}^T(\dot{\boldsymbol{M}}^* - 2\boldsymbol{C}^*(\boldsymbol{x}, \dot{\boldsymbol{x}}))\, \dot{\boldsymbol{x}}$$

Applying the skew-symmetric property: $\dot{\boldsymbol{x}}^T\, (\dot{\boldsymbol{M}}^* - 2\boldsymbol{C}^*)\, \dot{\boldsymbol{x}} = 0 \;\; \forall \;\; \dot{\boldsymbol{x}}$, yields

$$\dot{V} = \dot{\boldsymbol{x}}^T\, (\boldsymbol{M}^*\ddot{\boldsymbol{x}} + \boldsymbol{C}^*(\boldsymbol{x}, \dot{\boldsymbol{x}})\dot{\boldsymbol{x}} + \boldsymbol{g}^*(\boldsymbol{x}))$$

In stick-fixed stability analyses, the dynamics of the control inputs is neglected. Hence, we simply consider the autonomous system:

$$\boldsymbol{M}^*(\boldsymbol{x})\ddot{\boldsymbol{x}} + \boldsymbol{C}^*(\dot{\boldsymbol{x}}, \boldsymbol{x})\dot{\boldsymbol{x}} + \boldsymbol{D}^*(\dot{\boldsymbol{x}}, \boldsymbol{x})\dot{\boldsymbol{x}} + \boldsymbol{g}^*(\boldsymbol{x}) = 0$$

Applying this equation to the expression for $\dot{V}$, finally yields:

$$\dot{V} = -\dot{\boldsymbol{x}}^T \boldsymbol{D}^* \dot{\boldsymbol{x}}$$

According to Theorem 2, sufficient conditions for stick-fixed stability (assuming $\boldsymbol{J}(\boldsymbol{x})$ to be non-singular) are:

(i) $\boldsymbol{M}^* = \boldsymbol{J}^{-T}\boldsymbol{M}\boldsymbol{J}^{-1} > 0$ which is satisfied if the inertia matrix $\boldsymbol{M} > 0$.

(ii) $\boldsymbol{D}^* = \boldsymbol{J}^{-T}\boldsymbol{D}\boldsymbol{J}^{-1} > 0$ which is satisfied if the damping matrix $\boldsymbol{D} > 0$.

The first condition simply states that the inertia of the system must be positive definite. Indeed, this is satisfied for marine vehicles. The second condition simply states the system must be dissipative. A special solution to these results is obtained by considering the well known linear ship steering equations of motion.

Example: Application to the Linear Ship Dynamics

The above derived stick-fixed stability criterion can easily be related to the vehicle's hydrodynamic derivatives. This is best illustrated by considering the linear ship steering equations of motion. Linearizing the ship dynamics about the constant forward speed $u = u_o$ and assuming that $\boldsymbol{M} = \boldsymbol{M}^T$ suggests the model

$$\boldsymbol{M}\ddot{\boldsymbol{q}} + \boldsymbol{D}\dot{\boldsymbol{q}} = 0$$

where

$$\begin{bmatrix} m - Y_{\dot{v}} & mx_G - Y_{\dot{r}} \\ mx_G - N_{\dot{v}} & Iz - N_{\dot{r}} \end{bmatrix} \begin{bmatrix} \dot{v} \\ \dot{r} \end{bmatrix} + \begin{bmatrix} -Y_v & mu_o - Y_r \\ -N_v & mx_G u_o - N_r \end{bmatrix} \begin{bmatrix} v \\ r \end{bmatrix} = 0$$

Notice, that the two terms mu_o and $mx_G u_o$ arising from the linearization of the $\boldsymbol{C}$ matrix, are included in the $\boldsymbol{D}$ matrix instead. This is done to avoid the difficulties with the skew-symmetric property which is violated i.e. $C_{ij} \neq -C_{ji}$, when we are only considering 2 DOF (sway and yaw). Requiring that $det(\boldsymbol{D}) > 0$ yields:

$$Y_v(N_r - mx_G u_o) - N_v(Y_r - mu_o) > 0$$

This verifies the well known stability condition of Abkowitz (1964), for the straight line stability of ships.

4.2.2 Barbălat's Lyapunov-Like Lemma Applied to Stick-Free Stability Analyses

Lyapunov's direct method cannot be applied to non-autonomous systems. By *non-autonomous systems* we mean systems that can be expressed as

$$\dot{\boldsymbol{x}} = \boldsymbol{f}(\boldsymbol{x}, t)$$

where $\boldsymbol{f}$ explicitly depends on the time t. Stability analysis techniques for non-autonomous system can be used to study the motion stability of a system tracking a time-varying reference

trajectory. It is well known that the motion stability problem can be transformed into an equivalent stability problem around an equilibrium point by considering the system's error dynamics instead of the system's state dynamics. Although the original system is autonomous, tracking of time-varying trajectories implies that the equivalent system will be non-autonomous. For non-autonomous systems it is convenient to use Barbălat's lemma to prove global stability, Barbălat (1959):

Lemma 1 (Barbălat's Lemma)
If the function $g(t)$ has a finite limit as $t \to \infty$, is differentiable and $\dot{g}(t)$ is uniformly continuous, then $\dot{g}(t) \to 0$ as $t \to \infty$.

A Lyapunov-like version of Barbălat's lemma is found in Slotine and Li (1991):

Lemma 2 (Barbălat's Lyapunov-Like Lemma for Global Stability)
Assume that there exists a scalar function $V(\boldsymbol{x}, t)$ satisfying:

- *$V(\boldsymbol{x}, t)$ is lower bounded*
- *$\dot{V}(\boldsymbol{x}, t)$ is negative semi-definite*
- *$\dot{V}(\boldsymbol{x}, t)$ is uniformly continuous in time*

then $\dot{V}(\boldsymbol{x}, t) \to 0$ as $t \to \infty$.

Sufficient conditions for the first and last condition are:

Remark 1 (Lower boundness)
A sufficient condition for the scalar function $V(\boldsymbol{x}, t)$ to be lower bounded is that $V(\boldsymbol{x}, t)$ is positive semi-definite i.e.

$$V(\boldsymbol{x}, t) \geq 0 \qquad \forall\, t \geq t_0$$

Remark 2 (Uniform Continuity)
A sufficient condition for a differentiable function $\dot{V}(\boldsymbol{x}, t)$ to be uniformly continuous is that its derivative $\ddot{V}(\boldsymbol{x}, t)$ is bounded $\forall\, t \geq t_o$.

In this section, it will be shown how Barbălat's Lyapunov-like lemma can be used in stick-free stability analysis of underwater vehicles. The design methodology is best illustrated by considering a simple example.

Example: Nonlinear Feedback Linearization

Assume that we want to control the vehicle's linear and angular velocities. Let the error dynamics be denoted as $\dot{\tilde{\boldsymbol{q}}} = \dot{\boldsymbol{q}} - \dot{\boldsymbol{q}}_d$ *where* $\dot{\boldsymbol{q}}_d$ *is the desired state vector. For mechanical systems, Slotine and Li (1987) suggest defining a Lyapunov-like function candidate:*

$$V(\dot{\tilde{\boldsymbol{q}}}, t) = \frac{1}{2}\, \dot{\tilde{\boldsymbol{q}}}^T \boldsymbol{M} \dot{\tilde{\boldsymbol{q}}}$$

which can be interpreted as the "pseudo kinetic" energy of the vehicle. Differentiating V *with respect to time (assuming* $\boldsymbol{M} = \boldsymbol{M}^T$*) yields:*

$$\dot{V} = \dot{\tilde{\boldsymbol{q}}}^T \left(\boldsymbol{M} \ddot{\tilde{\boldsymbol{q}}} + \boldsymbol{C}(\dot{\boldsymbol{q}}) \dot{\tilde{\boldsymbol{q}}} \right)$$

Here we have used the skew-symmetric property: $\dot{\tilde{\boldsymbol{q}}}^T (\dot{\boldsymbol{M}} - 2\boldsymbol{C}) \dot{\tilde{\boldsymbol{q}}} = 0 \;\; \forall \;\; \dot{\tilde{\boldsymbol{q}}}$*. Substituting Eq. 2.38 into the expression for* $\dot{V}$ *yields:*

$$\dot{V} = \dot{\tilde{\boldsymbol{q}}}^T \left(\boldsymbol{B}\boldsymbol{u} - \boldsymbol{M}\ddot{\boldsymbol{q}}_d - \boldsymbol{C}\dot{\boldsymbol{q}}_d - \boldsymbol{D}\dot{\boldsymbol{q}}_d - \boldsymbol{g} \right) - \dot{\tilde{\boldsymbol{q}}}^T \boldsymbol{D} \dot{\tilde{\boldsymbol{q}}}$$

This suggests that the control law should be selected as

$$\boldsymbol{u} = \boldsymbol{B}^{+} (\boldsymbol{M}\ddot{\boldsymbol{q}}_d + \boldsymbol{C}\dot{\boldsymbol{q}}_d + \boldsymbol{D}\dot{\boldsymbol{q}}_d + \boldsymbol{g} - \boldsymbol{K}_D \dot{\tilde{\boldsymbol{q}}})$$

where $\boldsymbol{K}_D$ *is a positive definite regulator gain matrix of appropriate dimension. Hence,*

$$\dot{V} = -\dot{\tilde{\boldsymbol{q}}}^T \left(\boldsymbol{D} + \boldsymbol{K}_D \right) \dot{\tilde{\boldsymbol{q}}} \;\leq\; 0$$

Notice that $\dot{V} \leq 0$ *implies that* $V(t) \leq V(0)$*, and therefore that* $\dot{\tilde{\boldsymbol{q}}}$ *is bounded. This in turn implies that* $\ddot{V}$ *is bounded. Hence,* $\dot{V}$ *must be uniformly continuous. Finally, application of Barbălat's lemma shows that* $\dot{V} \rightarrow 0$ *which implies that* $\dot{\tilde{\boldsymbol{q}}} \rightarrow 0$ *as* $t \rightarrow \infty$*.*

Chapter 5

Autopilot Design

Conventional autopilot design based on linear theory starts from the assumption that the 6 DOF underwater vehicle equations of motion can be fairly described as a linear model linearized around an equilibrium point. This may be a rough approximation for many control and guidance applications. Indeed, underwater vehicles performing coupled manoeuvres at some speed are known to be highly nonlinear in their dynamics and kinematics. In such cases autopilots based on linear control theory can yield poor performance. It is a common assumption that linear control design is much simpler than its nonlinear counterpart. However, exploiting the structure of the nonlinear equations of motion often yields a relative simple nonlinear autopilot design. This will be shown in this chapter. The following topics are emphasized:

- Conventional autopilot design
- Autopilot design based on feedback linearization techniques
- Autopilot design based on sliding control
- Passivity-based adaptive autopilot design

5.1 Conventional Autopilot Design

This section briefly describes two frequently used linear control design techniques in the autopilot design of marine vehicles.

5.1.1 Proportional Integral Derivative (PID) Control

Most existing ROV-systems use a series of single-input single-output (SISO) controllers of P-type where each controller is designed for the control of one DOF. PID-controllers are used

only in more advanced ROV systems. This suggests that the desired forces and moments are calculated as

$$\tau_i = K_{P_i}\,\tilde{x}_i(t) + K_{D_i}\,\dot{\tilde{x}}_i(t) + K_{I_i}\int_o^t \tilde{x}_i(\tau)\,d\tau \quad \text{for} \quad i = 1,..,6$$

where K_{P_i}, K_{D_i} and K_{I_i} are the regulator gains and $\tilde{x}_i$ is the tracking error for the i-th DOF, respectively. The input matrix is then used to calculate the control input vector $\boldsymbol{u}$, c.f. Section 2.8.4.

$$\boldsymbol{u} = \boldsymbol{B}^{\dagger}(\dot{\boldsymbol{q}})\boldsymbol{\tau}$$

This approach is extremely sensitive to uncertainties in the input matrix $\boldsymbol{B}$ as well as the non-optimal tuning of the regulator parameters due to the time-varying behaviour of the hydrodynamic parameters. Hence, such autopilots should be used for vehicles which are meant to perform low speed non-coupled manoeuvres such as a simple "crab-wise motion". An example of this approach, is the control system of the EAVE-EAST vehicle at the University of New-Hampshire, Venkatachalam *et al.* (1985). A block diagram of the control system is shown in Fig. 5.1.

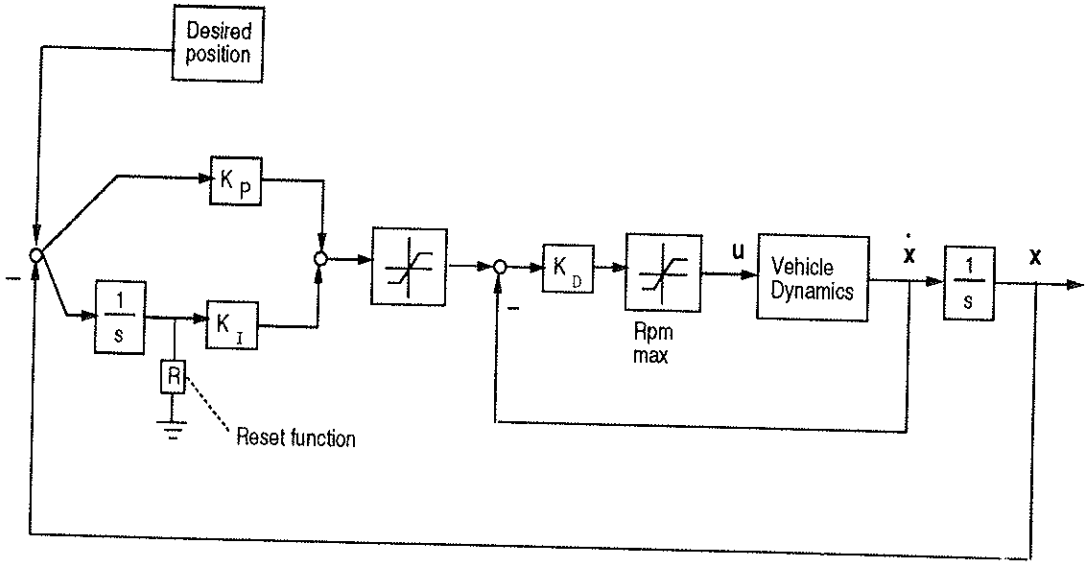

Figure 5.1: The EAVE-EAST Proportional Integral Derivative Controller, Venkatachalam *et al.* (1985)

As seen from the figure, the PID-control system for the EAVE-EAST vehicle is modified to handle saturation and integral wind-up.

5.1.2 Linear Quadratic Optimal Control Design

Linear quadratic (LQ) optimal control design is based on minimization on the linear quadratic performance index representing the control objective. Consider the linear state space model:

$$\begin{aligned} \dot{\boldsymbol{x}} &= \boldsymbol{A}\boldsymbol{x} + \boldsymbol{B}\boldsymbol{u} + \boldsymbol{C}\boldsymbol{v} \\ \boldsymbol{y} &= \boldsymbol{D}\boldsymbol{x} \end{aligned}$$

where $\boldsymbol{x}$ is the state vector, $\boldsymbol{u}$ is the input vector, $\boldsymbol{v}$ is the disturbance vector and $\boldsymbol{y}$ is the desired output vector. Let J be a performance index weighting the tracking error vector against the control power i.e.

$$Min\ J = \frac{1}{2}\int_o^\infty (\tilde{\boldsymbol{y}}^T \boldsymbol{Q}\tilde{\boldsymbol{y}} + \boldsymbol{u}^T \boldsymbol{P}\boldsymbol{u})\, d\tau$$

Here $\boldsymbol{P} > 0$ and $\boldsymbol{Q} \geq 0$ are the weighting matrices and $\tilde{\boldsymbol{y}} = \boldsymbol{y} - \boldsymbol{y}_c$ is the tracking error vector. The commanded input vector is denoted $\boldsymbol{y}_c$.

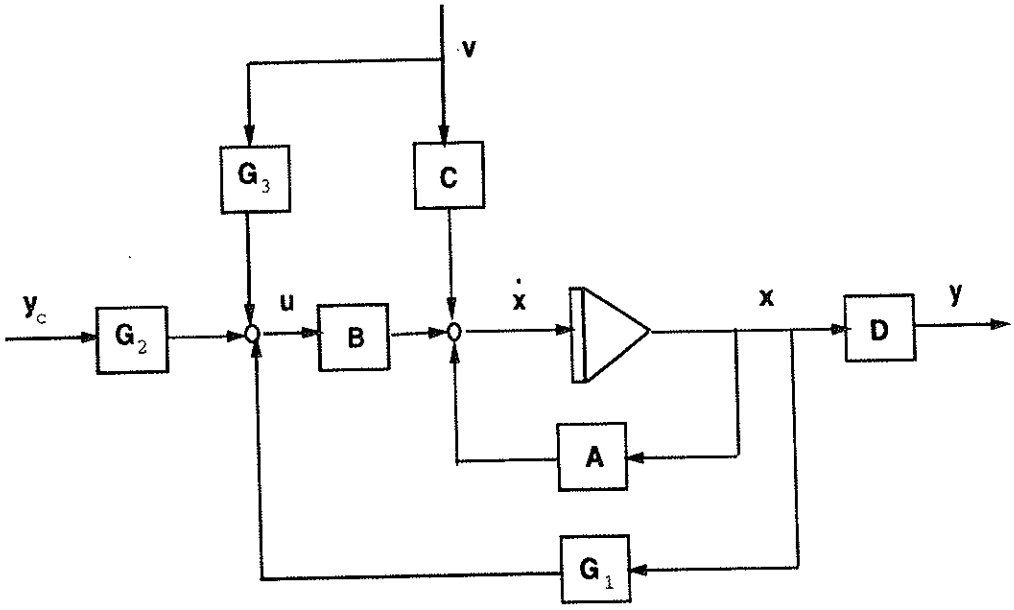

Figure 5.2: Linear Quadratic Optimal Autopilot

The optimal solution is well known, see e.g. Athans and Falb (1966), and can be written as:

$$\boldsymbol{u} = \boldsymbol{G}_1\,\boldsymbol{x} + \boldsymbol{G}_2\,\boldsymbol{y}_c + \boldsymbol{G}_3\boldsymbol{v}$$

A block diagram of the control system is shown in Fig. 5.2. Assuming $\boldsymbol{y}_c = const.$ and $\boldsymbol{v} = const.$ yield the following steady-state solution:

$$\begin{aligned}
\boldsymbol{G}_1 &= -\boldsymbol{P}^{-1}\boldsymbol{B}^T\boldsymbol{R}_S \\
\boldsymbol{G}_2 &= -\boldsymbol{P}^{-1}\boldsymbol{B}^T(\boldsymbol{A}+\boldsymbol{B}\boldsymbol{G}_1)^{-T}\boldsymbol{D}^T\boldsymbol{Q} \\
\boldsymbol{G}_3 &= \boldsymbol{P}^{-1}\boldsymbol{B}^T(\boldsymbol{A}+\boldsymbol{B}\boldsymbol{G}_1)^{-T}\boldsymbol{R}_S\boldsymbol{C}
\end{aligned}$$

Here $\boldsymbol{R}_S$ is the steady-state solution of the algebraic Riccati equation (ARE):

$$\boldsymbol{R}_S\boldsymbol{A} + \boldsymbol{A}^T\boldsymbol{R}_S - \boldsymbol{R}_S\boldsymbol{B}\boldsymbol{P}^{-1}\boldsymbol{B}^T\boldsymbol{R}_S + \boldsymbol{D}^T\boldsymbol{Q}\boldsymbol{D} = 0$$

Optimal state estimation (Kalman filtering) can be used to realize the autopilot in the case when not all states are measured. For instance, the LQG/LTR design methodology have been applied to underwater vehicles by Milliken (1984) and Triantafyllou and Grosenbaugh (1991). Loop shaping techniques like the LQG/LTR (Loop Transfer Recovery) design methodology, allow the designer to deal with robustness issues in a systematic manner. Indeed, robust stability (RS) can be guaranteed if bounds on the uncertainties are known. On the contrary, robust performance (RP) is still an unsolved problem. A linear controller design can be checked for RP by performing a structured singular value analysis. This technique is often referred to as the $\mu-analysis$ technique in the technical literature, see e.g. Maciejowski (1990). Nevertheless, the design of a so-called μ—optimal controller is still an active area for research.

5.2 Feedback Linearization

In this section feedback linearization techniques are discussed. Parametric uncertainties are discussed in the context of self-tuning and adaptive feedback linearization schemes. The basic idea with feedback linearization is to transform the nonlinear systems dynamics into a linear system. Conventional control techniques like pole placement and linear quadratic optimal control theory can then be applied to the linear system. In robotics, this technique is commonly referred to as *computed torque* control. The basic idea of nonlinear decoupling is quite old, Freund (1973). More recent work, such as Sastry and Isidori (1989) has formalized the idea to a large class of nonlinear systems.

5.2.1 Review of Input-Output Feedback Linearization

Nonlinear Affine Systems

Let us first consider MIMO nonlinear systems which are linear in control or affine, Sastry and Isidori (1989). These systems can be expressed as

$$\begin{aligned} \dot{\boldsymbol{x}} &= \boldsymbol{f}(\boldsymbol{x}) + \boldsymbol{G}(\boldsymbol{x})\boldsymbol{u} \\ \boldsymbol{y} &= \boldsymbol{h}(\boldsymbol{x}) \end{aligned} \tag{5.1}$$

with $\boldsymbol{x} \in \Re^n$, $\boldsymbol{y} \in \Re^m$, $\boldsymbol{u} \in \Re^p$ and $\boldsymbol{f}(\boldsymbol{x})$, $\boldsymbol{G}(\boldsymbol{x})$ and $\boldsymbol{h}(\boldsymbol{x})$ smooth. Differentiating the output $\boldsymbol{y}$ with respect to time yields

$$\dot{\boldsymbol{y}} = \boldsymbol{H}_x(\boldsymbol{x})\boldsymbol{f}(\boldsymbol{x}) + \boldsymbol{H}_x(\boldsymbol{x})\boldsymbol{G}(\boldsymbol{x})\boldsymbol{u}$$

where $\boldsymbol{H}_x(\boldsymbol{x}) = \frac{\partial \boldsymbol{h}(\boldsymbol{x})}{\partial \boldsymbol{x}}$ is the Jacobian. This control problem may be reduced to that of controlling the linear system

$$\dot{\boldsymbol{y}} = \boldsymbol{v}$$

where the choice: $\boldsymbol{v} = \dot{\boldsymbol{y}}_d - \boldsymbol{K}_P(\boldsymbol{y} - \boldsymbol{y}_d)$ yields the error equation

$$\dot{\boldsymbol{e}} + \boldsymbol{K}_P\boldsymbol{e} = 0 \tag{5.2}$$

Here $\boldsymbol{K}_P$ is a positive definite regulator gain matrix of appropriate dimension, $\boldsymbol{y}_d$ is the desired output vector and $\boldsymbol{e} = \boldsymbol{y} - \boldsymbol{y}_d$ is the tracking error vector. If the system Eq. 5.1 is *square* i.e. $m = p$, and $\boldsymbol{H}_x(\boldsymbol{x})\boldsymbol{G}(\boldsymbol{x})$ is nonsingular for all $\boldsymbol{x} \in \Re^n$, the actual control input vector $\boldsymbol{u}$ could be calculated as:

$$\boldsymbol{u} = (\boldsymbol{H}_x(\boldsymbol{x})\boldsymbol{G}(\boldsymbol{x}))^{-1}[\boldsymbol{v} - \boldsymbol{H}_x(\boldsymbol{x})\boldsymbol{f}(\boldsymbol{x})]$$

This approach fails if $\boldsymbol{H}_x(\boldsymbol{x})\boldsymbol{G}(\boldsymbol{x})$ is singular. In the singular case we must continue to differentiate the output y_j until one of the control inputs appear. Let r_j denote the system's relative degree i.e. the smallest number of differentiations the output y_j has to be differentiated for one of the control inputs to appear. The total relative degree is defined as $r = r_1 + ... + r_m$. Let us consider the case of $r < n$. Defining $\boldsymbol{G} = [\boldsymbol{g}_1, \ldots, \boldsymbol{g}_p]$ and

$$L_{\boldsymbol{f}}h_j = \frac{\partial h_j(\boldsymbol{x})}{\partial \boldsymbol{x}}\boldsymbol{f}(\boldsymbol{x}); \qquad L_{\boldsymbol{g}_j}h_j = \frac{\partial h_j(\boldsymbol{x})}{\partial \boldsymbol{x}}\boldsymbol{g}_j(\boldsymbol{x})$$

as the Lie derivatives of h_j with respect to $\boldsymbol{f}$ and $\boldsymbol{g}_j$, respectively, implies that Eq. 5.1 can be expressed as in Sastry and Isidori (1989),

$$y_j^{(r_j)} = L_{\boldsymbol{f}}^{r_j} h_j + \sum_{i=1}^{m} L_{\boldsymbol{g}_i}(L_{\boldsymbol{f}}^{r_j-1} h_j) u_i \tag{5.3}$$

where $(j = 1, 2, ..., m)$. The smallest integer r_j is found by requiring that at least one of the Lie derivatives $L_{\boldsymbol{g}_i}(L_{\boldsymbol{f}}^{r_j-1} h_j) \neq 0 \ \forall \ \boldsymbol{x}$. Notice that if the control input does not appear after at least r_j differentiations the system will not be controllable. Let $\boldsymbol{G}^*(\boldsymbol{x})$ be the $m \times m$ decoupling matrix defined as

$$\boldsymbol{G}^*(\boldsymbol{x}) = \begin{bmatrix} L_{\boldsymbol{g}_1}(L_{\boldsymbol{f}}^{r_1-1} h_1) & \dots & L_{\boldsymbol{g}_m}(L_{\boldsymbol{f}}^{r_1-1} h_1) \\ \vdots & & \vdots \\ L_{\boldsymbol{g}_1}(L_{\boldsymbol{f}}^{r_m-1} h_m) & \dots & L_{\boldsymbol{g}_m}(L_{\boldsymbol{f}}^{r_m-1} h_m) \end{bmatrix}$$

and

$$\boldsymbol{f}^*(\boldsymbol{x}) = (\ L_{\boldsymbol{f}}^{r_1} h_1, ..., L_{\boldsymbol{f}}^{r_m} h_m \ )^T$$

Hence, Eq. 5.3 can be expressed in a compact form as:

$$\begin{bmatrix} y_1^{(r_1)} \\ \vdots \\ y_m^{(r_m)} \end{bmatrix} = \boldsymbol{f}^*(\boldsymbol{x}) + \boldsymbol{G}^*(\boldsymbol{x}) \begin{bmatrix} u_1 \\ \vdots \\ u_m \end{bmatrix} \tag{5.4}$$

The equivalent linear system to be controlled is:

$$y^{(r_j)} = v_j \quad , \quad j = 1..m \tag{5.5}$$

If $\boldsymbol{G}^*(\boldsymbol{x})$ is non-singular the nonlinear feedback control law

$$\boldsymbol{u} = (\boldsymbol{G}^*(\boldsymbol{x}))^{-1} [\boldsymbol{v} - \boldsymbol{f}^*(\boldsymbol{x})] \tag{5.6}$$

yields the decoupled system Eq. 5.5 directly. A system with relative degree $(r_1, ..., r_m)$ can be transformed into a so-called *normal form* by applying a *diffeomorphism* $(\boldsymbol{\zeta}, \boldsymbol{z}) = T(\boldsymbol{x})$ defined as:

$$\begin{array}{cccc} \zeta_1^1 = h_1 & \zeta_2^1 = L_{\boldsymbol{f}} h_1 & \dots & \zeta_{r_1}^1 = L_{\boldsymbol{f}}^{r_1-1} h_1 \\ \vdots & & & \vdots \\ \zeta_1^m = h_m & \zeta_2^m = L_{\boldsymbol{f}} h_m & \dots & \zeta_{r_m}^m = L_{\boldsymbol{f}}^{r_m-1} h_m \end{array}$$

where $\boldsymbol{\zeta}$ denotes the *external dynamics*. Using the fact that $\boldsymbol{x} = T^{-1}(\boldsymbol{\zeta}, \boldsymbol{z})$ implies that Eq. 5.4 can be expressed as

$$
\begin{aligned}
\dot{\zeta}_1^j &= \zeta_2^j \\
&\vdots \\
\dot{\zeta}_{r_j}^j &= f_j^*(T^{-1}(\boldsymbol{\zeta}, \boldsymbol{z})) + \sum_{i=1}^{m} G_{ji}^*(T^{-1}(\boldsymbol{\zeta}, \boldsymbol{z}))u_i \\
y_j &= \zeta_1^j
\end{aligned}
$$

where $(j = 1, 2, ..., m)$ and

$$\dot{\boldsymbol{z}} = \boldsymbol{\phi}(\boldsymbol{\zeta}, \boldsymbol{z}) + \boldsymbol{\Psi}(\boldsymbol{\zeta}, \boldsymbol{z})\boldsymbol{u} \tag{5.7}$$

The state vector $\boldsymbol{z}$ denotes the *internal dynamics* and

$$
\begin{aligned}
\phi_k(\boldsymbol{\zeta}, \boldsymbol{z}) &= L_{\boldsymbol{f}}\zeta_k(\boldsymbol{x}) \\
\Psi_{ki}(\boldsymbol{\zeta}, \boldsymbol{z}) &= L_{\boldsymbol{g}_i}\zeta_k(\boldsymbol{x})
\end{aligned}
$$

where $(k = 1, ..., n - r)$ and $(i = 1, ..., m)$. The *zero-dynamics* of the nonlinear system is defined as the dynamics of the system when the outputs are constrained to be identically zero i.e. $\boldsymbol{\zeta}(t) = 0$. This is obtained by choosing the control inputs as:

$$\boldsymbol{u}(t) = -\left[\boldsymbol{G}^*(T^{-1}(0, \boldsymbol{z}))\right]^{-1} \boldsymbol{f}^*(T^{-1}(0, \boldsymbol{z}))$$

Eliminating $\boldsymbol{u}$ from Eq. 5.7 yields the zero dynamics:

$$\dot{\boldsymbol{z}} = \boldsymbol{\phi}(0, \boldsymbol{z}) - \boldsymbol{\Psi}(0, \boldsymbol{z})\left[\boldsymbol{G}^*(T^{-1}(0, \boldsymbol{z}))\right]^{-1} \boldsymbol{f}^*(T^{-1}(0, \boldsymbol{z}))$$

Notice that the zero dynamics are made unobservable by state feedback. The nonlinear system Eq. 5.1 is said to be *non-minimum phase* if the zero dynamics are unstable and *asymptotically minimum phase* if the zero dynamics are asymptotically stable, Byrnes and Isidori (1984). For minimum phase systems, feedback linearization results in bounding tracking if the desired motion trajectory is bounded. The proof is given in Sastry and Isidori (1989).

Input-Output Feedback Linearization of a more General Model Class

Although Eq. 5.1 is a fairly general model description, not all systems can be modelled using this structure. A feedback linearization scheme for the more general model class

$$\begin{aligned} \dot{\boldsymbol{x}} &= \boldsymbol{f}(\boldsymbol{x},\boldsymbol{u}) \\ \boldsymbol{y} &= \boldsymbol{h}(\boldsymbol{x}) \end{aligned}$$

is derived in Fossen and Foss (1991). Let γ_j be the smallest number of differentiations of the output y_j for one of the derivatives $\dot{u}_i$ to appear, then

$$y_j^{(\gamma_j)} = L_{\boldsymbol{f}}^{\gamma_j} h_j + \frac{\partial}{\partial \boldsymbol{u}} \left(L_{\boldsymbol{f}}^{\gamma_j - 1} h_j \right) \dot{\boldsymbol{u}} \quad , \quad j = 1, ..., m$$

or equivalently

$$\begin{bmatrix} y_1^{(\gamma_1)} \\ \vdots \\ y_m^{(\gamma_m)} \end{bmatrix} = \overline{\boldsymbol{f}}(\boldsymbol{x},\boldsymbol{u}) + \overline{\boldsymbol{G}}(\boldsymbol{x},\boldsymbol{u}) \begin{bmatrix} \dot{u}_1 \\ \vdots \\ \dot{u}_m \end{bmatrix}$$

where $\overline{f}_j(\boldsymbol{x},\boldsymbol{u}) = L_{\boldsymbol{f}}^{\gamma_j} h_j(\boldsymbol{x})$ and

$$\overline{\boldsymbol{G}}(\boldsymbol{x},\boldsymbol{u}) = \begin{bmatrix} \frac{\partial}{\partial u_1}\left(L_{\boldsymbol{f}}^{\gamma_1 - 1} h_1 \right) & \cdots & \frac{\partial}{\partial u_m}\left(L_{\boldsymbol{f}}^{\gamma_1 - 1} h_1 \right) \\ \vdots & & \vdots \\ \frac{\partial}{\partial u_1}\left(L_{\boldsymbol{f}}^{\gamma_m - 1} h_m \right) & \cdots & \frac{\partial}{\partial u_m}\left(L_{\boldsymbol{f}}^{\gamma_m - 1} h_m \right) \end{bmatrix}$$

The nonlinear control law (assuming that $\overline{\boldsymbol{G}}(\boldsymbol{x},\boldsymbol{u})$ is non-singular)

$$\dot{\boldsymbol{u}} = \left(\overline{\boldsymbol{G}}(\boldsymbol{x},\boldsymbol{u}) \right)^{-1} \left[\boldsymbol{v} - \overline{\boldsymbol{f}}(\boldsymbol{x},\boldsymbol{u}) \right]$$

yields the decoupled system:

$$y_j^{(\gamma_j)} = v_j \quad \text{for} \quad j = 1, ..., m$$

Example: Nonlinear Thruster Interactions

This new approach allows the designer to model nonlinear thruster interactions, for example, more closely. In other words, underwater vehicle systems in the form

$$\boldsymbol{M}\ddot{\boldsymbol{q}} + \boldsymbol{C}(\dot{\boldsymbol{q}})\dot{\boldsymbol{q}} + \boldsymbol{D}(\dot{\boldsymbol{q}})\dot{\boldsymbol{q}} + \boldsymbol{g}(\boldsymbol{x}) = \boldsymbol{\tau}(\dot{\boldsymbol{q}}, \boldsymbol{u})$$

where the control force and moment vector $\boldsymbol{\tau}$ is not linear in control, i.e. the input vector $\boldsymbol{u}$. We recall from Section 2.8 that the thruster force could be approximated as:

$$T \approx \rho\, D^4\, (\alpha + \beta\, J_o)\, n\, |n| \quad \textit{where} \quad J_o = \frac{(1-w)V}{nD}$$

which is equivalent to

$$\tau = b_1\, u\, |u| + b_2\, \dot{q}\, |u|$$

with $b_1 = \rho D^4 \alpha$ and $b_2 = \rho D^3 (1-w)\beta$. The input is simply $u = n$ while the vehicle's speed is $\dot{q} = V$. This justifies the use of the more general model class.

Feedback linearization techniques are easily applicable to the nonlinear underwater vehicle's equations of motion. This is illustrated in the next two sections.

5.2.2 Decoupling in the Vehicle-Fixed Reference Frame

q-frame Formulation

The decoupling of the vehicle's dynamics in the vehicle-fixed reference frame will be denoted as the q-frame formulation. The control objective is to transform the vehicle dynamics into a linear system $\ddot{\boldsymbol{q}} = \boldsymbol{a}_q$, where $\boldsymbol{a}_q$ can be interpreted as a commanded acceleration vector. The q-frame formulation should be used to control the vehicle's linear and angular velocities. Consider the nonlinear ROV dynamics, Eq. 2.38, which can be compactly expressed as:

$$\boldsymbol{M}\ddot{\boldsymbol{q}} + \boldsymbol{n}(\boldsymbol{x}, \dot{\boldsymbol{q}}) = \boldsymbol{B}(\dot{\boldsymbol{q}})\boldsymbol{u} \tag{5.8}$$

Here $\boldsymbol{x}$ and $\dot{\boldsymbol{q}}$ are assumed to be measured and $\boldsymbol{n}$ is the nonlinear vector:

$$\boldsymbol{n}(\boldsymbol{x}, \dot{\boldsymbol{q}}) = \boldsymbol{C}(\dot{\boldsymbol{q}})\dot{\boldsymbol{q}} + \boldsymbol{D}(\dot{\boldsymbol{q}})\dot{\boldsymbol{q}} + \boldsymbol{g}(\boldsymbol{x})$$

The nonlinearities can be cancelled out by simply selecting the control law as

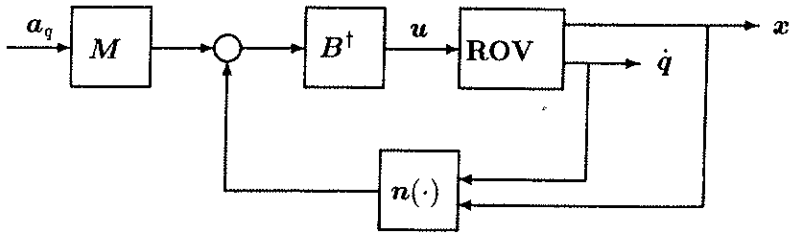

Figure 5.3: Nonlinear Decoupling

$$\boldsymbol{u} = \boldsymbol{B}^{\dagger}(\dot{\boldsymbol{q}}) \; [\boldsymbol{M}\boldsymbol{a}_q + \boldsymbol{n}(\dot{\boldsymbol{q}}, \boldsymbol{x})]$$

where the commanded acceleration vector $\boldsymbol{a}_q$ can be chosen by e.g. pole placement or linear quadratic optimal control theory. Let λ be the control bandwidth, $\dot{\boldsymbol{q}}_d$ the desired linear and angular velocity vector and $\tilde{\dot{\boldsymbol{q}}} = \dot{\boldsymbol{q}} - \dot{\boldsymbol{q}}_d$ the velocity tracking error. Then the commanded acceleration vector

$$\boldsymbol{a}_q = \ddot{\boldsymbol{q}}_d - \lambda \tilde{\dot{\boldsymbol{q}}}$$

yields the first-order error dynamics

$$\boldsymbol{M} \; (\ddot{\boldsymbol{q}} - \boldsymbol{a}_q) = \boldsymbol{M} \; (\ddot{\tilde{\boldsymbol{q}}} + \lambda \tilde{\dot{\boldsymbol{q}}}) = 0$$

The calculation of the commanded acceleration vector is shown in Figure 5.4.

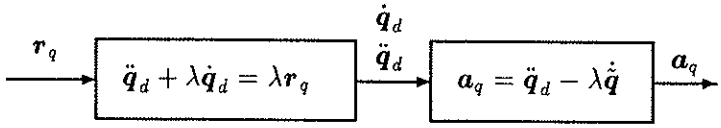

Figure 5.4: Calculation of the commanded acceleration (q-frame formulation).

The reference model is simply chosen as a first-order model with $\boldsymbol{r}_q$ as the commanded input vector. Note that in steady state $\dot{\boldsymbol{q}}_d(\infty) = \boldsymbol{r}_q$.

Example: Surge Velocity Control System

Consider a simplified model of a marine vehicle in surge

$$m\,\dot{u} + d\,|u|\,u = \tau$$

The commanded acceleration is calculated as:

$$a_q = \dot{u}_d - \lambda(u - u_d)$$

This suggests that the control law should be calculated as:

$$\tau = m\,(\dot{u}_d - \lambda(u - u_d)) + d\,|u|\,u$$

In robotics, it is usual to choose the commanded acceleration as

$$\boldsymbol{a}_q = \ddot{\boldsymbol{q}}_d - 2\lambda\dot{\tilde{\boldsymbol{q}}} - \lambda^2\tilde{\boldsymbol{q}}$$

where $\boldsymbol{q}$ is the manipulator joint angles. This yields the second-order error dynamics:

$$\boldsymbol{M}\,(\ddot{\boldsymbol{q}} - \boldsymbol{a}_q) = \boldsymbol{M}\,(\ddot{\tilde{\boldsymbol{q}}} + 2\lambda\dot{\tilde{\boldsymbol{q}}} + \lambda^2\tilde{\boldsymbol{q}}) = 0$$

For underwater vehicles the virtual vector $\boldsymbol{q}$ has no physical meaning. If the control objective is to control the vehicle's position and orientation in the earth-fixed reference frame, the following approach should be used instead.

5.2.3 Decoupling in the Earth-Fixed Reference Frame

x-frame Formulation

In the x-frame formulation the vehicle's dynamics and kinematics are decoupled into the earth-fixed reference frame i.e. $\ddot{\boldsymbol{x}} = \boldsymbol{a}_x$ where $\boldsymbol{a}_x$ can be interpreted as the earth-fixed commanded acceleration. The robotic counterpart to the x-frame formulation is feedback linearization in task-space coordinates, see e.g. Egeland (1987). The representation discussed in this section is the basis for the adaptive feedback linearization scheme presented in Section 5.2.5. Consider the ROV's dynamics and kinematics

$$\begin{aligned} \boldsymbol{M}\ddot{\boldsymbol{q}} + \boldsymbol{n}(\dot{\boldsymbol{q}}, \boldsymbol{x}) &= \boldsymbol{B}(\dot{\boldsymbol{q}})\boldsymbol{u} \\ \dot{\boldsymbol{x}} &= \boldsymbol{J}(\boldsymbol{x})\,\dot{\boldsymbol{q}} \end{aligned} \tag{5.9}$$

where $\boldsymbol{J}(\boldsymbol{x})$ is the kinematic transformation matrix and where both $\boldsymbol{x}$ and $\dot{\boldsymbol{q}}$ are assumed measured. Differentiation of the kinematic equation with respect to time yields

$$\ddot{\boldsymbol{q}} = \boldsymbol{J}^{-1}(\ddot{\boldsymbol{x}} - \dot{\boldsymbol{J}}\dot{\boldsymbol{q}})$$

The nonlinear control law

$$\boldsymbol{u} = \boldsymbol{B}^{\dagger}(\dot{\boldsymbol{q}}) \ [\boldsymbol{M}\boldsymbol{a}_q + \boldsymbol{n}(\dot{\boldsymbol{q}}, \boldsymbol{x})] \tag{5.10}$$

applied to the ROV equations of motion, yields:

$$\boldsymbol{M}(\ddot{\boldsymbol{q}} - \boldsymbol{a}_q) = \boldsymbol{M}\boldsymbol{J}^{-1}(\ddot{\boldsymbol{x}} - \dot{\boldsymbol{J}}\dot{\boldsymbol{q}} - \boldsymbol{J}\boldsymbol{a}_q) = 0$$

Defining

$$\boldsymbol{M}^* = \boldsymbol{J}^{-T}\boldsymbol{M}\boldsymbol{J}^{-1} \quad \text{and} \quad \boldsymbol{a}_x = \dot{\boldsymbol{J}}\dot{\boldsymbol{q}} + \boldsymbol{J}\boldsymbol{a}_q$$

yields the linear decoupled system:

$$\boldsymbol{M}^*(\ddot{\boldsymbol{x}} - \boldsymbol{a}_x) = 0$$

This suggests that the commanded acceleration $\boldsymbol{a}_x$ should be chosen as:

$$\boldsymbol{a}_x = \ddot{\boldsymbol{x}}_d - 2\lambda\dot{\tilde{\boldsymbol{x}}} - \lambda^2\tilde{\boldsymbol{x}}$$

In the implementation of the control law, Eq. 5.10, the commanded acceleration in the q-frame is calculated as:

$$\boldsymbol{a}_q = \boldsymbol{J}^{-1}(\boldsymbol{a}_x - \dot{\boldsymbol{J}}\dot{\boldsymbol{q}})$$

This is shown in Figure 5.5. The reference model is chosen such that the commanded input vector $\boldsymbol{r}_x$ is equal to the steady state reference vector i.e. $\boldsymbol{x}_d(\infty) = \boldsymbol{r}_x$.

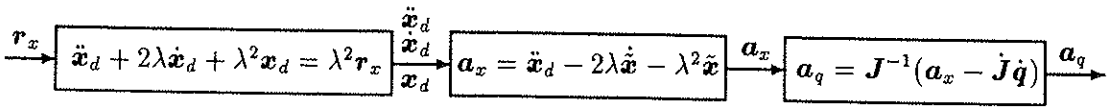

Figure 5.5: Calculation of commanded acceleration (x-frame formulation).

Example: Heading Control System

Consider the simplified model of an underwater vehicle in yaw

$$m\,\dot{r} + d\,|r|\,r = \tau \quad , \qquad \dot{\psi} = r$$

Hence, the commanded acceleration can be calculated as:

$$a_x = \dot{r}_d - 2\lambda(r - r_d) - \lambda^2(\psi - \psi_d)$$

where r_d is the desired angular velocity and ψ_d is the desired heading angle. For this particular example $a_q = a_x$, which yields the decoupling control law:

$$\tau = m\left(\dot{r}_d - 2\lambda(r - r_d) - \lambda^2(\psi - \psi_d)\right) + d\,|r|\,r$$

5.2.4 Self-Tuning Feedback Linearization

A self-tuning controller (STC) can be defined as a controller where the parameters are calculated on-line by a (recursive) parameter estimator. STC based on ARMAX models has been tested out on the Seapup ROV by Goheen (1986). Both nonlinear feedback linearization and sliding control techniques can be combined with a parameter estimator to improve their performance. A large number of recursive prediction error methods (RPM) are available for this purpose. The most known parameter estimators are probably the recursive least square (RLS) and the recursive maximum likelihood (RML) methods. We will exclusively use least square estimation to illustrate the idea of self-tuning feedback linearization. The feedback linearization control law, Eq. 5.10, can be replaced by

$$\boldsymbol{u} = \boldsymbol{B}^{\dagger}(\dot{\boldsymbol{q}})\,\left[\hat{\boldsymbol{M}}\,\boldsymbol{a}_q + \hat{\boldsymbol{n}}(\dot{\boldsymbol{q}}, \boldsymbol{x})\right]$$

where the hat denotes the parameter estimates. Consider the nonlinear underwater vehicle equations of motion Eq. 5.9 which can be parameterized as:

$$\boldsymbol{\tau} = \boldsymbol{M}\,\ddot{\boldsymbol{q}} + \boldsymbol{n}(\dot{\boldsymbol{q}}, \boldsymbol{x}) = \boldsymbol{\Phi}(\ddot{\boldsymbol{q}}, \dot{\boldsymbol{q}}, \boldsymbol{x})\,\boldsymbol{\theta}$$

Here $\boldsymbol{\Phi}$ is a known regressor matrix of appropriate dimension and $\boldsymbol{\theta}$ is the unknown parameter vector. Hence, the prediction error can be defined as

$$\boldsymbol{e}(t) = \boldsymbol{\Phi}(\ddot{\boldsymbol{q}}, \dot{\boldsymbol{q}}, \boldsymbol{x})\,\hat{\boldsymbol{\theta}} - \boldsymbol{\tau}$$

where $\hat{\boldsymbol{\theta}}$ is the estimated parameter vector.

Least-Square Estimation

The unknown parameters can be estimated by using a least-square scheme with constant forgetting factor λ. Consider the cost index

$$Min\ J = \frac{1}{2}\int_o^t e^{-\lambda(t-\tau)}\boldsymbol{e}^T(\tau)\boldsymbol{e}(\tau)\ d\tau$$

The forgetting factor (typically 0.96-0.99) ensures that past data are given less influence than current data in the estimation of the current parameters. This is particularly useful when dealing with time-varying parameters. The solution of the minimization problem is well known and can be written as

$$\dot{\hat{\boldsymbol{\theta}}} = -\boldsymbol{P}(t)\,\boldsymbol{\Phi}^T\,\boldsymbol{e} \tag{5.11}$$

with the gain update

$$\frac{d}{dt}(\boldsymbol{P}^{-1}) = -\lambda\,\boldsymbol{P}^{-1} + \boldsymbol{\Phi}^T\boldsymbol{\Phi}$$

In the implementation of the LS algorithm it is desirable to rewrite the gain update such that the matrix inversion of $\boldsymbol{P}$ is avoided. Using the fact that

$$\frac{d}{dt}(\boldsymbol{P}^{-1}\boldsymbol{P}) = 0 \quad \Rightarrow \quad \frac{d}{dt}(\boldsymbol{P}^{-1}) = -\boldsymbol{P}^{-1}\,\frac{d}{dt}(\boldsymbol{P})\,\boldsymbol{P}^{-1}$$

yields

$$\frac{d}{dt}(\boldsymbol{P}) = \lambda\,\boldsymbol{P} - \boldsymbol{P}\boldsymbol{\Phi}^T\boldsymbol{\Phi}\boldsymbol{P}$$

To avoid the difficulties with vanishing gain in the absence of persistent excitation, numerous techniques can be used. For instance, the gain update can be modified to

$$\frac{d}{dt}(\boldsymbol{P}) = \lambda_1\,\boldsymbol{P} - \lambda_2\boldsymbol{P}\boldsymbol{\Phi}^T\boldsymbol{\Phi}\boldsymbol{P} \tag{5.12}$$

where λ_1 tends to increase the adaption gain and λ_2 tends to decrease the adaption gain. The choices of λ_1 and λ_2 are discussed by Landau and Lozano (1981). On-line parameter estimation should not be used to estimate a large number of parameters. Like other indirect schemes, self-tuning feedback linearization requires that the system must be persistently exciting (PE) i.e. parameter convergence occurs if $\exists\ T > 0$ and $\beta \geq \alpha > 0$ such that

$$\beta\boldsymbol{I} \geq \frac{1}{T}\int_s^{s+T}\boldsymbol{\Phi}(t)\boldsymbol{\Phi}^T(t)\ dt \geq \alpha\boldsymbol{I} \quad , \quad \forall\ s \in \Re_+$$

This requirement is quite harsh when considering a general underwater vehicle in 6 DOF. The requirement of PE can be removed by using direct adaptive control schemes, instead.

In a direct adaptive control scheme global asymptotic stability of the tracking error can be proven without requiring the parameter error vector to converge to zero. This condition can be relaxed to one where the parameter error vector must be bounded i.e. $\tilde{\boldsymbol{\theta}} < \infty$. This is the topic for the next section. Parameter convergence is described more closely in e.g. Anderson *et al.* (1986).

5.2.5 Adaptive Feedback Linearization

The adaptive feedback linearization scheme for robot manipulators is usually formulated in the q-frame, i.e. in the joint coordinates. This is due to the fact that for a large number of robot manipulators, the desired task-space coordinates can be transformed to desired joint coordinates by applying the manipulator's inverse kinematics. However, in control and guidance applications the kinematic transformation does not exist. Nevertheless, this problem can be avoided by formulating the adaptive parameter updating law directly in the x-frame. One such approach uses the vehicle's Jacobian instead of the unknown inverse kinematics.

Previous work by Horowitz and Tomizuka (1986) is based on Popov's hyperstability theory which can be used to prove global stability for the overall system. However by applying Lyapunov-like stability theory for non-autonomous systems the derivation of the adaptive scheme is often much simpler. This means that the application of Barbălat's Lyapunov-like lemma, implies that we can avoid solving the Popov integral inequality and the Kalman-Yakubovitch lemma. This is advantage as the mathematical manipulations required to satisfy the requirements imposed by the Popov integral inequality can be quite laborious. In this section it will be shown how the original scheme proposed by Horowitz and Tomizuka (1986) can be relatively easily represented in the x-frame by applying Lyapunov-like stability theory.

x-frame Formulation

Again, consider the nonlinear equations of motion Eq. 5.8. Taking the control law to be

$$\boldsymbol{u} = \boldsymbol{B}^{\dagger}(\dot{\boldsymbol{q}}) \left[\hat{\boldsymbol{M}}\boldsymbol{a}_q + \hat{\boldsymbol{n}}(\boldsymbol{x}, \dot{\boldsymbol{q}})\right]$$

where the hat denotes the adaptive estimates, yields the error dynamics:

$$\boldsymbol{M}(\ddot{\boldsymbol{q}} - \boldsymbol{a}_q) = (\hat{\boldsymbol{M}} - \boldsymbol{M})\boldsymbol{a}_q + (\hat{\boldsymbol{n}}(\boldsymbol{x}, \dot{\boldsymbol{q}}) - \boldsymbol{n}(\boldsymbol{x}, \dot{\boldsymbol{q}}))$$

Since, the underwater vehicle equations are assumed to be linear in their parameters, we can apply the parameterization

$$(\hat{\boldsymbol{M}} - \boldsymbol{M})\boldsymbol{a}_q + (\hat{\boldsymbol{n}}(\boldsymbol{x}, \dot{\boldsymbol{q}}) - \boldsymbol{n}(\boldsymbol{x}, \dot{\boldsymbol{q}})) = \boldsymbol{\Phi}(\boldsymbol{x}, \dot{\boldsymbol{q}}, \boldsymbol{a}_q)\tilde{\boldsymbol{\theta}}$$

where $\tilde{\boldsymbol{\theta}} = \hat{\boldsymbol{\theta}} - \boldsymbol{\theta}$ is the parameter error vector.

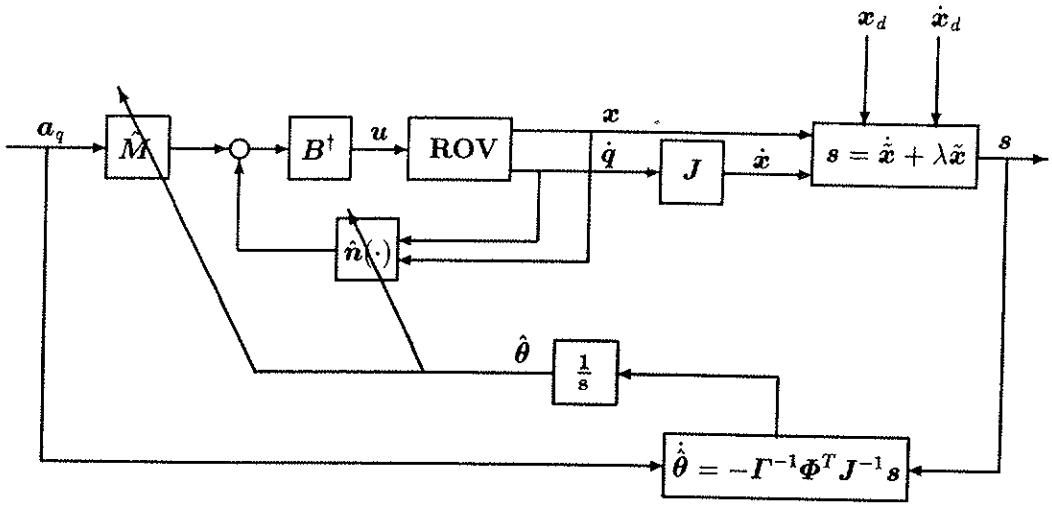

Figure 5.6: Adaptive feedback linearization applied to the nonlinear underwater vehicle equations of motion

Using the result $\boldsymbol{a}_x = \dot{\boldsymbol{J}}\dot{\boldsymbol{q}} + \boldsymbol{J}\boldsymbol{a}_q$, yields:

$$\boldsymbol{M}\boldsymbol{J}^{-1}(\ddot{\boldsymbol{x}} - \boldsymbol{a}_x) = \boldsymbol{\Phi}(\boldsymbol{x}, \dot{\boldsymbol{q}}, \boldsymbol{a}_q)\tilde{\boldsymbol{\theta}}$$

Premultiplying this expression with $\boldsymbol{J}^{-T}$ and letting $\boldsymbol{M}^* = \boldsymbol{J}^{-T}\boldsymbol{M}\boldsymbol{J}^{-1}$ yields the x-frame error dynamics:

$$\boldsymbol{M}^*(\ddot{\boldsymbol{x}} - \boldsymbol{a}_x) = \boldsymbol{J}^{-T}\boldsymbol{\Phi}(\boldsymbol{x}, \dot{\boldsymbol{q}}, \boldsymbol{a}_q)\tilde{\boldsymbol{\theta}}$$

By pole placement we choose the commanded acceleration vector as

$$\boldsymbol{a}_x = \ddot{\boldsymbol{x}}_d - 2\lambda\dot{\tilde{\boldsymbol{x}}} - \lambda^2\tilde{\boldsymbol{x}} \quad , \quad \lambda > 0$$

and

$$\boldsymbol{s} = \dot{\tilde{\boldsymbol{x}}} + \lambda\tilde{\boldsymbol{x}}$$

Hence, the error dynamics can be expressed as:

$$\boldsymbol{M}^*(\dot{\boldsymbol{s}} + \lambda\boldsymbol{s}) = \boldsymbol{J}^{-T}\boldsymbol{\Phi}(\boldsymbol{x}, \dot{\boldsymbol{q}}, \boldsymbol{a}_q)\tilde{\boldsymbol{\theta}}$$

To prove global stability we propose to use a Lyapunov-like function candidate:

$$V(\boldsymbol{s},\tilde{\boldsymbol{\theta}},t)=\frac{1}{2}\left(\boldsymbol{s}^T\boldsymbol{M}^*\boldsymbol{s}+\tilde{\boldsymbol{\theta}}^T\boldsymbol{\Gamma}\tilde{\boldsymbol{\theta}}\right) \quad , \quad \boldsymbol{M}^*=(\boldsymbol{M}^*)^T>0$$

Differentiating V with respect to time (assuming $\dot{\boldsymbol{M}}^*=0$) yields

$$\dot{V}=\boldsymbol{s}^T\boldsymbol{M}^*\dot{\boldsymbol{s}}+\dot{\tilde{\boldsymbol{\theta}}}^T\boldsymbol{\Gamma}\tilde{\boldsymbol{\theta}}$$

where $\boldsymbol{\Gamma}$ is a positive definite weighting matrix of appropriate dimension. Substituting the error dynamics into the expression for $\dot{V}$ yields:

$$\dot{V}=-\lambda\,\boldsymbol{s}^T\boldsymbol{M}^*\boldsymbol{s}+(\boldsymbol{s}^T\boldsymbol{J}^{-T}\tilde{\boldsymbol{\Phi}}+\dot{\tilde{\boldsymbol{\theta}}}^T\boldsymbol{\Gamma})\tilde{\boldsymbol{\theta}}$$

This suggest the parameter update law (assuming $\dot{\boldsymbol{\theta}}=0$):

$$\dot{\tilde{\boldsymbol{\theta}}}=-\boldsymbol{\Gamma}^{-1}\boldsymbol{\Phi}^T(\boldsymbol{x},\dot{\boldsymbol{q}},\boldsymbol{a}_q)\boldsymbol{J}^{-1}(\boldsymbol{x})\;\boldsymbol{s}$$

which finally yields:

$$\dot{V}=-\lambda\,\boldsymbol{s}^T\boldsymbol{M}^*\boldsymbol{s}\leq 0$$

Hence, global stability and asymptotic convergence of $\tilde{\boldsymbol{x}}$ to zero are guaranteed by applying Barbălat's Lyapunov-like lemma. We also notice that the parameter vector $\tilde{\boldsymbol{\theta}}$ will be bounded i.e. $\tilde{\boldsymbol{\theta}}<\infty$. Hence, PE is not required to guarantee the tracking error to converge to zero. Slotine and Li (1987) have showed that the assumption of $\dot{\boldsymbol{M}}^*=0$ can be removed by applying the skew-symmetric property $\boldsymbol{s}^T(\dot{\boldsymbol{M}}^*-2\boldsymbol{C}^*)\boldsymbol{s}=0$ together with passivity theory. This is described more closely in Section 5.4. A more general approach which allows the time-varying matrix $\dot{\boldsymbol{M}}$ to be included in the control law is discussed by Johansson (1990). He shows that the algorithm of Slotine and Li (1987) actually can be viewed as a special case of a more general direct adaptive control law based on Lyapunov stability. This approach is particularly interesting since global stability is proven by using a Lyapunov function instead of Barbălat's Lyapunov-like lemma. An alternative to adaptive feedback linearization techniques is the explicit model reference adaptive control (MRAC) scheme of Landau and Lozano (1981). This scheme has been successfully applied to underwater robotic vehicles by Yuh (1990).

Simulation Study: Adaptive Autopilot for the NEROV Underwater Vehicle

Consider the following simplified 4 DOF model of the NEROV vehicle in surge, sway, heave and yaw:

$$\begin{aligned} \boldsymbol{M}\,\ddot{\boldsymbol{q}} + \boldsymbol{C}(\dot{\boldsymbol{q}})\,\dot{\boldsymbol{q}} + \boldsymbol{D}(\dot{\boldsymbol{q}})\,\dot{\boldsymbol{q}} = \boldsymbol{\tau} \quad &, \quad \dot{\boldsymbol{q}} = (u, v, w, r)^T \\ \dot{\boldsymbol{x}} = \boldsymbol{J}(\boldsymbol{x})\,\dot{\boldsymbol{q}} \quad &, \quad \boldsymbol{x} = (x, y, z, \psi)^T \end{aligned}$$

The expressions and numerical values for $\boldsymbol{M}$, $\boldsymbol{C}$, $\boldsymbol{D}$ and $\boldsymbol{J}$ are found in Appendix A.

The adaptive control law is:

$$\begin{aligned} \boldsymbol{\tau} &= \hat{\boldsymbol{M}}\boldsymbol{a}_q + \hat{\boldsymbol{C}}(\dot{\boldsymbol{q}})\dot{\boldsymbol{q}} + \hat{\boldsymbol{D}}(\dot{\boldsymbol{q}})\dot{\boldsymbol{q}} = \boldsymbol{\Phi}(\dot{\boldsymbol{q}}, \boldsymbol{a}_q)\,\hat{\boldsymbol{\theta}} \\ \dot{\hat{\boldsymbol{\theta}}} &= -\boldsymbol{\Gamma}^{-1}\boldsymbol{\Phi}^T(\dot{\boldsymbol{q}}, \boldsymbol{a}_q)\boldsymbol{J}^{-1}(\boldsymbol{x})\,\boldsymbol{s} \end{aligned}$$

The x-frame formulation is used to control the vehicle's position (x, y, z) and heading angle ψ. We chose the reference model and the commanded acceleration vector as:

Reference model:	$\ddot{\boldsymbol{x}}_d + 2\lambda\dot{\boldsymbol{x}}_d + \lambda^2\boldsymbol{x}_d = \lambda^2\boldsymbol{r}_x$
Commanded acceleration:	$\boldsymbol{a}_x = \ddot{\boldsymbol{x}}_d - 2\lambda\dot{\tilde{\boldsymbol{x}}} - \lambda^2\tilde{\boldsymbol{x}}$
	$\boldsymbol{a}_q = \boldsymbol{J}^{-1}(\boldsymbol{a}_x - \dot{\boldsymbol{J}}\dot{\boldsymbol{q}})$

On the contrary, if we want to control the vehicle's linear and angular velocities (u, v, w, r) the q-frame formulation should be used. In the simulation study, the initial parameter estimates were chosen as $\hat{\boldsymbol{\theta}}(0) = 0$. The desired and actual outputs for: $\lambda = 1$, $\boldsymbol{\Gamma} = 0.001\ \boldsymbol{I}$ and a sampling rate of 10 Hz are shown in Figure 5.7. From the figure, it is seen that the performance of the adaptive controller is extremely good. Also note that the tracking error converge to zero after a while.

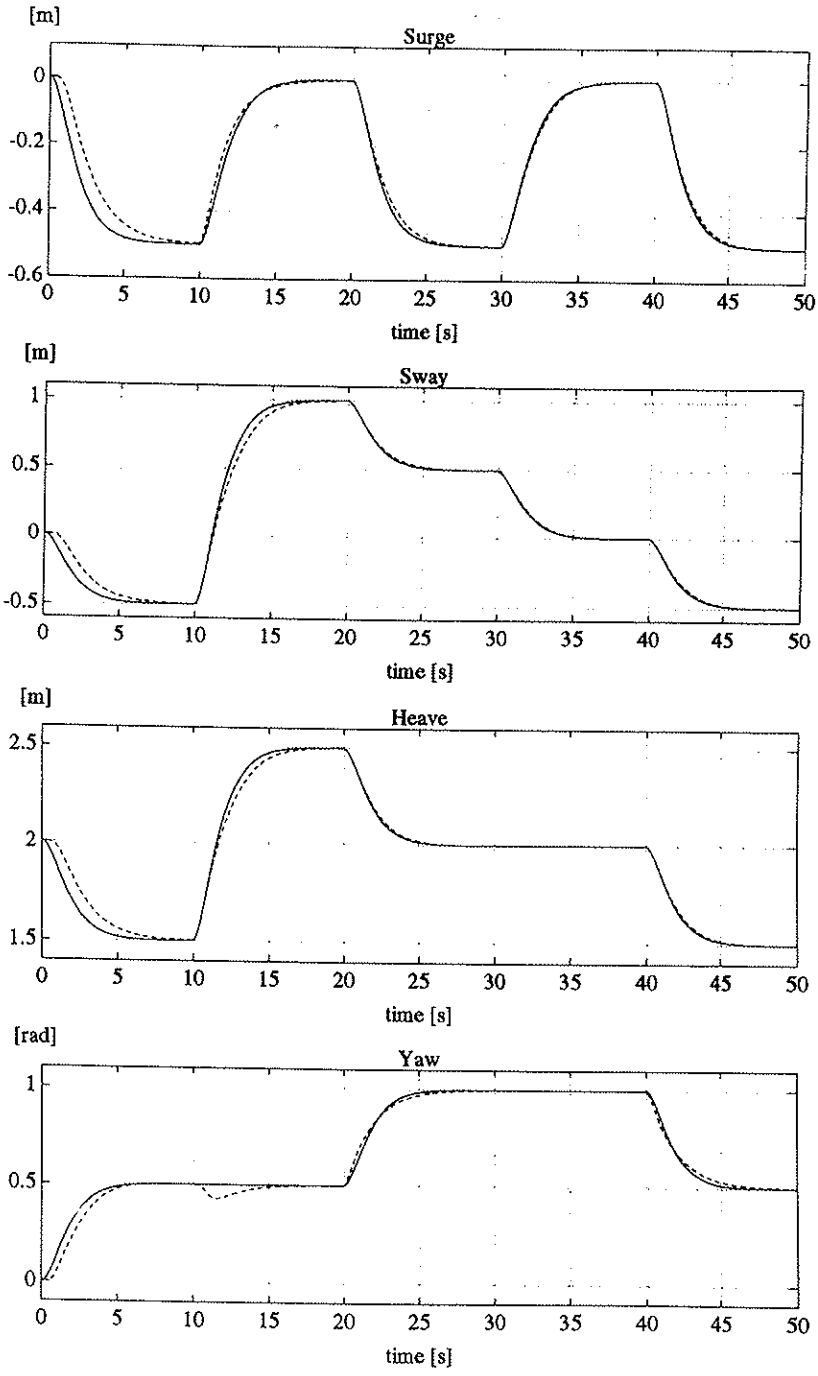

Figure 5.7: Desired and actual outputs in surge, sway, heave and yaw for the adaptive autopilot (x-frame formulation).

5.3 Sliding Control

The sliding control design methodology is described in detail by Slotine and Li (1991). Sliding control has been applied successfully in the control of underwater vehicles. Yoerger and Slotine(1984, 1985) have proposed to use a series of single-input single-output (SISO) continuous time controllers based on sliding mode control. Recent work by Yoerger and Slotine (1991) discusses how adaptive sliding control can be applied to underwater vehicles. Cristi *et al.* (1990) discuss adaptive sliding mode control of AUVs in the dive plane. Sliding mode controllers have been successfully implemented for the JASON vehicle Yoerger *et al.* (1986) and the MUST vehicle Dougherty and Woolweaver (1990). The experiments show that sliding mode controllers have significant advantageous to traditional linear control theory.

5.3.1 SISO Sliding Control Applied to Underwater Vehicles

This approach is based on a slightly modified version of the sliding controller proposed by Yoerger and Slotine (1984) and Yoerger and Slotine (1985). Consider the simplified ROV model:

$$M_{ii}\ddot{q}_i + n_i(\dot{q}_i) = \tau_i \quad \text{and} \quad \dot{x}_i = \dot{q}_i \quad i = 1..6$$

where all kinematic and dynamic cross-coupling terms terms are neglected. Here, τ_i is the input, M_{ii} is the diagonal element of the inertia matrix $\boldsymbol{M}$ and n_i corresponds to the quadratic damping term in the nonlinear vector $\boldsymbol{n}$ i.e.

$$\boldsymbol{M} = \begin{bmatrix} m - X_{\dot{u}} & 0 & 0 & 0 & 0 & 0 \\ 0 & m - Y_{\dot{v}} & 0 & 0 & 0 & 0 \\ 0 & 0 & m - Z_{\dot{w}} & 0 & 0 & 0 \\ 0 & 0 & 0 & Ix - K_{\dot{p}} & 0 & 0 \\ 0 & 0 & 0 & 0 & Iy - M_{\dot{q}} & 0 \\ 0 & 0 & 0 & 0 & 0 & Iz - N_{\dot{r}} \end{bmatrix}$$

$$\boldsymbol{n}(\dot{\boldsymbol{q}}) = \begin{bmatrix} -X_{u|u|}\, u|u|, & -Y_{v|v|}\, v|v|, & -Z_{w|w|}\, w|w|, & -K_{p|p|}\, p|p|, & -M_{q|q|}\, q|q|, & -N_{r|r|}\, r|r| \end{bmatrix}^T$$

Uncertainties in the model are compensated for in the control design. For notational simplicity, let us write the ROV model as:

$$m\ddot{x} + d\,|\dot{x}|\dot{x} = \tau \quad \text{where} \quad m > 0; \quad d > 0$$

Here $m = M_{ii}$, $d\,\dot{x}|\dot{x}| = n_i(\dot{q}_i)$ and $\tau = \tau_i$. We also assume that both $\dot{x}$ and x are measured. Define a measure of tracking (sliding surface)

$$s = \dot{\tilde{x}} + \lambda\tilde{x}$$

where $\tilde{x} = x - x_d$ is the tracking error and λ is the control bandwidth. It is convenient to define a virtual reference x_r satisfying

$$\dot{x}_r = \dot{x}_d - \lambda\tilde{x} \quad \Rightarrow \quad s = \dot{x} - \dot{x}_r$$

Consider the scalar Lyapunov-like function candidate

$$V(s,t) = \frac{1}{2} m\, s^2 \quad , \quad m > 0$$

Differentiating V with respect to time (assuming $\dot{m} = 0$) yields

$$\dot{V} = s\, m\, (\ddot{x} - \ddot{x}_r) = s\, (\, \tau - d\, |\dot{x}|\dot{x} - m\ddot{x}_r\,) = -d\, |\dot{x}|s^2 + s(\tau - m\ddot{x}_r - d\, |\dot{x}|\dot{x}_r)$$

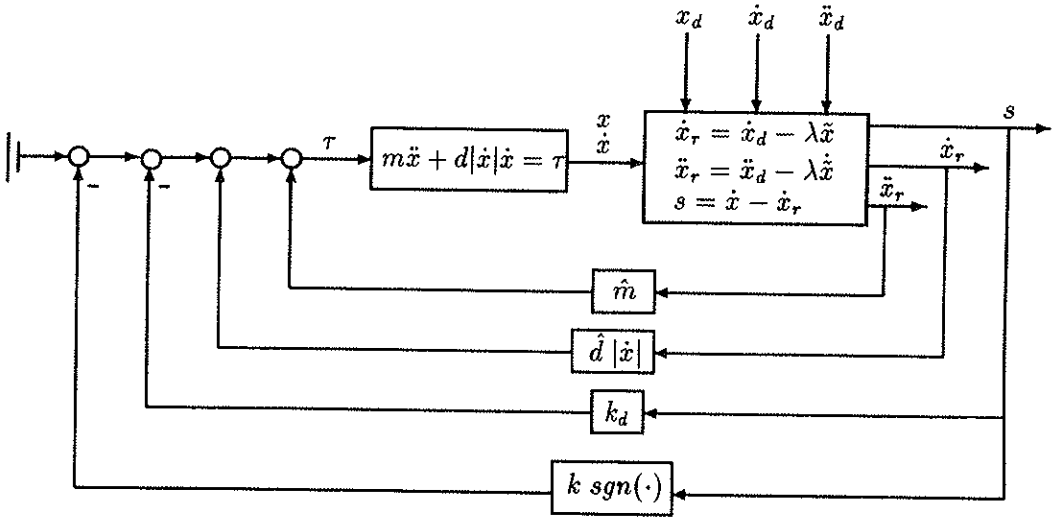

Figure 5.8: SISO sliding control applied to underwater vehicles

Taking the control law to be

$$\tau = \hat{m}\ddot{x}_r + \hat{d}\,|\dot{x}|\dot{x}_r - k_d\, s - k\ sgn(s) \quad , \quad k_d > 0$$

where $\hat{m}$ and $\hat{d}$ are the estimates of m and d, respectively, yields

$$\dot{V} = -(\, k_d + d\,|\dot{x}|\,)\, s^2 + (\, \tilde{m}\ddot{x}_r + \tilde{d}\,|\dot{x}|\dot{x}_r\,)\, s - k\,|s|$$

Here $\tilde{m} = \hat{m} - m$ and $\tilde{d} = \hat{d} - d$. Conditions on the switching gain k are found by requiring that $\dot{V} \leq 0$. The particular choice

$$k \geq |\tilde{m}\ddot{x}_r + \tilde{d}\,|\dot{x}|\,\dot{x}_r| + \eta \quad \text{with} \quad \eta > 0$$

implies that

$$\dot{V} \leq -(\, k_d + d\,|\dot{x}|\,)\, s^2 - \eta\,|s| \leq 0$$

This is due to the fact that $(\, k_d + d|\dot{x}|\,) > 0 \quad \forall\, \dot{x}$. Note that $\dot{V} \leq 0$ implies that $V(t) \leq V(0)$, and therefore that s is bounded. This in turn implies that $\ddot{V}$ is bounded. Hence $\dot{V}$ must be uniformly continuous. Finally, application of Barbălat's lemma then shows that $s \to 0$ and thus $\tilde{x} \to 0$ as $t \to \infty$.

Chattering

It is well known that the switching term $k\,sgn(s)$ can lead to chattering. Chattering must be eliminated for the controller to perform properly. Slotine and Li (1991) suggest to smooth out the control law discontinuity inside a boundary layer by replacing the $sgn(\cdot)$ function in the control law with

$$sat(s/\phi) = \begin{cases} 1 & \text{if} \quad \frac{s}{\phi} > 1 \\ s/\phi & \text{if} \quad -1 \leq \frac{s}{\phi} \leq 1 \\ -1 & \text{if} \quad \frac{s}{\phi} < -1 \end{cases}$$

where ϕ should be interpreted as the boundary layer thickness. This substitution will in fact assign a lowpass filter structure to the dynamics of the sliding surface s. The boundary layer thickness can also be made time-varying to exploit the maximum control bandwidth available. This is described more closely in Slotine and Li (1991).

Simulation Study: SISO Sliding Control Applied to an Underwater Vehicle

Consider the simplified model of an underwater vehicle in surge:

$$m\,\ddot{x} + d\,\dot{x}\,|\dot{x}| = \tau \tag{5.13}$$

with $m = 200\ kg$ *and* $d = 50\ kg/m$.

The SISO sliding controller can be expressed as:

$$\tau = \hat{m}\,\ddot{x}_r + \hat{d}\,|\dot{x}|\dot{x}_r - k_d\,s - k\,sat(s/\phi) \quad , \quad k_d > 0 \tag{5.14}$$

The following two cases were studied:

- **(1) PD-controller:**

$$\begin{array}{ll} \hat{m} = 0 & k_d = 500 \\ \hat{d} = 0 & k = 0 \end{array}$$

- **(2) Sliding controller:**

$$\begin{array}{lll} \hat{m} & = 0.6\,m & \tilde{m} \leq 0.5\,m \\ \hat{d} & = 1.5\,d & \tilde{d} \leq 0.5\,d \\ k & = \left| \left(\tilde{m}\,\ddot{x}_r + \tilde{d}\,|\dot{x}|\,\dot{x}_r\right) \right| + 0.1 & k_d = 200 \end{array}$$

Notice that the first case simply corresponds to the PD control law:

$$\tau = -k_d\,s = -k_d\,\dot{\tilde{x}} - \lambda\,k_d\,\tilde{x}$$

In the simulation study the closed loop bandwidth was chosen as: $\lambda = 1$ *for both controllers. The boundary layer thickness was chosen as* $\phi = \pm\,0.35$ *for the sliding controller while the sampling rate was set at 10 Hz. The simulation results are shown in Figure 5.9 and 5.10. It is seen from the figures that the performance of the sliding controller is much better than the performance of the PD-controller. Note that control input for the sliding controller is relatively smooth due to the lowpass filter structure of the boundary layer.*

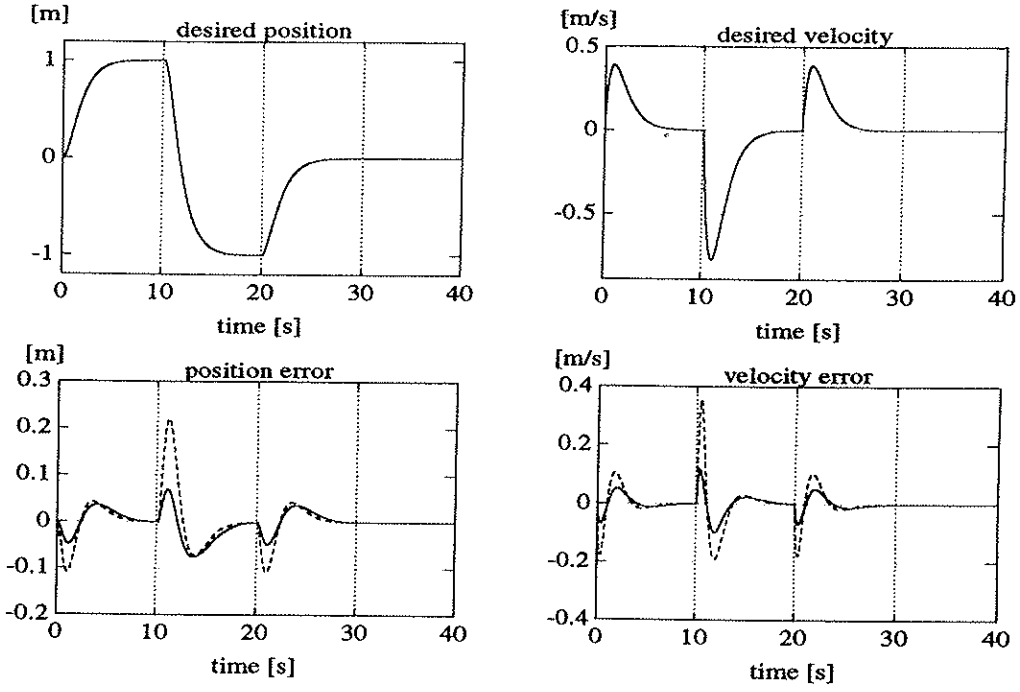

Figure 5.9: Performance study of the sliding controller (solid) and the PD-controller (dotted).

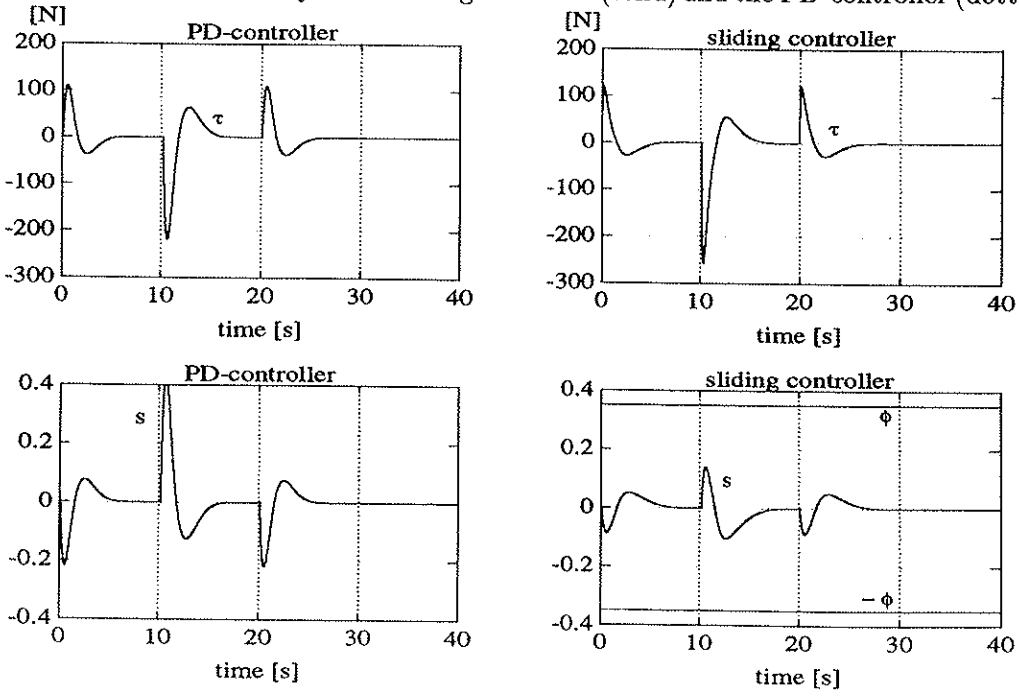

Figure 5.10: Control inputs and sliding surfaces for the PD-controller and the sliding controller.

5.3.2 Sliding Control of MIMO Nonlinear Systems

MIMO Nonlinear Systems with Arbitrary Relative Degree

These results are published in Fossen and Foss (1991) and are mainly an extension of the results of Slotine and Li (1991). The sliding design methodology is described in detail by e.g. Utkin (1977) and Slotine (1983). The basic idea of sliding controller design is to provide a systematic approach to the problem of designing a robust controller in the case of modelling inaccuracies. This can be achieved by replacing the error equation, Eq. 5.2, by

$$\dot{\boldsymbol{s}} + \boldsymbol{k}.\times \boldsymbol{sgn}(\boldsymbol{s}) = \boldsymbol{w}(t) \quad \text{where} \quad k_i > \sup_t \mid w_i(t) \mid ; \qquad i = 1, 2, ..., m$$

Here $\boldsymbol{s}$ is a measure of tracking and $\boldsymbol{w}(t)$ represents all the external signals. The switching term $\boldsymbol{k}.\times \boldsymbol{sgn}(\boldsymbol{s})$ can be interpreted as a vector of elements $k_i\ sgn(s_i)$. If all k_i satisfy the above inequality, then $\boldsymbol{s}$ goes to zero in finite time. Define a sliding surface, Fossen and Foss (1991),

$$s_j = (\frac{d}{dt} + \lambda_j)^{r_j - 1} e_j \quad \text{where} \quad e_j = y_j - y_{j,d} \tag{5.15}$$

where λ_j is a positive scalar specifying the control bandwidth and $y_{j,d}$ is the desired trajectory. For systems of relative degree $r_j = 1$, Eq. 5.15 simply yields $s_j = e_j$. Define a virtual reference vector $\boldsymbol{\alpha}_d$ with elements $\alpha_{d,j}$ such that

$$\dot{s}_j = y_j^{(r_j)} - \alpha_{d,j} \quad , \quad j = 1, ..., m \tag{5.16}$$

For the system

$$\begin{bmatrix} y_1^{(r_1)} \\ \vdots \\ y_m^{(r_m)} \end{bmatrix} = \boldsymbol{f}^*(\boldsymbol{x}) + \boldsymbol{G}^*(\boldsymbol{x}) \begin{bmatrix} u_1 \\ \vdots \\ u_m \end{bmatrix}$$

where $\boldsymbol{f}^*$ and $\boldsymbol{G}^*$ are defined in Section 5.2.1, we propose a control law (assuming $\boldsymbol{G}^*(\boldsymbol{x})$ is non-singular)

$$\boldsymbol{u} = (\hat{\boldsymbol{G}}^*(\boldsymbol{x}))^{-1} \left[\boldsymbol{\alpha}_d - \hat{\boldsymbol{f}}^*(\boldsymbol{x}) - \boldsymbol{k}.\times \boldsymbol{sgn}(\boldsymbol{s}) \right] \tag{5.17}$$

Here the hat denotes the estimates of the nonlinear functions. The bounds of the elements k_i may be derived by applying Barbălat's lemma. Notice, that the existence of $\boldsymbol{u}$ is influenced by the choice of the controlled variables $\boldsymbol{y}$ i.e. the existence of the inverse of $\boldsymbol{G}^*(\boldsymbol{x})$.

Assume that the parametric uncertainties in the nonlinear functions $\boldsymbol{f}^*$ and $\boldsymbol{G}^*$ satisfy the following bounds

$$\begin{aligned} \mid \hat{f}_j^*(\boldsymbol{x}) - f_j^*(\boldsymbol{x}) \mid &\leq \delta_i \\ \boldsymbol{G}^*(\boldsymbol{x}) = (\boldsymbol{I} + \boldsymbol{\Delta})\hat{\boldsymbol{G}}^*(\boldsymbol{x}) \quad &, \quad \mid \Delta_{ij} \mid \leq U_{ij} \end{aligned} \tag{5.18}$$

where $(i = 1, ..., m)$, $(j = 1, ..., m)$ and $\overline{\sigma}(\boldsymbol{\Delta}) < 1$. Consider a Lyapunov-like function candidate:

$$V(\boldsymbol{s}, t) = \frac{1}{2}\boldsymbol{s}^T\boldsymbol{s} \tag{5.19}$$

Differentiating $V(\boldsymbol{s}, t)$ with respect to time and substituting Eqs. 5.4, 5.16, 5.17 and 5.18 yields

$$\dot{V} = \boldsymbol{s}^T\dot{\boldsymbol{s}} = \boldsymbol{s}^T \left[(\boldsymbol{f}^* - \hat{\boldsymbol{f}}^*) + \boldsymbol{\Delta}(\boldsymbol{\alpha}_d - \hat{\boldsymbol{f}}^*) - (\boldsymbol{I} + \boldsymbol{\Delta})\, \boldsymbol{k}. \times \boldsymbol{sgn}(\boldsymbol{s}) \right] \tag{5.20}$$

From this it is seen that if $k_i \geq k_i'$ $\forall$ i where the vector $\boldsymbol{k}'$ satisfies

$$(\boldsymbol{I} - \overline{\boldsymbol{U}})\, \boldsymbol{k}' = \boldsymbol{\delta} + \boldsymbol{U} \mid \boldsymbol{\alpha}_d - \hat{\boldsymbol{f}}^*(\boldsymbol{x}) \mid + \boldsymbol{\eta} \tag{5.21}$$

with $\boldsymbol{U}$ as an $m \times m$ matrix with elements U_{ij} and $\overline{\boldsymbol{U}}$ defined as

$$\overline{\boldsymbol{U}} = \begin{bmatrix} U_{11} & -U_{12} & \dots & -U_{1m} \\ -U_{21} & U_{22} & & -U_{2m} \\ \vdots & & \ddots & \vdots \\ -U_{m1} & -U_{m2} & \dots & U_{mm} \end{bmatrix} \tag{5.22}$$

the sliding condition

$$\dot{V} \leq -\boldsymbol{\eta}^T \mid \boldsymbol{s} \mid = \sum_{i=1}^{m} -\eta_i \mid s_i \mid \leq 0 \quad , \quad \eta_i > 0 \tag{5.23}$$

is satisfied. Hence, applying Barbălat's Lyapunov-like lemma ensures that $\boldsymbol{s} \to 0$ and thus $\boldsymbol{e} \to 0$. The proof is found in Appendix B.

5.3.3 MIMO Sliding Control Applied to Underwater Vehicles

It is straightforward to apply the results from the previous sections to the MIMO underwater vehicle equations of motion. For attitude control of Hamiltonian spacecraft Slotine and Benedetto (1990) suggest using a Lyapunov-like function candidate

$$V(\boldsymbol{s},t) = \frac{1}{2}\,\boldsymbol{s}^T\boldsymbol{M}^*\boldsymbol{s} \quad , \quad \boldsymbol{M}^* = (\boldsymbol{M}^*)^T > 0$$

to prove global stability. This function can also be applied in the stability analyses of underwater vehicles in 6 DOF. Differentiating V with respect to time yields:

$$\dot{V} = \boldsymbol{s}^T\boldsymbol{M}^*\dot{\boldsymbol{s}} + \frac{1}{2}\boldsymbol{s}^T\dot{\boldsymbol{M}}^*\boldsymbol{s} - \boldsymbol{s}^T\boldsymbol{C}^*\boldsymbol{s} + \boldsymbol{s}^T\boldsymbol{C}^*\boldsymbol{s}$$

Define a measure of tracking $\boldsymbol{s}$ such that

$$\boldsymbol{s} = \dot{\tilde{\boldsymbol{x}}} + \lambda\tilde{\boldsymbol{x}} \quad \text{where} \quad \tilde{\boldsymbol{x}} = \boldsymbol{x} - \boldsymbol{x}_d \quad \text{is the tracking error}$$

and a virtual reference vector $\boldsymbol{x}_r$ satisfying

$$\boldsymbol{s} = \dot{\boldsymbol{x}} - \dot{\boldsymbol{x}}_r \quad \text{where} \quad \dot{\boldsymbol{x}}_r = \dot{\boldsymbol{x}}_d - \lambda\tilde{\boldsymbol{x}}$$

Applying the skew-symmetric property $\boldsymbol{s}^T(\dot{\boldsymbol{M}}^* - \boldsymbol{C}^*)\boldsymbol{s} = 0 \quad \forall\ \boldsymbol{s}$ to the expression for $\dot{V}$ yields

$$\dot{V} = \boldsymbol{s}^T\boldsymbol{M}^*(\ddot{\boldsymbol{x}} - \ddot{\boldsymbol{x}}_r) + \boldsymbol{s}^T\boldsymbol{C}^*(\dot{\boldsymbol{x}} - \dot{\boldsymbol{x}}_r)$$

Substituting the nonlinear ROV model, Eq. 2.41, into the expression for $\dot{V}$ yields:

$$\dot{V} = -\boldsymbol{s}^T\boldsymbol{D}^*\boldsymbol{s} + \boldsymbol{s}^T(\boldsymbol{B}^*\boldsymbol{u} - \boldsymbol{M}^*\ddot{\boldsymbol{x}}_r - \boldsymbol{C}^*\dot{\boldsymbol{x}}_r - \boldsymbol{D}^*\dot{\boldsymbol{x}}_r - \boldsymbol{g}^*)$$

Fossen and Sagatun(1991a, 1991b) show that the representation of the control law of Slotine and Benedetto (1990) can be simplified by defining a virtual reference vector $\boldsymbol{q}_r$ satisfying the transformation

$$\dot{\boldsymbol{x}}_r = \boldsymbol{J}(\boldsymbol{x})\,\dot{\boldsymbol{q}}_r$$

From this we obtain

$$\begin{aligned}\dot{\boldsymbol{q}}_r &= \boldsymbol{J}^{-1}(\boldsymbol{x})\,\dot{\boldsymbol{x}}_r \\ \ddot{\boldsymbol{q}}_r &= \boldsymbol{J}^{-1}(\boldsymbol{x})\,(\ddot{\boldsymbol{x}}_r - \dot{\boldsymbol{J}}(\boldsymbol{x})\boldsymbol{J}^{-1}(\boldsymbol{x})\,\dot{\boldsymbol{x}}_r)\end{aligned}$$

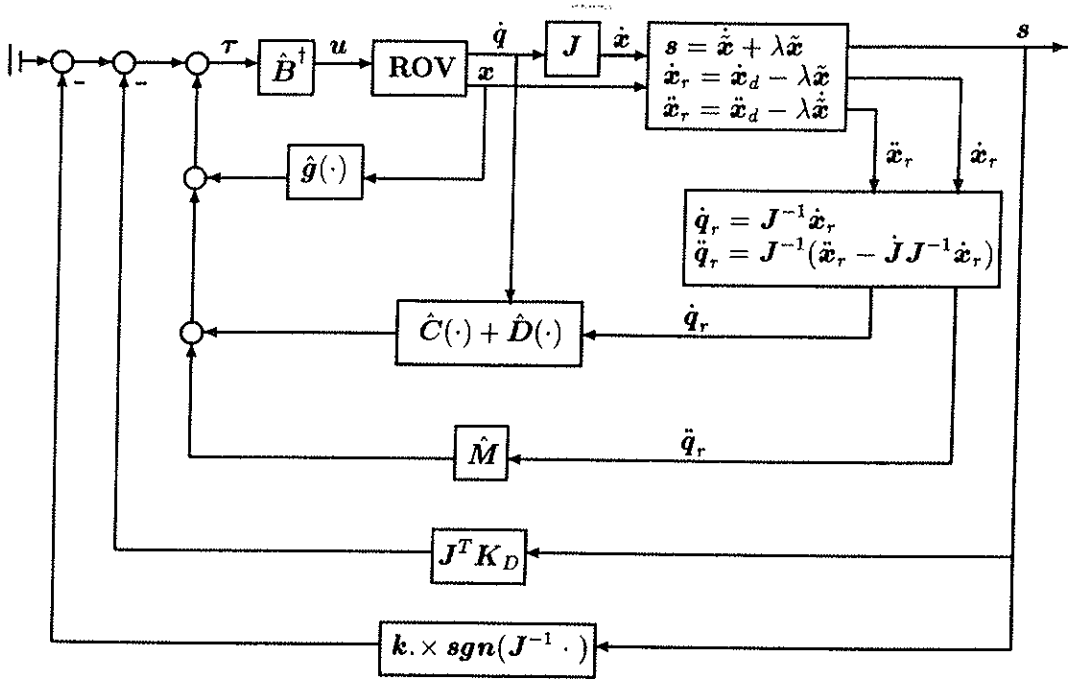

Figure 5.11: MIMO sliding control applied to underwater vehicles

Hence, the expression for $\dot{V}$ can be expressed as

$$\dot{V} = -s^T D^* s + (J^{-1}s)^T(Bu - M\ddot{q}_r - C\dot{q}_r - D\dot{q}_r - g) \tag{5.24}$$

Let us initially assume that the input matrix $\boldsymbol{B}$ is known and restrict our discussion to underwater vehicles with equal or more control inputs than controllable DOF i.e. $p \geq n$. Hence, a generalized inverse $\boldsymbol{B}^{\dagger}$ can be used in the decoupling. Uncertainties in the input matrix matrix will be treated in Section 5.4.3. Let the estimates of the the terms $\boldsymbol{M}$, $\boldsymbol{C}$, $\boldsymbol{D}$ and $\boldsymbol{g}$ be denoted as $\hat{\boldsymbol{M}}$, $\hat{\boldsymbol{C}}$, $\hat{\boldsymbol{D}}$ and $\hat{\boldsymbol{g}}$, then the nonlinear control law, Fossen and Sagatun (1991a), is

$$\boldsymbol{u} = \boldsymbol{B}^{\dagger}[\underbrace{\hat{\boldsymbol{M}}\ddot{\boldsymbol{q}}_r + \hat{\boldsymbol{C}}\dot{\boldsymbol{q}}_r + \hat{\boldsymbol{D}}\dot{\boldsymbol{q}}_r + \hat{\boldsymbol{g}}}_{Feedforward\ term} - \underbrace{\boldsymbol{J}^T\boldsymbol{K}_D\,\boldsymbol{s}}_{PD-controller} - \underbrace{\boldsymbol{k}\,.\times\,\boldsymbol{sgn}\,(\boldsymbol{J}^{-1}\boldsymbol{s})}_{Robustifying\ term}]$$

where $\boldsymbol{K}_D$ is a positive semi-definite regulator gain matrix of appropriate dimension and the operator $.\times$ is used to denote the Schur product i.e. element-by-element multiplication.

This in turn implies

$$\dot{V} = -\boldsymbol{s}^T(\boldsymbol{D}^* + \boldsymbol{K}_D)\boldsymbol{s} + (\boldsymbol{J}^{-1}\boldsymbol{s})^T(\tilde{\boldsymbol{M}}\ddot{\boldsymbol{q}}_r + \tilde{\boldsymbol{C}}\dot{\boldsymbol{q}}_r + \tilde{\boldsymbol{D}}\dot{\boldsymbol{q}}_r + \tilde{\boldsymbol{g}}) - \boldsymbol{k}^T \mid \boldsymbol{J}^{-1}\boldsymbol{s} \mid$$

Here $\tilde{\boldsymbol{M}} = \hat{\boldsymbol{M}} - \boldsymbol{M}$, $\tilde{\boldsymbol{C}} = \hat{\boldsymbol{C}} - \boldsymbol{C}$, $\tilde{\boldsymbol{D}} = \hat{\boldsymbol{D}} - \boldsymbol{D}$ and $\tilde{\boldsymbol{g}} = \hat{\boldsymbol{g}} - \boldsymbol{g}$. This suggests that the elements k_i of the switching gain vector $\boldsymbol{k}$ should be chosen as:

$$k_i \geq \mid \tilde{\boldsymbol{M}}\ddot{\boldsymbol{q}}_r + \tilde{\boldsymbol{C}}(\dot{\boldsymbol{q}})\dot{\boldsymbol{q}}_r + \tilde{\boldsymbol{D}}(\dot{\boldsymbol{q}})\dot{\boldsymbol{q}}_r + \tilde{\boldsymbol{g}}(\boldsymbol{x})\mid_i + \eta_i \quad , \quad \eta_i > 0 \tag{5.25}$$

This in turn implies

$$\dot{V} \leq -\boldsymbol{s}^T(\boldsymbol{D}^* + \boldsymbol{K}_D)\boldsymbol{s} - \boldsymbol{\eta}^T\,(\boldsymbol{J}^{-1}\boldsymbol{s}) \leq 0$$

This is due to the fact that the dissipative matrix $\boldsymbol{D} > 0$ and the regulator gain matrix $\boldsymbol{K}_D \geq 0$ implies that $(\boldsymbol{J}^{-T}\boldsymbol{D}\boldsymbol{J}^{-1} + \boldsymbol{K}_D) > 0$. Hence, $\boldsymbol{s}$ is bounded and $\dot{V}$ is uniformly continuous. Therefore, Barbălat's lemma ensures that $\boldsymbol{s} \rightarrow 0$ and thus $\tilde{\boldsymbol{x}} \rightarrow 0$ as $t \rightarrow \infty$.
In Section 5.4.1 it will be shown that adaptive and sliding control can be successfully combined to reduce the parametric uncertainties. Hybrid (adaptive and sliding) control compensating for uncertainties in the input matrix $\boldsymbol{B}$ is discussed in Section 5.4.3. An alternative approach to an adaptive controller is using a STC. This is the topic for the next section.

5.3.4 Self-Tuning Sliding Control

A nonlinear RPE method has been applied in the self-tuning sliding controller proposed by Fossen and Balchen (1988). The STC is simulated for an underwater vehicle in 3 DOF. Let us assume that the parameter estimates satisfy the following bounds

$$|\theta_j - \hat{\theta}_j| \leq \tilde{\theta}_j \quad , \quad j = 1,..r$$

where r is the number of parameters and $\boldsymbol{\theta}$ is an unknown parameter vector found from the linear parameterization

$$\boldsymbol{\tau} = \boldsymbol{M}\ddot{\boldsymbol{q}} + \boldsymbol{C}(\dot{\boldsymbol{q}})\dot{\boldsymbol{q}} + \boldsymbol{D}(\dot{\boldsymbol{q}})\dot{\boldsymbol{q}} + \boldsymbol{g}(\boldsymbol{x}) = \boldsymbol{\Phi}(\ddot{\boldsymbol{q}}, \dot{\boldsymbol{q}}, \boldsymbol{x})\,\boldsymbol{\theta}$$

where $\boldsymbol{\Phi}$ as a known regressor matrix . This requires that $\ddot{\boldsymbol{q}}$, $\dot{\boldsymbol{q}}$ and $\boldsymbol{x}$ are measured. The switching gains in Eq. 5.25 can be replaced by

$$k_i \geq \sum_{j=1}^{r} |\Phi_{ij}(\ddot{\boldsymbol{q}}, \dot{\boldsymbol{q}}, \boldsymbol{x})\;\tilde{\theta}_j| + \eta_i \quad , \quad \eta_i > 0$$

where (i=1,2,...,n) and $\tilde{\theta}_j$ is the uncertainty of the j-th parameter estimate. This in turn suggests that the control law should be calculated as

$$\boldsymbol{\tau} = \left[\hat{\boldsymbol{M}}\ddot{\boldsymbol{q}}_r + \hat{\boldsymbol{C}}\dot{\boldsymbol{q}}_r + \hat{\boldsymbol{D}}\dot{\boldsymbol{q}}_r + \hat{\boldsymbol{g}} - \boldsymbol{J}^T\boldsymbol{K}_D\,\boldsymbol{s} - \boldsymbol{k}\;.\times\; \boldsymbol{sgn}\,(\boldsymbol{J}^{-1}\boldsymbol{s})\right]$$

where the hat denotes the estimated parameters. The unknown parameters are updated according to Eqs. 5.11 and 5.12. As in the self-tuning feedback linearization case, PE is required to guarantee the parameter error to converge to zero. This suggests that the self-tuning sliding controller should only be used when a relatively small number of parameters are to be estimated. If this is not the case, the direct adaptive control scheme presented in the next section could be advantageous.

Simulation Study: Self-Tuning Sliding Control Applied to an Underwater Vehicle

Again, consider the simplified ROV model in surge

$$m\,\ddot{x} + d\,\dot{x}\,|\dot{x}| = \tau$$

with $m = 200\ kg$ *and* $d = 50\ kg/m$. *The parameter and regressor vectors are*

$$\boldsymbol{\Phi} = (\ \ddot{x} \quad |\dot{x}|\dot{x}\ ) \qquad , \qquad \boldsymbol{\theta} = (\ m \quad d\ )^T$$

while the prediction error is defined as:

$$e = \boldsymbol{\Phi}\,\hat{\boldsymbol{\theta}} - \tau$$

Hence, the parameter vector is updated as:

$$\begin{aligned} \dot{\hat{\boldsymbol{\theta}}} &= -\boldsymbol{P}\boldsymbol{\Phi}^T e \\ \dot{\boldsymbol{P}} &= \lambda\,\boldsymbol{P} - \boldsymbol{P}\boldsymbol{\Phi}^T\boldsymbol{\Phi}\boldsymbol{P} \end{aligned}$$

In the simulation study the sampling rate was set at 10 Hz. The initial parameter estimates were chosen as $\hat{m}(0) = \hat{d}(0) = 0$ *while the initial adaption gain was chosen as* $\boldsymbol{P}(0) = 10\,\boldsymbol{I}$. *The simulation was performed with* $\lambda = 0.96$ *and the control input was simply chosen as*

$$\tau = \tau_o \sin(2\pi \frac{t}{T})$$

with $\tau_o = 15$ *and* $T = 10$. *The convergence of the parameter estimates are shown in Figure 5.12.*

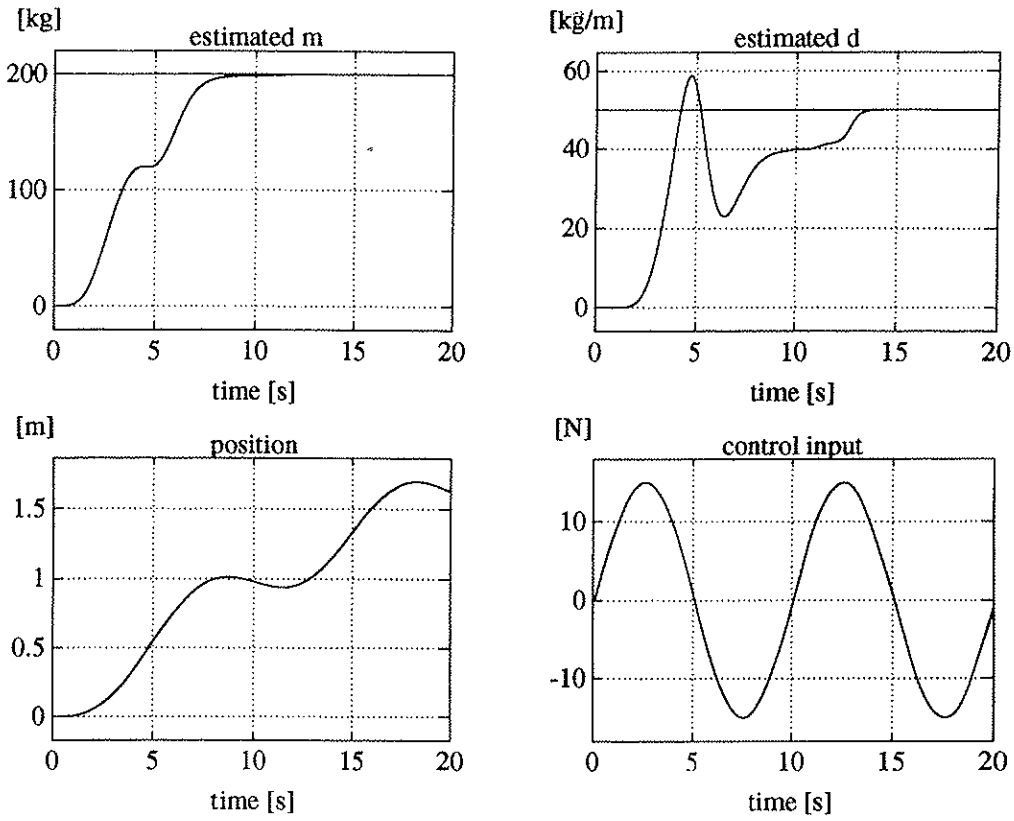

Figure 5.12: Parameter estimates, actual position and control input.

Notice that the estimated parameters converge to their actual values in less than 15 seconds due to the PE control input. The vehicle should perform a self-test each time the ROV undergoes a configuration change. The self-test could simply be a cycle of known inputs to each thruster. Then, the parameter estimates obtained from the self-test should be used to calculate the sliding control law Eq. 5.14.

5.4 Passivity Based Adaptive Control Design

In this section a passivity based adaptive autopilot design for underwater vehicles will be discussed. The proposed autopilot is general enough for dynamic positioning as well as tracking of a time-varying reference trajectories in 6 DOF. The autopilot design will be divided into three steps: (1) parameter estimation, (2) adaptive compensation of sea currents and (3) compensation of input uncertainties. A block diagram of the autopilot is shown in Figure 5.13.

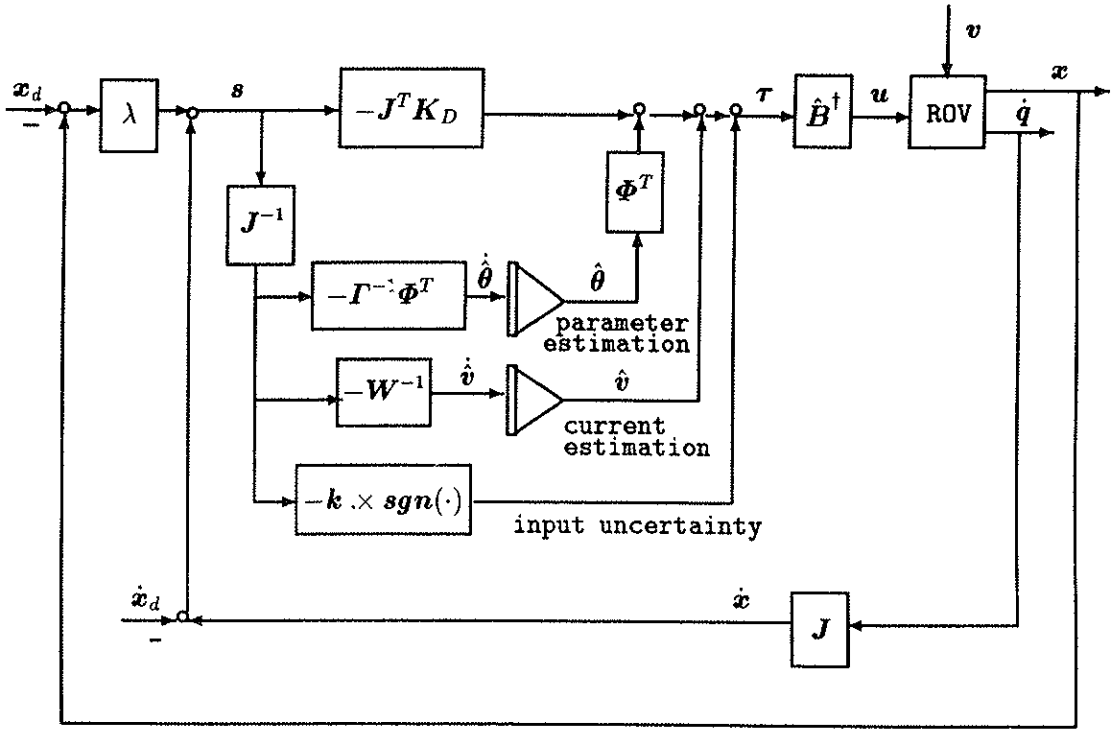

Figure 5.13: Nonlinear adaptive autopilot design for underwater vehicles

As seen from the block diagram, the inner loop (Section 5.4.1) represents the parameter update law. The next loop is an adaptive feedforward term for the compensation of slowly varying sea currents (Section 5.4.2). Finally, the third loop shows how uncertainties in the input matrix due to partly known thruster characteristics can be compensated for by adding a discontinuous term to the adaptive control law (Section 5.4.3). This loop compensates for uncertainties due to the expression:

$$\boldsymbol{u} = \hat{\boldsymbol{B}}^{\dagger}(\dot{\boldsymbol{q}})\,\boldsymbol{\tau} \tag{5.26}$$

which is strongly influenced of the accuracy of the estimate

$$\hat{B}_{ij} = \rho\, D^4\, \hat{K}_{T_{ij}}(J_o); \qquad i = 1,2,..,n \qquad j = 1,2..,p$$

Generation of the desired force and moment vector $\boldsymbol{\tau}$ can be done by applying direct adaptive control theory. This is the topic for the next section.

5.4.1 Global Stable Adaptive Control Design

(i) PBAC

Passivity based adaptive control (PBAC) schemes, Slotine and Li (1987), Sadegh and Horowitz (1987) and Kelly and Carelli (1988), exploit the skew-symmetric property of $\dot{\boldsymbol{M}} - 2\boldsymbol{C}$, c.f. Ortega and Spong (1988). The parameter update law in this section is based on an extension of the results of Slotine and Li (1987) and Slotine and Benedetto (1990) to underwater vehicles. The results are published in Fossen and Sagatun(1991a, 1991b). Consider the nonlinear underwater vehicle equations of motion, Eq. 2.41,

$$\boldsymbol{M}^*(\boldsymbol{x})\ddot{\boldsymbol{x}} + \boldsymbol{C}^*(\boldsymbol{x},\dot{\boldsymbol{x}})\dot{\boldsymbol{x}} + \boldsymbol{D}^*(\boldsymbol{x},\dot{\boldsymbol{x}})\dot{\boldsymbol{x}} + \boldsymbol{g}^*(\boldsymbol{x}) = \boldsymbol{J}^{-T}\boldsymbol{\tau}$$

Assume the desired trajectory: $\ddot{\boldsymbol{x}}_d$, $\dot{\boldsymbol{x}}_d$ and $\boldsymbol{x}_d$ to be bounded. Let $\tilde{\boldsymbol{x}} = \boldsymbol{x} - \boldsymbol{x}_d$ be the tracking error and $\tilde{\boldsymbol{\theta}}$ be the parameter error vector. Define a measure of tracking $\boldsymbol{s}$ as

$$\boldsymbol{s} = \dot{\tilde{\boldsymbol{x}}} + \lambda\tilde{\boldsymbol{x}} \tag{5.27}$$

where λ is a strictly positive constant which may be interpreted as the control bandwidth. It is convenient to rewrite Eq. 5.27 as

$$\boldsymbol{s} = \dot{\boldsymbol{x}} - \dot{\boldsymbol{x}}_r \quad \text{where} \quad \dot{\boldsymbol{x}}_r = \dot{\boldsymbol{x}}_d - \lambda\tilde{\boldsymbol{x}}$$

To prove global stability, Slotine and Benedetto (1990) suggest using a Lyapunov-like function candidate

$$V(\boldsymbol{s},\tilde{\boldsymbol{\theta}},t) = \frac{1}{2}\left(\boldsymbol{s}^T\boldsymbol{M}^*\boldsymbol{s} + \tilde{\boldsymbol{\theta}}^T\boldsymbol{\Gamma}\tilde{\boldsymbol{\theta}}\right) \quad , \quad \boldsymbol{M}^* = (\boldsymbol{M}^*)^T > 0$$

where $\boldsymbol{\Gamma}$ is a symmetric positive definite weighting matrix of appropriate dimension. Differentiating V with respect to time and using the skew-symmetric property $\dot{\boldsymbol{x}}^T(\dot{\boldsymbol{M}}^* - 2\boldsymbol{C}^*)\,\dot{\boldsymbol{x}} = 0 \;\forall\; \dot{\boldsymbol{x}}$, yields:

$$\dot{V} = -\boldsymbol{s}^T\boldsymbol{D}^*\boldsymbol{s} + \dot{\tilde{\boldsymbol{\theta}}}^T\boldsymbol{\Gamma}\tilde{\boldsymbol{\theta}} + \boldsymbol{s}^T(\boldsymbol{J}^{-T}\boldsymbol{\tau} - \boldsymbol{M}^*\ddot{\boldsymbol{x}}_r - \boldsymbol{C}^*\dot{\boldsymbol{x}}_r - \boldsymbol{D}^*\dot{\boldsymbol{x}}_r - \boldsymbol{g}^*)$$

Fossen and Sagatun(1991a, 1991b) define a virtual vector $\dot{\boldsymbol{q}}_r$ which satisfies the transformation:

$$\dot{\boldsymbol{x}}_r = \boldsymbol{J}(\boldsymbol{x})\, \dot{\boldsymbol{q}}_r$$

Hence, the virtual reference vectors $\dot{\boldsymbol{q}}_r$ and $\ddot{\boldsymbol{q}}_r$ can be calculated as:

$$\begin{aligned} \dot{\boldsymbol{q}}_r &= \boldsymbol{J}^{-1}(\boldsymbol{x})\dot{\boldsymbol{x}}_r \\ \ddot{\boldsymbol{q}}_r &= \boldsymbol{J}^{-1}(\boldsymbol{x})(\ddot{\boldsymbol{x}}_r - \dot{\boldsymbol{J}}(\boldsymbol{x})\boldsymbol{J}^{-1}(\boldsymbol{x})\dot{\boldsymbol{x}}_r) \end{aligned}$$

We now notice that the unknown terms $\boldsymbol{M}^*, \boldsymbol{C}^*, \boldsymbol{D}^*$ and $\boldsymbol{g}^*$ can be parameterized as

$$\boldsymbol{M}^*\ddot{\boldsymbol{x}}_r + \boldsymbol{C}^*\dot{\boldsymbol{x}}_r + \boldsymbol{D}^*\dot{\boldsymbol{x}}_r + \boldsymbol{g}^* = \boldsymbol{J}^{-T}\left[\boldsymbol{M}\ddot{\boldsymbol{q}}_r + \boldsymbol{C}\dot{\boldsymbol{q}}_r + \boldsymbol{D}\dot{\boldsymbol{q}}_r + \boldsymbol{g}\right] = \boldsymbol{J}^{-T}\boldsymbol{\Phi}(\boldsymbol{x}, \dot{\boldsymbol{q}}, \dot{\boldsymbol{q}}_r, \ddot{\boldsymbol{q}}_r)\,\boldsymbol{\theta}$$

where $\boldsymbol{\theta}$ is an unknown parameter vector and $\boldsymbol{\Phi}$ is a known regressor matrix of appropriate dimension. We have here assumed that the terms $\boldsymbol{M}^*$, $\boldsymbol{C}^*$, $\boldsymbol{D}^*$ and $\boldsymbol{g}^*$ are linear in their parameters. By using $\boldsymbol{q}_r$ instead of $\boldsymbol{x}_r$ in the parameterization, the transformation matrix $\boldsymbol{J}(\boldsymbol{x})$ is avoided in the expression for the regressor matrix. This yields:

$$\dot{V} = -\boldsymbol{s}^T\boldsymbol{D}^*\boldsymbol{s} + (\boldsymbol{J}^{-1}\boldsymbol{s})^T(\boldsymbol{\tau} - \boldsymbol{\Phi}\,\boldsymbol{\theta}) + \dot{\tilde{\boldsymbol{\theta}}}^T\boldsymbol{\Gamma}\tilde{\boldsymbol{\theta}} \tag{5.28}$$

Let the control law be chosen as

$$\boldsymbol{\tau} = \boldsymbol{\Phi}\,\hat{\boldsymbol{\theta}} - \boldsymbol{J}^T\boldsymbol{K}_D\boldsymbol{s} \tag{5.29}$$

where $\hat{\boldsymbol{\theta}}$ is the estimated parameter vector and $\boldsymbol{K}_D$ is a symmetric positive regulator gain matrix of appropriate dimension. Then, the parameter update law

$$\dot{\hat{\boldsymbol{\theta}}} = -\boldsymbol{\Gamma}^{-1}\boldsymbol{\Phi}^T(\boldsymbol{x}, \dot{\boldsymbol{q}}, \dot{\boldsymbol{q}}_r, \ddot{\boldsymbol{q}}_r)\boldsymbol{J}^{-1}(\boldsymbol{x})\,\boldsymbol{s}$$

yields

$$\dot{V} = -\boldsymbol{s}^T(\boldsymbol{K}_D + \boldsymbol{D}^*)\boldsymbol{s} \leq 0$$

This is due to the fact that the dissipative term $\boldsymbol{D} > 0$ implies that $\boldsymbol{D}^* = \boldsymbol{J}^{-T}\boldsymbol{D}\boldsymbol{J}^{-1} > 0$. Hence, global stability is guaranteed by applying Barbălat's Lyapunov-like lemma. This in turn implies that the tracking error vector converges to zero i.e. $\tilde{\boldsymbol{x}} \to 0$ and that the parameter error vector is bounded i.e. $||\tilde{\boldsymbol{\theta}}|| < \infty$. The boundness of the parameter error vector and the global asymptotic stability of the tracking error allows a large number of parameters to be estimated. Global asymptotic stability of the parameter error vector cannot be guaranteed without requiring the input vector to be PE.

(ii) VS-PBAC

An alternative parameter update law can be found by deriving a variable structure passivity based adaptive controller (VS-PBAC). The variable structure model reference adaptive controller (VS-MRAC) of Tso *et al.* (1991) uses the parameterization of Craig (1988) which requires both acceleration measurements and that the estimated inertia matrix is invertible. These limiting conditions may be removed by applying the parameterization of Slotine and Li (1987). In this section it will be shown that it is straightforward to generalize the results of Tso *et al.* (1991) to the scheme of Slotine and Li (1987). The results are published in Fossen and Balchen (1991).

Define a Lyapunov-like function candidate:

$$V(\boldsymbol{s},\tilde{\boldsymbol{\theta}},t)=\frac{1}{2}\boldsymbol{s}^T\boldsymbol{M}^*\boldsymbol{s} \quad , \quad \boldsymbol{M}^*=(\boldsymbol{M}^*)^T>0$$

Hence, Eq. 5.28 reduces to:

$$\dot{V}=-\boldsymbol{s}^T\boldsymbol{D}^*\boldsymbol{s}+(\boldsymbol{J}^{-1}\boldsymbol{s})^T(\boldsymbol{\tau}-\boldsymbol{\Phi}\,\boldsymbol{\theta})$$

Let the control law be

$$\boldsymbol{\tau}=\boldsymbol{\Phi}\,\hat{\boldsymbol{\theta}}-\boldsymbol{J}^T\boldsymbol{K}_D\boldsymbol{s}$$

where $\hat{\boldsymbol{\theta}}$ is the estimated parameter vector and $\boldsymbol{K}_D$ is a symmetric positive definite regulator gain matrix of appropriate dimension. This in turn implies that:

$$\dot{V}=-\boldsymbol{s}^T(\boldsymbol{D}^*+\boldsymbol{K}_D)\boldsymbol{s}+(\boldsymbol{J}^{-1}\boldsymbol{s})^T\boldsymbol{\Phi}(\hat{\boldsymbol{\theta}}-\boldsymbol{\theta})$$

We know notice that the last term in the expression for $\dot{V}$ can be written as:

$$(\boldsymbol{J}^{-1}\boldsymbol{s})^T\boldsymbol{\Phi}(\hat{\boldsymbol{\theta}}-\boldsymbol{\theta})=\sum_{i=1}^{r}(\hat{\theta}_i-\theta_i)(\boldsymbol{\Phi}^T\boldsymbol{J}^{-1}\boldsymbol{s})_i$$

Then, the parameter update law

$$\hat{\theta}_i=-\theta_i^*\;sgn\left[(\boldsymbol{\Phi}^T\boldsymbol{J}^{-1}\boldsymbol{s})_i\right] \quad , \quad |\theta_i|\leq\theta_i^*$$

yields

$$\dot{V}=-\boldsymbol{s}^T(\boldsymbol{K}_D+\boldsymbol{D}^*)\boldsymbol{s}-\sum_{i=1}^{r}\theta_i^*\;|\boldsymbol{\Phi}^T\boldsymbol{J}^{-1}\boldsymbol{s}|_i-\sum_{i=1}^{r}\theta_i\;(\boldsymbol{\Phi}^T\boldsymbol{J}^{-1}\boldsymbol{s})_i\leq 0 \qquad ,$$

Assuming $||\boldsymbol{\Phi}||<\infty$, Barbălat's Lyapunov-like lemma ensures that $\boldsymbol{s}\rightarrow 0$, thus the tracking error vector $\tilde{\boldsymbol{x}}$ converges to zero.

Simulation Study: Simplified Model of an Underwater Vehicle

The performance of the PD-controller, the PBAC and the VS-PBAC was compared by studying a simplified model of an underwater vehicle in surge:

$$m\,\ddot{x} + d\,\dot{x}|\dot{x}| = \tau$$

Here $m = 150\ kg$ *and* $d = 50\ kg/m$. *The adaptive control law is:*

$$\tau = \hat{m}\,\ddot{x}_r + \hat{d}\,|\dot{x}|\dot{x}_r - K_D s \quad , \quad K_D > 0$$

The following three cases were studied:

- **(1) PD-controller:**

$$\hat{m} = 0$$
$$\hat{d} = 0$$

- **(2) PBAC:**

$$\dot{\hat{m}} = -\frac{1}{\gamma_1}\,\ddot{x}_r s \qquad \gamma_1 = 0.001$$
$$\dot{\hat{d}} = -\frac{1}{\gamma_2}\,|\dot{x}|\dot{x}_r s \qquad \gamma_2 = 0.001$$

- **(3) VS-PBAC:**

$$\hat{m} = -m^*\,sgn(\ddot{x}_r s) \qquad m^* \geq |m|$$
$$\hat{d} = -d^*\,sgn(|\dot{x}|\dot{x}_r s) \qquad d^* \geq |d|$$

In the simulations we chose $\hat{m}(0) = \hat{d}(0) = 0$ *for the adaptive controller and* $m^* = 1.5\,|m|$, $d^* = 1.5\,|d|$ *for the VS-PBAC. The regulator gain was chosen as* $K_D = 150$ *for all three cases. The sampling rate was set at 20 Hz. The simulation results are shown in Figures 5.14 and 5.15. It is seen that the performance of the VS-PBAC is extremely good except for the chattering in the control input. Hence, implementation of the VS-PBAC requires that the control input must be filtered. This will probably reduce some of the performance. The PBAC also performs quite well particularly compared to the somewhat sluggish performance of the PD-controller. It is seen that the performance of the PBAC is improved after a while as a result of the parameter convergence.*

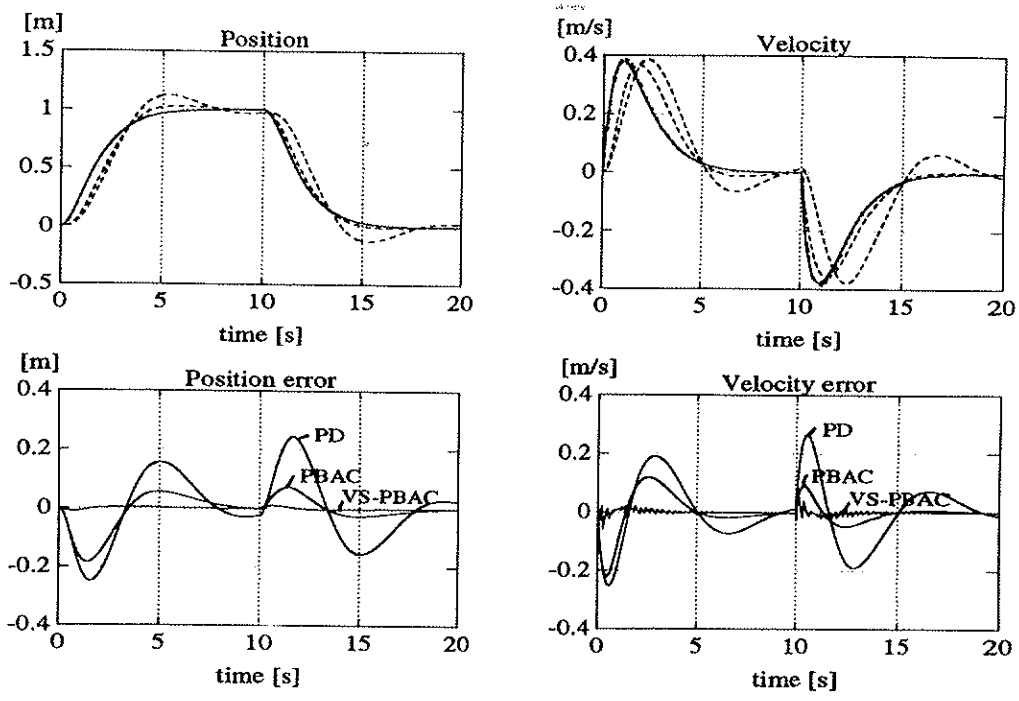

Figure 5.14: Performance study of PBAC, VS-PBAC and PD-controller

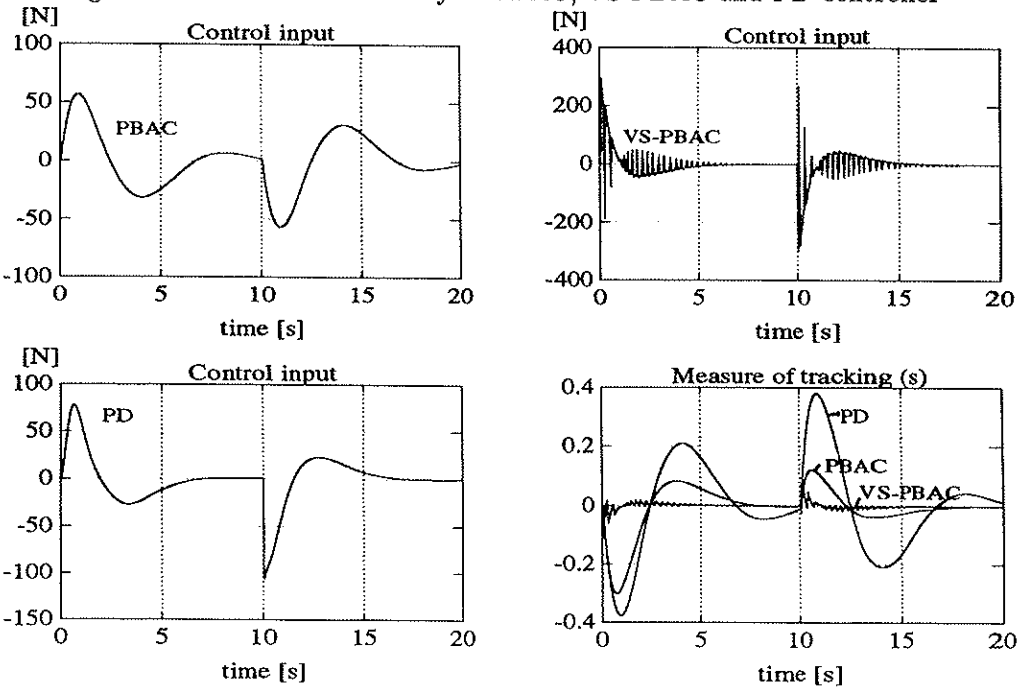

Figure 5.15: Control inputs and measure of tracking for PBAC, VS-PBAC and PD-controller

5.4.2 Adaptive Compensation of Current Induced Disturbances

Sea currents may dramatically reduce the performance of the control system. Fossen and Balchen (1991) suggest adding an adaptive feedforward term to the nonlinear control law to compensate for slowly varying environmental disturbances. Hence, in the nonlinear underwater vehicle equations of motion, we will assume that the earth-fixed current velocity components $\dot{x}_f$, $\dot{y}_f$ and $\dot{z}_f$ are constant or at least slowly varying. The current velocity vector referred to the vehicle-fixed reference frame is:

$$\begin{bmatrix} u_f \\ v_f \\ w_f \end{bmatrix} = \boldsymbol{J}_1^{-1}(\phi,\theta,\psi) \begin{bmatrix} \dot{x}_f \\ \dot{y}_f \\ \dot{z}_f \end{bmatrix}$$

where the coordinate transformation matrix $\boldsymbol{J}_1$ is defined in Section 2.1. We will also assume that all terms which include components of the fluid velocity vector can be lumped together into a total current disturbance vector $\boldsymbol{v}$ such that:

$$\begin{aligned} \boldsymbol{M}\ddot{\boldsymbol{q}} + \boldsymbol{C}(\dot{\boldsymbol{q}})\dot{\boldsymbol{q}} + \boldsymbol{D}(\dot{\boldsymbol{q}})\dot{\boldsymbol{q}} + \boldsymbol{g}(\boldsymbol{x}) + \boldsymbol{v}(t) &= \boldsymbol{\tau} \\ \dot{\boldsymbol{v}} = \boldsymbol{\eta}(t) \quad , \quad \boldsymbol{\eta}(t) &\text{ is white noise} \end{aligned} \tag{5.30}$$

The assumption that current disturbances can be linearly superpositioned in the nonlinear equations of motion radically reduces the number of parameters to be estimated. The disadvantage of this assumption is that model misalignments are imposed. However, simulations show that this is an extremely good assumption. The corresponding x-frame representation of the model is:

$$\boldsymbol{M}^*(\boldsymbol{x})\ddot{\boldsymbol{x}} + \boldsymbol{C}^*(\boldsymbol{x},\dot{\boldsymbol{x}})\dot{\boldsymbol{x}} + \boldsymbol{D}^*(\boldsymbol{x},\dot{\boldsymbol{x}})\dot{\boldsymbol{x}} + \boldsymbol{g}^*(\boldsymbol{x}) + \boldsymbol{v}^*(\boldsymbol{x}) = \boldsymbol{J}^{-T}(\boldsymbol{x})\boldsymbol{\tau}$$

Here, the new term $\boldsymbol{v}^*$ is defined as:

$$\boldsymbol{v}^*(\boldsymbol{x}) = \boldsymbol{J}^{-T}(\boldsymbol{x})\boldsymbol{v}$$

Consider a modified Lyapunov-like function candidate:

$$V(\boldsymbol{s},\tilde{\boldsymbol{\theta}},\tilde{\boldsymbol{v}},t) = \frac{1}{2}(\boldsymbol{s}^T\boldsymbol{M}^*\boldsymbol{s} + \tilde{\boldsymbol{\theta}}^T\boldsymbol{\Gamma}\tilde{\boldsymbol{\theta}} + \tilde{\boldsymbol{v}}^T\boldsymbol{W}\tilde{\boldsymbol{v}})$$

where $\boldsymbol{\Gamma}$ and $\boldsymbol{W}$ are symmetric positive definite weighting matrices. $\tilde{\boldsymbol{v}} = \hat{\boldsymbol{v}} - \boldsymbol{v}$ is the environmental disturbance error vector. Hence, the expression for $\dot{V}$ is modified to

$$\dot{V} = -\boldsymbol{s}^T\boldsymbol{D}^*\boldsymbol{s} + (\boldsymbol{J}^{-1}\boldsymbol{s}^T)^T(\boldsymbol{\tau} - \boldsymbol{\Phi}\,\boldsymbol{\theta} - \boldsymbol{v}) + \dot{\tilde{\boldsymbol{\theta}}}^T\boldsymbol{\Gamma}\tilde{\boldsymbol{\theta}} + \dot{\tilde{\boldsymbol{v}}}^T\boldsymbol{W}\tilde{\boldsymbol{v}}$$

where $\boldsymbol{\Phi}$ is found from the standard linear parameterization:

$$\boldsymbol{M}\ddot{\boldsymbol{q}}_r + \boldsymbol{C}\dot{\boldsymbol{q}}_r + \boldsymbol{D}\dot{\boldsymbol{q}}_r + \boldsymbol{g} = \boldsymbol{\Phi}(\boldsymbol{x},\dot{\boldsymbol{q}},\dot{\boldsymbol{q}}_r,\ddot{\boldsymbol{q}}_r)\,\boldsymbol{\theta}$$

Adding an adaptive feedforward term in the nonlinear control law Eq. 5.29 yields

$$\boldsymbol{\tau} = \boldsymbol{\Phi}\,\hat{\boldsymbol{\theta}} + \hat{\boldsymbol{v}} - \boldsymbol{J}^T\boldsymbol{K}_D\boldsymbol{s} \tag{5.31}$$

This in turn, suggests that the parameter adaption laws should be chosen as

$$\dot{\hat{\boldsymbol{\theta}}} = -\boldsymbol{\Gamma}^{-1}\boldsymbol{\Phi}^T(\boldsymbol{x},\dot{\boldsymbol{q}},\dot{\boldsymbol{q}}_r,\ddot{\boldsymbol{q}}_r)\boldsymbol{J}^{-1}(\boldsymbol{x})\,\boldsymbol{s}$$

$$\dot{\hat{\boldsymbol{v}}} = -\boldsymbol{W}^{-1}\boldsymbol{J}^{-1}(\boldsymbol{x})\,\boldsymbol{s} \tag{5.32}$$

which yields

$$\dot{V} = -\boldsymbol{s}^T(\boldsymbol{K}_D + \boldsymbol{D}^*)\boldsymbol{s} \leq 0$$

Hence, it is seen that slowly varying environmental disturbances can be compensated for by using the modified control law Eq. 5.31 where the feedforward term is updated through Eq. 5.32.

Simulation Study: Dynamic Positioning of the NEROV Vehicle

Again, consider the 4 DOF NEROV nonlinear equations of relative *motion, Appendix A. This corresponds to the state vectors* $\boldsymbol{x} = (x,y,z,\psi)^T$ *and* $\dot{\boldsymbol{q}} = (u,v,w,r)^T$. *The adaptive controller suggests that we write the system in the form of Eq. 5.30. Fluid motion in the x- and y-directions* (u_f *and* v_f) *caused by currents suggests that the unknown disturbance vector should be chosen as*

$$\boldsymbol{v} = (v_1\ v_2\ 0\ v_3)^T$$

for the model in Appendix A. Hence, the adaptive controller should be based on the "current-free" terms:

$$\boldsymbol{M} = \begin{bmatrix} m - X_{\dot{u}} & 0 & 0 & 0 \\ 0 & m - Y_{\dot{v}} & 0 & 0 \\ 0 & 0 & m - Z_{\dot{w}} & 0 \\ 0 & 0 & 0 & I_z - N_{\dot{r}} \end{bmatrix} \qquad \boldsymbol{C}(\dot{\boldsymbol{q}}_r) = \begin{bmatrix} 0 & -mr & 0 & Y_{\dot{v}}v \\ mr & 0 & 0 & -X_{\dot{u}}u \\ 0 & 0 & 0 & 0 \\ -Y_{\dot{v}}v & X_{\dot{u}}u & 0 & 0 \end{bmatrix}$$

$$\boldsymbol{D}(\dot{\boldsymbol{q}}) = -\begin{bmatrix} X_u + X_{u|u|}|u| & 0 & 0 & 0 \\ 0 & Y_u + Y_{v|v|}|v| & 0 & 0 \\ 0 & 0 & Z_w + Z_{w|w|}|w| & 0 \\ 0 & 0 & 0 & N_r + N_{r|r|}|r| \end{bmatrix} \qquad \boldsymbol{g}(\boldsymbol{x}) = \begin{bmatrix} 0 \\ 0 \\ 0 \\ 0 \end{bmatrix}$$

$$\boldsymbol{B}(\dot{\boldsymbol{q}}) = \begin{bmatrix} K_{T_{11}} & K_{T_{12}} & 0 & 0 & 0 & 0 \\ 0 & 0 & -K_{T_{23}} & K_{T_{24}} & 0 & 0 \\ 0 & 0 & 0 & 0 & K_{T_{35}} & K_{T_{36}} \\ -l_1 K_{T_{11}} & l_2 K_{T_{12}} & 0 & 0 & 0 & 0 \end{bmatrix} \qquad \boldsymbol{J}(\boldsymbol{x}) = \begin{bmatrix} c\psi & -s\psi & 0 & 0 \\ s\psi & c\psi & 0 & 0 \\ 0 & 0 & 1 & 0 \\ 0 & 0 & 0 & 1 \end{bmatrix}$$

where all components of the fluid motion vector are removed. The desired outputs in surge and sway were fixed at $x_d = 1$ and $y_d = 1$ m while the depth was switched between $z_d = 2$ m and $z_d = 3$ m. The desired heading angle was shifted between $\psi_d = \pm 30$ deg, see Figure 5.17. An unknown constant current with $\dot{x}_f = 0.9$ m/s, $\dot{y}_f = -0.8$ m/s and $\dot{z}_f = 0.0$ m/s was injected after $t = 5s$. Hence,

$$\begin{bmatrix} u_f \\ v_f \\ w_f \end{bmatrix} = \begin{bmatrix} \cos\psi & \sin\psi & 0 \\ -\sin\psi & \cos\psi & 0 \\ 0 & 0 & 1 \end{bmatrix} \begin{bmatrix} \dot{x}_f \\ \dot{y}_f \\ \dot{z}_f \end{bmatrix}$$

The current induced disturbance used in the simulation study are shown in Figure 5.16

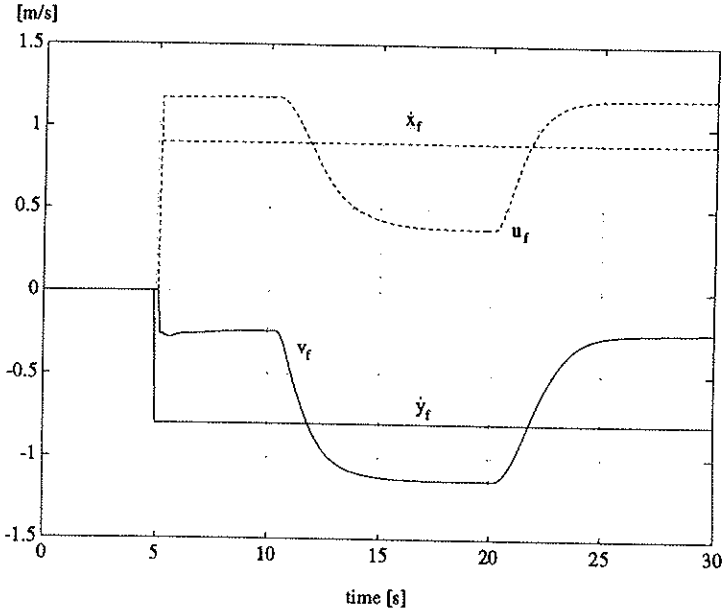

Figure 5.16: Sea current velocities in the earth-fixed and the vehicle-fixed reference frame.

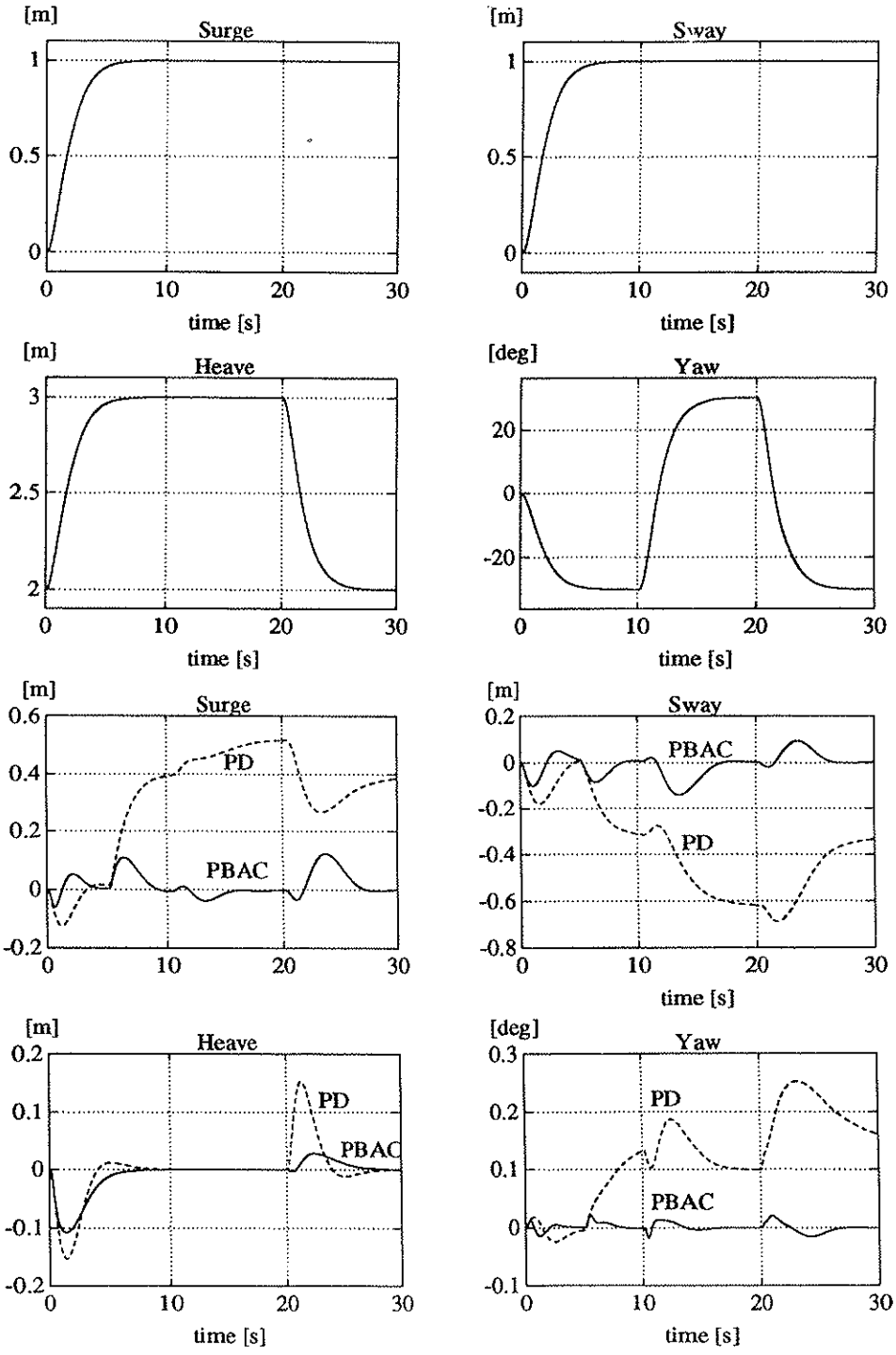

Figure 5.17: Desired outputs (upper plots) and tracking errors (lower plots) in surge, sway, heave and yaw.

The regulator parameters were chosen as $\boldsymbol{K}_D = diag(500, 500, 500, 250)$, $\boldsymbol{\Gamma} = 0.001\ \boldsymbol{I}$, $\boldsymbol{W} = 0.001\ \boldsymbol{I}$ *and* $\lambda = 1$. *The sampling rate was set at 10 Hz. The tracking errors for the PD-controller and the PBAC are shown in Figure 5.17. The control inputs for the PBAC are shown in Figure 5.18.*

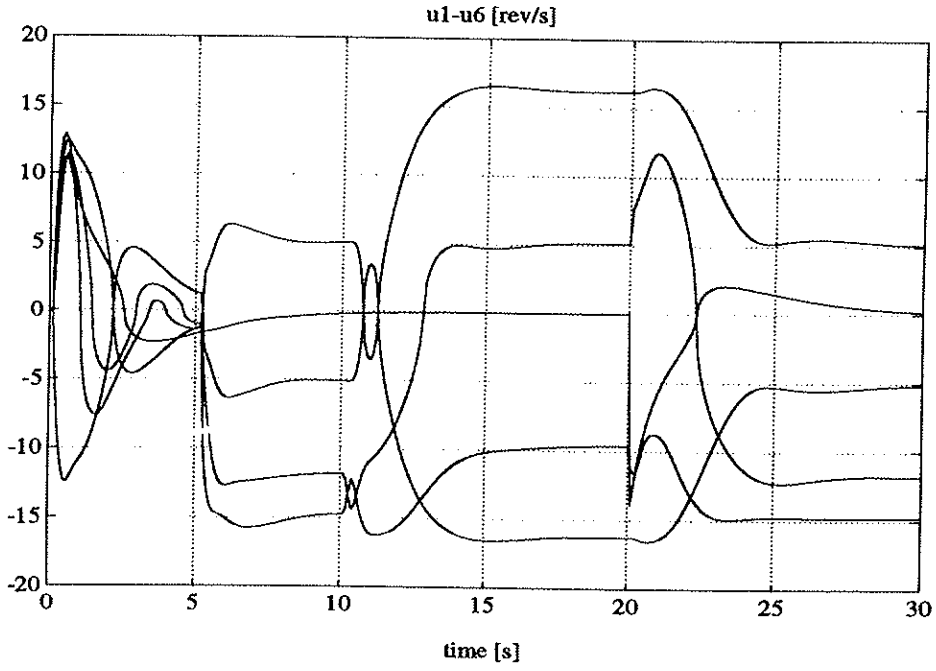

Figure 5.18: Control inputs for the PBAC with feedforward term.

Notice that there is a relatively small increase in the tracking error at $t = 5s$ *where the current disturbances are injected. This shows that the adaptive controller yields high performance even for relatively large current velocities as well as model misalignments. The errors in the regressor matrix, due the assumption that current disturbances could be linearly superpositioned in the nonlinear underwater vehicle equations of motion, did not the reduce the performance of the controller. Other simulations also verified this.*

5.4.3 Compensation of Input Uncertainties

It is well known that input uncertainties, c.f. Eq. 5.26, are crucial for the robustness of the control system. For underwater vehicles this uncertainty is due to partly known thruster and control surface characteristics. This problem was first studied by Fossen and Sagatun(1991a, 1991b). They suggest that the input uncertainty can be incorporated in the

control design simply by assuming that the uncertainties on the input matrix $\boldsymbol{B}$ were on multiplicative from

$$\boldsymbol{B}(\dot{\boldsymbol{q}}) = (\boldsymbol{I} + \boldsymbol{\Delta})\, \hat{\boldsymbol{B}}(\dot{\boldsymbol{q}}) \quad , \quad |\, \boldsymbol{\Delta}_{ij} \,| \leq U_{ij} \tag{5.33}$$

Here $\boldsymbol{I}$ is the $n \times n$ identity matrix and $\boldsymbol{\Delta}$ is an $n \times n$ unknown uncertainty matrix.

Hybrid (Adaptive and Sliding) Control

Substituting Eq. 5.33 into Eq. 5.28 yields

$$\dot{V} = -\boldsymbol{s}^T \boldsymbol{D}^* \boldsymbol{s} + (\boldsymbol{J}^{-1}\boldsymbol{s})^T \left[(\boldsymbol{I} + \boldsymbol{\Delta})\, \hat{\boldsymbol{B}}\boldsymbol{u} - \boldsymbol{\Phi}\, \boldsymbol{\theta} \right] + \tilde{\boldsymbol{\theta}}^T \boldsymbol{\Gamma} \tilde{\boldsymbol{\theta}}$$

Taking the control law to be, Fossen and Sagatun(1991a, 1991b),

$$\boldsymbol{u} = \hat{\boldsymbol{B}}^{\dagger} \left[\boldsymbol{\Phi}\, \hat{\boldsymbol{\theta}} - \boldsymbol{J}^T \boldsymbol{K}_D\, \boldsymbol{s} - \boldsymbol{k} \,.\times\, \boldsymbol{sgn}\,(\boldsymbol{J}^{-1}\boldsymbol{s}) \right] \quad , \quad \boldsymbol{K}_D \geq 0$$

yields

$$\dot{V} = -\boldsymbol{s}^T (\boldsymbol{D}^* + \boldsymbol{K}_D)\boldsymbol{s} + (\boldsymbol{J}^{-1}\boldsymbol{s})^T \left[\boldsymbol{\Delta}\, (\boldsymbol{\Phi}\, \hat{\boldsymbol{\theta}} - \boldsymbol{J}^T \boldsymbol{K}_D \boldsymbol{s}) - (\boldsymbol{I} + \boldsymbol{\Delta})\, \boldsymbol{k} \,.\times\, \boldsymbol{sgn}(\boldsymbol{J}^{-1}\boldsymbol{s}) \right]$$

After some straightforward calculations it is possible to show that the switching gain vector $\boldsymbol{k}$ should be selected such that the elements $k_i \geq k_i'$ $\forall\, i$ where $\boldsymbol{k}'$ is

$$\boldsymbol{k}' = (\boldsymbol{I} - \overline{\boldsymbol{U}})^{-1} \left[\boldsymbol{U}\, |\, \boldsymbol{\Phi}\, \hat{\boldsymbol{\theta}} - \boldsymbol{J}^T \boldsymbol{K}_D \boldsymbol{s}\, | + \boldsymbol{\eta} \right]$$

Here the matrix $\boldsymbol{U}$ is defined in Eq. 5.33 and the matrix $\overline{\boldsymbol{U}}$ is defined as

$$\overline{\boldsymbol{U}} = \begin{bmatrix} U_{11} & -U_{12} & \dots & -U_{1n} \\ -U_{21} & U_{22} & & -U_{2n} \\ \vdots & & \ddots & \vdots \\ -U_{n1} & -U_{n2} & \dots & U_{nn} \end{bmatrix}$$

The proof basically follows that of Eq. 5.21 in Appendix B. Substituting these expressions into the expression for $\dot{V}$ finally yields:

$$\dot{V} \leq -\boldsymbol{s}^T (\boldsymbol{D}^* + \boldsymbol{K}_D)\boldsymbol{s} - \boldsymbol{\eta}^T\, (\boldsymbol{J}^{-1}\boldsymbol{s}) \leq 0$$

As in the previous case, Barbălat's lemma ensures that $\boldsymbol{s} \rightarrow 0$ and thus $\tilde{\boldsymbol{x}} \rightarrow 0$ as $t \rightarrow \infty$. A simulation study of the controller is found in Fossen and Sagatun(1991a, 1991b).

Integral Control

Although the controllers discussed in this chapter all are of PD-type, integral action can be obtained by simply letting $\int_o^t \tilde{\boldsymbol{x}}(\tau)\, d\tau$ be the variable of interest. Hence, the measure of tracking $\boldsymbol{s} = \dot{\tilde{\boldsymbol{x}}} + \lambda\tilde{\boldsymbol{x}}$ should be replaced by:

$$\boldsymbol{s} = \dot{\tilde{\boldsymbol{x}}} + 2\lambda\tilde{\boldsymbol{x}} + \lambda^2 \int_o^t \tilde{\boldsymbol{x}}(\tau)\, d\tau$$

This in turn implies that the adaptive control law

$$\boldsymbol{\tau} = \boldsymbol{\Phi}\,\hat{\boldsymbol{\theta}} - \boldsymbol{J}^T \boldsymbol{K}_D \boldsymbol{s}$$

can be expressed as

$$\boldsymbol{\tau} = \boldsymbol{\Phi}\,\hat{\boldsymbol{\theta}} - \boldsymbol{J}^T \Big(\underbrace{\boldsymbol{K}_D}_{K_D^*}\dot{\tilde{\boldsymbol{x}}} + \underbrace{2\lambda\boldsymbol{K}_D}_{K_P^*}\tilde{\boldsymbol{x}} + \underbrace{\lambda^2\boldsymbol{K}_D}_{K_I^*} \int_o^t \tilde{\boldsymbol{x}}(\tau)\, d\tau \Big)$$

where K_P^*, K_D^* and K_I^* are the proportional, derivative and integral gains, respectively.

Chapter 6

Optimal State Estimation

When designing underwater navigation systems it is sought to design the state estimator in such a manner that the measurement model does not dependent on the vehicle's hydrodynamic parameters. The time-varying behaviour of the hydrodynamic parameters due to unknown disturbances and different operating conditions can drastically reduce the performance of the state estimator. We also require a navigation system which is independent of the vehicle we are using. Hence, we will exclusively use the vehicle's kinematic equations in our design.

The navigation system can be designed by applying well known Kalman filtering techniques to combine the different sensors in an "optimal" manner. Under certain conditions like observability, a state estimator (Kalman filter) also allows us to estimate the unmeasured states. In this chapter, we will show how the different sensors can be integrated in two independent state estimators, each designed for:

- Estimation of position $\boldsymbol{x}_1 = (x, y, z)^T$ and linear velocities $\dot{\boldsymbol{q}}_1 = (u, v, w)^T$.
- Estimation of Euler angles $\boldsymbol{x}_2 = (\phi, \theta, \psi)^T$ and angular velocities $\dot{\boldsymbol{q}}_2 = (p, q, r)^T$.

Recall that all the proposed nonlinear autopilots in the previous chapter were based on full state feedback i.e. the assumption that: $\boldsymbol{x} = (x, y, z, \phi, \theta, \psi)^T$ and $\dot{\boldsymbol{q}} = (u, v, w, p, q, r)^T$ were measurable. In many applications this is not realistic. Hence, we will show how acceptable estimates of $\boldsymbol{x}$ and $\dot{\boldsymbol{q}}$ can be obtained. The state vector estimates will be denoted by $\hat{\boldsymbol{x}}$ and $\hat{\dot{\boldsymbol{q}}}$, respectively.

6.1 Review of Optimal State Estimation

In control and guidance applications it is convenient to use a continuous-discrete version of the extended Kalman filter to design the integrated navigation system. This particular representation of the Kalman filter allows us to use continuous models for both the state estimator and error covariance propagation while the state estimate update and error covariance update are discrete. This implies that the continuous models can be sampled at a very high sampling rate to avoid numerical difficulties while the measurement update rate can be chosen differently for each sensors. This is particularly useful when having a large number of sensors with different bandwidths. A summary of the continuous-discrete extended Kalman filter is given in Table 6.1.

Table 6.1: Summary of continuous-discrete extended Kalman filter, Gelb *et al.* (1988).

System model Measurement model	$\dot{\boldsymbol{x}} = \boldsymbol{f}(\boldsymbol{x}(t), t) + \boldsymbol{v}(t)$; $\quad \boldsymbol{v}(t) \sim N(0, \boldsymbol{V}(t))$ $\boldsymbol{y}_k = \boldsymbol{h}_k(\boldsymbol{x}(t_k)) + \boldsymbol{w}_k$; $\quad k = 1, 2...$; $\quad \boldsymbol{w}_k \sim N(0, \boldsymbol{W}_k)$
Initial conditions Other assumptions	$\boldsymbol{x}(0) \sim N(\hat{\boldsymbol{x}}_o, \hat{\boldsymbol{X}}_o)$ $E[\boldsymbol{v}(t)\boldsymbol{w}_k^T] = 0$ for all k and all t
State estimate propagation Error covariance propagation	$\dot{\hat{\boldsymbol{x}}} = \boldsymbol{f}(\hat{\boldsymbol{x}}(t), t)$ $\dot{\hat{\boldsymbol{X}}} = \boldsymbol{A}(\hat{\boldsymbol{x}}(t), t)\, \hat{\boldsymbol{X}}(t) + \hat{\boldsymbol{X}}(t)\, \boldsymbol{A}^T(\hat{\boldsymbol{x}}(t), t) + \boldsymbol{V}(t)$
Gain matrix State estimate update Error covariance update	$\boldsymbol{K}_k = \hat{\boldsymbol{X}}_k(-)\boldsymbol{D}_k^T(\hat{\boldsymbol{x}}_k(-))\, \left[\boldsymbol{D}_k(\hat{\boldsymbol{x}}_k(-))\hat{\boldsymbol{X}}_k(-)\boldsymbol{D}_k^T(\hat{\boldsymbol{x}}_k(-)) + \boldsymbol{W}_k\right]^{-1}$ $\hat{\boldsymbol{x}}_k(+) = \hat{\boldsymbol{x}}_k(-) + \boldsymbol{K}_k\, [\boldsymbol{y}_k - \boldsymbol{h}_k(\hat{\boldsymbol{x}}_k(-))]$ $\hat{\boldsymbol{X}}_k(+) = [\boldsymbol{I} - \boldsymbol{K}_k\boldsymbol{D}_k(\hat{\boldsymbol{x}}_k(-))]\, \hat{\boldsymbol{X}}_k(-)\, [\boldsymbol{I} - \boldsymbol{K}_k\boldsymbol{D}_k(\hat{\boldsymbol{x}}_k(-))]^T +$ $\hat{\boldsymbol{X}}_k(-)\boldsymbol{D}_k^T(\hat{\boldsymbol{x}}_k(-))\boldsymbol{W}_k^{-1}\boldsymbol{D}_k(\hat{\boldsymbol{x}}_k(-))\hat{\boldsymbol{X}}_k(-)$
Definitions	$\boldsymbol{A}(\hat{\boldsymbol{x}}(t), t) = \left.\frac{\partial \boldsymbol{f}(\boldsymbol{x}(t), t)}{\partial \boldsymbol{x}(t)}\right\|_{\boldsymbol{x}(t)=\hat{\boldsymbol{x}}(t)}$ $\boldsymbol{D}(\hat{\boldsymbol{x}}_k(-)) = \left.\frac{\partial \boldsymbol{h}(\boldsymbol{x}(t_k))}{\partial \boldsymbol{x}(t_k)}\right\|_{\boldsymbol{x}(t_k)=\hat{\boldsymbol{x}}_k(-)}$

Recall from Section 2.1 that the kinematic equations can be expressed as:

$$\begin{aligned} \dot{\boldsymbol{x}}_1 &= \boldsymbol{J}_1(\boldsymbol{x}_2)\,\dot{\boldsymbol{q}}_1; \quad & \boldsymbol{x}_1 &= (x,y,z)^T; \quad & \dot{\boldsymbol{q}}_1 &= (u,v,w)^T \\ \dot{\boldsymbol{x}}_2 &= \boldsymbol{J}_2(\boldsymbol{x}_2)\,\dot{\boldsymbol{q}}_2; \quad & \boldsymbol{x}_2 &= (\phi,\theta,\psi)^T; \quad & \dot{\boldsymbol{q}}_2 &= (p,q,r)^T \end{aligned}$$

where $\boldsymbol{J}_1(\boldsymbol{x}_2)$ and $\boldsymbol{J}_2(\boldsymbol{x}_2)$ are two transformation matrices. This decoupled structure will be exploited in the next sections.

6.2 Estimation of Position and Linear Velocities

Underwater positioning of underwater vehicles are usually based on hydroacoustic navigation like super short base-line (SSBS), short base-line (SBS) and long base-line (LBS) systems. In the Ocean Basin Laboratory at the Marine Technology Center, MARINTEK the measurements from four hydroacoustic transducers can be used to calculate the earth-fixed position vector (x, y, z). The hydroacoustic positioning system can be improved by integrating a depth sensor in the measurement model. Similarly the linear velocities can be measured by using a Doppler sonar. However, a Doppler sonar is often found too expensive for many commercial applications.

Example I: Position Measurements

A hydroacoustic positioning system can be combined with a pressure meter. This suggests the following measurement models:

- **Pressure meter:**

  The static pressure at a depth z is modelled as

  $$y_1 = \rho g z + p_o$$

  where p_o is the atmospheric pressure at the water surface, ρ is the water density and g is the acceleration of gravity.

- **Hydroacoustic navigation system:**

  The distance between the transducer and the vehicle can be expressed as

  $$y_i = \sqrt{(x-x_i)^2 + (y-y_i)^2 + (z-z_i)^2} \qquad i = 2,3,...,n$$

  where (x_i, y_i, z_i) is the global position of sensor number i.

The position measurement system is shown in Figure 6.1. Notice that if $n > 3$ we have redundancy in the sensor system since only three measurements are required to calculate the global position (x, y, z). Redundant measurements can be used to improve the state estimates since it reduces the sensitivity to wild-points.

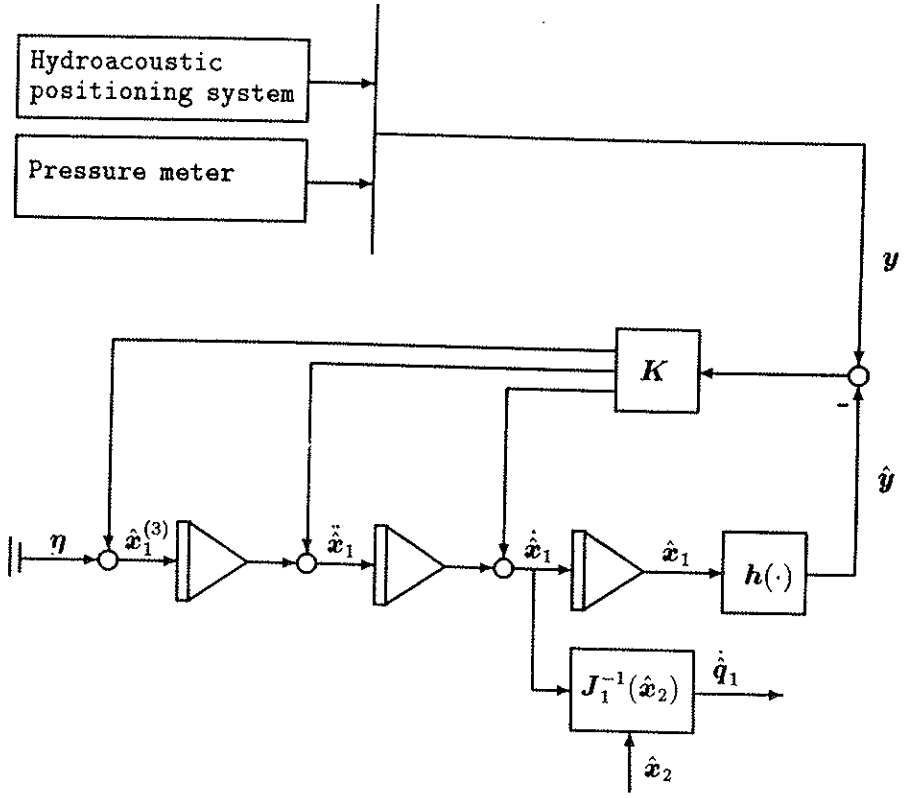

Figure 6.1: Optimal estimation of position and linear velocities based on position measurements.

The design can be further improved by including acceleration measurements in the model. This is illustrated in the next example.

Example II: Position and Acceleration Measurements

- **Linear acceleration meter:**

  We recall from Newton's 2nd law of linear momentum, Section 2.2, that the linear accelerations can be expressed as:

$$\begin{aligned} a_x &= \dot{u} - vr + wq - l_{x_1}(q^2 + r^2) + l_{y_1}(pq - \dot{r}) + l_{z_1}(pr + \dot{q}) \\ a_y &= \dot{v} - wp + ur - l_{y_2}(r^2 + p^2) + l_{z_2}(qr - \dot{p}) + l_{x_2}(qp + \dot{r}) \\ a_z &= \dot{w} - uq + vp - l_{z_3}(p^2 + q^2) + l_{x_3}(rp - \dot{q}) + l_{y_3}(rq + \dot{p}) \end{aligned}$$

  where $(l_{x_i}, l_{y_i}, l_{z_i})$ is the distance between the location of the i-th acceleration meter and the vehicle's centre of gravity. It is necessary to bias the output from the vertical acceleration meter to allow for the acceleration component of $1g$ due to gravity. Compensating for the effect of gravity, c.f. Section 2.4.3, suggests that the output from the acceleration meters can be written as

$$\begin{aligned} n_x &= \sin\theta + \frac{a_x}{g} \\ n_y &= -\cos\theta \sin\phi + \frac{a_y}{g} \\ n_z &= 1 - \cos\theta\cos\phi + \frac{a_z}{g} \end{aligned}$$

  where the outputs n_x, n_y and n_z are in g. Note that the output n_z is biased with $1g$.

Figure 6.2 shows how the acceleration measurement can be included in the state estimator. This design is superior to the first design since more sensor information is available. The first example is based on the assumptions that the jerk can be described as white noise i.e. $\boldsymbol{x}^{(3)} = \eta(t)$ where $\eta(t)$ as white noise. This assumption can be violated if the vehicle's acceleration is changing fast. The first method can also yield poor velocity estimates if the position measurements are noisy.

Simulation Study: Estimation of Linear Velocities

In the simulation study we used a measurement model similar to that in Example I to describe two of the hydroacoustic transducers located in the Ocean Basin Laboratory at NTH. Besides this we included a model of one single depth sensor in the measurement model. The measurement noise used in the simulation study was obtained from experimental time-series of the hydroacoustic transducers and a Keller EI-72 pressure meter. From Figure 6.1 it is

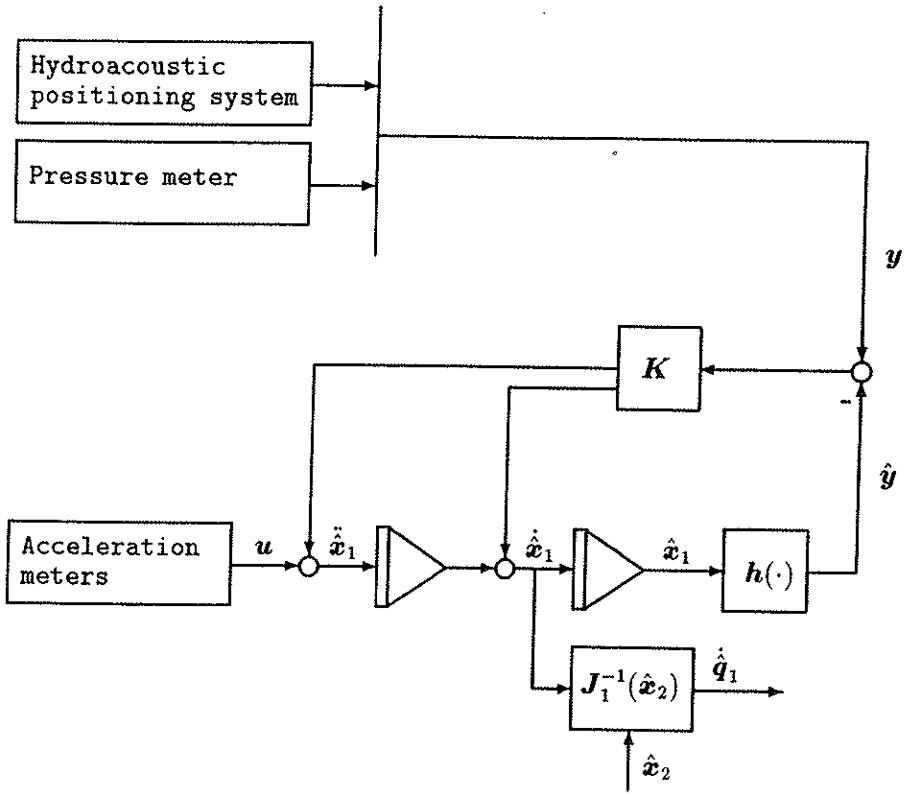

Figure 6.2: Optimal estimation of position and linear velocities based on position and acceleration measurements.

seen that the estimator can be decoupled in one model for surge, sway and heave, respectively. Hence, the state and error covariance propagation can be written as:

$$\dot{\hat{\boldsymbol{\eta}}}_i = \boldsymbol{A}_i \hat{\boldsymbol{\eta}}_i = \begin{bmatrix} 0 & 1 & 0 \\ 0 & 0 & 1 \\ 0 & 0 & 0 \end{bmatrix} \hat{\boldsymbol{\eta}}_i; \qquad i = 1..3$$

$$\dot{\hat{\boldsymbol{X}}}_i = \boldsymbol{A}_i \boldsymbol{X}_i(t) + \boldsymbol{X}_i(t)\boldsymbol{A}_i^T + \boldsymbol{V}_i; \qquad i = 1..3$$

where $\boldsymbol{\eta}_i = (\eta_{i1}, \eta_{i2}, \eta_{i3})^T$ *and* $\boldsymbol{V}_i = diag\ (v_{i1}, v_{i2}, v_{i3})$. *The corresponding state updates at time k are:*

$$\hat{\boldsymbol{\eta}}_{1,k}(+) \;=\; \hat{\boldsymbol{\eta}}_{1,k}(-) + \boldsymbol{K}_1\ [x_k - \hat{x}_k(-)]$$

$$\begin{aligned}\hat{\boldsymbol{\eta}}_{2,k}(+) &= \hat{\boldsymbol{\eta}}_{2,k}(-) + \boldsymbol{K}_2\ [y_k - \hat{y}_k(-)] \\ \hat{\boldsymbol{\eta}}_{3,k}(+) &= \hat{\boldsymbol{\eta}}_{3,k}(-) + \boldsymbol{K}_3\ [z_k - \hat{z}_k(-)]\end{aligned}$$

This simple structure can only be applied to systems where the number of sensors are equal to the number of positions to be estimated. We must also require that there is an inverse mapping of the physical measurement model $\boldsymbol{y} = \boldsymbol{h}(x, y, z)$ *such that the state vector can be calculated as* $(x, y, z)^T = \boldsymbol{h}^{-1}(\boldsymbol{y})$. *Indeed, this is true for the system:*

$$\begin{aligned}\boldsymbol{y}_1 &= \rho g\ z + p_o + w_1 \\ \boldsymbol{y}_2 &= \sqrt{(x - x_1)^2 + (y - y_1)^2 + (z - z_1)^2} + w_2 \\ \boldsymbol{y}_3 &= \sqrt{(x - x_2)^2 + (y - y_2)^2 + (z - z_2)^2} + w_3\end{aligned}$$

Here (x_1, y_1, z_1) *and* (x_2, y_2, z_2) *are the fixed locations of the hydroacoustic transducers and* w_i *(i=1,2,3) is the measurement noise. The simulation results are shown in Figure 6.3.*

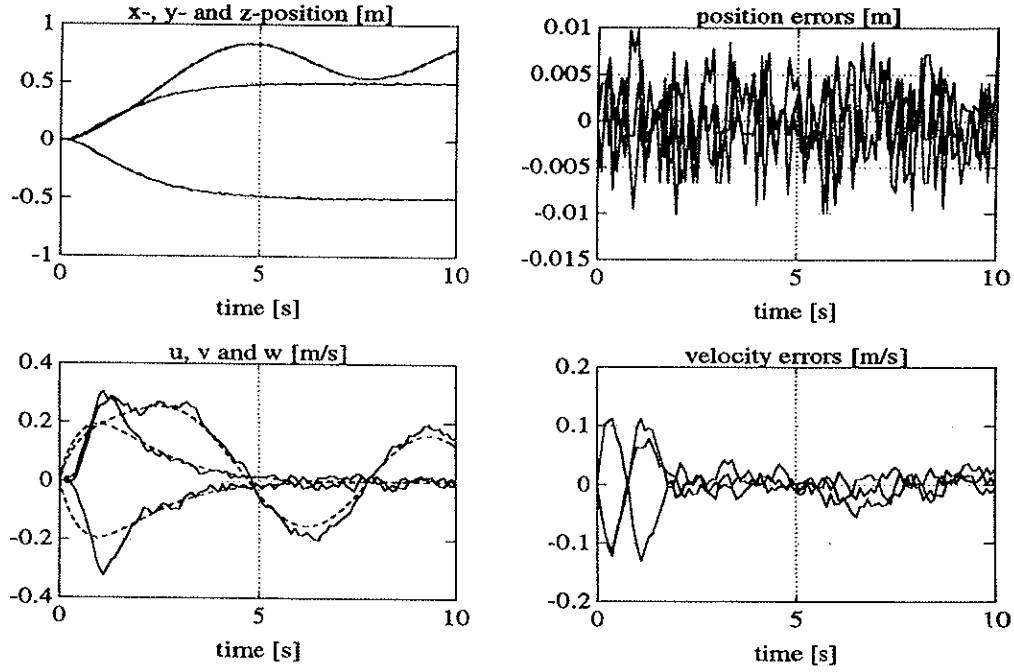

Figure 6.3: Upper left: actual (dotted) and estimated (solid) positions, upper right: position errors, lower left: actual (dotted) and estimated (solid) linear velocities and lower right: linear velocity errors.

6.3 Estimation of Euler Angles and Angular Velocities

In this section we will describe how an optimal state estimator for the estimation of Euler angles and angular rates can be designed. The sensor system is based standard inexpensive sensors.

Example III: Euler Angles and Angular Rate Measurements

The most basic sensors which can be used to measure the Euler angles and the angular rates are:

- **Inclinometers:**

  An inclinometer responds to the normal component of the gravitational acceleration. For an underwater vehicle this implies that we can only measure the roll and pitch angle and not the heading angle since there is no horizontal gravitational acceleration component. Hence, the measurement model can be written as:

$$y_1 = \phi$$

$$y_2 = \theta$$

- **Compass:**

  The vehicle's heading angle can be measured by applying a simple flux-gate compass which can be described with the measurement model:

$$y_3 = \psi$$

- **Angular rate sensors:**

  Angular rate sensors can be used to measure the Euler axis rates:

$$\begin{aligned} \dot{\phi} &= p + \sin\phi \tan\theta \, q + \cos\phi \tan\theta \, r \\ \dot{\theta} &= \cos\phi \, q - \sin\phi \, r \\ \dot{\psi} &= \frac{\sin\phi}{\cos\theta} q + \frac{\cos\phi}{\cos\theta} r \end{aligned}$$

or the vehicle-fixed rates

$$\begin{aligned} p &= \dot{\phi} - \sin\theta\,\dot{\psi} \\ q &= \cos\phi\,\dot{\theta} + \cos\theta\sin\phi\,\dot{\psi} \\ r &= -\sin\phi\,\dot{\theta} + \cos\theta\cos\phi\,\dot{\psi} \end{aligned}$$

The most simple sensors are usually based on the last principle. In Figure 6.4 it is shown how two inclinometers, a compass and a three-axial vehicle-fixed angular rate sensor can be integrated in a Kalman filter. This approach uses the three-axial rate sensor as input for the state estimator. An alternative method is shown in Figure 6.5 where all the sensor measurements are included in the output vector $\boldsymbol{y}$.

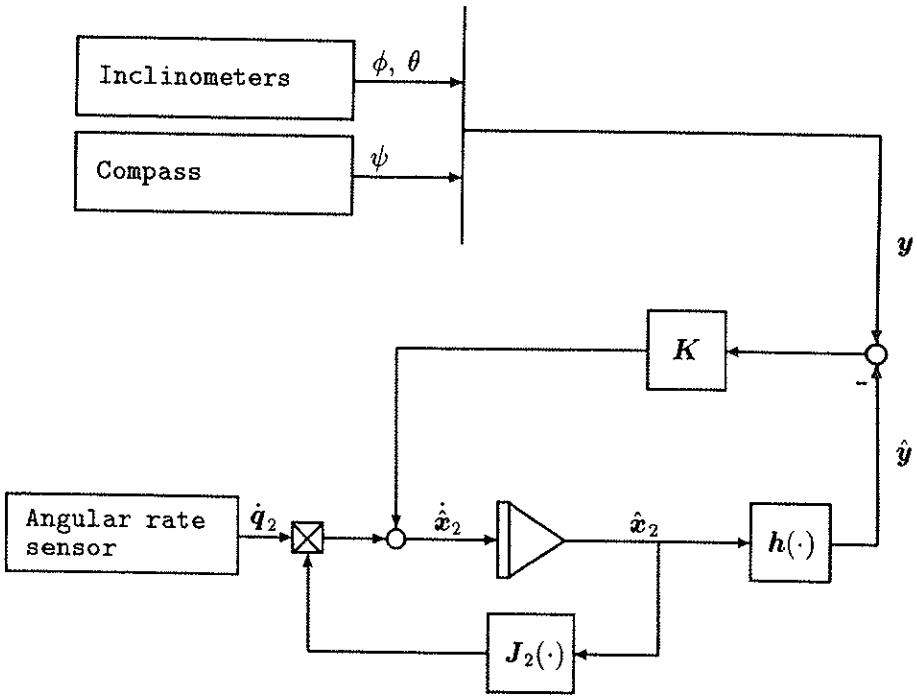

Figure 6.4: Optimal estimation of Euler angles and angular rates.

It should be noted that the sensor systems discussed in this chapter are not the only solution to the underwater navigation problem. There are, of course, other sensor configuration. By applying more expensive sensors like gyroscopes, Doppler sonars etc. different block diagrams can be obtained. Nevertheless, the basic ideas of underwater integrated navigation

systems have been discussed. The proposed block diagrams are easy to implement and quite inexpensive compared to more advanced sensor systems used in military applications, for example.

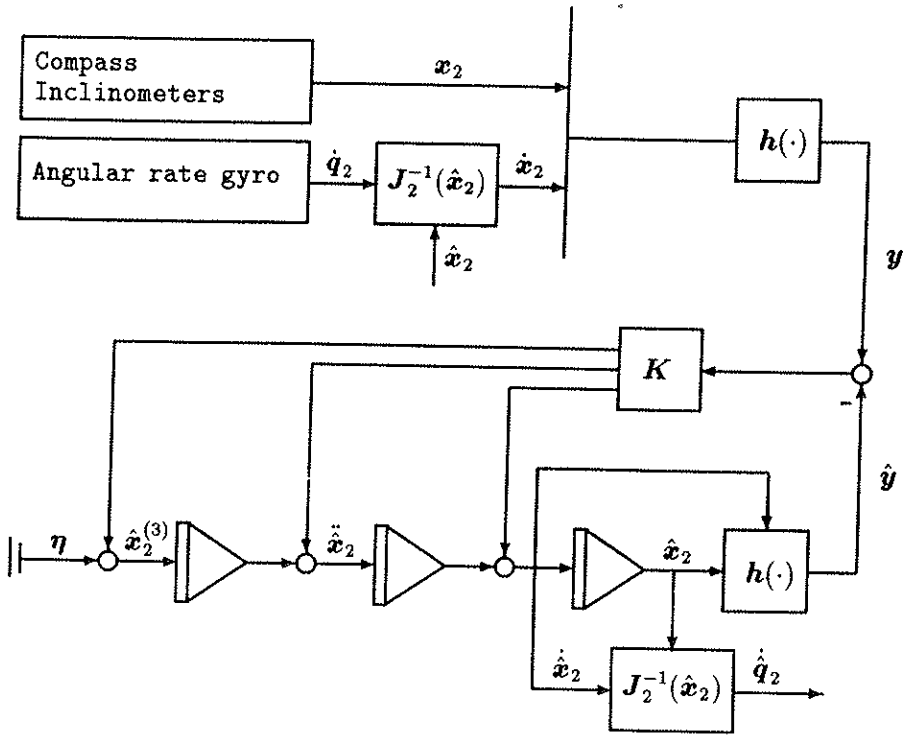

Figure 6.5: Optimal estimation of Euler angles and angular rates.

Experimental Results: The NEROV Sensor System

The experimental results are based on the NEROV sensor system, Fossen and Sagatun (1991d), which consists of the following sensors:

- **One ARS-C331-1A three-axial rate sensor (Watson Industries Inc.)**
- **Two LSOP-90 electric inclinometers (Schaevitz Inc.)**
- **One RFC-250 flux-gate compass (Robertson Tritech A/S).**

These sensors are used to measure the Euler angles and the body-fixed angular rates. The sensors are integrated in a Kalman filter structure similar to that in Figure 6.5. In the experiment a sampling rate of 20 Hz was used. The initial measurement covariance matrix was chosen as

$$W(0) = diag\,(\sigma^2_{inc}, \sigma^2_{inc}, \sigma^2_{comp}, \sigma^2_{rate}, \sigma^2_{rate}, \sigma^2_{rate})$$

with the following values for the sensors static standard deviations:

$$\begin{aligned} \sigma_{inc} &= 0.30 \text{ deg} \\ \sigma_{comp} &= 0.75 \text{ deg} \\ \sigma_{rate} &= 0.25 \text{ deg/s} \end{aligned}$$

A simple wild-point algorithm was designed by updating the measurement covariance matrix as (i=1..6):

$$W_{ii}(k) = \begin{cases} \infty & if \quad | y_i(k+1) - y_i(k) | > \alpha\, \sigma_i(k) \\ W_{ii}(0) & else \end{cases}$$

where $\sigma_i(k)$ is the standard deviation of the i-th measurement at time k and α is a constant typically chosen in the interval $3 < \alpha < 9$. A continuous version of the Kalman filter was used i.e.

$$\dot{\hat{\boldsymbol{x}}} = \boldsymbol{A}\,\hat{\boldsymbol{x}}(t) + \boldsymbol{K}(t)\,[\boldsymbol{y}(t) - \boldsymbol{h}(\hat{\boldsymbol{x}}(t))]$$

$$\boldsymbol{h}(\hat{\boldsymbol{x}}(t)) = \boldsymbol{D}\,\hat{\boldsymbol{x}}(t)$$

where

$$\boldsymbol{A} = \begin{bmatrix} 0_{3\times3} & I_{3\times3} & 0_{3\times3} \\ 0_{3\times3} & 0_{3\times3} & I_{3\times3} \\ 0_{3\times3} & 0_{3\times3} & 0_{3\times3} \end{bmatrix} \quad \boldsymbol{D} = \begin{bmatrix} I_{3\times3} \\ I_{3\times3} \\ 0_{3\times3} \end{bmatrix} \quad \boldsymbol{K}(t) = \hat{\boldsymbol{X}}\boldsymbol{D}^T\boldsymbol{W}^{-1}(t)$$

The steady state error covariance matrix satisfies

$$\boldsymbol{A}\hat{\boldsymbol{X}} + \hat{\boldsymbol{X}}\boldsymbol{A}^T - \hat{\boldsymbol{X}}\boldsymbol{D}^T\boldsymbol{W}^{-1}\boldsymbol{D}\hat{\boldsymbol{X}} + \boldsymbol{V} = 0$$

This equation can be solved off-line for all possible "wild-point combinations" of the diagonal elements in $\boldsymbol{W}$. Since the state estimator consists of three integrators, we decided to choose the covariance matrix $\boldsymbol{V}$ as:

$$\boldsymbol{V} = \begin{bmatrix} \frac{1}{6}\,T^3v^2\,I_{3\times3} & 0_{3\times3} & 0_{3\times3} \\ 0_{3\times3} & \frac{1}{2}\,T^2v^2\,I_{3\times3} & 0_{3\times3} \\ 0_{3\times3} & 0_{3\times3} & Tv^2\,I_{3\times3} \end{bmatrix}$$

where T is the sampling rate and v is the maximum deviation in jerk i.e. $|\boldsymbol{x}^{(3)}| \leq v$. This relationship was obtained by simply integrating the constant v three times. The experimental results for the rolling and pitching motion are shown in Figures 6.6 and 6.7, respectively. The NEROV sensor system is described more closely in Fossen and Sagatun (1991d) and Tillman Hansen and Osen (1991).

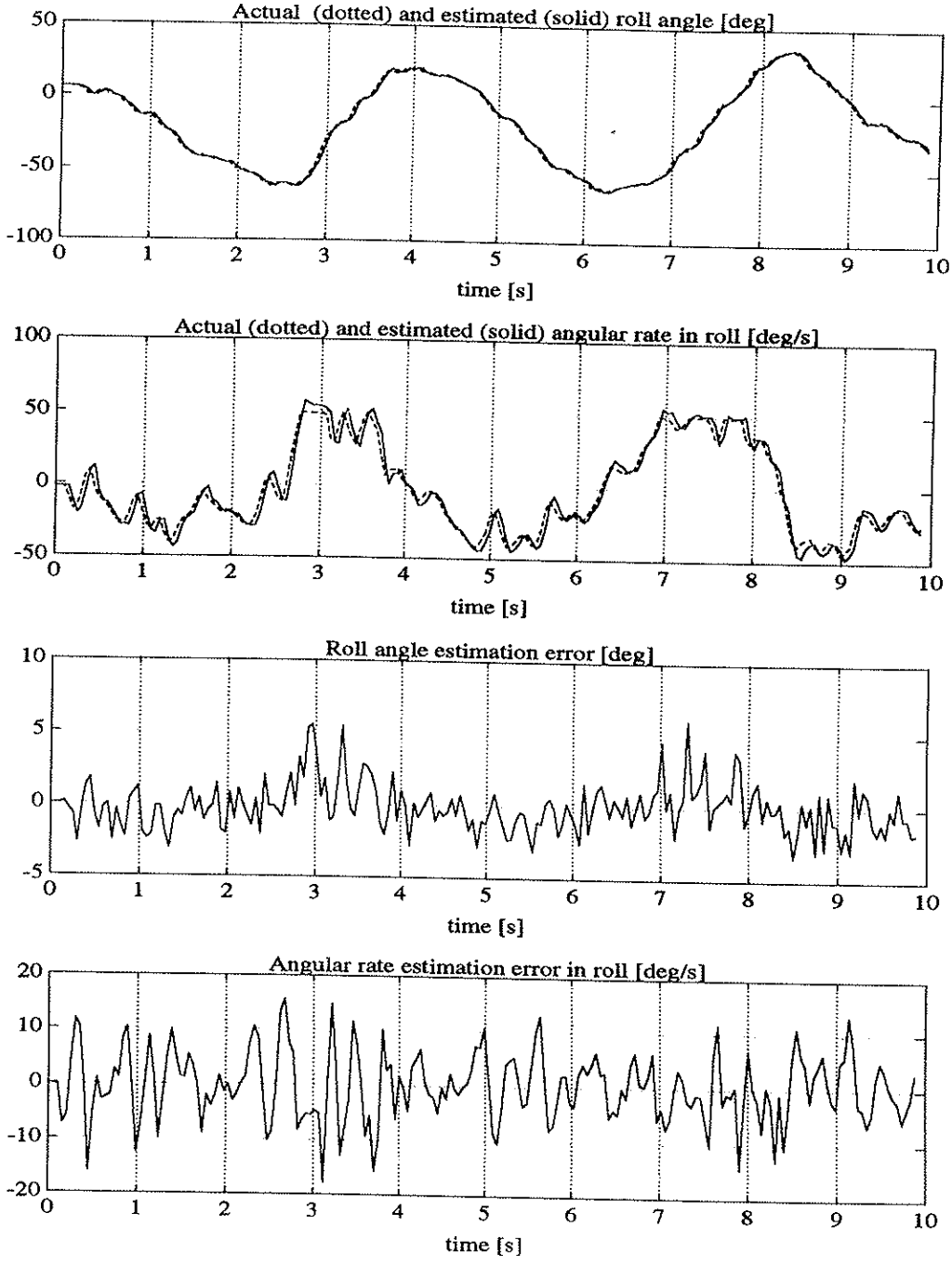

Figure 6.6: Experimental results: rolling motion.

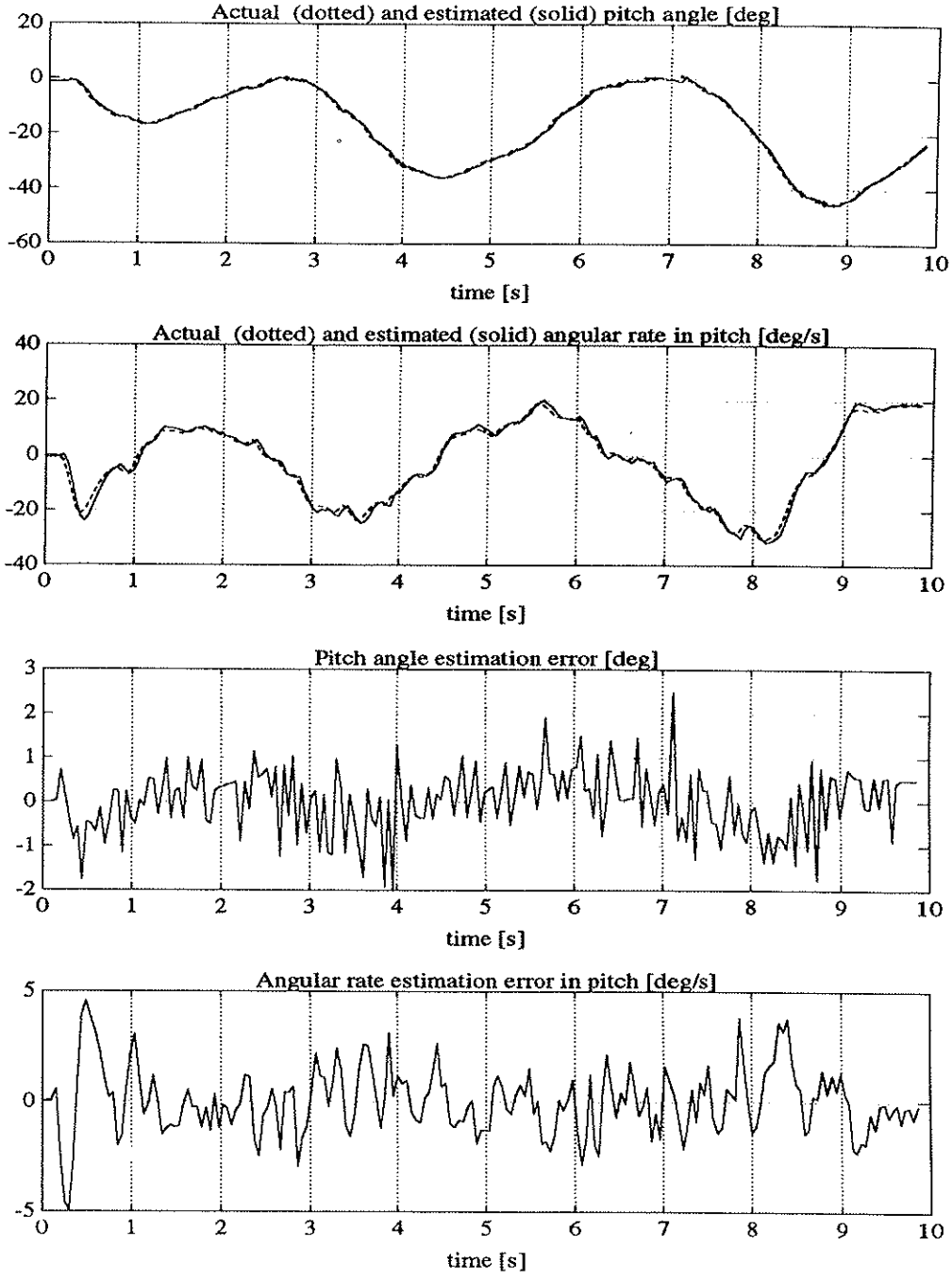

Figure 6.7: Experimental results: pitching motion.

Chapter 7

Conclusions and Recommendations

This chapter concludes the work already presented and suggests areas where additional studies would be beneficial.

7.1 Conclusions

The main purpose of this work have been to derive a comprehensive 6 DOF nonlinear ROV model and investigate the feasibility of nonlinear control system techniques for the autopilot design for underwater vehicles.

The main motivation for using nonlinear models and control theory is that small underwater vehicles are known to operate over a large number of operating points with no specific speed dominating. Thus a linear control design will be quite laborious, since linearization and gain scheduling techniques must be applied to each of the vehicle's operating points. A nonlinear model should also be used if the vehicle is allowed to perform coupled manoeuvres at some speed. Another advantage of a nonlinear design is that the nonlinear kinematics, thruster forces and hydrodynamic forces due to quadratic drag, Coriolis, centrifugal and added mass coupling terms etc. can be understood and compensated for in the control design. Understanding and modelling these effects can also be used to improve the robustness and performance of the ROV. Uncertainties due to partly known thruster characteristics can particularly yield poor performance. The experimental thruster characteristics of the NEROV vehicle were obtained from an open water test to illustrate this problem. These results were used to derive a nonlinear model of the thruster forces. Uncertainties in the experimental data were compensated for in the control design.

It is shown how the nonlinear underwater vehicle equations of motion can be written in a compact form nearly similar to the representation used in robot manipulator control i.e.

- Vehicle dynamics:

$$M\ddot{q} + C(\dot{q})\dot{q} + D(\dot{q})\dot{q} + g(x) = B(\dot{q})u \tag{7.1}$$

- Kinematics

$$\dot{x} = J(x)\dot{q} \tag{7.2}$$

This representation is highly advantageous when designing nonlinear controllers which are based on the well known properties of mechanical system analyses like the positiveness of the damping matrix ($D > 0$), the positiveness and symmetry of the inertia matrix ($M = M^T > 0$) and the skew-symmetry of $\dot{M} - 2C$. By exploiting these properties it is shown how advanced nonlinear control theory yields a relative simple autopilot design. Indeed, advanced nonlinear control design was found often to be simpler and more intuitive than its linear counterpart. The following three nonlinear control design techniques are discussed in depth:

- **Feedback linearization techniques.**
- **Sliding control.**
- **Passivity based control.**

Based on the nonlinear equations of motion, Eqs. 7.1 and 7.2, globally stable autopilots for underwater vehicles were both derived in the earth-fixed and vehicle-fixed reference frames. These representations are classified as:

(i) **q-frame formulation.**
In the q-frame formulation the vehicle's controller is formulated in the vehicle-fixed reference frame. This representation is intended for control of the vehicle's linear and angular velocities. Only the vehicle's dynamic equation of motion, Eq. 7.1, is used by the controller.

(ii) **x-frame formulation.**
The x-frame formulation is intended for position and orientation control. Hence, the vehicle's controller is formulated in the earth-fixed reference frame in this representation. Both the vehicle's dynamic and kinematic equations of motion, Eqs. 7.1 and 7.2, are used by the controller.

Model Imperfectness due to parametric uncertainties is compensated by deriving adaptive and self-tuning versions of the above control schemes. For the passivity based adaptive controller a new parameterization which simplifies the representation of the adaptive controller was derived. The adaptive scheme has also been modified to deal with slowly varying environmental disturbances by adding an adaptive feedforward term to the nonlinear controller. Especial care has been taken to compensate for input uncertainties due to partly known thruster characteristics. This was done by deriving a hybrid (adaptive and sliding) controller. Global stability is proven for all controllers by applying Barbălat's Lyapunov-like lemma. An experimental model of the NEROV vehicle was used in the simulation study.

Some new contributions to stick-fixed and stick-free stability analyses of underwater vehicles in 6 DOF have been discussed. These stability criteria were based on well known techniques like the Routh's stability criterion, Lyapunov's linearization method, Lyapunov's direct method for autonomous systems and advanced Lyapunov theory like Barbălat's Lyapunov-like lemma for non-autonomous systems.

Finally, navigation systems for underwater vehicles have been discussed. All the proposed sensor systems were based on optimal filtering and state estimation (Kalman filtering). Since a ROV's hydrodynamic parameters are not perfectly known, a state estimator should be designed such that it is independent of the vehicle's hydrodynamic parameters. This was achieved by exclusively using the kinematic equations of motion. Experimental and simulation results based on the NEROV sensor system were used to verify two of the proposed methods.

7.2 Recommendations for Further Work

It is hoped that the NEROV vehicle will be operative in spring 1991 such that the nonlinear controllers can be implemented and tested in the Ocean Basin Laboratory at the Marine Technology Center (MARINTEK). These experiments should be compared with the performance of a state-of-the-art linear controller. The complexity of the chosen model as well as the robustness for errors in the regressor matrix have to be investigated more closely.

Particular focus should be placed on environmental disturbances. Although the PBAC discussed in this thesis can compensate for slowly varying disturbances like sea currents, special attention should be given to waves. In the wave affected zone it might be natural to separate the vehicle's model into a low frequency (LF) and a high frequency part (HF) similar to the approach used in dynamic positioning of ships by Balchen *et al.* (1976). For underwater vehicles capable of moving in 6 DOF this is still an unsolved problem, mainly due to the difficulties of estimating the wave motion when model uncertainties are present.

A future application could be to replace the hydroacoustic navigation system with e.g. an underwater camera to determine the earth-fixed x- and y-coordinates. Hence, offshore pipeline tracking and inspection could be performed with a fully autonomous underwater vehicle. Besides this, AUVs can also be used in telerobotic research. In teleoperation it is desirable to remove the time delay in the communication channel caused by a hydroacoustic communication link, for instance. This could easily be tested in the Ocean Basin Laboratory.

Appendix A

The NEROV Vehicle

A.1 The NEROV General Arrangement

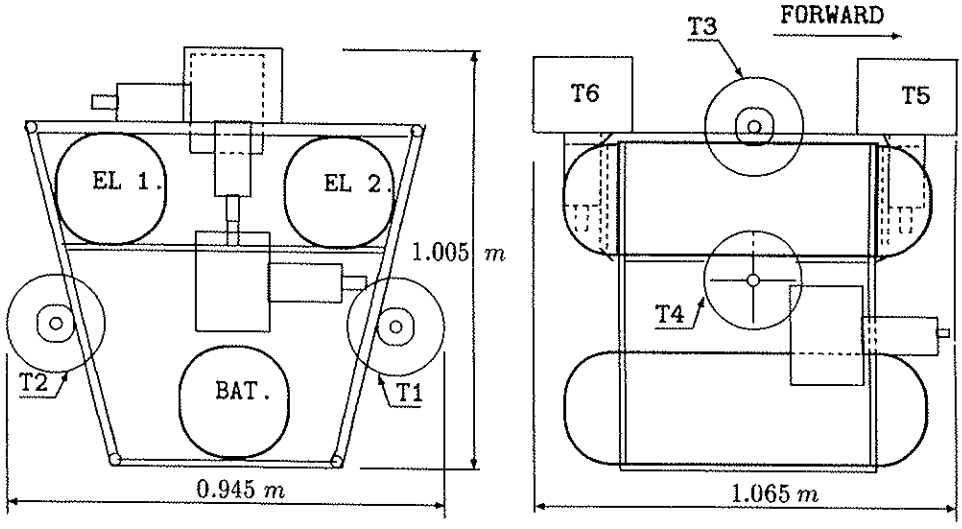

A.2 The NEROV Equations of Motion

The underwater vehicle equations of motion are based on the following assumptions:

1. The axes of the local coordinate system were found to deviate with less than 2 degrees with the principal axes of inertia of the vehicle. This suggested that the inertia tensor could be chosen as a diagonal matrix i.e. $I_{xy} = I_{xz} = I_{yz} = 0$.

2. The vehicle's origin was chosen to coincide with the CG i.e. $\boldsymbol{r}_G = (0, 0, 0)^T$

3. xz- and yz-plane symmetries suggested that the vehicle's CB could be described with only one component, namely $\boldsymbol{r}_B = (0, 0, z_B)^T$.

4. The vehicle is neutrally buoyant which implies that $W = B$.

5. Only diagonal elements of the added mass matrix $\boldsymbol{M}_A$ and damping matrix $\boldsymbol{D}$ are considered.

Underwater Vehicle Dynamics and Kinematics

The NEROV equations of motion can be expressed in a compact form as

$$\boldsymbol{M}\ddot{\boldsymbol{q}}_r + \boldsymbol{C}(\dot{\boldsymbol{q}}_r)\dot{\boldsymbol{q}}_r + \boldsymbol{D}(\dot{\boldsymbol{q}}_r)\dot{\boldsymbol{q}}_r + \boldsymbol{g}(\boldsymbol{x}) = \boldsymbol{B}(\dot{\boldsymbol{q}}_r)\,\boldsymbol{u}$$

$$\dot{\boldsymbol{x}} = \boldsymbol{J}(\boldsymbol{x})\dot{\boldsymbol{q}}$$

Here $\boldsymbol{M}$ is an $n \times n$ inertia matrix including hydrodynamic added mass, $\boldsymbol{C}$ is an $n \times n$ nonlinear matrix including Coriolis, centrifugal and added mass terms, $\boldsymbol{D}$ is a 6×6 matrix of dissipative terms, such as potential damping, viscous damping and skin friction, $\boldsymbol{B}$ is an $n \times p$ input matrix, $\boldsymbol{g}$ is an $n \times 1$ vector of restoring forces and moments and $\boldsymbol{J}$ is an $n \times n$ transformation matrix. For the NEROV vehicle it was convenient to derive both simplified 6 DOF and 4 DOF models.

Simplified 6 DOF Model (n=6, p=6)

$$\boldsymbol{M} = \begin{bmatrix} m - X_{\dot{u}} & 0 & 0 & 0 & 0 & 0 \\ 0 & m - Y_{\dot{v}} & 0 & 0 & 0 & 0 \\ 0 & 0 & m - Z_{\dot{w}} & 0 & 0 & 0 \\ 0 & 0 & 0 & I_x - K_{\dot{p}} & 0 & 0 \\ 0 & 0 & 0 & 0 & I_y - M_{\dot{q}} & 0 \\ 0 & 0 & 0 & 0 & 0 & I_z - N_{\dot{r}} \end{bmatrix}$$

$$\boldsymbol{C}(\dot{\boldsymbol{q}}_r) = \begin{bmatrix} 0 & -mr & mq & 0 & -Z_{\dot{w}}w_r & Y_{\dot{v}}v_r \\ mr & 0 & -mp & Z_{\dot{w}}w_r & 0 & -X_{\dot{u}}u_r \\ -mq & mp & 0 & -Y_{\dot{v}}v_r & X_{\dot{u}}u_r & 0 \\ 0 & -Z_{\dot{w}}w_r & Y_{\dot{v}}v_r & 0 & (I_z - N_{\dot{r}})r & -(I_y - M_{\dot{q}})q \\ Z_{\dot{w}}w_r & 0 & -X_{\dot{u}}u_r & -(I_z - N_{\dot{r}})r & 0 & (I_x - K_{\dot{p}})p \\ -Y_{\dot{v}}v_r & X_{\dot{u}}u_r & 0 & (I_y - M_{\dot{q}})q & -(I_x - K_{\dot{p}})p & 0 \end{bmatrix}$$

$$\boldsymbol{D}(\dot{\boldsymbol{q}}_r) = -\begin{bmatrix} X_u + X_{u|u|}|u_r| & 0 & 0 & 0 & 0 & 0 \\ 0 & Y_u + Y_{v|v|}|v_r| & 0 & 0 & 0 & 0 \\ 0 & 0 & Z_w + Z_{w|w|}|w_r| & 0 & 0 & 0 \\ 0 & 0 & 0 & K_p + K_{p|p|}|p| & 0 & 0 \\ 0 & 0 & 0 & 0 & M_q + M_{q|q|}|q| & 0 \\ 0 & 0 & 0 & 0 & 0 & N_r + N_{r|r|}|r| \end{bmatrix}$$

$$\boldsymbol{g}(\boldsymbol{x}) = \begin{bmatrix} 0 \\ 0 \\ 0 \\ z_B B \cos\theta \sin\phi \\ z_B B \sin\theta \\ 0 \end{bmatrix}$$

$$\boldsymbol{B}(\dot{\boldsymbol{q}}) = \begin{bmatrix} K_{T_{11}} & K_{T_{12}} & 0 & 0 & 0 & 0 \\ 0 & 0 & -K_{T_{23}} & K_{T_{24}} & 0 & 0 \\ 0 & 0 & 0 & 0 & K_{T_{35}} & K_{T_{36}} \\ 0 & 0 & l_3 K_{T_{23}} & -l_4 K_{T_{24}} & 0 & 0 \\ 0 & 0 & 0 & 0 & -l_5 K_{T_{35}} & l_6 K_{T_{36}} \\ -l_1 K_{T_{11}} & l_2 K_{T_{12}} & 0 & 0 & 0 & 0 \end{bmatrix}$$

The 6 DOF kinematic transformation matrix $\boldsymbol{J}(\boldsymbol{x})$ is described in Section 2.1.

Simplified 4 DOF Model (n=4, p=6)

This model is based on the additional assumption that the vehicle is metacentre stable such that the vehicle's rolling and pitching motion can be neglected This in turn requires the vehicle to be "balanced" such that $\overline{BG}_z >> 0$.

$$\boldsymbol{M} = \begin{bmatrix} m - X_{\dot{u}} & 0 & 0 & 0 \\ 0 & m - Y_{\dot{v}} & 0 & 0 \\ 0 & 0 & m - Z_{\dot{w}} & 0 \\ 0 & 0 & 0 & I_z - N_{\dot{r}} \end{bmatrix} \qquad \boldsymbol{C}(\dot{\boldsymbol{q}}_r) = \begin{bmatrix} 0 & -mr & 0 & Y_{\dot{v}} v_r \\ mr & 0 & 0 & -X_{\dot{u}} u_r \\ 0 & 0 & 0 & 0 \\ -Y_{\dot{v}} v_r & X_{\dot{u}} u_r & 0 & 0 \end{bmatrix}$$

$$\boldsymbol{D}(\dot{\boldsymbol{q}}_r) = -\begin{bmatrix} X_u + X_{u|u|}|u_r| & 0 & 0 & 0 \\ 0 & Y_u + Y_{v|v|}|v_r| & 0 & 0 \\ 0 & 0 & Z_w + Z_{w|w|}|w_r| & 0 \\ 0 & 0 & 0 & N_r + N_{r|r|}|r| \end{bmatrix} \qquad \boldsymbol{g}(\boldsymbol{x}) = \begin{bmatrix} 0 \\ 0 \\ 0 \\ 0 \end{bmatrix}$$

$$\boldsymbol{B}(\dot{\boldsymbol{q}}) = \begin{bmatrix} K_{T_{11}} & K_{T_{12}} & 0 & 0 & 0 & 0 \\ 0 & 0 & -K_{T_{23}} & K_{T_{24}} & 0 & 0 \\ 0 & 0 & 0 & 0 & K_{T_{35}} & K_{T_{36}} \\ -l_1 K_{T_{11}} & l_2 K_{T_{12}} & 0 & 0 & 0 & 0 \end{bmatrix} \qquad \boldsymbol{J}(\boldsymbol{x}) = \begin{bmatrix} c\psi & -s\psi & 0 & 0 \\ s\psi & c\psi & 0 & 0 \\ 0 & 0 & 1 & 0 \\ 0 & 0 & 0 & 1 \end{bmatrix}$$

A.3 Simulation Model

Some of the hydrodynamic parameters of the NEROV vehicle were found by full-scale experiments in the Ocean Basin Laboratory at the Marine Technology Research Institute (MARINTEK), Fossen and Sagatun (1991c).

The simulation model used in this thesis is based on the following numerical values:

(1) Hydrodynamic Derivatives and Damping Coefficients:

$X_{\dot{u}}$	=	-30 kg	X_u	=	-80 kg/s	$X_{u\|u\|}$	=	-120 kg/m
$Y_{\dot{v}}$	=	-110 kg	Y_v	=	-110 kg/s	$Y_{v\|v\|}$	=	-200 kg/m
$Z_{\dot{w}}$	=	-80 kg	Z_w	=	-100 kg/s	$Z_{w\|w\|}$	=	-150 kg/m
$K_{\dot{p}}$	=	-15 $kg\,m$	K_p	=	-30 $kg\,m/s$	$K_{p\|p\|}$	=	-50 $kg\,m$
$M_{\dot{q}}$	=	-20 $kg\,m$	M_q	=	-40 $kg\,m/s$	$M_{q\|q\|}$	=	-40 $kg\,m$
$N_{\dot{r}}$	=	-1 $kg\,m$	N_r	=	-10 $kg\,m/s$	$N_{r\|r\|}$	=	-15 $kg\,m$

(2) Weight and Balance Data:

The weight and balance data were found by simple experimental set-ups at the Division of Engineering Cybernetics (NTH), Fossen and Sagatun (1991c). The z-axis is positive upwards.

x_G	=	0 m	x_B	=	0 m			
y_G	=	0 m	y_B	=	0 m	$\overline{V}$	=	0.0183 m^3
z_G	=	0 m	z_B	=	0.04 m	m	=	180 kg
I_x	=	25 $kg\,m^2$	I_y	=	29 $kg\,m^2$	I_z	=	28 $kg\,m^2$
I_{xy}	=	0 $kg\,m^2$	I_{xz}	=	0 $kg\,m^2$	I_{yz}	=	0 $kg\,m^2$

Appendix B

Proof of Equation 5.21

Consider Eq. 5.20 which can be expressed as:

$$\begin{aligned}\dot{V} &= \boldsymbol{s}^T \left[(\boldsymbol{f}^* - \hat{\boldsymbol{f}}^*) + \boldsymbol{\Delta}(\boldsymbol{\alpha}_d - \hat{\boldsymbol{f}}^*) - (\boldsymbol{I} + \boldsymbol{\Delta})\, \boldsymbol{k}.\times\, \boldsymbol{sgn}(\boldsymbol{s}) \right] \\ &= \sum_{i=1}^{m} s_i \left[(f_i^* - \hat{f}_i^*) + \sum_{j=1}^{m} \Delta_{ij}(\alpha_{d,j} - \hat{f}_j^*) - (1+\Delta_{ii})\, k_i\, sgn(s_i) - \sum_{j=1,\, j\neq i}^{m} \Delta_{ij}\, k_j\, sgn(s_j) \right]\end{aligned}$$

Recall that the uncertainties are assumed to satisfy the following bounds:

$$\begin{aligned} \mid f_j^*(\boldsymbol{x}) - \hat{f}_j^*(\boldsymbol{x}) \mid \leq \delta_i \\ G^*(\boldsymbol{x}) = (\boldsymbol{I} + \boldsymbol{\Delta})\hat{G}^*(\boldsymbol{x}) \quad , \quad \mid \Delta_{ij} \mid \leq U_{ij} \end{aligned}$$

where $(i = 1, ..., m)$, $(j = 1, ..., m)$ and $\overline{\sigma}(\boldsymbol{\Delta}) < 1$. Hence

$$\dot{V} \leq -\boldsymbol{\eta}^T |\boldsymbol{s}| = -\sum_{i=1}^{m} \eta_i\, |s_i| \leq 0 \quad , \quad (\eta_i > 0 \ , \ i = 1, .., m)$$

if the switching gains k_i satisfy

$$(1 - U_{ii})\, k_i \geq -\sum_{j=1,\, j\neq i}^{m} U_{ij}\, k_j + \delta_i + \sum_{j=1}^{m} U_{ij} |\alpha_{d,j} - \hat{f}_j^*| + \eta_i$$

for $(i = 1, .., m)$. This in turn implies that there exists a $k_i \geq k_i'$ for $(i = 1, .., m)$ such that:

$$\begin{bmatrix} 1-U_{11} & U_{12} & \cdots & U_{1m} \\ U_{21} & 1-U_{22} & & U_{2m} \\ \vdots & & \ddots & \vdots \\ U_{m1} & U_{m2} & \cdots & 1-U_{mm} \end{bmatrix} \begin{bmatrix} k_1' \\ \vdots \\ k_m' \end{bmatrix} = \begin{bmatrix} \delta_1 \\ \vdots \\ \delta_m \end{bmatrix} + \begin{bmatrix} U_{11} & U_{12} & \cdots & U_{1m} \\ U_{21} & U_{22} & & U_{2m} \\ \vdots & & \ddots & \vdots \\ U_{m1} & U_{m2} & \cdots & U_{mm} \end{bmatrix} \begin{bmatrix} |\, \alpha_{d,1} - \hat{f}_1^* \,| \\ \vdots \\ |\, \alpha_{d,m} - \hat{f}_m^* \,| \end{bmatrix} + \begin{bmatrix} \eta_1 \\ \vdots \\ \eta_m \end{bmatrix}$$

Defining a matrix $\overline{U}$ as:

$$\overline{U} = \begin{bmatrix} U_{11} & -U_{12} & \dots & -U_{1m} \\ -U_{21} & U_{22} & & -U_{2m} \\ \vdots & & \ddots & \vdots \\ -U_{m1} & -U_{m2} & \dots & U_{mm} \end{bmatrix}$$

finally yields

$$(I - \overline{U})\, \boldsymbol{k}' = \boldsymbol{\delta} + \boldsymbol{U} \mid \boldsymbol{\alpha}_d - \hat{\boldsymbol{f}}^*(\boldsymbol{x}) \mid + \boldsymbol{\eta}$$

which concludes the proof.

References

M. A. Abkowitz (1964). Lectures on Ship Hydrodynamics- Steering and Manoeuvrability. Technical Report Hy-5, Hydro- and Aerodynamic's Laboratory, Lyngby, Denmark.

M. Abkowitz (1969). *Stability and Motion Control of Ocean Vehicle.* MIT Press, Boston, Massachusetts.

E. E. Allmendinger (1990), editor. *Submersible Vehicle Systems Design.* The Society of Naval Architects and Marine Engineers, 601 Pavonia Avenue, Jersey City, N. J. 07306.

B. D. O. Anderson, R. R. Bitmead, C. R. Johnson, Jr., P. V. Kokotovic, R. L. Kosut, I. M. Y. Mareels, L. Praly, and B. D. Riedle (1986). *Stability of Adaptive Systems.* MIT Press, Cambridge, Massachusetts.

M. Athans and P. L. Falb (1966), editors. *Optimal Control.* McGraw-Hill Book Company, New York.

J. G. Balchen (1963). *Reguleringsteknikk Bind 1.* TAPIR, N-7034 Trondheim, Norway (in Norwegian).

J. G. Balchen (1990). *Ulineære Systemer og Stabilitetsteori.* Institutt for teknisk kybernetikk, Norges tekniske høgskole, N-7034 Trondheim, Norway (in Norwegian).

J. G. Balchen, N. A. Jenssen, and S. Sælid (1976). Dynamic Positioning Using Kalman Filtering and Optimal Control Theory. In *IFAC/IFIP Symposium on Automation in Offshore Oil Field Operation*, (North-Holland Publishing Company).

Barbălat (1959). Systèmes d'Èquations Diffèrentielles d'Oscillations Non Linèaires. *Revue de Mathèmatiques Pures et Appliquèes*, Vol. 4, No. 2, pp. 267–270. Acadèmie de la Rèpublique Populaire Roumaine (in French).

M. Blanke (1981). *Ship Propulsion Losses Related to Automated Steering and Prime Mover Control.* Ph.D thesis, The Technical University of Denmark, Lyngby.

C. Byrnes and A. Isidori (1984). A Frequency Domain Philosophy for Nonlinear Systems with Application to Stabilization and Adaptive Control. In *Proceedings of the IEEE Conf. on Decision and Control*, pp. 1569–1573, Las Vegas, NV.

J. J. Craig (1988). *Adaptive Control of Mechanical Manipulators.* Addison-Wesley, Reading, Massachusetts.

R. Cristi, F. A. Papoulias, and A. J. Healey (1990). Adaptive Sliding Mode Control of Autonomous Underwater Vehicles in the Dive Plane . *IEEE Oceanic Engineering*, OE-15, No. 3, pp. 152–160.

I. Dand and M. J. Every (1983). An Overview of the Hydrodynamics of Umbilical Cables and Vehicles. In *Proceedings of the SUBTECH'83 Conference*, paper no. 10.4.

F. Dougherty and G. Woolweaver (1990). At-Sea Testing of an Unmanned Underwater Vehicle Flight Control System. In *Symposium on Autonomous Underwater Technology*, pp. 65–68, Washington, DC, USA.

O. Egeland (1985). *Robotmanipulatorer.* Institutt for teknisk kybernetikk, Norges tekniske høgskole, N-7034 Trondheim, Norway (in Norwegian).

O. Egeland (1987). *Cartesian Control of Industrial Robots with Redundant Degrees of Freedom.* Dr.ing thesis, Division of Engineering Cybernetics, Norwegian Institute of Technology, March 1987.

O. Egeland (1991). The Norwegian Research Programme on Advanced Robotic Systems. In *International Symposium on Advanced Robot Technology (ISART)*, Tokyo, Japan, March 1991.

O. M. Faltinsen (1990a). *Sea Loads on Ships and Offshore Structures.* Cambridge University Press, New York.

O. M. Faltinsen (1990b). *Lecture Notes in Sink-Source Methods and Wave-Induced Loads.* Division of Marine Hydrodynamics, Norwegian Institute of Technology, N-7034 Trondheim, Norway.

J. Feldman (1979). DTMSRDC Revised Standard Submarine Equations of Motion. Technical Report DTNSRDC-SPD-0393-09, Naval Ship Research and Development Center, Washington D.C.

T. I. Fossen (1990). Adaptive Feedback Linearization of Systems with Significant Actuator Dynamics. *Modeling, Identification and Control*, MIC-11, No. 3, pp. 169–179.

T. I. Fossen (1991). Adaptive Macro-Micro Control of Nonlinear Underwater Robotic Systems. In *Proceedings of the 5th International Conference on Advanced Robotics (ICAR)*, Pisa, Italy, June 1991.

T. I. Fossen and J. G. Balchen (1988). Modelling and Nonlinear Self-Tuning Robust Trajectory Control of an Autonomous Underwater Vehicle. *Modeling, Identification and Control*, MIC-9, No. 4, pp. 165–177.

T. I. Fossen and J. G. Balchen (1991). The NEROV Autonomous Underwater Vehicle. In *Proceedings of the OCEANS'91 Conference*, Honolulu, Hawaii, USA, October 1991.

T. I. Fossen and B. A. Foss (1991). Sliding Control of MIMO Nonlinear Systems. In *Proceedings of the 1991 European Control Conference*, Grenoble, France, July 1991.

T. I. Fossen and S. I. Sagatun (1991a). Adaptive Control of Nonlinear Underwater Robotic Systems. In *Proceedings of the IEEE Conference on Robotics and Automation*, pp. 1687–1695, Sacramento, California, April 1991.

T. I. Fossen and S. I. Sagatun (1991b). Adaptive Control of Nonlinear Systems: A Case Study of Underwater Robotic Systems. *Journal of Robotic Systems*, JRS-8, No. 3.

T. I. Fossen and S. I. Sagatun (1991c). The Norwegian Experimental Remotely Operated Vehicle (NEROV) Equations of Motion. Technical Report 91-4-W, Division of Engineering Cybernetics, Norwegian Institute of Technology, N-7034 Trondheim, Norway.

T. I. Fossen and S. I. Sagatun (1991d). The Norwegian Experimental Remotely Operated Vehicle (NEROV) Sensor System. Technical Report 91-2-W, Division of Engineering Cybernetics, Norwegian Institute of Technology, N-7034 Trondheim, Norway.

E. Freund (1973). Decoupling and Pole Assignment in Nonlinear Systems. *Electronics Letter*, EL-9, No. 16, 1973.

A. Gelb, J. F. Kasper, Jr., R. A. Nash, Jr., C. F. Price, and A. A. Sutherland, Jr. (1988). *Applied Optimal Estimation.* MIT Press, Boston, Massachusetts.

M. Gertler (1959). The DTMB Planar Motion Mechanism System. In *Proceedings of Symposium on Towing Tank Facilities, Instrumentation and Measuring Techniques*, Zagreb, Yugoslavia, September 1959.

M. Gertler and G. R. Hagen (1967). Standard Equations of Motion for Submarine Simulation. Technical Report DTMB 2510, Naval Ship Research and Development Center, Washington D.C.

K. R. Goheen (1986). *The Modelling and Control of Remotely Underwater Operated Vehicles.* Ph.D thesis, Dept. of Mechanical Eng.,University College London, July 1986.

M. D. Haskind (1954). On Wave Motions of a Heavy Fluid. *Prikl. Mat. Mekh.*, PMM-18, pp. 15–26.

Hasselmann et al. (1973). Measurements of Wind-Wave Growth and Swell Decay during the Joint North Sea Wave Project (JONSWAP). *Deutschen Hydrografischen Zeitschrift*, Ergängsungheft, Reihe A(8°), No. 12.

R. Horowitz and M. Tomizuka (1986). An Adaptive Control Scheme for Mechanical Manipulators-Compensation of Nonlinearity and Decoupling Control. Technical Report No. 80-WA/DSC-6, ASME.

D. E. Humphreys and K. W. Watkinson (1978). Prediction of the Acceleration Hydrodynamic Coefficients for Underwater Vehicles from Geometric Parameters. Technical Report NCSL-TR-327-78, Naval Costal System Center, Panama City, Florida.

D. E. Humphreys and K. W. Watkinson (1982). Hydrodynamic Stability and Control Analyses of the UNH-EAVE Autonomous Underwater Vehicle. Technical Report A.R.A.P. Tech. Memo. No. 82-2, University of New-Hampshire, Marine Systems Engineering Laboratory, Durham, New-Hampshire 03824.

F. H. Imlay (1961). The Complete Expressions for Added Mass of a Rigid Body Moving in an Ideal Fluid. Technical Report DTMB 1528, David Taylor Model Basin, Washington D.C.

N. A. Jenssen (1980). *Estimation and Control in Dynamic Positioning of Vessels.* Dr.ing thesis, Division of Engineering Cybernetics, Norwegian Institute of Technology, December 1980.

R. Johansson (1990). Adaptive Control of Robot Manipulator Motion. *IEEE Transactions on Robotics and Automation*, RA-6, No. 4, pp. 483–490.

S. Kalske (1989). Motion Dynamics of Subsea Vehicles. Technical report, Technical Research Centre of Finland, Vuorimiehentie 5, SF-02150 Espoo, Finland, January 1989.

T. R. Kane, P. W. Likins, and D. A. Levinson (1983). *Spacecraft dynamics.* McGraw-Hill, New York, NY.

R. Kelly and R. Carelli (1988). Input-Output Analysis of an Adaptive Computed Torque plus Compensation Control for Manipulators. In *Proceedings of the 27th IEEE Conference on Decision and Control*, Austin, Texas.

R. A. Kleppaker, K. Vetsgård, J. O. Hallset, and J. G. Balchen (1986). The Application of a Free-Swimming ROV in Aquaculture. In *IFAC Symposium on Automation and Dataprocessing in Aquaculture*, Trondheim, Norway, August 1986.

C. G. Källström (1979). *Identification and Adaptive Control Applied to Ship Steering.* Ph.D thesis, Dept. of Automatic Control, Lund Institute of Technology, Sweden.

H. Lamb (1932). *Hydrodynamics.* Cambridge University Press, London, UK.

I. D. Landau and R. Lozano (1981). Unification of Discrete Time Explicit Model Reference Adaptive Control Designs. *Automatica*, AUT-17, No. 4, pp. 593–611.

D. J. Lewis, J. M. Lipscombe, and P. C. Thomasson (1984). The Simulation of Remotely Operated Vehicles. In *Proceedings of the ROV'84 Conference*, pp. 245–251.

H. Lie, B. Sortland, and W. Lian (1989). Design of ROV Umbilical Configurations to Improve ROV Operability. In *Proceedings of of the OMAE'89 Conference*, The Hague, The Netherlands, March 1989.

M. A. Lyapunov (1907). Problème Gènèrale de la Stabilitè de Mouvement. *Ann. Fac. Sci. Toulouse*, Vol. 9, pp. 203–474. (Translation of a paper published in Comm. Soc. math. Kharkow 1893, reprinted in Ann. math Studies, Vol. 17, Princeton 1949).

J. M. Maciejowski (1990), editor. *Multivariable Feedback Design.* Addison-Wesley, Wokingham, England.

H. Mahesh, J. Yuh, and R. Lakshmi (1991). Control of Underwater Robots in Working Mode. In *Proceedings of IEEE International Conference on Robotics and Automation*, pp. 2630–2635, Sacramento, California, April 1991.

L. G. Milliken (1984). *Multivariable Control of an Underwater Vehicles.* Ph.D thesis, Massachusetts Institute of Technology, May 1984.

L. M. Milne-Thomson (1968). *Theoretical Hydrodynamics.* MacMillan Education Ltd., London, UK.

J. R. Morison, M. P. O'Brien, J. W. Johnson, and S. A. Schaaf (1950). The Force Exerted by Surface Waves on Piles. *Pet. Trans*, PT-189, pp. 149–154.

D. Myrhaug (1986). *Havmiljøbeskrivelse.* Institutt for marin hydrodynamikk, Norges tekniske høgskole, N-7034 Trondheim, Norway (in Norwegian).

J. N. Newman (1977). *Marine Hydrodynamics.* MIT Press, Massachusetts.

N. H. Norrbin (1970). Theory and Observation on the use of a Mathematical Model for Ship Maneuvering in Deep and Confined Waters. In *the 8th Symposium on Naval Hydrodynamics*, Pasadena, California.

R. Ortega and M. W. Spong (1988). Adaptive Motion Control of Rigid Robots: A Tutorial. In *Proceedings of the 27th Conference on Decision and Control*, pp. 1575–1584, Austin, Texas.

J. Roskam (1982). *Airplane Flight Dynamics and Automatic Flight Control.* Roskam Aviation and Engineering Corporation, Route 4, Box 274, Ottawa, Kansas 66067.

Ø. J. Rødseth (1990). Research on Autonomous Underwater Vehicles in Norway. In *Proceedings Seminar on Autonomous Underwater Vehicles, association for structural improvement of the shipbuilding industry*, Tokyo, Japan.

N. Sadegh and R. Horowitz (1987). Stability Analysis of an Adaptive Controller for Robotic Manipulators. In *Proceedings of IEEE International Conference on Robotics and Automation*, pp. 1223–1229, Raleigh, North Carolina.

S. I. Sagatun (1991). *Dynamic Positioning of Underwater Vehicles.* Dr.ing thesis, Division of Engineering Cybernetics, Norwegian Institute of Technology, N-7034 Trondheim, Norway (to be published).

S. I. Sagatun and T. I. Fossen (1990a). Computer-Controlled Underwater Robot Manipulator. In *Proceedings of the 22nd Offshore Technology Conference*, pp. 123–129, Houston, Texas, May 1990.

S. I. Sagatun and T. I. Fossen (1990b). Design Study of The Norwegian Experimental Remotely Operated Vehicle (NEROV). Technical Report 90-57-W, Division of Engineering Cybernetics, Norwegian Institute of Technology, N-7034 Trondheim, Norway.

S. I. Sagatun and T. I. Fossen (1991a). The Norwegian Experimental Remotely Operated Vehicle (NEROV) Propulsion System. Technical Report 91-1-W, Division of Engineering Cybernetics, Norwegian Institute of Technology, N-7034 Trondheim, Norway.

S. I. Sagatun and T. I. Fossen (1991b). The Norwegian Experimental Remotely Operated Vehicle (NEROV) Computer System. Technical Report 91-3-W, Division of Engineering Cybernetics, Norwegian Institute of Technology, N-7034 Trondheim, Norway.

S. I. Sagatun and T. I. Fossen (1991c). The Norwegian Experimental Remotely Operated Vehicle (NEROV). In *Proceedings of the ROV'91 Conference*, Hollywood, Florida, May 1991.

S. S. Sastry and A. Isidori (1989). Adaptive Control of Linearizable Systems. *IEEE Trans. Automatic Control*, TAC-34, No. 11, pp. 1123–1131.

J. J. E. Slotine (1983). *Tracking Control of Nonlinear Systems using Sliding Surfaces.* Ph.D thesis, MIT Dept. of Aero. and Astrodynamics, Cambridge, MA, May 1983.

J. J. E. Slotine and M. D. Di Benedetto (1990). Hamiltonian Adaptive Control of Spacecraft. *IEEE Trans. Automatic Control*, TAC-35, No. 7, pp. 848–852.

J. J. E. Slotine and W. Li (1987). Adaptive Manipulator Control. A Case Study. In *Proceedings of the 1987 IEEE Conf. on Robotics and Automation*, pp. 1392–1400, Raleigh, North Carolina.

J. J. E. Slotine and W. Li (1991). *Applied Nonlinear Control.* Prentice-Hall Int., Englewood Cliffs, New Jersey 07632.

SNAME (1950). The Society of Naval Architects and Marine Engineers. Nomenclature for Treating the Motion of a Submerged Body Through a Fluid. In *Technical and Research Bulletin 1-5.*

S. Sælid, N. A. Jenssen, and J. G. Balchen (1983). Design and Analysis of a Dynamic Positioning System Based on Kalman Filtering and Optimal Control. *IEEE Transaction on Automatic Control*, TAC-28, No. 3, pp. 331–339.

E. Tillman Hansen and O. L. Osen (1991). *Prosjektoppgave i Fag: 43190.* Institutt for teknisk kybernetikk, Norges tekniske høgskole, N-7034 Trondheim, Norway (in Norwegian).

S. J. Tinker (1982). Identification of Submarine Dynamics from Free-Model Test. In *Proceedings of the DRG Seminar*, The Netherlands, April 1982.

M. S. Triantafyllou and A. M. Amzallag (1984). A New Generation of Underwater Unmanned Tethered Vehicles Carrying Heavy Equipment at Large Depths. Technical Report MITSG 85-30TN, MIT Sea Grant, Boston, Massachusetts.

M. S. Triantafyllou and M. A. Grosenbaugh (1991). Robust Control For Underwater Vehicle Systems With Time Delays. *IEEE Oceanic Engineering*, OE-16, No. 1, pp. 146–152.

S. K. Tso, Y. Xu, and H. Y. Shum (1991). Variable Structure Model Reference Adaptive Control of Robot Manipulators. In *Proceedings of IEEE International Conference on Robotics and Automation*, pp. 2148–2153, Sacramento, California, April 1991.

I. U. Utkin (1977). Variable Structure Systems with Sliding Modes. *IEEE Transactions on Automatic Control*, TAC-22, No. 2, pp. 212–222, April 1977.

R. Venkatachalam, D. E. Limbert, and J. C. Jalbert (1985). Design and Simulation of a Crab-Wise Motion Controller for the EAVE-EAST Submersible. In *Proceedings of the ROV'85 Conference.*

H. Walderhaug (1990). *Marin Hydrodynamikk Grunnkurs.* Institutt for marin hydrodynamikk, Norges tekniske høgskole, N-7034 Trondheim, Norway (in Norwegian).

K. Wendel (1956). Hydrodynamic Masses and Hydrodynamic Moments of Inertia. Technical report, TMB Translation 260, July 1956.

D. R. Yoerger and J. J. E. Slotine (1984). Nonlinear Trajectory Control of Autonomous Underwater Vehicles using the Sliding Methodology. In *Proceedings of the ROV' 84 Conference*, pp. 245–251.

D. R. Yoerger and J. J. E. Slotine (1985). Robust Trajectory Control of Underwater Vehicles. *IEEE Oceanic Engineering*, OE-10, No. 4, pp. 462–470.

D. R. Yoerger and J. J. E. Slotine (1991). Adaptive Sliding Control of an Experimental Underwater Vehicle. In *Proceedings of IEEE International Conference on Robotics and Automation*, pp. 2746–2751, Sacramento, California, April 1991.

D. R. Yoerger, J. B. Newman, and J. J. E. Slotine (1986). Supervisory Control System for the JASON ROV. *IEEE Oceanic Engineering*, OE-11, No. 3, pp. 392–400.

D. R. Yoerger, J. G. Cooke, and J. J. E. Slotine (1990). The Influence on Thruster Dynamics on Underwater Vehicle Behavior and Their Incorporation Into Control Systems Design. *IEEE Oceanic Engineering*, OE-15, No. 3, pp. 167–179.

J. Yuh (1990). Modeling and Control of Underwater Robotic Vehicles. *IEEE Transactions on Systems, Man and Cybernetics*, TSMC-20, No. 6, pp. 1475–1483.

W. W. Zhou (1987). *Identification of Nonlinear Marine Systems.* Ph.D thesis, Servolaboratoriet, The Technical University of Denmark, Lyngby, Denmark.

K. J. Åström and C. G. Källström (1976). Identification of Ship Steering Dynamics. *Automatica*, AUT-12, 1976.

K. J. Åström and B. Wittenmark (1989). *Adaptive Control.* Addision-Wesley Publishing Company, Reading, Massachusetts.

Index